THE UNIVERSITY OF WARWICK

Library Declaration and Deposit Agreement

1. STUDENT DETAILS

Please complete the following:

Full name: ……

University ID number: ……

2. THESIS DEPOSIT

2.1 Under your registration at the University, you are required to deposit your thesis with the University in BOTH hard copy and in digital format. The digital copy should normally be saved as a single pdf file.

2.2 The hard copy will be housed in the University Library. The digital copy will be deposited in the University's Institutional Repository (WRAP). Unless otherwise indicated (see 2.6 below), this will be made immediately openly accessible on the Internet and will be supplied to the British Library to be made available online via its Electronic Theses Online Service (EThOS) service.
[At present, theses submitted for a Master's degree by Research (MA, MSc, LLM, MS or MMedSci) are not being deposited in WRAP and not being made available via EthOS. This may change in future.]

2.3 In exceptional circumstances, the Chair of the Board of Graduate Studies may grant permission for an embargo to be placed on public access to the thesis **in excess of two years**. This must be applied for when submitting the thesis for examination (further information is available in the *Guide to Examinations for Higher Degrees by Research*.)

2.4 If you are depositing a thesis for a Master's degree by Research, the options below only relate to the hard copy thesis.

2.5 If your thesis contains material protected by third party copyright, you should consult with your department, and if appropriate, deposit an abridged hard and/or digital copy thesis.

2.6 Please tick one of the following options for the availability of your thesis (guidance is available in the *Guide to Examinations for Higher Degrees by Research)***:**

☐ Both the hard and digital copy thesis can be made publicly available immediately

☐ The hard copy thesis can be made publicly available immediately and the digital copy thesis can be made publicly available after a period of two years (*should you subsequently wish to reduce the embargo period please inform the Library*)

☐ Both the hard and digital copy thesis can be made publicly available after a period of two years (*should you subsequently wish to reduce the embargo period please inform the Library*)

☐ Both the hard copy and digital copy thesis can be made publicly available after _____ (insert time period in excess of two years). **This option requires the prior approval of the Chair of the Board of Graduate Studies (see 2.3 above)**

The University encourages users of the Library to utilise theses as much as possible, and unless indicated below users will be able to photocopy your thesis.

☐ I **do not** wish for my thesis to be photocopied

3. GRANTING OF NON-EXCLUSIVE RIGHTS

Whether I deposit my Work personally or through an assistant or other agent, I agree to the following:

- Rights granted to the University of Warwick and the British Library and the user of the thesis through this agreement are non-exclusive. I retain all rights in the thesis in its present version or future versions. I agree that the institutional repository administrators and the British Library or their agents may, without changing content, digitise and migrate the thesis to any medium or format for the purpose of future preservation and accessibility.

4. DECLARATIONS

I DECLARE THAT:

- I am the author and owner of the copyright in the thesis and/or I have the authority of the authors and owners of the copyright in the thesis to make this agreement. Reproduction of any part of this thesis for teaching or in academic or other forms of publication is subject to the normal limitations on the use of copyrighted materials and to the proper and full acknowledgement of its source.

- The digital version of the thesis I am supplying is either the same version as the final, hard-bound copy submitted in completion of my degree once any minor corrections have been completed, or is an abridged version (see 2.5 above).

- I have exercised reasonable care to ensure that the thesis is original, and does not to the best of my knowledge break any UK law or other Intellectual Property Right, or contain any confidential material.

- I understand that, through the medium of the Internet, files will be available to automated agents, and may be searched and copied by, for example, text mining and plagiarism detection software.

- At such time that my thesis will be made publically available digitally (see 2.6 above), I grant the University of Warwick and the British Library a licence to make available on the Internet the thesis in digitised format through the Institutional Repository and through the British Library via the EThOS service.

- If my thesis does include any substantial subsidiary material owned by third-party copyright holders, I have sought and obtained permission to include it in any version of my thesis available in digital format and that this permission encompasses the rights that I have granted to the University of Warwick and to the British Library.

5. LEGAL INFRINGEMENTS

I understand that neither the University of Warwick nor the British Library have any obligation to take legal action on behalf of myself, or other rights holders, in the event of infringement of intellectual property rights, breach of contract or of any other right, in the thesis.

Please sign this agreement and ensure it is bound into the final hard bound copy of your thesis, which should be submitted to Student Reception, Senate House.

Student's signature: .....…… Date: .....

Synthesis and Self-Assembly of Linear and Cyclic Degradable Graft Copolymers

Rebecca Williams

Submitted for the degree of Doctor of Philosophy

THE UNIVERSITY OF WARWICK

Department of Chemistry

August 2014

For my parents, Andrew and Anne Williams.

Table of Contents

List of Figures

List of Schemes

List of Tables

Acknowledgements

Firstly, I must thank my supervisors and mentors Rachel and Andrew for not only their continued support throughout my PhD and MChem, but more importantly for believing in me. Without your support, guidance and encouragement, none of this would be possible.

I am also grateful to all members of the Dove and O'Reilly groups, past and present, for their advice and friendship. Thank you for making the lab such a cheerful and pleasant place to work. I doubt I will ever work with such fantastic colleagues again. In particular I am grateful to Ian and Guillaume simply for understanding.

Thank you to my soon-to-be husband Benben for supporting me throughout the past four years of my PhD and beyond. I'm sorry for neglecting you at times, but I hope you realise by now, I don't love chemistry more than you! Thank you for looking after me and believing in me, but more importantly, for teaching me to look after and believe in myself.

Finally, thank you to my wonderful family, including Morgan and Max, to whom I am forever indebted. You know what you have done for me and without you I would not be where I am today.

Declaration of Authorship

This thesis is submitted to the University of Warwick in support of my application for the degree of Doctor of Philosophy. It has been composed by myself and has not been submitted in any previous application for any degree. The work presented (including data generated and data analysis) was carried out by the author except in the cases outlined below:

- The MALDI-TOF data in Chapter 2 was obtained and analysed by Dr Ian Barker (University of Warwick);
- The DSC data in Chapter 3 was obtained and analysed by Dr Richard Todd (University of Warwick);
- The TEM images in Chapter 3 were obtained by Dr Joseph Patterson (University of Warwick);
- The SAXS data in Chapter 5 was obtained and analysed by Dr Anaïs Pitto-Barry (Australian Synchrotron facility and University of Warwick);
- The cryo-TEM images in Chapter 5 were obtained by Matthew van Hulle (Eindhoven University of Technology).

Publications

Orthogonal Modification of Norbornene-Functional Degradable Polymers, R. J. Williams, R. K. O'Reilly and A. P. Dove, *ACS Macro Lett.*, 2012, **1**, 1285 – 1290 (**Chapter 2**).

Degradable Graft Copolymers by Ring-Opening and Reversible Addition-Fragmentation Chain Transfer Polymerization, R. J. Williams, R. K. O'Reilly and A. P. Dove, *Polym. Chem.*, 2012, **3**, 2156 – 2164 (**Chapter 3**).

Abstract

This thesis explores the use of ring-opening polymerisation (ROP) and reversible addition-fragmentation chain transfer (RAFT) polymerisation to prepare linear and cyclic graft copolymers with a polycarbonate backbone. The solution properties and self-assembly behaviour of these linear and cyclic graft copolymers with hydrophilic side arms is also described.

Chapter 1 introduces the polymerisation techniques used in this thesis, namely ROP and RAFT, and provides a review of the self-assembly of polymers that possess a cyclic topology.

In Chapter 2, the synthesis and ROP of a novel cyclic carbonate monomer bearing pendent norbornene functionality is described. Successful post-polymerisation modification of the norbornene functionality is demonstrated for a range of addition reactions; 1,3-dipolar cycloaddition, inverse electron demand Diels-Alder reaction and radical thiol-ene addition, and is also shown to provide access to multi-functional polycarbonates. Attempts to prepare graft copolymers *via* the grafting of thiol-terminated polymer chains to the norbornene-functional polycarbonate backbone are also described.

Chapter 3 describes the optimised synthesis of linear graft copolymers *via* the ROP of a RAFT chain transfer agent (CTA)-functional cyclic carbonate monomer and subsequent RAFT polymerisation to grow polymer chains from the RAFT CTA sites located along the resulting polycarbonate backbone. This methodology was used to prepare a polycarbonate-*g*-poly(*N*-isopropylacrylamide) amphiphilic copolymer and its self-assembly to afford degradable, thermoresponsive particles is demonstrated.

In Chapter 4, the optimised procedures developed in Chapter 3 for the preparation of linear graft copolymers are applied to the preparation of well-defined cyclic graft copolymers with a degradable cyclic polycarbonate backbone and a range of side arm compositions.

Chapter 5 investigates the solution properties and self-assembly behaviour of linear and cyclic graft copolymers with hydrophilic poly(*N*-acryloylmorpholine) side arms and a hydrophobic polycarbonate backbone, prepared using the methodologies developed in Chapters 3 and 4.

Chapter 6 provides a summary of the key findings of Chapters 2 – 5 and Chapter 7 provides the experimental methods of this thesis.

Abbreviations

$\boldsymbol{\delta}$	Chemical shift
$\boldsymbol{Đ_M}$	Dispersity
$\boldsymbol{\lambda}$	Wavelength
δ-VL	δ-valerolactone
ε-CL	ε-caprolactone
AFM	Atomic force microscopy
AIBN	2,2'-Azobis(isobutyronitrile)
Ar	Aromatic
ATRP	Atom transfer radical polymerisation
bis-MPA	2,2'-Bis(hydroxymethyl) propionic acid
br	Broad
cmc	Critical micelle concentration
cryoTEM	Cryogenic transmission electron microscopy
CTA	Chain transfer agent
CuAAC	Copper-catalysed alkyne-azide cycloaddition
d	Doublet
$\mathbf{DA_{inv}}$	Inverse electron demand Diels-Alder reaction
$\boldsymbol{D_{av}}$	Average diameter
DBU	1,8-Diazabicyclo[5.4.0]undec-7-ene
DCTB	Trans-2-[3-(4-*tert*-butylphenyl)-2-methyl-2-propylidene] malonitrile
DDMAT	1-Dodecyl-S'-(α,α'-dimethyl-α''-acetic acid)
$\boldsymbol{D_h}$	Hydrodynamic diameter

DLS	Dynamic light scattering
DMAP	4-(Dimethylamino)pyridine
DMF	*N*,*N*-Dimethylformamide
DOSY	Diffusion-ordered NMR spectroscopy
DP	Degree of polymerisation
DSC	Differential scanning calorimetry
DTT	Dithiothreitol
EDC	*N*-(3-Dimethyl-aminopropyl)-*N*'-ethylcarbodiimide
eq	Equivalents
ESI MS	Electrospray ionisation mass spectrometry
FT-IR	Fourier transform infrared
$\boldsymbol{I(q)}$	Scattering intensity
$\boldsymbol{J}$	Coupling constant
$\boldsymbol{k_{eq}}$	Equilibrium rate constant
LA	Lactic acid or lactide
LAM	Less activated monomer
LCST	Lower critical solution temperature
m	Multiplet
MA	Methyl acrylate
MAM	More activated monomer
MALDI ToF MS	Matrix-assisted laser desorption ionisation time of flight mass spectrometry
$\boldsymbol{M_n}$	Number average molecular weight
MTBD	7-Methyl-1,5,7-triazabicyclo[4.4.0]dec-5-ene

M_w	Weight average molecular weight
[M]/[I]	Monomer-to-initiator ratio
m/z	Mass-to-charge ratio
N_{agg}	Aggregation number
NAM	*N*-Acryloylmorpholine
NHC	*N*-Heterocyclic carbene
Nb	Norbornene
NiPAm	*N*-Isopropylacrylamide
NMP	Nitroxide mediated polymerisation
NMR	Nuclear magnetic resonance
PAA	Poly(acrylic acid)
PBA	Poly(butyl acrylate)
PBd	Poly(butadiene)
PBO	Poly(butylene oxide)
PC	Polycarbonate
PCEVE	Poly(chloroethyl vinyl ether)
PCL	Poly(ε-caprolactone)
PD	Polydispersity
PDEAEMA	Poly(2-(diethylamino) ethyl methacrylate)
PDMAEMA	Poly(2-(dimethylamino) ethyl methacrylate)
PEG	Poly(ethylene glycol)
PEO	Poly(ethylene oxide)
PHEMA	Poly(2-hydroxyethyl methacrylate)
PI	Poly(isoprene)

PFP	Pentafluorophenyl
PLA	Poly(lactide)
PMA	Poly(methyl acrylate)
PMDETA	*N,N,N′,N″*-Pentamethyldiethylenetriamine
PMEO$_2$MA	Poly(2-(2-methoxy-ethoxy) ethyl methacrylate)
PMMA	Poly(methyl methacrylate)
POEGMA	Poly(oligo(ethylene glycol) methyl ether methacrylate)
PPFS	Poly(pentafluorostyrene)
PPO	Poly(propylene oxide)
PS	Poly(styrene)
pTSA	*p*-Toluenesulfonic acid
PVL	Poly(δ-valerolactone)
q	Quartet
q	Scattering vector
RAFT	Reversible addition-fragmentation chain transfer
RDRP	Reversible deactivation radical polymerisation
$\boldsymbol{R}_\mathbf{h}$	Hydrodynamic radius
REMP	Ring-expansion metathesis polymerisation
RI	Refractive index
ROMP	Ring-opening metathesis polymerisation
ROP	Ring-opening polymerisation
rt	Room temperature
s	Singlet
SAXS	Small angle x-ray scattering

SEC	Size exclusion chromatography
SLD	Scattering length density
t	Triplet
TBD	1,5,7-Triazabicyclo[4.4.0]dec-5-ene
TEG	Triethylene glycol methylether
TEGA	Triethylene glycol methylether acrylate
TEM	Transmission electron microscopy
TEMPO	2,2,6,6-Tetramethylpiperdine-1-oxyl
$\boldsymbol{T}_{\mathbf{g}}$	Glass transition temperature
THF	Tetrahydrofuran
THPA	Tetrahydropyran acrylate
$\boldsymbol{T}_{\mathbf{m}}$	Melting transition temperature
TMC	Trimethylene carbonate
UV	Ultraviolet
UV/vis	Ultraviolet/visible

1 Introduction

1.0 Overview

This chapter is divided into two sections; the first introduces the concept of "controlled" polymerisation techniques, with particular attention given to the polymerisation techniques used in this thesis; ring-opening and reversible addition-fragmentation chain transfer polymerisations, while the second section focuses on the application of controlled polymerisation techniques in the synthesis and self-assembly of cyclic polymers.

1.1 Introduction

Since the birth of polymer chemistry in the mid 19th century, polymers have become essential to everyday life. Originally, polymers were developed for their bulk macroscopic properties and indeed a lack of appropriate analytical techniques meant that microscopic, structural properties could not be readily probed or manipulated. With the vast development of polymerisation techniques and analytical methods over the last century, the control of polymer molecular weight, architecture, composition, the precise introduction of functionality, and even the exact sequence of polymer chains is now possible. Such precise control over the structure and functionality of polymers has allowed their development as macromolecular building blocks, *i.e*. components that form a more complex, hierarchical system. Examples include the use of amphiphilic block copolymers in self-assembly to form vehicles for drug delivery or the use of multi-armed water-soluble polymers in the preparation of hydrogels for tissue engineering applications.

1.2 Polymerisation Techniques

Conventional polymerisation techniques; whether step-growth or chain-growth, are typically uncontrolled processes resulting in the formation of ill-defined polymers, with unpredictable molecular weights, broad dispersities and a lack of chain-end functionality. Conversely, a living polymerisation proceeds in the absence of chain termination or chain transfer and affords well-defined polymers with predictable molecular weights and narrow molecular weight distributions. The difference in evolution of molecular weight between conventional step-growth, chain-growth and living polymerisations is shown in Figure 1.1 and highlights how in a living polymerisation, molecular weight is directly correlated to monomer conversion.

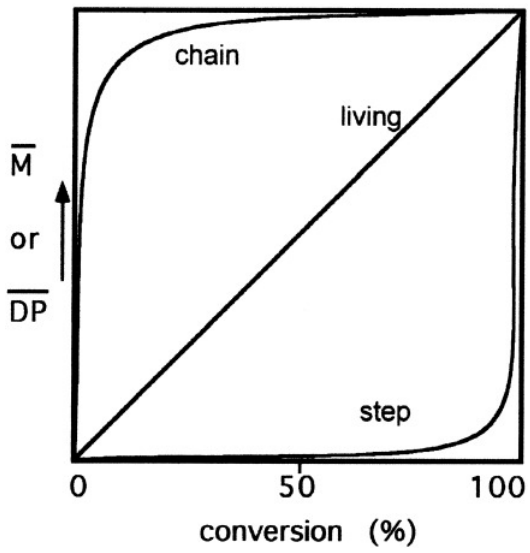

Figure 1.1. The evolution of molecular weight *versus* monomer conversion for a chain-growth, step-growth and living polymerisation.[1]

1.2.1 Living Polymerisations

For a polymerisation to be defined as "living" it must fulfill certain criteria:[2]

- The number of growing polymer chains is constant throughout the polymerisation and independent of monomer conversion;
- The degree of polymerisation and number average molecular weight of the polymers is directly proportional to monomer conversion;
- The molecular weight of the polymers can be controlled by the ratio of monomer and initiator;
- The polymerisation proceeds until all monomer is consumed (100% monomer conversion) and the addition of more monomer results in further polymerisation;
- Polymers with a narrow molecular weight distribution are produced;
- Chain end functionalised polymers can be prepared;
- Block copolymers can be formed by the sequential addition of a second monomer.

Anionic polymerisations have been categorised as living, with the first example reported by Swarc in 1956,[3] demonstrating the anionic polymerisation of styrene using sodium naphthalene as an initiator. However, these ionic polymerisation techniques suffer from poor functional group tolerance, stringent reaction conditions, the need for extremely high levels of monomer and solvent purity and the need to completely eliminate water and oxygen from the polymerisation system. As a consequence, alternative polymerisation techniques have been developed that exhibit "*pseudo*-living" or "controlled" behaviour and possess a higher tolerance to functional groups and trace

impurities. Examples of "controlled" polymerisation techniques include; reversible deactivation radical polymerisation (RDRP) techniques,[4-8] ring-opening polymerisation (ROP)[9] and ring-opening metathesis polymerisation (ROMP).[10, 11]

1.2.2 Reversible Deactivation Radical Polymerisation

Reversible deactivation radical polymerisations combine the advantages of both living and radical polymerisations, through meeting many of the criteria of a living polymerisation whilst being much simpler techniques to undertake. There are three main steps in a conventional free radical polymerisation; initiation, propagation and termination. During initiation, initiator species undergo homolysis to form radicals which subsequently react with monomer to become the first monomer unit of the polymer chain. Propagation is the addition of further monomer units to the growing polymer chain. Termination occurs mainly *via* radical-radical coupling by either recombination or disproportionation, resulting in the formation of dead polymer chains that can no longer propagate (Scheme 1.1). Chain transfer can also occur where the

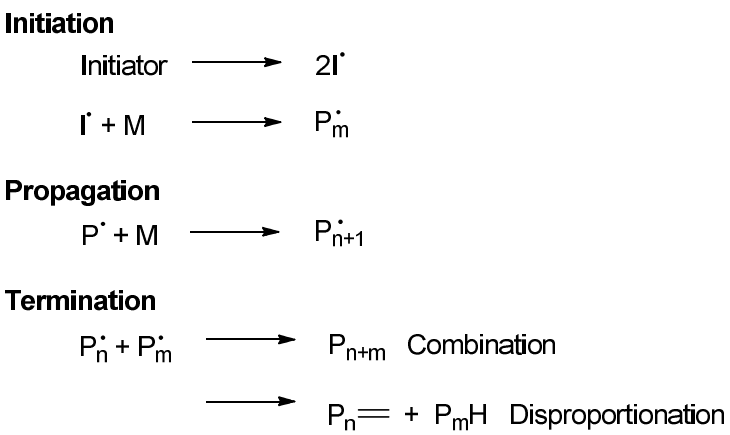

Scheme 1.1. Mechanism of a free radical polymerisation.

propagating radical is transferred to another atom, creating a dead polymer chain. All these processes occur concurrently, resulting in ill-defined polymers with unpredictable molecular weights and broad dispersities.

In order to control a radical polymerisation *i.e.* minimise the amount of termination and ensure the rate of initiation is faster than the rate of propagation, the concentration of active radicals in the polymerisation system must be reduced. In RDRP the concentration of propagating radicals is controlled by establishing a dynamic equilibrium between a low concentration of propagating polymer chains and a greater concentration of dormant polymer chains.[5] The equilibrium is rapid, ensuring all polymer chains have an equal chance of propagation and can grow at a constant rate, leading to polymers with narrow molecular weight distributions. Termination does still occur during RDRP but is limited to only a small percent of the total polymer chains.

The three main RDRP techniques are atom transfer radical polymerisation (ATRP),[12-17] nitroxide mediated polymerisation (NMP)[18-21] and reversible addition-fragmentation chain transfer polymerisation (RAFT).[22-28] ATRP and NMP both utilise the persistent radical effect to create an equilibrium between active and dormant polymer chains, a halide radical coordinated to a transition metal-ligand complex in ATRP and a nitroxide radical in NMP (Scheme 1.2). As a consequence of the stability of the dormant species, the equilibrium favours a low concentration of active radicals.

1.2.3 Reversible Addition Fragmentation Chain Transfer Polymerisation

In RAFT polymerisation the equilibrium between active and dormant chains is established by the addition of a thiocarbonyl compound, known as the RAFT

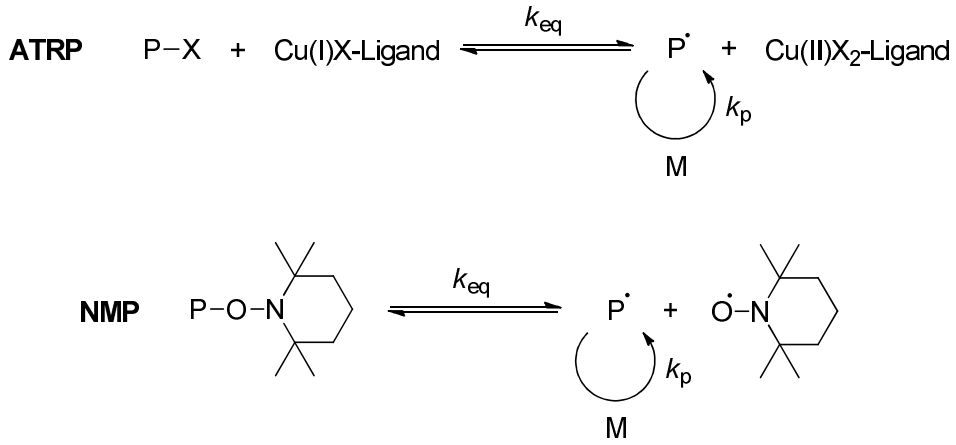

Scheme 1.2. Equilibrium steps of ATRP and NMP.

chain transfer agent (CTA), to a conventional radical polymerisation. The thiocarbonyl species adds to the propagating polymer chains and thus limits the number of polymer chains with an active radical chain end. An equilibrium is established between a large amount of polymer chains with thiocarbonyl end groups and a small number of polymer chains with a radical at the chain end. The thiocarbonyl group rapidly shuttles between polymer chains ensuring all polymer chains have an equal chance of propagation and grow at a constant rate, resulting in a narrow molecular weight distribution.[29]

The RAFT polymerisation process is initiated in the same way as a conventional free radical polymerisation through decomposition of a thermal initiator to yield a radical species, $I^{\cdot}$, which subsequently reacts with monomer (Scheme 1.3. (i)). The growing polymer chain ($P_n^{\cdot}$) then reacts with the thiocarbonyl group of the CTA forming a radical polymer intermediate. This intermediate can then fragment in one of two ways; to form either a polymeric CTA and release the R-group or revert back to the initial growing polymer chain and CTA (ii). The radical R-group ($R^{\cdot}$) can then act as an initiating group by reacting with

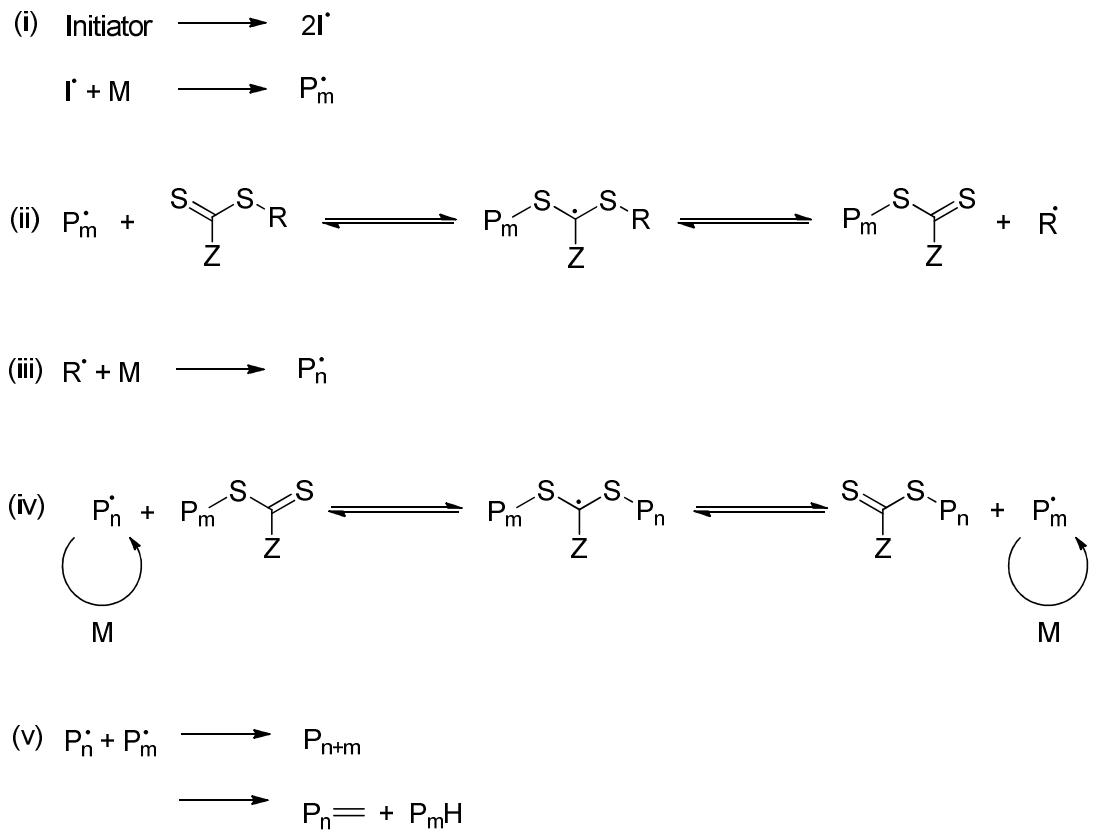

Scheme 1.3. Mechanism of RAFT polymerisation.

monomer, forming new polymer chains (iii). Once all CTA has been consumed, all polymers (P_n and P_m) now take part in the main equilibrium (iv) between active and dormant species, rapidly switching between propagating polymer chains and dormant thiocarbonyl-capped polymers. Termination can still occur but is significantly minimised compared to conventional free radical polymerisations, as a result of this low concentration of radical species.

The structure of the RAFT CTA, specifically the identity of the Z- and R-groups, can have a significant effect on polymerisation and therefore careful choice of CTA is needed.[30] The identity of the Z-group affects the stability of the thiocarbonyl group and therefore the stability of the radical intermediate in the main equilibrium of RAFT polymerisation.[31] Hence, the stability bestowed by the Z-group must be balanced to allow addition to the thiocarbonyl double

bond, as well as allowing fragmentation of the polymer chains to enable propagation.

There are four main types of CTA depending on the structure of the Z-group; dithioesters, trithiocarbonates, dithiocarbamates and xanthates (Figure 1.2), and with correct choice of CTA type, effective polymerisation control can be achieved for a wide range of monomers. More activated monomers (MAMs), such as styrenes, acrylates, methacrylates, acrylamides and methacrylamides, form comparatively stable radicals and therefore the polymerisation of MAMs is better controlled by CTAs with stabilising Z-groups, which are more susceptible to radical attack, such as dithioesters and trithiocarbonates. Conversely, dithiocarbamates and xanthates provide good control over less activated monomers (LAMs), such as *N*-vinyl pyrrolidone, vinyl acetate and other vinyl ester monomers. For dithiocarbamates and xanthates, the lone pair of the respective nitrogen or oxygen atom is delocalised onto the thiocarbonyl group, lowering its reactivity and susceptibility to radical attack.

The identity of the R-group is also important; it must be a good leaving group compared to the propagating polymer chain and be able to effectively re-initiate

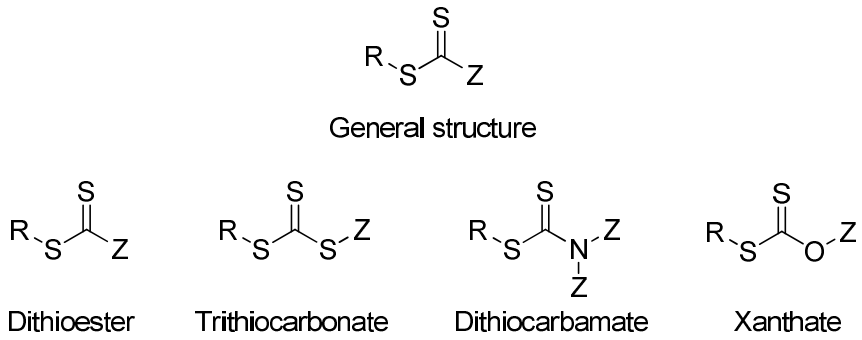

Figure 1.2. Types of RAFT chain transfer agent.

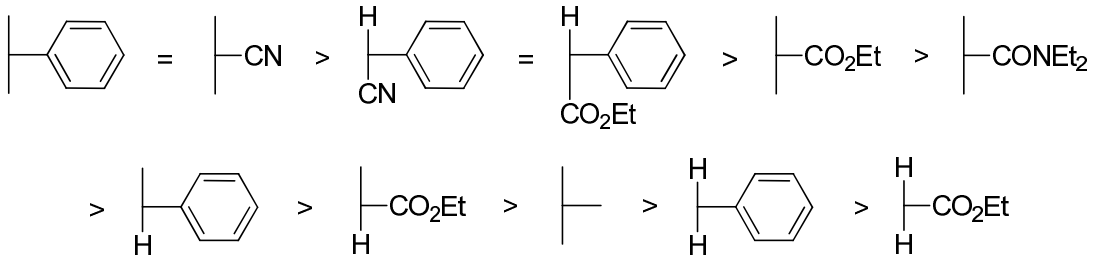

Figure 1.3. RAFT CTA R-groups, decreasing fragmentation rate from left to right.

polymerisation (Figure 1.3).[32] Thus, by judicious choice of Z- and R-groups it is possible to control the polymerisation of a large array of monomers, making RAFT a very versatile and attractive technique. Furthermore, the incorporation of a thiocarbonyl group onto the polymer chain end provides the opportunity for post-polymerisation modification of polymer chains prepared by RAFT.[33, 34] The thiocarbonyl group can be transformed into an alkene by thermal elimination or a thiol *via* reaction with amines or reducing agents, can act as a dienophile in hetero-Diels-Alder reactions and react with functionalised radical species.

1.2.4 Ring-Opening Polymerisation

A ring-opening polymerisation is defined as a polymerisation in which a cyclic monomer yields a polymer consisting of acyclic repeat units or repeat units that contain fewer cycles than the monomer. This definition encompasses an extremely large range of cyclic monomers, including but not limited to lactones,[35, 36] carbonates,[37] ethers,[38] sulfides,[39] lactams,[40] oxazolines,[41] phosphonates,[42] and siloxanes.[43] As a consequence of the structural diversity of these monomers, there are several mechanisms by which ROP can occur and

many of these polymerisations can be categorised as either "living" or "controlled".[9]

The ring-opening polymerisation of cyclic esters has emerged as an area of particular interest.[35, 36, 44-49] The resulting aliphatic polyesters may be both biocompatible and (bio)degradable and have consequently found applications in the biomedical arena; for drug delivery and tissue engineering, and as degradable replacements for conventional commodity plastics.[44, 50-54] Polyesters are traditionally prepared *via* the polycondensation of hydroxyacids or a difunctional carboxylic acid and a diol,[47, 55] where the latter approach relies upon precise stoichiometry. The resulting polymers are generally limited to low molecular weights and possess broad dispersities, furthermore, long reaction times and high temperatures are often required. The ROP of cyclic esters provides a controlled alternative to prepare degradable aliphatic polyesters, with predictable molecular weights, narrow molecular weight distributions and end-group control, and hence affords polymers with extremely well-defined and tunable bulk properties. The ROP of cyclic esters has been demonstrated with a range of catalysts, including metal-based catalysts,[56-60] organic catalysts[61-64] and enzymes.[65-67]

1.2.4.1 Metal-Catalysed ROP

Both well-defined metal coordination complexes[57, 58, 60] and simple metal salts,[68] such as metal alkoxides,[59] have been demonstrated to effectively catalyse the ROP of cyclic esters *via* either an anionic or coordination-insertion mechanism (Scheme 1.4). Anionic ROP proceeds *via* nucleophilic attack of the initiating anion at the carbonyl group of the cyclic ester, generating anionic propagating

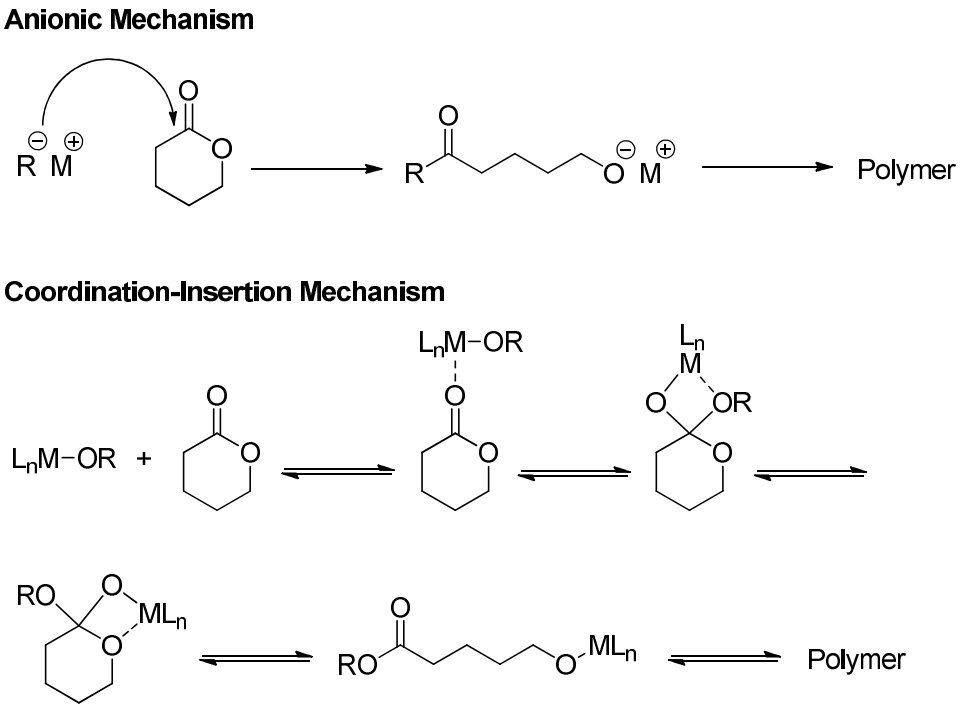

Scheme 1.4. Metal catalysed ROP of cyclic esters; (top) *via* an anionic mechanism, (bottom) *via* a coordination-insertion mechanism.

species. In a coordination-insertion mechanism, the carboxyl oxygen atom of the cyclic ester monomer coordinates to the metal centre of the coordination complex and is subsequently inserted into the metal-oxygen bond of the metal alkoxide group. While the use of metal-based catalysts has been highly successful in the preparation of well-defined polyesters, the resulting polymers are often contaminated with trace metal impurities. These impurities can be costly and time consuming to remove and if left in the polymer can prevent its use in metal-sensitive applications, including the biomedical and microelectronic fields of research.

1.2.4.2 Organocatalysed ROP

Within the last two decades significant advances have been made in the field of organocatalytic ROP, offering an attractive alternative to traditional metal-

based ROP catalysts.[61-64] Small molecule organic catalysts are often commercially available or can be synthesised in relatively few steps and unlike many metal-based catalysts, organic catalysts are generally air and moisture stable, making their preparation, storage and handling considerably easier. Organocatalysts can be easily removed from the resulting polyesters *via* simple washing procedures or the use of ion exchange resins, as a consequence of their acidic or basic nature.

The first example of organocatalysed ROP was reported by Hedrick and coworkers in 2001 for the polymerisation of lactide using 4-(dimethylamino)pyridine (DMAP) as the polymerisation catalyst.[69] Polymerisations were well controlled, exhibiting low dispersity values, however slow polymerisation times were reported. Subsequent research by the same group investigated the use of *N*-heterocyclic carbenes (NHCs) in the ROP of cyclic esters which were found to be highly active catalysts, with significantly increased rates of polymerisation compared to DMAP catalysed ROP.[70] The activity of the NHC catalysts could be controlled through variation of the *N*-substituent[71] and consequently were applied to the ROP of a wide range of cyclic esters, as well as other cyclic monomers, including carbonates,[72] epoxides[73, 74] and siloxanes.[75, 76] The use of NHC catalysts has also been applied to the successful preparation of well-defined cyclic poly(lactide) (PLA),[77, 78] other cyclic polyesters[79-82] and cyclic poly(carbosiloxane)s,[83] *via* manipulation of the zwitterionic polymerisation mechanism, in the absence of an initiating alcohol (Scheme 1.5). As a consequence of the acute air and moisture sensitivity of NHCs, the *in situ* generation of NHCs from air stable derivatives has also been investigated.[84-90]

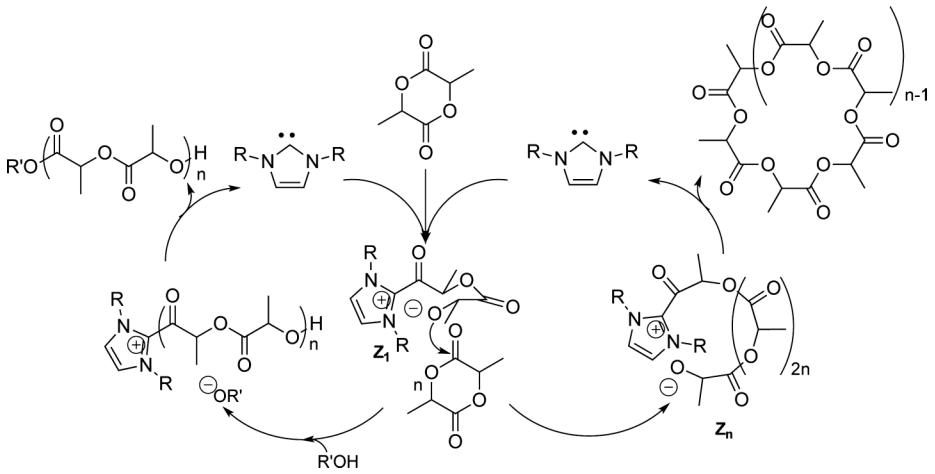

Scheme 1.5. NHC mediated ROP of lactide in the presence and absence of an alcohol initiator.[81]

A significant advancement in the field of organocatalytic ROP was made with the development of bifunctional thiourea-amine catalyst systems.[91] These systems allow the concurrent activation of the cyclic monomer and initiating alcohol through H-bonding (Figure 1.4). The initial thiourea-amine catalyst system investigated incorporated both functionalities on the same molecule, however, dividing the functionalities between separate molecules allowed tuning of the polymerisation activity through variation of the tertiary amine. Consequently, (-)-sparteine was found to exhibit an excellent balance between reactivity and selectivity.[92]

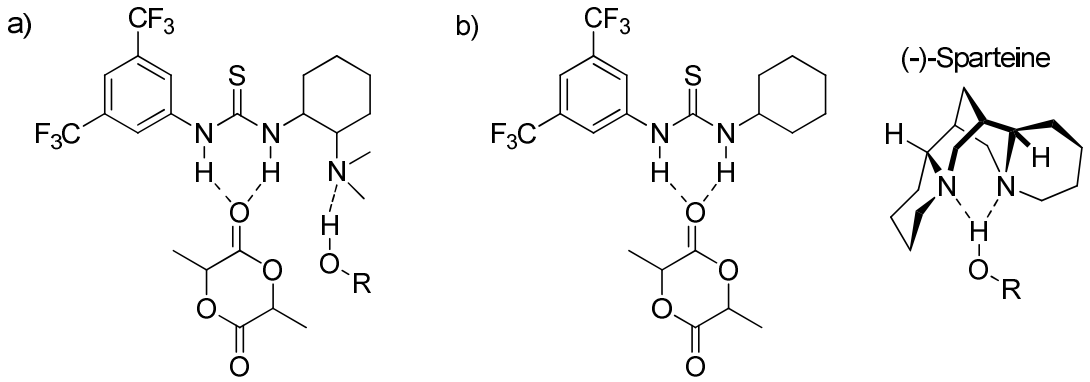

Figure 1.4. Dual activation of lactide and an alcohol initiator *via* H-bonding with a) bifunctional thiourea-amine or b) thiourea and (-)-sparteine.

The application of organic "superbases" as ROP catalysts has also received considerable attention. 1,8-Diazabicyclo[5.4.0]undec-7-ene (DBU) and 7-methyl-1,5,7-triazabicyclo[4.4.0]dec-5-ene (MTBD) (Figure 1.5) were found to exhibit high catalytic activity and low dispersity values for the polymerisation of lactide[93] and the cyclic carbonate monomer, trimethylene carbonate,[72] as well as other functional cyclic carbonates[94, 95] and phosphoesters,[96-98] *via* an activated initiator mechanism. Whilst these catalysts are successful for the polymerisation of LA, cyclic carbonates and cyclic phosphoesters, they have proved ineffective for the polymerisation of lactones,[93] where additional activation of the lactone *via* H-bonding with a thiourea cocatalyst is required for successful polymerisation (Figure 1.5). The "superbase" 1,5,7-triazabicyclo[4.4.0]dec-5-ene (TBD) possesses the ability to activate both the cyclic monomer and initiating alcohol and therefore demonstrates extremely high activity in ROP in the polymerisation of lactide, lactones,[93, 99, 100] cyclic carbonates[72] and cyclic phosphoesters.[96-98] Furthermore, as a consequence of this high activity TBD has been able to polymerise monomers which exhibit low levels of ring strain, for example, large lactones such as ω-pentadecalactone,[101]

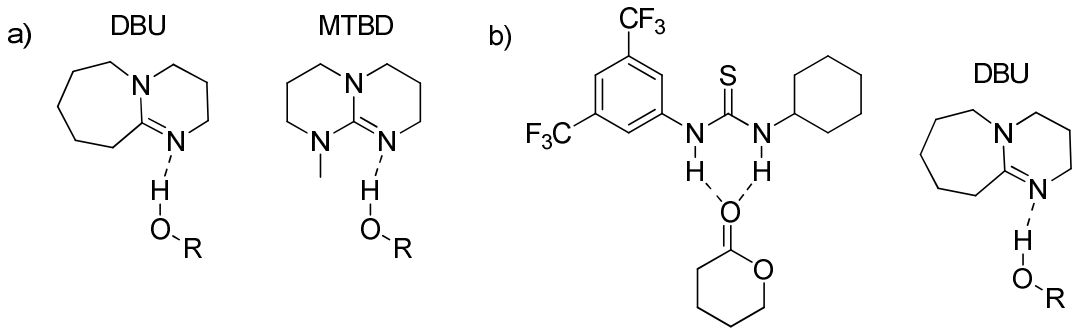

Figure 1.5. a) Activation of an alcohol initiator *via* H-bonding with DBU and MTBD. b) Dual activation of an alcohol initiator and lactone *via* H-bonding with DBU and thiourea cocatalyst respectively.

as well as sterically hindered lactides,[102] lactones[103, 104] and cyclic carbonates.[105] In addition to the aforementioned catalysts which function through nucleophilic attack, organocatalysed cationic polymerisation has also been demonstrated for the ring-opening of cyclic esters *via* protonation and activation of the carbonyl group of the monomer. Strong acids such as trifluoromethanesulfonic acid,[106] methanesulfonic acid,[107] diphenyl phosphate[108] and phosphoramidic acid[109] are capable of activating both the monomer and initiating alcohol simultaneously.[110]

1.2.4.3 Polycarbonates *via* ROP

As a consequence of their low toxicity, biocompatibility and biodegradability, aliphatic polycarbonates have received increasing attention as materials for biomedical applications, including controlled drug release and tissue engineering.[37, 111, 112] In addition, aliphatic polycarbonates possess some advantages over aliphatic polyesters when applied to this field of research, such as greater stability and improved mechanical properties. Polycarbonates exhibit greater *in vitro* and *in vivo* stability than polyesters as a result of differing hydrolysis mechanisms.[113-120] The hydrolytic chain scission of a polyester results in the formation of a carboxylic acid terminated polymer chain, which will subsequently auto-catalyse further degradation of the polyester. Contrastingly, chain scission of a polycarbonate will yield a less acidic carbonic acid end group, that will readily decompose to release CO_2, forming a hydroxyl end group and preventing end-group mediated auto-catalysed degradation (Scheme 1.5). As a result of these different hydrolysis mechanisms, the *in vivo* degradation of polycarbonates occurs predominantly

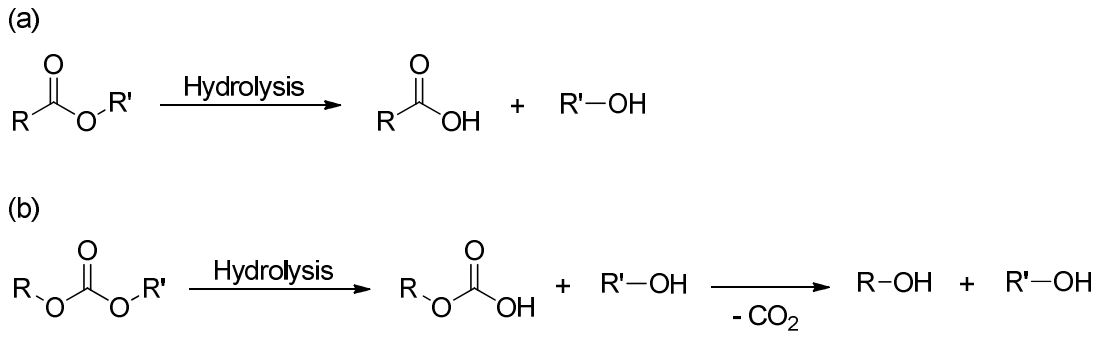

Scheme 1.6. Hydrolysis of (a) an ester *vs* (b) a carbonate.

via enzymatic surface erosion,[113, 118] whereas polyesters undergo auto-catalysed bulk degradation.[119] Furthermore, the acidic degradation products of polyesters can cause harmful inflammation of the surrounding tissue.

Aliphatic polycarbonates are typically amorphous polymers, with low glass transition temperatures (T_g), compared to polyesters, which are often semi-crystalline. Consequently, polycarbonates are more suitable materials for soft tissue engineering compared to polyesters, and possess beneficial mechanical properties.[114, 115] To this end, polycarbonates are often copolymerised with polyesters to improve the mechanical properties of the polymer, where the copolymerisation of polyesters and polycarbonates allows the fine-tuning of other properties, *e.g.* degradation.[119, 120]

There are three main approaches for the preparation of polycarbonates; the polycondensation of diols with phosgene,[37, 112, 121] the copolymerisation of carbon dioxide and epoxides[122-128] and the ROP of cyclic carbonate monomers[37, 129, 130] (Scheme 1.6). The synthesis of polycarbonates *via* polycondensation suffers from the disadvantages of step-growth polymerisations, notably the requirement for the precise stoichiometry of monomers, often leading to polymers with low molecular weights and broad dispersities. Furthermore, the

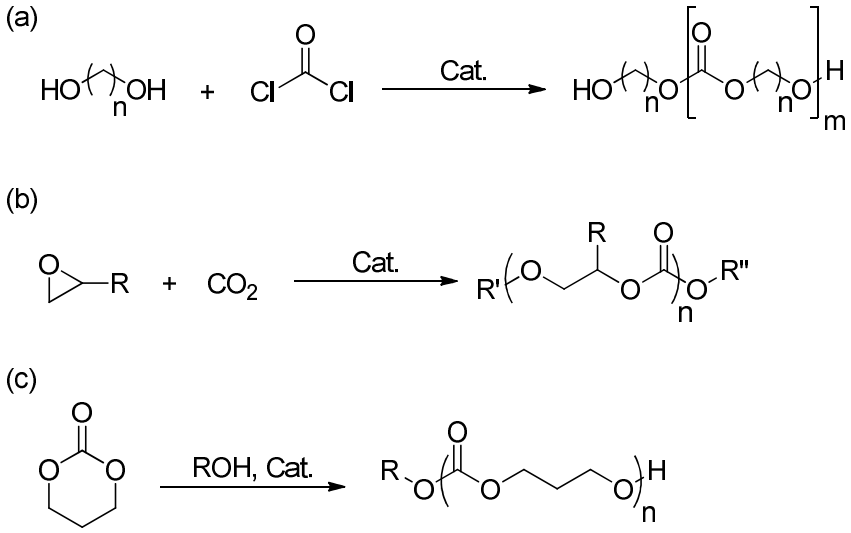

Scheme 1.7. Preparation of polycarbonates *via* (a) polycondensation, (b) copolymerisation of epoxides and CO_2 and (c) ROP.

use of toxic reagents such as phosgene is undesirable. The copolymerisation of CO_2 and epoxides has received increasing attention as a sustainable alternative for the production of polycarbonates. A wide range of metal catalysts have been developed to control such polymerisations, however the use of high temperatures and pressures is generally required and polymerisations suffer from limited molecular weights and side reactions, including the formation of ether linkages and cyclic carbonates.

The ROP of cyclic carbonate monomers offers a controlled alternative to the preparation of polycarbonates, where the resulting well-defined polymers display predictable molecular weights, narrow molecular weight distributions and excellent end-group fidelity. Furthermore, the versatile synthesis of six membered cyclic carbonate monomers with pendent functionality has allowed access to a library of functional polycarbonates, adding even greater appeal to this methodology.[131, 132]

1.2.4.4 Functional Polycarbonates

The introduction of functionality to a polymer can impart desirable properties to the material that allow its tailoring towards a specific application.[133-135] The incorporation of functionality into polycarbonates is an area of great current interest and has allowed precise control over the physical properties of polycarbonates and the attachment of relevant therapeutic, biological or fluorescent molecules.[136-138] To enable the preparation of functional polycarbonates, a variety of methods to prepare functional cyclic carbonate monomers have been developed.[131, 132] These methods have primarily focused on the ring closure of 1,3-diols using phosgene derivatives, to prepare six membered cyclic carbonates (Figure 1.6). 2,2'-Bis(hydoxymethyl) propionic acid (bis-MPA), a 1,3-diol with a pendent carboxylic acid group, has received considerable attention as a feedstock for functional six membered cyclic carbonates (Scheme 1.8). The desired functional group may be directly coupled to the carboxylic acid of bis-MPA, under acidic or basic conditions (route A), however to incorporate more sensitive functionalities the use of an acetonide protection-deprotection strategy is required to protect the diol (route B). This increases the number of steps required to prepare the functional carbonate monomer and involves the preparation of a different intermediate during each monomer synthesis. To overcome this problem, Hedrick and coworkers have

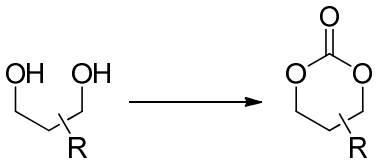

Figure 1.6. Ring-closure of a 1,3-diol.

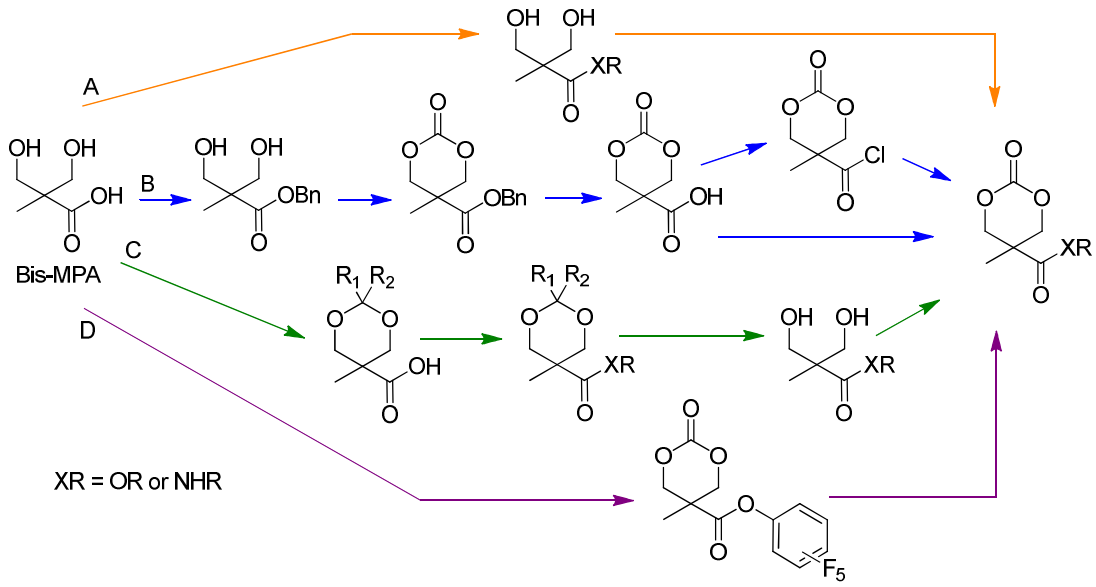

Scheme 1.8. Synthesis of functional cyclic carbonates derived from bis-MPA.

pioneered two methods to prepare common intermediates for the synthesis of functional cyclic carbonate monomers derived from bis-MPA. In the first approach, the carboxylic acid of bis-MPA was protected by conversion to a benzyl ester before ring-closure of the diol.[139] Subsequent deprotection *via* hydrogenation yielded a carboxylic acid functional cyclic carbonate scaffold, ready for further reaction with amines or alcohols to yield the desired functional carbonate monomer (route C). In their alternative approach, functional cyclic carbonate monomers could be prepared in two steps *via* reaction of bis-MPA with bis(pentafluorophenyl)carbonate, yielding a pentafluorophenyl-functional cyclic carbonate, followed by reaction with the desired functional amine or alcohol (route D).[140-142] Other 1,3-diols have also been reported as feedstocks for the production of functional cyclic carbonate monomers,[143] including amino acids,[144] sugars,[105] pentaerythritol[145] and glycerol.[146] These versatile strategies for monomer synthesis have resulted in a

plethora of functional cyclic carbonate monomers and consequently a large range of functionalised polycarbonates.[147-150]

1.3 Cyclic Polymers

The properties of polymers are not only controlled through polymer functionality and composition, but also through control of polymer topology and architecture. The major advancement of controlled and living polymerisation techniques has enabled the preparation of a range of well-defined complex polymer architectures, including block, star,[151-154] graft,[155-159] branched[160-163] and cyclic.[164-167] Of these polymer architectures, cyclic polymers are perhaps the least explored as a consequence of the difficulty in both their preparation and purification. Despite these difficulties, cyclic polymers are of significant interest as a result of the unique properties they exhibit in comparison to analogous linear polymers.

1.3.1 Synthesis of Cyclic Polymers

The existence of cyclic polymers has been long established in nature with the discovery of circular DNA[168] and in synthetic chemistry as cyclic contaminants in step-growth polymerisations. Indeed, original synthetic methods to prepare cyclic polymers were based upon the ring-chain equilibrium of poly(dimethylsiloxane),[169, 170] where cyclic species were separated from linear polymers through laborious fractional precipitations and preparative size exclusion chromatography.[171] Despite the obvious limitations of this method, it allowed the first investigation of cyclic polymer properties, verifying the unique behaviour of cyclic topologies.

Recent synthetic breakthroughs have since allowed the preparation of well-defined cyclic polymers in the absence of linear impurities, as well as a diverse range of more complex cyclic architectures. There are now two main

approaches to prepare cyclic polymers; ring-closure[172-174] and ring-expansion.[175] The synthesis of cyclic polymers has been extensively reviewed,[164-167, 176] so only an overview of these techniques will be given.

Ring-closure techniques involve the coupling of the reactive chain ends of a linear polymer to yield a cyclic polymer (Figure 1.7). Ring-closure can be achieved through the bimolecular homodifunctional coupling of a linear polymer with a small molecule linker or the unimolecular homodifunctional or heterodifunctional coupling of a linear polymer. The development of living and controlled polymerisation techniques has allowed the preparation of polymers with high chain end functionality. Furthermore, in all ring-closure techniques, the use of highly efficient coupling reactions is crucial to ensure high purity cyclic polymers.

In a bimolecular ring-closure strategy, the linear polymer first undergoes an intermolecular reaction with the small molecule linker, forming an intermediate species which then undergoes intramolecular cyclisation. Reactions are performed at high dilution or *pseudo*-high dilution to avoid the intermediate species reacting with another polymer chain, however the concentration of reactants must be sufficiently high for the first step of this method to be effective. Furthermore, precise 1:1 stoichiometry of the linear polymer and small molecule linker is needed. To overcome the limitations of bimolecular ring-closure, electrostatic interactions between the linear polymer chain ends and small molecule linker can be used to template cyclisation.[177] In contrast, for unimolecular ring-closure techniques, high dilution alone is required to suppress polymer-polymer coupling side reactions, as such this method has

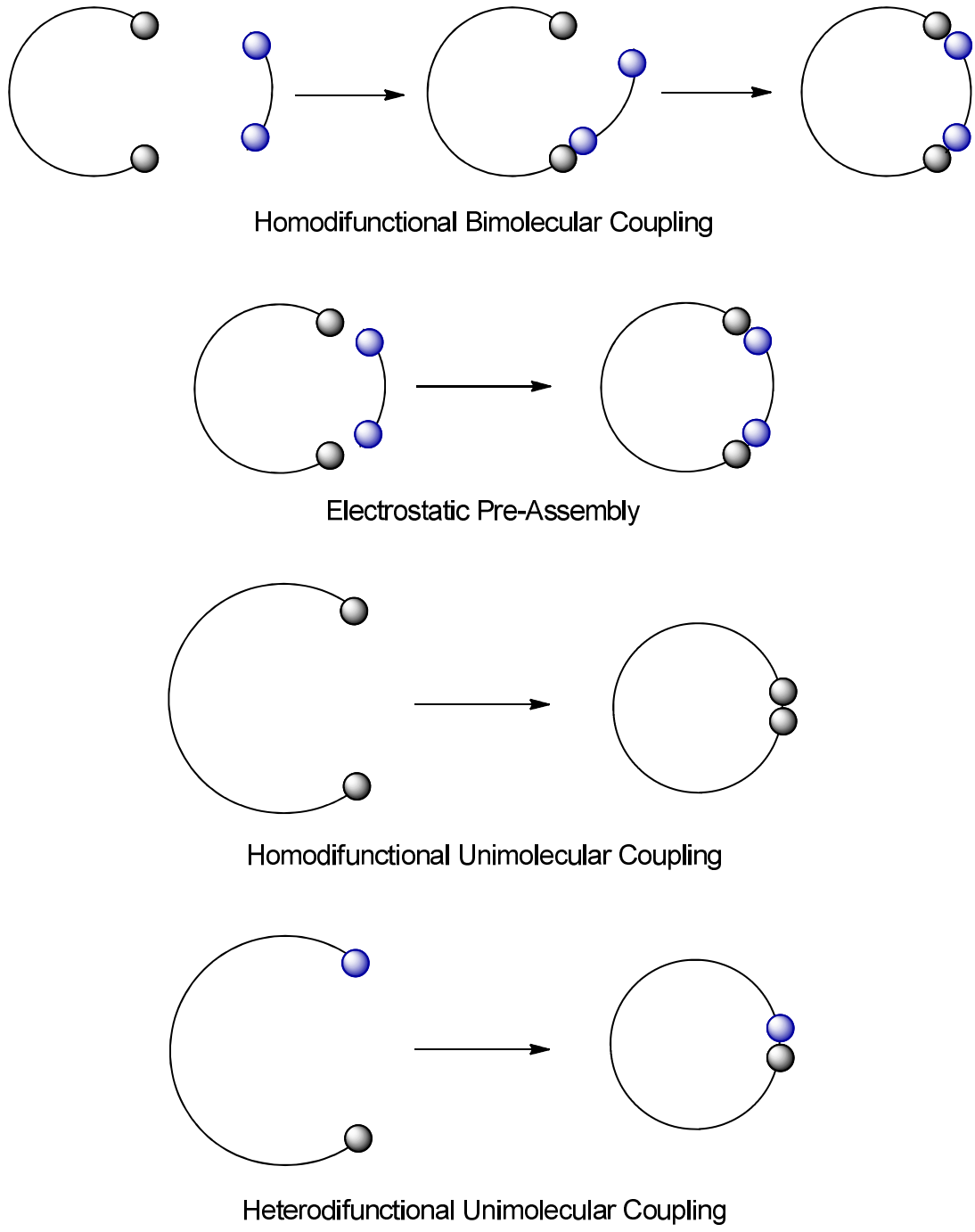

Figure 1.7. Synthesis of cyclic polymers *via* ring-closure.

been highly successful in the preparation of well-defined cyclic polymers and is generally favoured over bimolecular ring-closure.

Ring-expansion techniques involve the successive insertion of a cyclic monomer into a cyclic catalyst,[178] initiator[175] or propagating species[78] (Figure 1.8). Ring-expansion techniques do not require high dilution and therefore afford cyclic

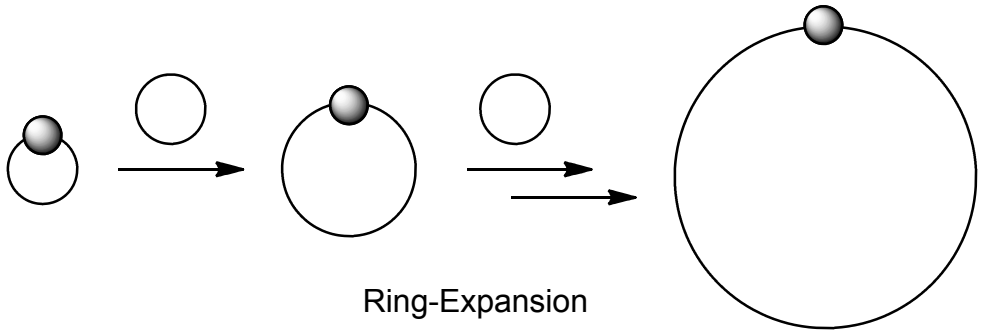

Figure 1.8. Synthesis of cyclic polymers *via* ring-expansion.

polymers in considerably higher yields than ring-closure techniques. However, careful catalyst design is required to ensure the formation of high molecular weight cyclic polymers with low dispersities and to ensure elimination of the catalyst from the final polymer.

The advances made in cyclic polymer synthesis, controlled polymerisation techniques and highly efficient coupling "click" reactions,[179] have also allowed for the preparation of a diverse range of cyclic polymer topologies including tadpole,[180] sun-shaped,[181] theta-shaped,[182] figure-of-eight[183] and other multi-cyclic topologies [177] (Figure 1.9).

1.3.2 Topological Effects

Cyclic polymers possess many unique physical properties in comparison to their linear polymer analogues, in both bulk and solution.[164, 166, 184] These differences provide opportunities for exploitation in many applications, as well as increasing our fundamental understanding of structure-property relationships. Cyclic polymers possess smaller hydrodynamic volumes[185, 186] and radii of gyration[187, 188] in comparison to their linear counterparts as a consequence of the more confined conformation of cyclic polymer chains. This

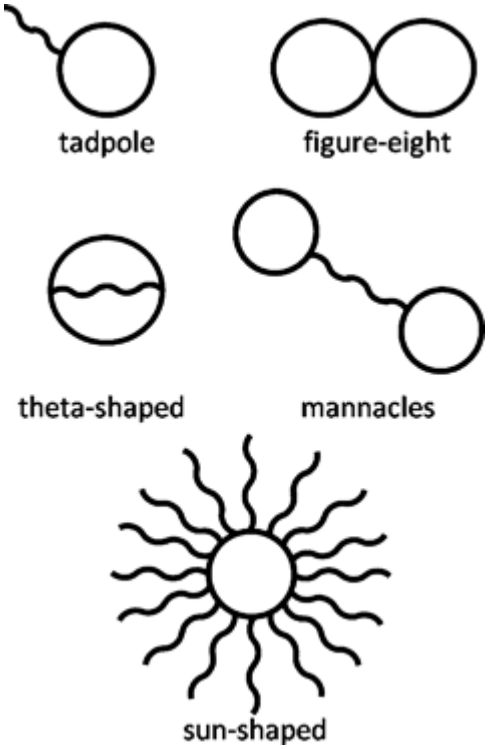

Figure 1.9. Complex cyclic polymer architectures.[167]

difference has been exploited in the characterisation of cyclic polymers by size exclusion chromatography (SEC) analysis, where cyclic polymers exhibit longer retention times and therefore lower apparent molecular weights than the equivalent linear polymers of the same molecular weight.

As a consequence of their smaller hydrodynamic volume and lack of chain ends, cyclic polymers exhibit significantly higher critical entanglement molecular weights than analogous linear polymers. Similarly, the solution viscosities and melt viscosities of cyclic polymers are lower than the equivalent linear polymers.[187, 189] Interestingly, the melt viscosities of blends of cyclic and linear polymers are higher than either component, as a consequence of the threading of linear chains through cyclic polymer chains.[190]

The glass transition temperatures (T_g) of analogous linear and cyclic polymers exhibit very different trends.[191, 192] Cyclic polymers exhibit higher T_g values

than their linear counterparts as a consequence of the different mobilities of cyclic and linear polymers. Cyclic polymers are inherently less mobile than linear polymers because of their confined nature, smaller volumes and lack of chain ends. Furthermore, because of a lack of polymer chain ends, cyclic polymers show very little dependence of T_g on molecular weight, except at very low molecular weights.[191] The melting transition temperatures (T_m) of cyclic and linear polymers also exhibit similar differences in behaviour.

Cyclic and linear polymers are known to exhibit different modes of diffusion.[193] The accepted mode of diffusion for linear polymers is a reptation mechanism; this process is governed by the mobility of the polymer chain ends. As cyclic polymers do not possess chain ends, diffusion must occur by a different mechanism, however this precise mode of diffusion has yet to be elucidated.

The unique structural and physical properties of cyclic polymers have been exploited in a variety of applications. Hawker and coworkers recently reported the use of cyclic block copolymers to prepare thin films for lithography applications, where the reduced volume of the cyclic polymer allowed a 30% decrease in domain spacing, compared to the corresponding linear diblock copolymer (Figure 1.10).[194] Zhang *et al*. prepared cyclic polymer based gels *via* a combination of ring-opening metathesis polymerisation and thiol-ene chemistry. The gels prepared from cyclic polymers were found to exhibit markedly different swelling and mechanical properties in comparison to the equivalent gels comprised of linear polymers.[195] In addition, Szoka and coworkers reported that cyclic polymers have longer *in vivo* circulation times and higher tumor accumulation compared to linear analogues.[196, 197]

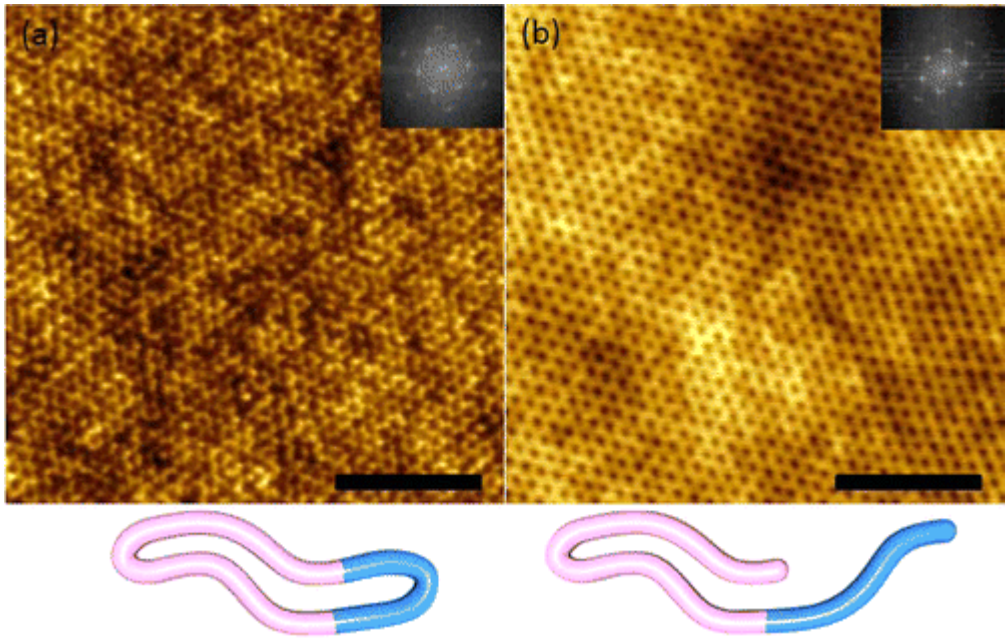

Figure 1.10. AFM height images of cyclic and linear PS-*b*-PEO thin films (scale bar = 250 nm).[194]

1.4 Self-Assembly

Self-assembly is ubiquitous with nature and everyday life; the membranes of living cells are comprised of self-assembled phospholipids and countless cleaning products and cosmetics contain self-assembled surfactants. Consequently, the solution self-assembly of amphiphilic molecules is an area of significant research.[198-203] Amphiphiles self-assemble in selective solvents to minimise unfavourable hydrophobic-hydrophilic interactions. A small molecule amphiphile consists of a hydrophobic tail and a hydrophilic head group, and the resulting morphology of the self-assembled molecule is determined by the packing parameter, $p = v/a_o l_c$, where v is the volume of the hydrophobic tail, a_o is the contact area of the hydrophilic head group and l_c is the length of the hydrophobic tail. Spherical micelles are favoured when $p < 1/3$, cylindrical micelles are favoured when $1/3 < p < 1/2$ and vesicles when $1/2 < p < 1$.[204]

1.4.1 Self-Assembly of Linear Block Copolymers

The major advancement of controlled polymerisation techniques has allowed the preparation of well-defined amphiphilic polymers that will self-assemble into well-defined aggregates in a selective solvent. Self-assembled polymeric aggregates exhibit greater stability than small molecule aggregates,[205] as a result of their superior mechanical and physical properties, and consequently polymeric self-assemblies have been utilised as catalytic nanoreactors,[206-208] drug delivery vehicles[137, 138, 209-216] and molecular imaging agents.[136, 217] Among the different architectures of amphiphilic polymer, linear block copolymer systems are by far the most studied. As a result the self-assembly of linear block copolymers is well established and has been extensively reviewed,[138, 212, 218-221] most recently by Mai and Eisenberg.[218]

A wide range of morphologies are accessible *via* the self-assembly of linear block copolymers,[222] including customary assemblies such as spherical and cylindrical micelles, vesicles and lamellae, as well as far more complex morphologies including multi-compartment micelles,[223, 224] helical micelles[225] and multi-lamellar "onion" vesicles.[226] The resulting morphology of a block copolymer aggregate is determined by three factors which govern the free energy of the system: the degree of stretching of the core forming block, the interfacial tension between the core and the solvated corona and the repulsive interactions of the corona chains.[212, 218] Consequently, the morphology of polymeric assemblies can be influenced by a wide range of variables that affect these three factors, including polymer composition, concentration, water content, assembly technique and the presence of additives. Furthermore, block copolymer assemblies may be defined as either thermodynamically stable or

kinetically frozen, depending on the mobility of the constituent polymer chains and employed method of assembly.[227, 228]

1.4.2 Self-Assembly of Cyclic Polymers

The chain architecture of amphiphilic polymers is also known to influence self-assembly behaviour, however reports of the self-assembly of non-linear polymer architectures are relatively limited. The recent advancement of controlled polymerisation techniques has allowed the preparation of a diverse range of amphiphilic non-linear polymers, including star, graft, branched and cyclic polymers, and consequently the self-assembly of non-linear polymers has gained increasing interest.[223, 229-239]

Interest in the solution self-assembly of cyclic polymers began in the mid 1990s,[240] not long after initial investigations into the solution self-assembly of linear block copolymers. However, as a consequence of the synthetic difficulties encountered in the preparation of well-defined, high purity cyclic polymers, this area of research remained comparatively limited. With the recent developments in cyclic polymer preparation allowing these synthetic difficulties to be overcome, studies of cyclic polymer self-assembly have received increasing attention. Cyclic amphiphilic polymers are expected to display unique self-assembly behaviour in comparison to linear polymers as a consequence of the reduced conformational freedom of cyclic polymers and their smaller hydrodynamic volumes. The rest of this chapter will seek to provide an overview of the limited, but growing field of cyclic polymer self-assembly in an attempt to elucidate the effect of cyclisation on aggregation. This overview will discuss the assembly of amphiphilic cyclic block copolymers,

in addition to more complex amphiphilic cyclic architectures, highlighting topological differences observed in comparison to the self-assembly behaviour of equivalent linear systems where appropriate.

1.4.2.1 Self-Assembly of Cyclic Block Copolymers

The earliest reported investigations into the effect of polymer cyclisation on self-assembly were undertaken by Booth and coworkers, studying cyclic diblock copolymers comprised of either poly(ethylene oxide)-*b*-poly(butylene oxide) (cyclic-PEO-*b*-PBO) or poly(ethylene oxide)-*b*-poly(propylene oxide) (cyclic-PEO-*b*-PPO).[240-242] The self-assembly behaviour of the cyclic diblock copolymers was compared with the self-assembly of linear triblock copolymers and linear diblock copolymers of equivalent composition. The authors reported similar aggregation behaviour for the cyclic diblock and linear triblock copolymers, with both polymers forming micellar assemblies, with comparable values of hydrodynamic radii (R_h) and critical micelle concentrations (cmc). One notable difference was observed when comparing the aggregation numbers (N_{agg}) of the cyclic diblock and linear triblock assemblies, with values of N_{agg} consistently higher for the cyclic diblock micelles, suggesting that cyclic diblock assemblies are denser than the equivalent linear triblock assemblies. When comparing the cyclic diblock copolymers with the linear diblock copolymers, a more distinct difference in self-assembly behaviour was observed. The linear diblock copolymer assemblies consistently exhibited significantly larger values of R_h and N_{agg} and lower cmc values, compared to both the cyclic diblock and linear triblock systems.

The findings of these initial studies can be explained by considering the respective conformation of the three polymer architectures in a micellar state (Figure 1.11). The cyclic diblock and linear triblock copolymers are entropically disfavoured because each polymer chain has two block junctions located at the solvent-core interface, in comparison to linear diblock copolymers which possess only one block junction. To this end, the cmc values for cyclic diblock and linear triblock copolymers will be higher than the equivalent linear diblock assemblies. The relative size of the resulting assemblies will also be influenced by the conformation of the different architectures. As the core-forming block of the linear diblock copolymer assembly is not required to loop and can stretch without restriction, the value of R_h for a linear diblock micellar assembly is expected to be larger than that of equivalent cyclic diblock or linear triblock assemblies. Furthermore, as a consequence of their unrestricted structure,

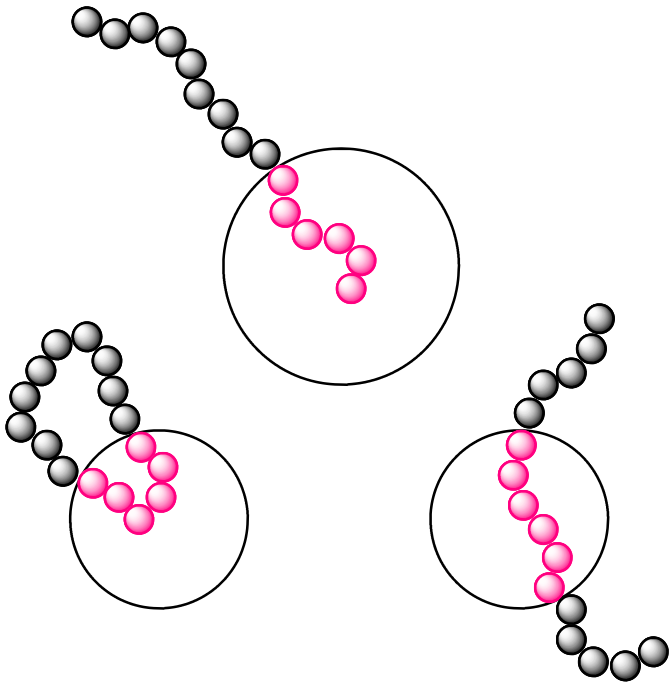

Figure 1.11. Chain conformations of linear diblock, cyclic diblock and linear triblock copolymers in a micellar state.

allowing better packing, linear diblock copolymer micelles are expected to be denser than micelles comprised of the equivalent cyclic diblock or linear triblock. In addition, because cyclic polymers possess smaller hydrodynamic volumes than linear polymers, the assembly of the cyclic diblock copolymer is expected to be smaller than the assembly of the linear triblock copolymer. Thus the observed respective particle sizes of cyclic diblock, linear diblock and linear triblock copolymers is a balance between their hydrodynamic volume, conformation and relative stretching and packing abilities. Booth and coworkers concluded that the cyclic diblock and linear triblock polymers form comparatively loose flower-like micelles, where the cyclic aggregate is smaller as a consequence of its smaller hydrodynamic volume. Whereas, the linear diblock copolymers form more conventional densely packed star-like micelles.

Subsequent studies by other research groups have also compared the self-assembly of cyclic diblock and linear diblock copolymers and reported similar findings. Ge *et al*. studied the self-assembly of cyclic poly(2-(2-methoxy-ethoxy) ethyl methacrylate)-*b*-poly(oligo(ethylene glycol) methyl ether methacrylate) (cyclic-PMEO_2MA-*b*-POEGMA) and cyclic poly(2-(dimethylamino) ethyl methacrylate)-*b*-poly(2-(diethylamino) ethyl methacrylate) (cyclic-PDMAEMA-*b*-PDEAEMA) in comparison to linear diblock copolymers of the same composition.[243] For both polymer systems, the cyclic diblock assembly exhibited a smaller hydrodynamic radius and higher cmc value than the equivalent linear diblock copolymer. Additionally, Zhang *et al*. observed that the hydrodynamic diameter of cyclic poly(ethylene glycol)-*b*-poly(ε-caprolactone) (PEO-*b*-PCL) micelles was approximately half that of linear PEO-*b*-PCL micelles (cyclic D_h = 15 nm, linear D_h = 27 nm) (Figure 1.12).[244] Whereas,

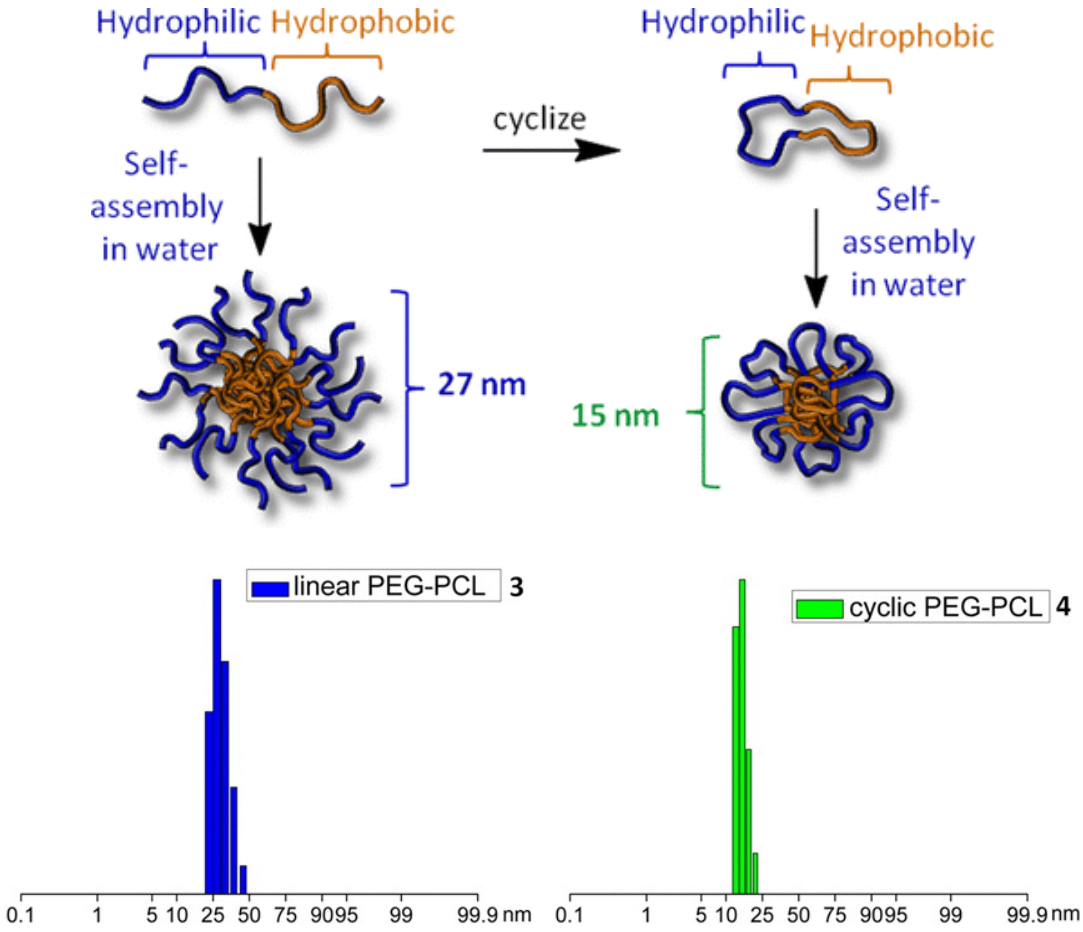

Figure 1.12. Light scattering data for cyclic and linear PCL-*b*-PEG.[244]

Hadjichristidis and coworkers reported a significantly larger aggregation number and hydrodynamic radius for aggregates of linear poly(styrene)-*b*-poly(butadiene) (PS-*b*-PBd) in DMF, a selective solvent for PS, in comparison to cyclic PS-*b*-PBd and linear PS-*b*-PBd-*b*-PS.[245] Surprisingly, when the same polymers were assembled in *n*-decane, a selective solvent for PBd, aggregates of the linear triblock copolymer, PS-*b*-PBd-*b*-PS, displayed the largest values of N_{agg} and R_h.

Isono *et al*. reported the self-assembly of cyclic poly(decyl glycidyl ether)-*b*-poly(2-(2-(2-methoxyethoxy)ethoxy ethyl glycidyl ether) and the equivalent linear diblock copolymer.[246] In contrast to previous examples, it was observed

that the cyclic diblock copolymer assemblies were larger than the assemblies of the linear diblock (cyclic D_h = 166 nm, linear D_h = 122 nm). However, considering the fully extended chain lengths of the linear and cyclic copolymers, these assemblies cannot be classical core-shell micelles and indeed further analysis of the assemblies by transmission electron microscopy (TEM) revealed large spherical compound structures. The increased complexity of these aggregates makes it harder to elucidate the effect of cyclisation on the particle dimensions. However, the observed difference in particle size may result from the reduced packing ability of cyclic polymer chains compared to linear polymers, resulting in a greater value of D_h for the cyclic diblock assembly.

Yamamoto and Tezuka compared the self-assembly behaviour of cyclic poly(butyl acrylate)-*b*-poly(ethylene oxide) (PBA-*b*-PEO) with respect to the linear triblock PBA-*b*-PEO-*b*-PBA.[247] Upon micellisation the hydrophilic block of the linear triblock copolymer is looped and in contrast to previous studies the linear triblock assembly is conformationally restricted in the corona and not the core. The cyclic diblock and linear triblock assemblies displayed comparable values of D_h and cmc (cyclic D_h = 20 nm, cmc = 0.14 mg/mL, linear D_h = 20 nm, cmc = 0.13 mg/mL). However, significantly different thermal stabilities were exhibited by the cyclic and linear assemblies, with the cyclic micelles displaying cloud points > 40 °C higher than the linear micelles. The lower thermal stability of the linear assemblies was attributed to the occurrence of inter-micelle bridging *via* dangling polymer chains in combination with dehydration, resulting in agglomeration at lower temperatures. In comparison, the cyclic polymer chains cannot form inter-micelle bridges and agglomeration will only occur as a consequence of polymer dehydration (Figure 1.13). Through

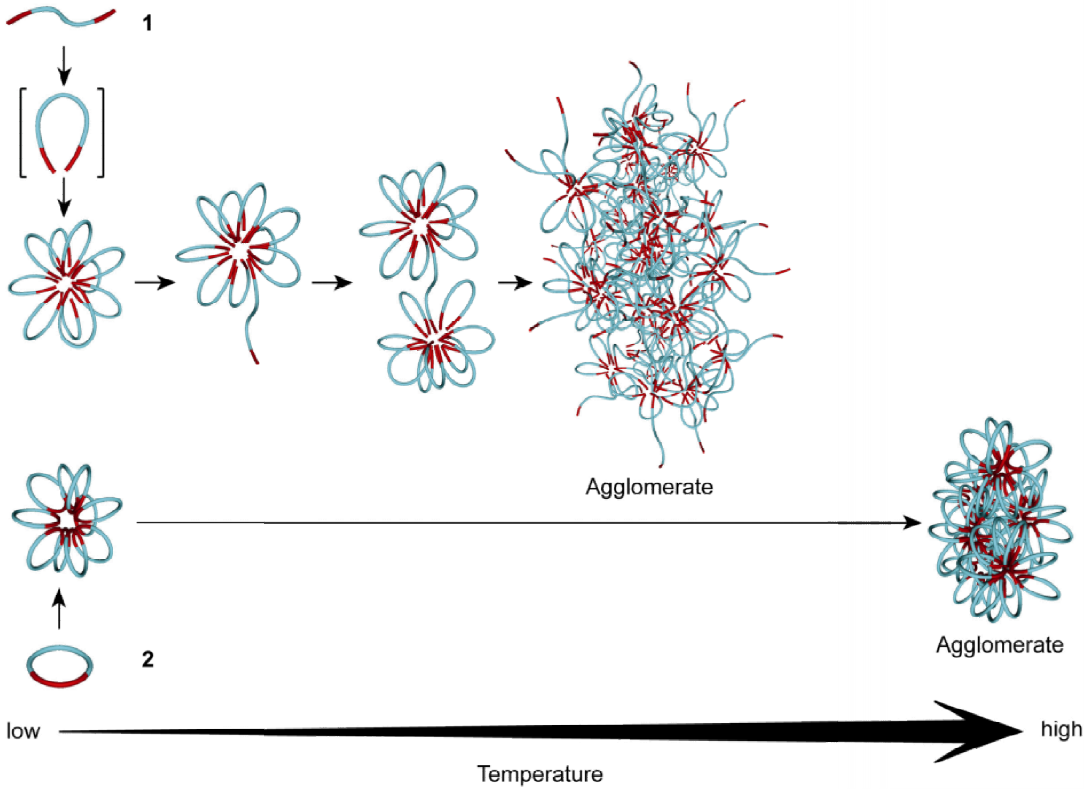

Figure 1.13. Modes of temperature induced agglomeration for cyclic diblock PBA-*b*-PEO and linear triblock PBA-*b*-PEO-*b*-PBA flower-like micelles.[247]

coassembly of the cyclic and linear polymers, micelles with tunable cloud point temperatures were observed. The same group has also reported that micelles of cyclic PBA-*b*-PEO and cyclic poly(methyl acrylate)-*b*-poly(ethylene oxide) (PMA-*b*-PEO) exhibit greater robustness in response to salt additives (NaCl and $MgSO_4$), when compared to their linear PBA-*b*-PEO-*b*-PBA and PMA-*b*-PEO-*b*-PMA counterparts.[248] The greater thermal and salt stabilities of the cyclic diblock assemblies were exploited through their use as catalytic nanoreactors in reactions that required elevated temperatures and high salt concentrations. Yamamoto and Ree have subsequently reported a detailed small angle x-ray scattering investigation that highlighted subtle structural differences between the cyclic PBA-*b*-PEO and linear PBA-*b*-PEO-*b*-PBA assemblies (Figure 1.14).[249] Both micelles were found to exhibit a core-fuzzy-shell structure, however the

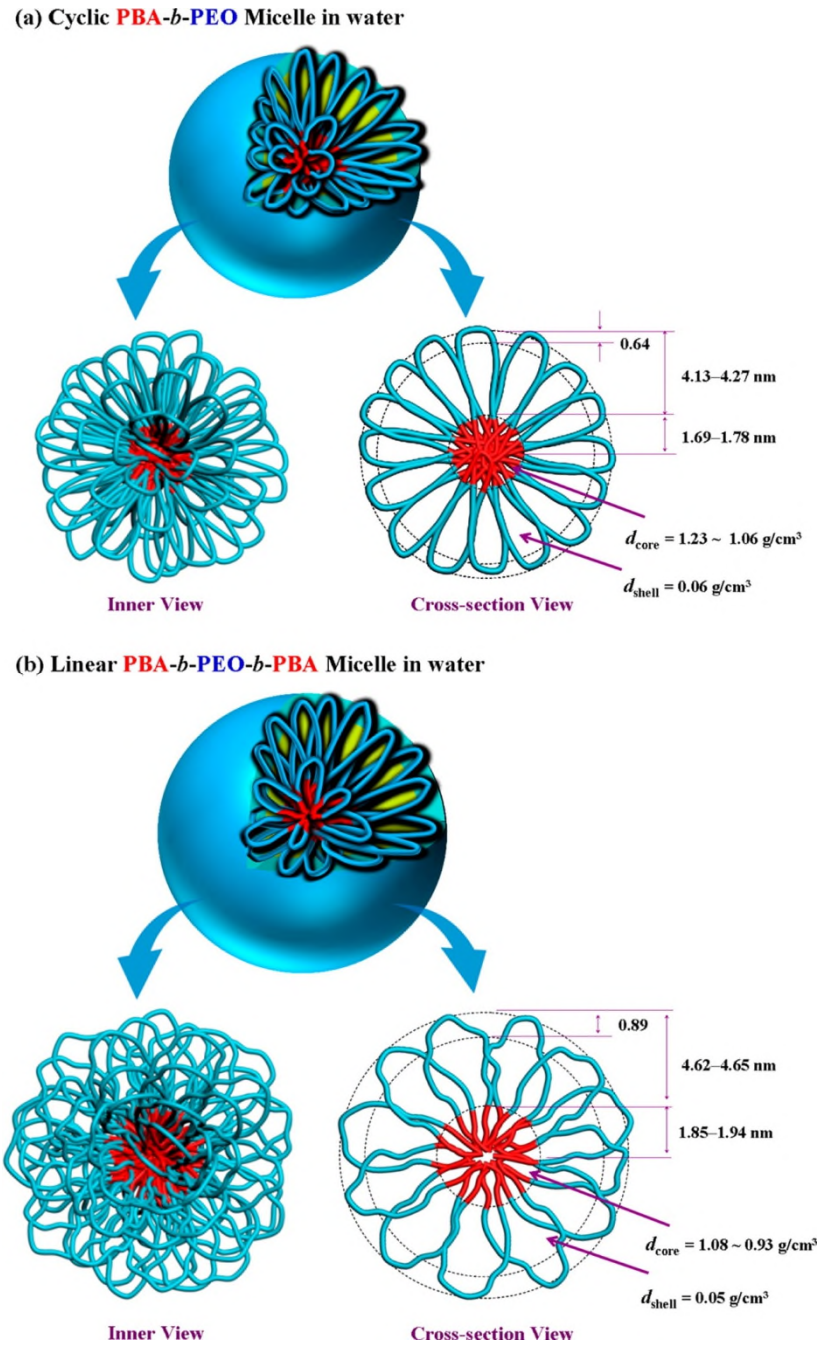

Figure 1.14. Structural representations of cyclic diblock PBA-*b*-PEO and linear triblock PBA-*b*-PEO-*b*-PBA micelles, structural parameters obtained from SAXS analysis.[249]

core and corona of the cyclic diblock copolymer micelle were more compact than the linear triblock copolymer micelle, as a result of the greater confinement and smaller effective volume of cyclic polymers.

The work highlighted so far has focused on the aggregation of cyclic block copolymers that possess a longer hydrophilic block relative to the hydrophobic

block or comparable hydrophilic and hydrophobic block lengths; such polymers assemble to form so-called "star-like" micelles. Borsali and coworkers reported the self-assembly behaviour of cyclic poly(styrene)-*b*-poly(isoprene) (PS-*b*-PI) copolymers, that possess a significantly longer core-forming PS block than the corona-forming PI block; these assemblies are commonly referred to as "crew-cut".[250-256] In contrast to the "star-like" assemblies discussed above, these "crew-cut" assemblies exhibited much greater structural and morphological differences with respect to their linear PS-*b*-PI analogues. The linear PS-*b*-PI copolymers were observed to form spherical micelles of consistent size and low dispersities, regardless of polymer concentration, temperature or solvent choice (*n*-alkane length). However, the morphology of the cyclic PS-*b*-PI copolymers was found to change dramatically as these parameters were varied and a transition from spherical flower-like micelles to giant worm-like micelles was observed (Figures 1.15 and 1.16). As was discussed in previous examples, the contrasting self-assembly behaviour between the cyclic and linear polymers arose as a result of the looped nature of the PS core block of the cyclic polymer assembly, restricting the packing of the core and resulting in unfavourable PS-solvent interactions. However, as a consequence of the large hydrophobic block in these "crew-cut" assemblies, the effect is more pronounced compared to examples of "star-like" micelles. To minimise unfavourable PS-solvent interactions, the flower-like micelles of the cyclic diblock copolymer cohere forming more energetically favourable worm-like micelles. The transition from flower-like micelles to worm-like micelles is more pronounced as polymer concentration and temperature are increased, as the probability of cohesive collisions increases. Furthermore, as the solvent quality for PS is reduced (*n*-

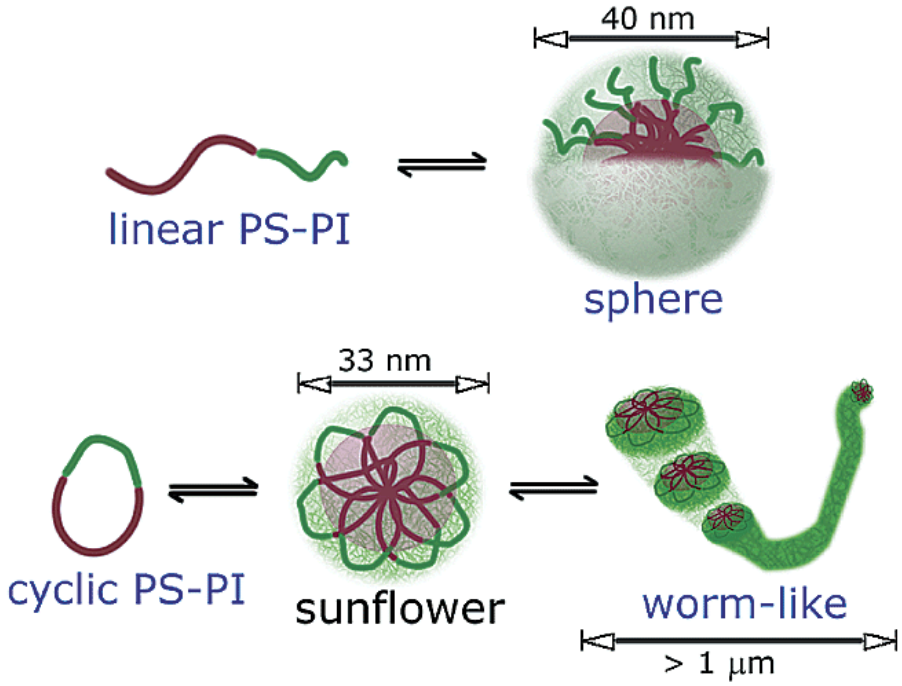

Figure 1.15. Contrasting self-assembly behaviour of linear and cyclic PS-*b*-PI.[252]

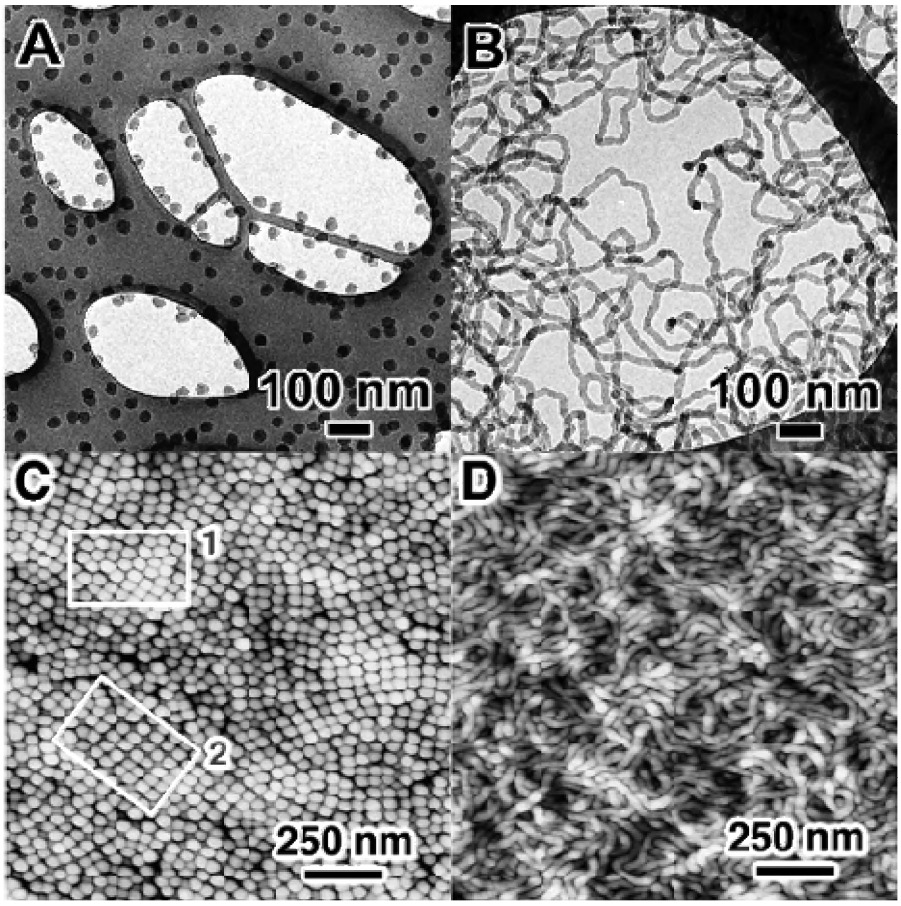

Figure 1.16. (A) Cryo-TEM image of linear PS-*b*-PI, (B) cryo-TEM image of cyclic PS-*b*-PI, (C) AFM image of linear PS-*b*-PI, (D) AFM image of cyclic PS-*b*-PI.[250]

pentane < *n*-heptane < *n*-decane), the driving force for cohesion is greater. Conversely, without the restrictive loop structure the spherical micelles of the linear polymer are more energetically favourable than the equivalent cyclic assemblies and possess no driving force for cohesion.

1.4.2.2 Self-Assembly of Complex Cyclic Architectures

In addition to the self-assembly of amphiphilic cyclic diblock copolymers, some examples of the self-assembly of more complex amphiphilic cyclic architectures have been reported. Wan *et al*. reported the self-assembly of an amphiphilic tadpole-shaped polymer; where a tadpole-shaped polymer consists of a cyclic polymer attached to a linear polymer chain.[257] The ring of the tadpole consisted of hydrophilic poly(*N*-isopropylacrylamide) (PNiPAm), whereas the linear tail consisted of hydrophobic poly(ε-caprolactone) (PCL). When the self-assembly behaviour of the amphiphilic tadpole was compared with that of the equivalent linear diblock assembly, the tadpole-shaped polymer was reported to form slightly larger assemblies than the linear diblock copolymer (tadpole R_h = 70 nm, linear R_h = 62 nm). This suggested that the incorporation of cycles in the tadpole-shaped polymer hindered packing of the polymer during aggregation, resulting in larger, less compact particles. As the values of R_h for both the tadpole-shaped polymer and linear polymer were larger than the maximum polymer chain length, the particles were ascribed to large compound structures. The viability of these tadpole and linear assemblies as drug carriers was investigated by loading the particles with doxorubicin hydrochloride and monitoring the subsequent release of the drug. The assemblies consisting of the tadpole-shaped polymer were found to exhibit faster release profiles,

confirming the less compact nature of the assembly compared to the equivalent linear system.

In direct contrast, when Isono *et al*. studied the self-assembly of tadpole-shaped polymers with a hydrophilic ring (poly(2-(2-(2-methoxyethoxy)ethoxy ethyl glycidyl ether)) and hydrophobic tail (poly(decyl glycidyl ether)), the tadpole assemblies displayed a significantly smaller solution diameter than the equivalent linear assemblies (tadpole D_h = 83 nm, linear D_h = 123 nm).[246] These aggregates were also reported to be large compound structures.

The self-assembly behaviour of tadpole-shaped polymers comprised of a hydrophobic ring and a hydrophilic tail has also been studied. Dong *et al*. prepared tadpole-shaped polymers with a poly(styrene) ring and a poly(ethylene oxide) tail.[258] Subsequent self-assembly afforded vesicles with an average solution diameter of 160 nm, whereas vesicles prepared from the analogous linear PS-*b*-PEO copolymer displayed a smaller solution diameter of 70 nm (Figure 1.17).

Lonsdale and Monteiro compared the self-assembly behaviour of different tadpole architectures comprised of hydrophobic poly(styrene) rings and hydrophilic poly(acrylic acid) (PAA) tails.[259] Depending on the block length of

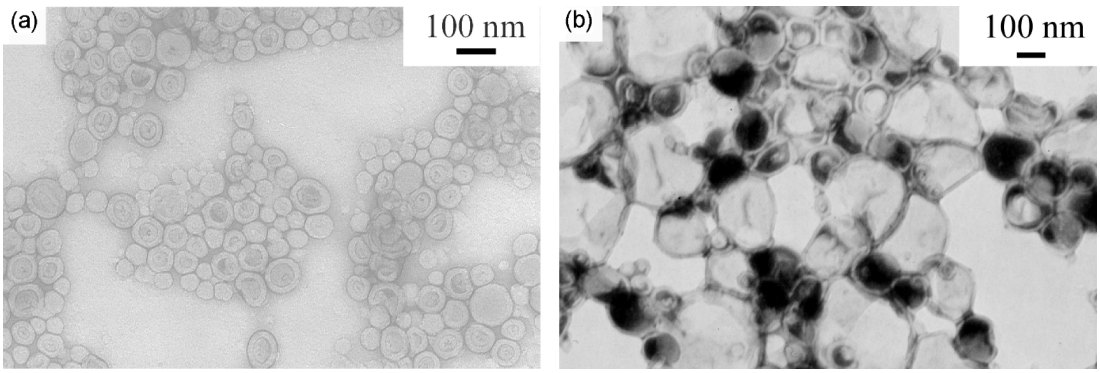

Figure 1.17. TEM images of (a) linear PS-*b*-PEO and (b) tadpole PS-*b*-PEO.[258]

the PAA tails, either "star-like" micelles or "crew-cut" vesicles were formed during self-assembly (Figure 1.18). Assemblies that possessed two PAA tails but only one PS ring formed the smallest structures because the presence of a second hydrophilic tail increased the hydrophilic volume of the polymer and therefore the curvature of the assembly. Conversely, as a consequence of reduced hydrophilic volume, assemblies with only one PAA tail but two PS rings formed the largest structures. The greater restriction of two polymer rings per chain may also hinder the packing of the hydrophobic block in comparison to

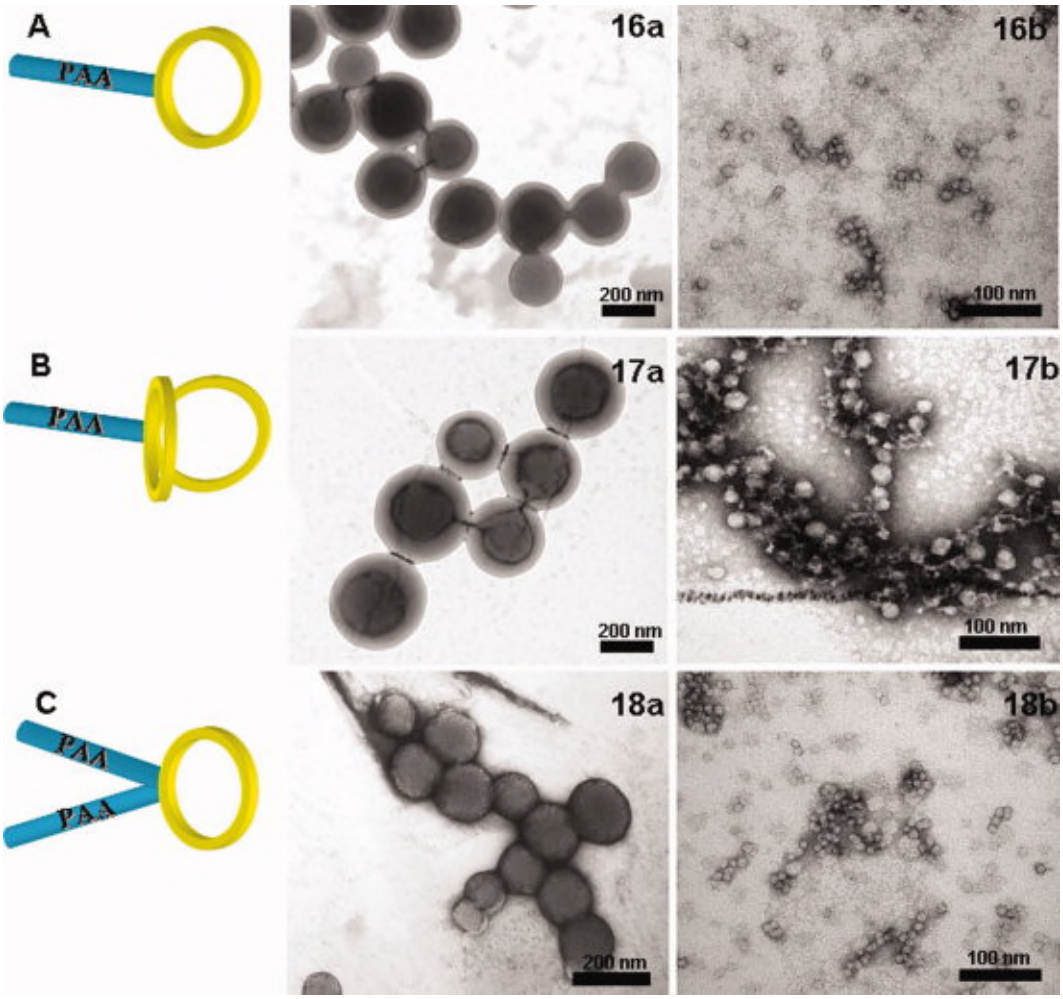

Figure 1.18. TEM images of PS-*b*-PAA tadpole-shaped polymers with varying architectures.[259]

the tadpole- shaped polymers with only one ring, contributing to the larger size of this assembly.

Similarly, when Fan *et al*. studied the self-assembly of an amphiphilic figure-of-eight shaped polymer in comparison to its precursor, a 4-armed amphiphilic star polymer, the assembly of the figure-of-eight shaped polymer exhibited a significantly larger solution diameter (figure-of-eight D_h = 42 nm, star D_h = 18 nm).[260] The 4-armed star polymer consisted of two PS arms and two PEO arms, whereas both rings in the figure-of-eight shaped polymer possessed a diblock PS-*b*-PEO structure. The conformation of the figure-of-eight shaped polymer is extremely restricted upon aggregation, which greatly limits its ability to pack during self-assembly and results in a considerably larger micelle size compared to the star copolymer system. Furthermore, micelles of this particular figure-of-eight polymer possess three core-solvent junctions reducing their entropic favourability, whereas micelles comprised of the star copolymer possess only one core-solvent junction per chain.

The self-assembly of jellyfish-shaped amphiphilic polymers has also been briefly investigated. Cai *et al*. prepared jellyfish-shaped polymers with a hydrophobic block copolymer ring comprised of PCL and poly(pentafluorostyrene) (PPFS), with hydrophilic PEG side arms attached to the latter block, yielding cyclic PCL-*b*-P(PFS-*g*-PEG).[261] Upon self-assembly in water, spherical micelles with a diameter of 50 - 60 nm were observed by scanning electron microscopy (SEM). No comparison with an equivalent linear structure was reported by the authors. In another example, Coulembier *et al*. prepared jellyfish-shaped polymers with a cyclic poly($_L$-lactide) (PLLA) backbone and three poly(methyl methacrylate) (PMMA) side arms.[262] When a

solution of the polymer in THF was deposited on a mica substrate and analysed by atomic force microscopy (AFM), short cylindrical structures, toroids and other structures were observed (Figure 1.19). The height and width of the cylinders and toroids corresponded to the diameter of the PLLA ring, suggesting the jellyfish assembled in a cofacial manner.

In a similar manner, Schappacher and Deffieux prepared well-defined polymeric nanotubes *via* the self-assembly of densely grafted, high molecular weight cyclic brush copolymers.[263] The cyclic polymer backbone consisted of poly(chloroethyl vinyl ether) that had been grafted with a mixture of randomly distributed PS and PI arms. The cyclic brush copolymers were found to self-assemble in heptane, a selective solvent for PI, to afford nanotubes with a diameter of *ca*. 100 nm and length of up to 700 nm (Figure 1.20). The diameter of the assemblies corresponded to the diameter of the cyclic brushes, again

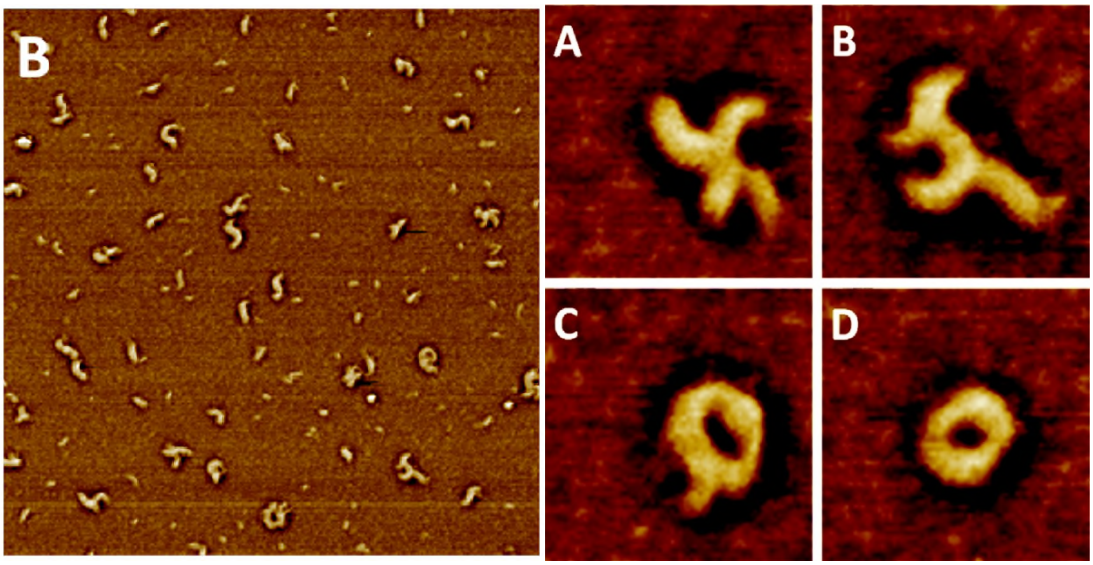

Figure 1.19. AFM phase images of PLLA-*g*-PMMA jellyfish (left image size = 1 μm x 1 μm, right image sizes = 100 nm x 100 nm).[262]

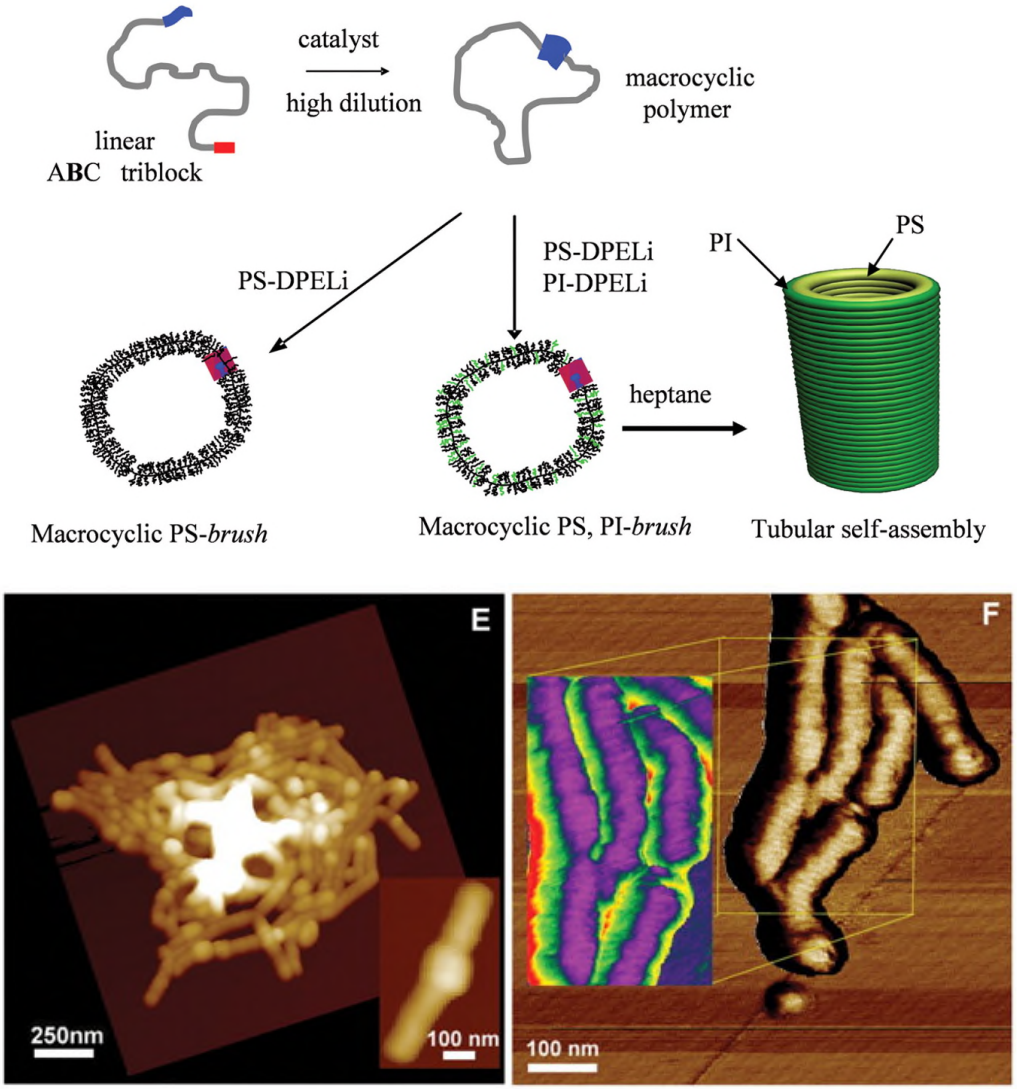

Figure 1.20. (Top) Preparation of PS and PS/PI cyclic brush copolymers. (Bottom) AFM images of PS/PI nanotubes.[263]

suggesting self-assembly occurred in a cofacial manner between cyclic brush copolymers.

These last two examples highlight the unique and significant self-assembly behaviour of polymers that possess a cyclic architecture, where these particular examples of self-assembly are impossible to achieve with polymers of a linear architecture.

1.5 Conclusions

In this chapter, the concept of living and controlled polymerisation techniques has been introduced, with particular attention given to the polymerisation techniques utilised in this thesis, namely organocatalytic ROP and RAFT polymerisation. The development of versatile methodologies to prepare functional aliphatic polycarbonates has also been discussed, and will be used and expanded in later chapters.

An introduction to the unique structural and physical properties of cyclic polymers has been given. Significant developments in the synthesis of high purity well-defined cyclic polymers have greatly expanded this field of research, which continues to grow. In particular, the cyclisation of amphiphilic polymers can have a profound effect of their self-assembly behaviour. A review of the self-assembly of cyclic polymers highlighted the effect cyclisation can have on particle dimensions, particle morphology and the packing of polymer chains within assemblies. Furthermore, the cyclisation of amphiphilic polymers can result in unique self-assembly behaviour that cannot be achieved through the self-assembly of linear polymers.

1.6 References

1. T. R. Darling, T. P. Davis, M. Fryd, A. A. Gridnev, D. M. Haddleton, S. D. Ittel, R. R. Matheson, G. Moad and E. Rizzardo, *J. Polym. Sci., Part A: Polym. Chem.*, 2000, **38**, 1706-1708.
2. R. P. Quirk and B. Lee, *Polym. Int.*, 1992, **27**, 359-367.
3. M. Szwarc, *Nature*, 1956, **178**, 1168-1169.
4. W. A. Braunecker and K. Matyjaszewski, *Prog. Polym. Sci.*, 2007, **32**, 93-146.
5. A. Goto and T. Fukuda, *Prog. Polym. Sci.*, 2004, **29**, 329-385.
6. K. Matyjaszewski, *Curr. Opin. Solid Stare Mater. Sci.*, 1996, **1**, 769-776.
7. K. Matyjaszewski, *Prog. Polym. Sci.*, 2005, **30**, 858-875.
8. K. Matyjaszewski and J. Spanswick, *Mater. Today*, 2005, **8**, 26-33.
9. S. Penczek, M. Cypryk, A. Duda, P. Kubisa and S. Słomkowski, *Prog. Polym. Sci.*, 2007, **32**, 247-282.
10. C. W. Bielawski and R. H. Grubbs, *Prog. Polym. Sci.*, 2007, **32**, 1-29.
11. S. Sutthasupa, M. Shiotsuki and F. Sanda, *Polym. J.*, 2010, **42**, 905-915.
12. M. Kamigaito, T. Ando and M. Sawamoto, *Chem. Rev.*, 2001, **101**, 3689-3746.
13. M. Kato, M. Kamigaito, M. Sawamoto and T. Higashimura, *Macromolecules*, 1995, **28**, 1721-1723.
14. K. Matyjaszewski, *Macromolecules*, 2012, **45**, 4015-4039.
15. K. Matyjaszewski, S. Gaynor and J.-S. Wang, *Macromolecules*, 1995, **28**, 2093-2095.
16. K. Matyjaszewski and J. Xia, *Chem. Rev.*, 2001, **101**, 2921-2990.

17. M. Ouchi, T. Terashima and M. Sawamoto, *Chem. Rev.*, 2009, **109**, 4963-5050.

18. M. K. Georges, R. P. N. Veregin, P. M. Kazmaier and G. K. Hamer, *Macromolecules*, 1993, **26**, 2987-2988.

19. C. J. Hawker, *J. Am. Chem. Soc.*, 1994, **116**, 11185-11186.

20. C. J. Hawker, A. W. Bosman and E. Harth, *Chem. Rev.*, 2001, **101**, 3661-3688.

21. D. H. Solomon, *J. Polym. Sci., Part A: Polym. Chem.*, 2005, **43**, 5748-5764.

22. C. Barner-Kowollik and S. Perrier, *J.Polym. Sci., Part A: Polym. Chem.*, 2008, **46**, 5715-5723.

23. J. Chiefari, Y. K. Chong, F. Ercole, J. Krstina, J. Jeffery, T. P. T. Le, R. T. A. Mayadunne, G. F. Meijs, C. L. Moad, G. Moad, E. Rizzardo and S. H. Thang, *Macromolecules*, 1998, **31**, 5559-5562.

24. G. Moad, E. Rizzardo and S. H. Thang, *Aust. J. Chem.*, 2005, **58**, 379-410.

25. G. Moad, E. Rizzardo and S. H. Thang, *Aust. J. Chem.*, 2006, **59**, 669-692.

26. G. Moad, E. Rizzardo and S. H. Thang, *Polymer*, 2008, **49**, 1079-1131.

27. G. Moad, E. Rizzardo and S. H. Thang, *Aust. J. Chem.*, 2009, **62**, 1402-1472.

28. S. Perrier and P. Takolpuckdee, *J. Polym. Sci., Part A: Polym. Chem.*, 2005, **43**, 5347-5393.

29. C. Barner-Kowollik, M. Buback, B. Charleux, M. L. Coote, M. Drache, T. Fukuda, A. Goto, B. Klumperman, A. B. Lowe, J. B. McLeary, G. Moad, M. J. Monteiro, R. D. Sanderson, M. P. Tonge and P. Vana, *J. Polym. Sci., Part A: Polym. Chem.*, 2006, **44**, 5809-5831.

30. D. J. Keddie, G. Moad, E. Rizzardo and S. H. Thang, *Macromolecules*, 2012, **45**, 5321-5342.

31. J. Chiefari, R. T. A. Mayadunne, C. L. Moad, G. Moad, E. Rizzardo, A. Postma and S. H. Thang, *Macromolecules*, 2003, **36**, 2273-2283.

32. Y. K. Chong, J. Krstina, T. P. T. Le, G. Moad, A. Postma, E. Rizzardo and S. H. Thang, *Macromolecules*, 2003, **36**, 2256-2272.

33. G. Moad, E. Rizzardo and S. H. Thang, *Polym. Int.*, 2011, **60**, 9-25.

34. H. Willcock and R. K. O'Reilly, *Polym. Chem.*, 2010, **1**, 149-157.

35. O. Dechy-Cabaret, B. Martin-Vaca and D. Bourissou, *Chem. Rev.*, 2004, **104**, 6147-6176.

36. P. Lecomte and C. Jérôme, in *Synthetic Biodegradable Polymers*, eds. B. Rieger, A. Künkel, G. W. Coates, R. Reichardt, E. Dinjus and T. A. Zevaco, Springer Berlin Heidelberg, 2012, vol. 245, pp. 173-217.

37. F. Suriano, O. Coulembier, J. L. Hedrick and P. Dubois, *Polym. Chem.*, 2011, **2**, 528-533.

38. A.-L. Brocas, C. Mantzaridis, D. Tunc and S. Carlotti, *Prog. Polym. Sci.*, 2013, **38**, 845-873.

39. A. Kameyama and T. Nishikubo, *Polym. J*, 2009, **41**, 1-15.

40. K. Hashimoto, *Prog. Polym. Sci.*, 2000, **25**, 1411-1462.

41. S. Kobayashi and H. Uyama, *J. Polym. Sci., Part A: Polym. Chem.*, 2002, **40**, 192-209.

42. Y.-C. Wang, Y.-Y. Yuan, J.-Z. Du, X.-Z. Yang and J. Wang, *Macromol. Biosci.*, 2009, **9**, 1154-1164.

43. J. Chojnowski, *J. Inorg. Organomet. Polym.*, 1991, **1**, 299-323.

44. R. J. Pounder and A. P. Dove, *Polym. Chem.*, 2010, **1**, 260-271.

45. M. J. Stanford and A. P. Dove, *Chem. Soc. Rev.*, 2010, **39**, 486-494.

46. C. M. Thomas, *Chem. Soc. Rev.*, 2010, **39**, 165-173.

47. C. K. Williams, *Chem. Soc. Rev.*, 2007, **36**, 1573-1580.

48. C. Jérôme and P. Lecomte, *Adv. Drug Deliv. Rev.*, 2008, **60**, 1056-1076.

49. A. P. Dove, *Chem. Commun.*, 2008, 6446-6470.

50. A.-C. Albertsson and I. K. Varma, *Biomacromolecules*, 2003, **4**, 1466-1486.

51. K. E. Uhrich, S. M. Cannizzaro, R. S. Langer and K. M. Shakesheff, *Chem. Rev.*, 1999, **99**, 3181-3198.

52. H. Seyednejad, A. H. Ghassemi, C. F. van Nostrum, T. Vermonden and W. E. Hennink, *J. Controlled Release*, 2011, **152**, 168-176.

53. L. S. Nair and C. T. Laurencin, *Prog. Polym. Sci.*, 2007, **32**, 762-798.

54. Y. Ohya, A. Takahashi and K. Nagahama, in *Polymers in Nanomedicine*, eds. S. Kunugi and T. Yamaoka, Springer Berlin Heidelberg, 2012, vol. 247, pp. 65-114.

55. A.-C. Albertsson and I. K. Varma, *Adv. Polym. Sci.*, 2002, **157**, 1-40.

56. N. Ajellal, J.-F. Carpentier, C. Guillaume, S. M. Guillaume, M. Helou, V. Poirier, Y. Sarazin and A. Trifonov, *Dalton Trans.*, 2010, **39**, 8363-8376.

57. J.-F. Carpentier, *Macromol. Rapid Commun.*, 2010, **31**, 1696-1705.

58. S. Dagorne, M. Normand, E. Kirillov and J.-F. Carpentier, *Coord. Chem. Rev.*, 2013, **257**, 1869-1886.

59. D. Mecerreyes and R. Jérôme, *Macromol. Chem. Phys.*, 1999, **200**, 2581-2590.

60. A. Sauer, A. Kapelski, C. Fliedel, S. Dagorne, M. Kol and J. Okuda, *Dalton Trans.*, 2013, **42**, 9007-9023.

61. A. P. Dove, *ACS Macro Lett.*, 2012, **1**, 1409-1412.

62. N. E. Kamber, W. Jeong, R. M. Waymouth, R. C. Pratt, B. G. G. Lohmeijer and J. L. Hedrick, *Chem. Rev.*, 2007, **107**, 5813-5840.

63. C. Thomas and B. Bibal, *Green Chem.*, 2014, **16**, 1687-1699.

64. M. K. Kiesewetter, E. J. Shin, J. L. Hedrick and R. M. Waymouth, *Macromolecules*, 2010, **43**, 2093-2107.

65. A.-C. Albertsson and R. K. Srivastava, *Adv. Drug Deliv. Rev.*, 2008, **60**, 1077-1093.

66. S. Matsumura, in *Enzyme-Catalyzed Synthesis of Polymers*, eds. S. Kobayashi, H. Ritter and D. Kaplan, Springer Berlin Heidelberg, 2006, vol. 194, pp. 95-132.

67. S. Kobayashi, *Macromol. Rapid Commun.*, 2009, **30**, 237-266.

68. H. R. Kricheldorf and I. Kreiser-Saunders, *Makromol. Chem.*, 1990, **191**, 1057-1066.

69. F. Nederberg, E. F. Connor, M. Möller, T. Glauser and J. L. Hedrick, *Angew. Chem. Int. Ed.*, 2001, **40**, 2712-2715.

70. E. F. Connor, G. W. Nyce, M. Myers, A. Möck and J. L. Hedrick, *J. Am. Chem. Soc.*, 2002, **124**, 914-915.

71. A. P. Dove, R. C. Pratt, B. G. G. Lohmeijer, D. A. Culkin, E. C. Hagberg, G. W. Nyce, R. M. Waymouth and J. L. Hedrick, *Polymer*, 2006, **47**, 4018-4025.

72. F. Nederberg, B. G. G. Lohmeijer, F. Leibfarth, R. C. Pratt, J. Choi, A. P. Dove, R. M. Waymouth and J. L. Hedrick, *Biomacromolecules*, 2006, **8**, 153-160.

73. J. Raynaud, C. Absalon, Y. Gnanou and D. Taton, *J. Am. Chem. Soc.*, 2009, **131**, 3201-3209.

74. J. Raynaud, W. N. Ottou, Y. Gnanou and D. Taton, *Chem. Commun.*, 2010, **46**, 3203-3205.

75. B. G. G. Lohmeijer, G. Dubois, F. Leibfarth, R. C. Pratt, F. Nederberg, A. Nelson, R. M. Waymouth, C. Wade and J. L. Hedrick, *Org. Lett.*, 2006, **8**, 4683-4686.

76. M. Rodriguez, S. Marrot, T. Kato, S. Stérin, E. Fleury and A. Baceiredo, *J. Organomet. Chem.*, 2007, **692**, 705-708.

77. W. Jeong, E. J. Shin, D. A. Culkin, J. L. Hedrick and R. M. Waymouth, *J. Am. Chem. Soc.*, 2009, **131**, 4884-4891.

78. D. A. Culkin, W. Jeong, S. Csihony, E. D. Gomez, N. P. Balsara, J. L. Hedrick and R. M. Waymouth, *Angew. Chem. Int. Ed.*, 2007, **46**, 2627-2630.

79. W. Jeong, J. L. Hedrick and R. M. Waymouth, *J. Am. Chem. Soc.*, 2007, **129**, 8414-8415.

80. E. J. Shin, H. A. Brown, S. Gonzalez, W. Jeong, J. L. Hedrick and R. M. Waymouth, *Angew. Chem. Int. Ed.*, 2011, **50**, 6388-6391.

81. H. A. Brown and R. M. Waymouth, *Acc. Chem. Res.*, 2013, **46**, 2585-2596.

82. H. A. Brown, S. Xiong, G. A. Medvedev, Y. A. Chang, M. M. Abu-Omar, J. M. Caruthers and R. M. Waymouth, *Macromolecules*, 2014, **47**, 2955-2963.

83. H. A. Brown, Y. A. Chang and R. M. Waymouth, *J. Am. Chem. Soc.*, 2013, **135**, 18738-18741.

84. O. Coulembier, A. P. Dove, R. C. Pratt, A. C. Sentman, D. A. Culkin, L. Mespouille, P. Dubois, R. M. Waymouth and J. L. Hedrick, *Angew. Chem. Int. Ed.*, 2005, **44**, 4964-4968.

85. O. Coulembier, B. G. G. Lohmeijer, A. P. Dove, R. C. Pratt, L. Mespouille, D. A. Culkin, S. J. Benight, P. Dubois, R. M. Waymouth and J. L. Hedrick, *Macromolecules*, 2006, **39**, 5617-5628.

86. S. Csihony, D. A. Culkin, A. C. Sentman, A. P. Dove, R. M. Waymouth and J. L. Hedrick, *J. Am. Chem. Soc.*, 2005, **127**, 9079-9084.

87. M. Fèvre, J. Pinaud, A. Leteneur, Y. Gnanou, J. Vignolle, D. Taton, K. Miqueu and J.-M. Sotiropoulos, *J. Am. Chem. Soc.*, 2012, **134**, 6776-6784.

88. G. W. Nyce, S. Csihony, R. M. Waymouth and J. L. Hedrick, *Chem. Eur. J.*, 2004, **10**, 4073-4079.

89. G. W. Nyce, T. Glauser, E. F. Connor, A. Möck, R. M. Waymouth and J. L. Hedrick, *J. Am. Chem. Soc.*, 2003, **125**, 3046-3056.

90. L. Zhang, F. Nederberg, R. C. Pratt, R. M. Waymouth, J. L. Hedrick and C. G. Wade, *Macromolecules*, 2007, **40**, 4154-4158.

91. A. P. Dove, R. C. Pratt, B. G. G. Lohmeijer, R. M. Waymouth and J. L. Hedrick, *J. Am. Chem. Soc.*, 2005, **127**, 13798-13799.

92. R. C. Pratt, B. G. G. Lohmeijer, D. A. Long, P. N. P. Lundberg, A. P. Dove, H. Li, C. G. Wade, R. M. Waymouth and J. L. Hedrick, *Macromolecules*, 2006, **39**, 7863-7871.

93. B. G. G. Lohmeijer, R. C. Pratt, F. Leibfarth, J. W. Logan, D. A. Long, A. P. Dove, F. Nederberg, J. Choi, C. Wade, R. M. Waymouth and J. L. Hedrick, *Macromolecules*, 2006, **39**, 8574-8583.

94. S. Onbulak, S. Tempelaar, R. J. Pounder, O. Gok, R. Sanyal, A. P. Dove and A. Sanyal, *Macromolecules*, 2012, **45**, 1715-1722.

95. J. Xu, F. Prifti and J. Song, *Macromolecules*, 2011, **44**, 2660-2667.

96. B. Clément, B. Grignard, L. Koole, C. Jérôme and P. Lecomte, *Macromolecules*, 2012, **45**, 4476-4486.

97. Y. Iwasaki and E. Yamaguchi, *Macromolecules*, 2010, **43**, 2664-2666.

98. S. Zhang, A. Li, J. Zou, L. Y. Lin and K. L. Wooley, *ACS Macro Lett.*, 2012, **1**, 328-333.

99. M. K. Kiesewetter, M. D. Scholten, N. Kirn, R. L. Weber, J. L. Hedrick and R. M. Waymouth, *J. Org. Chem.*, 2009, **74**, 9490-9496.

100. R. C. Pratt, B. G. G. Lohmeijer, D. A. Long, R. M. Waymouth and J. L. Hedrick, *J. Am. Chem. Soc.*, 2006, **128**, 4556-4557.

101. M. Bouyahyi, M. P. F. Pepels, A. Heise and R. Duchateau, *Macromolecules*, 2012, **45**, 3356-3366.

102. F. Jing and M. A. Hillmyer, *J. Am. Chem. Soc.*, 2008, **130**, 13826-13827.

103. H. Kim, J. V. Olsson, J. L. Hedrick and R. M. Waymouth, *ACS Macro Lett.*, 2012, **1**, 845-847.

104. M. T. Martello, A. Burns and M. Hillmyer, *ACS Macro Lett.*, 2011, **1**, 131-135.

105. K. Mikami, A. T. Lonnecker, T. P. Gustafson, N. F. Zinnel, P.-J. Pai, D. H. Russell and K. L. Wooley, *J. Am. Chem. Soc.*, 2013, **135**, 6826-6829.

106. D. Bourissou, B. Martin-Vaca, A. Dumitrescu, M. Graullier and F. Lacombe, *Macromolecules*, 2005, **38**, 9993-9998.

107. S. Gazeau-Bureau, D. Delcroix, B. Martín-Vaca, D. Bourissou, C. Navarro and S. Magnet, *Macromolecules*, 2008, **41**, 3782-3784.

108. K. Makiguchi, T. Satoh and T. Kakuchi, *Macromolecules*, 2011, **44**, 1999-2005.

109. D. Delcroix, A. Couffin, N. Susperregui, C. Navarro, L. Maron, B. Martin-Vaca and D. Bourissou, *Polym. Chem.*, 2011, **2**, 2249-2256.

110. N. Susperregui, D. Delcroix, B. Martin-Vaca, D. Bourissou and L. Maron, *J. Org. Chem.*, 2010, **75**, 6581-6587.

111. J. Feng, R.-X. Zhuo and X.-Z. Zhang, *Prog. Polym. Sci.*, 2012, **37**, 211-236.

112. J. Xu, E. Feng and J. Song, *J. Appl. Polym. Sci.*, 2014, **131**, DOI: 10.1002/app.39822.

113. K. J. Zhu, R. W. Hendren, K. Jensen and C. G. Pitt, *Macromolecules*, 1991, **24**, 1736-1740.

114. N. Andronova and A.-C. Albertsson, *Biomacromolecules*, 2006, **7**, 1489-1495.

115. B. L. Dargaville, C. Vaquette, H. Peng, F. Rasoul, Y. Q. Chau, J. J. Cooper-White, J. H. Campbell and A. K. Whittaker, *Biomacromolecules*, 2011, **12**, 3856-3869.

116. O. S. Kluin, H. C. van der Mei, H. J. Busscher and D. Neut, *Biomaterials*, 2009, **30**, 4738-4742.

117. Y. Zhang and R.-x. Zhuo, *Biomaterials*, 2005, **26**, 2089-2094.

118. Z. Zhang, R. Kuijer, S. K. Bulstra, D. W. Grijpma and J. Feijen, *Biomaterials*, 2006, **27**, 1741-1748.

119. A. P. Pêgo, M. J. A. Van Luyn, L. A. Brouwer, P. B. van Wachem, A. A. Poot, D. W. Grijpma and J. Feijen, *J. Biomed. Mater. Res. A*, 2003, **67A**, 1044-1054.

120. A. P. Pêgo, A. A. Poot, D. W. Grijpma and J. Feijen, *Macromol. Biosci.*, 2002, **2**, 411-419.

121. *US Pat.*, 3376261A, 1968.

122. D. J. Darensbourg, *Chem. Rev.*, 2007, **107**, 2388-2410.

123. D. J. Darensbourg, R. M. Mackiewicz, A. L. Phelps and D. R. Billodeaux, *Acc. Chem. Res.*, 2004, **37**, 836-844.

124. S. Inoue, H. Koinuma and T. Tsuruta, *J. Polym. Sci., Part B: Polym. Lett.*, 1969, **7**, 287-292.

125. X.-B. Lu, W.-M. Ren and G.-P. Wu, *Acc. Chem. Res.*, 2012, **45**, 1721-1735.

126. H. Sugimoto and S. Inoue, *J. Polym. Sci., Part A: Polym. Chem.*, 2004, **42**, 5561-5573.

127. H. Sugimoto and S. Inoue, *Pure Appl. Chem.*, 2006, **78**, 1823-1834.

128. G. W. Coates and D. R. Moore, *Angew. Chem. Int. Ed.*, 2004, **43**, 6618-6639.

129. W. H. Carothers, G. L. Dorough and F. J. van Natta, *J. Am. Chem. Soc.*, 1932, **54**, 761-772.

130. L. Mespouille, O. Coulembier, M. Kawalec, A. P. Dove and P. Dubois, *Prog. Polym. Sci.*, 2014, **39**, 1144-1164.

131. G. Rokicki, *Prog. Polym. Sci.*, 2000, **25**, 259-342.

132. S. Tempelaar, L. Mespouille, O. Coulembier, P. Dubois and A. P. Dove, *Chem. Soc. Rev.*, 2013, **42**, 1312-1336.

133. W. H. Binder and R. Sachsenhofer, *Macromol. Rapid Commun.*, 2007, **28**, 15-54.

134. P. L. Golas and K. Matyjaszewski, *Chem. Soc. Rev.*, 2010, **39**, 1338-1354.

135. M. A. Gauthier, M. I. Gibson and H.-A. Klok, *Angew. Chem. Int. Ed.*, 2009, **48**, 48-58.

136. Z. Ge and S. Liu, *Chem. Soc. Rev.*, 2013, **42**, 7289-7325.

137. F. Meng, Z. Zhong and J. Feijen, *Biomacromolecules*, 2009, **10**, 197-209.

138. J. Rodríguez-Hernández, F. Chécot, Y. Gnanou and S. Lecommandoux, *Prog. Polym. Sci.*, 2005, **30**, 691-724.

139. R. C. Pratt, F. Nederberg, R. M. Waymouth and J. L. Hedrick, *Chem. Commun.*, 2008, 114-116.

140. D. P. Sanders, K. Fukushima, D. J. Coady, A. Nelson, M. Fujiwara, M. Yasumoto and J. L. Hedrick, *J. Am. Chem. Soc.*, 2010, **132**, 14724-14726.

141. J. M. W. Chan, H. Sardon, A. C. Engler, J. M. García and J. L. Hedrick, *ACS Macro Lett.*, 2013, **2**, 860-864.

142. A. C. Engler, J. M. W. Chan, D. J. Coady, J. M. O'Brien, H. Sardon, A. Nelson, D. P. Sanders, Y. Y. Yang and J. L. Hedrick, *Macromolecules*, 2013, **46**, 1283-1290.

143. S. Venkataraman, N. Veronica, Z. X. Voo, J. L. Hedrick and Y. Y. Yang, *Polym. Chem.*, 2013, **4**, 2945-2948.

144. F. Sanda, J. Kamatani and T. Endo, *Macromolecules*, 2001, **34**, 1564-1569.

145. Z. Xie, C. Lu, X. Chen, L. Chen, Y. Wang, X. Hu, Q. Shi and X. Jing, *J. Polym. Sci., Part A: Polym. Chem.*, 2007, **45**, 1737-1745.

146. F. He, Y.-P. Wang, G. Liu, H.-L. Jia, J. Feng and R.-X. Zhuo, *Polymer*, 2008, **49**, 1185-1190.

147. J. A. Edward, M. K. Kiesewetter, H. Kim, J. C. A. Flanagan, J. L. Hedrick and R. M. Waymouth, *Biomacromolecules*, 2012, **13**, 2483-2489.

148. W. Chen, Y. Zou, J. Jia, F. Meng, R. Cheng, C. Deng, J. Feijen and Z. Zhong, *Macromolecules*, 2013, **46**, 699-707.

149. S. Venkataraman, A. L. Lee, H. T. Maune, J. L. Hedrick, V. M. Prabhu and Y. Y. Yang, *Macromolecules*, 2013, **46**, 4839-4846.

150. Z. Y. Ong, C. Yang, S. J. Gao, X.-Y. Ke, J. L. Hedrick and Y. Yan Yang, *Macromol. Rapid Commun.*, 2013, **34**, 1714-1720.

151. A. Blencowe, J. F. Tan, T. K. Goh and G. G. Qiao, *Polymer*, 2009, **50**, 5-32.

152. Y. Deng, S. Zhang, G. Lu and X. Huang, *Polym. Chem.*, 2013, **4**, 1289-1299.

153. H. Gao and K. Matyjaszewski, *Prog. Polym. Sci.*, 2009, **34**, 317-350.

154. K. Khanna, S. Varshney and A. Kakkar, *Polym. Chem.*, 2010, **1**, 1171-1185.

155. C. Feng, Y. Li, D. Yang, J. Hu, X. Zhang and X. Huang, *Chem. Soc. Rev.*, 2011, **40**, 1282-1295.

156. S. S. Sheiko, B. S. Sumerlin and K. Matyjaszewski, *Prog. Polym. Sci.*, 2008, **33**, 759-785.

157. D. Uhrig and J. Mays, *Polym. Chem.*, 2011, **2**, 69-76.

158. M. Zhang and A. H. E. Müller, *J. Polym. Sci., Part A: Polym. Chem.*, 2005, **43**, 3461-3481.

159. O. Azzaroni, *J. Polym. Sci., Part A: Polym. Chem.*, 2012, **50**, 3225-3258.

160. A. Carlmark, C. Hawker, A. Hult and M. Malkoch, *Chem. Soc. Rev.*, 2009, **38**, 352-362.

161. R. M. England and S. Rimmer, *Polym. Chem.*, 2010, **1**, 1533-1544.

162. K. Inoue, *Prog. Polym. Sci.*, 2000, **25**, 453-571.

163. B. I. Voit and A. Lederer, *Chem. Rev.*, 2009, **109**, 5924-5973.

164. K. Endo, in *New Frontiers in Polymer Synthesis*, ed. S. Kobayashi, Springer Berlin Heidelberg, 2008, vol. 217, pp. 121-183.

165. Z. Jia and M. J. Monteiro, *J. Polym. Sci., Part A: Polym. Chem.*, 2012, **50**, 2085-2097.

166. H. R. Kricheldorf, *J. Polym. Sci., Part A: Polym. Chem.*, 2010, **48**, 251-284.

167. B. A. Laurent and S. M. Grayson, *Chem. Soc. Rev.*, 2009, **38**, 2202-2213.

168. D. Freifelder, A. K. Kleinschmidt and R. L. Sinsheimer, *Science*, 1964, **146**, 254-255.

169. J. F. Brown and G. M. J. Slusarczuk, *J. Am. Chem. Soc.*, 1965, **87**, 931-932.

170. D. W. Scott, *J. Am. Chem. Soc.*, 1946, **68**, 2294-2298.

171. K. Dodgson, D. Sympson and J. A. Semlyen, *Polymer*, 1978, **19**, 1285-1289.

172. D. Geiser and H. Höcker, *Macromolecules*, 1980, **13**, 653-656.

173. G. Hild, A. Kohler and P. Rempp, *Eur. Polym. J.*, 1980, **16**, 525-527.

174. B. Vollmert and J.-x. Huang, *Makromol. Chem. Rapid Commun.*, 1980, **1**, 333-339.

175. H. R. Kricheldorf and S.-R. Lee, *Macromolecules*, 1995, **28**, 6718-6725.

176. J. N. Hoskins and S. M. Grayson, *Polym. Chem.*, 2011, **2**, 289-299.

177. H. Oike, H. Imaizumi, T. Mouri, Y. Yoshioka, A. Uchibori and Y. Tezuka, *J. Am. Chem. Soc.*, 2000, **122**, 9592-9599.

178. C. W. Bielawski, D. Benitez and R. H. Grubbs, *Science*, 2002, **297**, 2041-2044.

179. H. C. Kolb, M. G. Finn and K. B. Sharpless, *Angew. Chem. Int. Ed.*, 2001, **40**, 2004-2021.

180. M. Kubo, T. Hayashi, H. Kobayashi and T. Itoh, *Macromolecules*, 1998, **31**, 1053-1057.

181. M. Schappacher, C. Billaud, C. Paulo and A. Deffieux, *Macromol. Chem. Phys.*, 1999, **200**, 2377-2386.

182. Y. Tezuka, A. Tsuchitani, Y. Yoshioka and H. Oike, *Macromolecules*, 2002, **36**, 65-70.

183. M. Antonietti and K. J. Fölsch, *Makromol. Chem. Rapid Commun.*, 1988, **9**, 423-430.

184. T. Yamamoto and Y. Tezuka, *Polym. Chem.*, 2011, **2**, 1930-1941.

185. G. Hadziioannou, P. M. Cotts, G. ten Brinke, C. C. Han, P. Lutz, C. Strazielle, P. Rempp and A. J. Kovacs, *Macromolecules*, 1987, **20**, 493-497.

186. M. Duval, P. Lutz and C. Strazielle, *Makromol. Chem. Rapid Commun.*, 1985, **6**, 71-76.

187. J. Roovers, *J. Polym. Sci., Polym. Phys. Ed.*, 1985, **23**, 1117-1126.

188. M. Ragnetti, D. Geiser, H. Höcker and R. C. Oberthür, *Makromol. Chem.*, 1985, **186**, 1701-1709.

189. G. B. McKenna, G. Hadziioannou, P. Lutz, G. Hild, C. Strazielle, C. Straupe, P. Rempp and A. J. Kovacs, *Macromolecules*, 1987, **20**, 498-512.

190. D. J. Orrah, J. A. Semlyen and S. B. Ross-Murphy, *Polymer*, 1988, **29**, 1455-1458.

191. J. Roovers, *Macromolecules*, 1985, **18**, 1359-1361.

192. P. G. Santangelo, C. M. Roland, T. Chang, D. Cho and J. Roovers, *Macromolecules*, 2001, **34**, 9002-9005.

193. S. Habuchi, N. Satoh, T. Yamamoto, Y. Tezuka and M. Vacha, *Angew. Chem. Int. Ed.*, 2010, **49**, 1418-1421.

194. J. E. Poelma, K. Ono, D. Miyajima, T. Aida, K. Satoh and C. J. Hawker, *ACS Nano*, 2012, **6**, 10845-10854.

195. K. Zhang, M. A. Lackey, J. Cui and G. N. Tew, *J. Am. Chem. Soc.*, 2011, **133**, 4140-4148.

196. B. Chen, K. Jerger, J. M. J. Fréchet and F. C. Szoka Jr, *J. Controlled Release*, 2009, **140**, 203-209.

197. N. Nasongkla, B. Chen, N. Macaraeg, M. E. Fox, J. M. J. Fréchet and F. C. Szoka, *J. Am. Chem. Soc.*, 2009, **131**, 3842-3843.

198. T. Dwars, E. Paetzold and G. Oehme, *Angew. Chem. Int. Ed.*, 2005, **44**, 7174-7199.

199. H. F. Eicke, *Pure Appl. Chem.*, 1980, **52**, 1349-1357.

200. P. D. I. Fletcher, *Curr. Opin. Colloid Interface Sci.*, 1996, **1**, 101-106.

201. S. P. Moulik, *Curr. Sci.*, 1996, **71**, 368-376.

202. P. Schurtenberger, *Curr. Opin. Colloid Interface Sci.*, 1996, **1**, 773-778.

203. H. Hoffmann, *Adv. Mater.*, 1994, **6**, 116-129.

204. J. N. Israelachvili, D. J. Mitchell and B. W. Ninham, *J. Chem. Soc., Faraday Trans. 2*, 1976, **72**, 1525-1568.

205. B. M. Discher, Y.-Y. Won, D. S. Ege, J. C.-M. Lee, F. S. Bates, D. E. Discher and D. A. Hammer, *Science*, 1999, **284**, 1143-1146.

206. P. Cotanda, N. Petzetakis and R. K. O'Reilly, *MRS Communications*, 2012, **2**, 119-126.

207. A. Lu and R. K. O'Reilly, *Curr. Opin. Biotechnol.*, 2013, **24**, 639-645.

208. D. M. Vriezema, M. Comellas Aragonès, J. A. A. W. Elemans, J. J. L. M. Cornelissen, A. E. Rowan and R. J. M. Nolte, *Chem. Rev.*, 2005, **105**, 1445-1490.

209. M. Elsabahy and K. L. Wooley, *Chem. Soc. Rev.*, 2012, **41**, 2545-2561.

210. K. Kataoka, A. Harada and Y. Nagasaki, *Adv. Drug Deliv. Rev.*, 2001, **47**, 113-131.

211. V. P. Torchilin, *J. Controlled Release*, 2001, **73**, 137-172.

212. A. Blanazs, S. P. Armes and A. J. Ryan, *Macromol. Rapid Commun.*, 2009, **30**, 267-277.

213. A. Harada and K. Kataoka, *Prog. Polym. Sci.*, 2006, **31**, 949-982.

214. U. Kedar, P. Phutane, S. Shidhaye and V. Kadam, *Nanomed. Nanotechnology Biol. Med.*, 2010, **6**, 714-729.

215. N. Nishiyama and K. Kataoka, *Pharmacol. Ther.*, 2006, **112**, 630-648.

216. P. V. Pawar, S. V. Gohil, J. P. Jain and N. Kumar, *Polym. Chem.*, 2013, **4**, 3160-3176.

217. V. S. Trubetskoy, *Adv. Drug Deliv. Rev.*, 1999, **37**, 81-88.

218. Y. Mai and A. Eisenberg, *Chem. Soc. Rev.*, 2012, **41**, 5969-5985.

219. K. Nakashima and P. Bahadur, *Adv. Colloid Interface Sci.*, 2006, **123–126**, 75-96.

220. G. Riess, *Prog. Polym. Sci.*, 2003, **28**, 1107-1170.

221. M. D. Ward and P. R. Raithby, *Chem. Soc. Rev.*, 2013, **42**, 1619-1636.

222. L. Zhang and A. Eisenberg, *Science*, 1995, **268**, 1728-1731.

223. A. O. Moughton, M. A. Hillmyer and T. P. Lodge, *Macromolecules*, 2011, **45**, 2-19.

224. H. Cui, Z. Chen, S. Zhong, K. L. Wooley and D. J. Pochan, *Science*, 2007, **317**, 647-650.

225. S. Zhong, H. Cui, Z. Chen, K. L. Wooley and D. J. Pochan, *Soft Matter*, 2008, **4**, 90-93.

226. H. Shen and A. Eisenberg, *Angew. Chem. Int. Ed.*, 2000, **39**, 3310-3312.

227. R. C. Hayward and D. J. Pochan, *Macromolecules*, 2010, **43**, 3577-3584.

228. T. Nicolai, O. Colombani and C. Chassenieux, *Soft Matter*, 2010, **6**, 3111-3118.

229. G. M. Soliman, A. Sharma, D. Maysinger and A. Kakkar, *Chem. Commun.*, 2011, **47**, 9572-9587.

230. D. K. Smith, A. R. Hirst, C. S. Love, J. G. Hardy, S. V. Brignell and B. Huang, *Prog. Polym. Sci.*, 2005, **30**, 220-293.

231. D. K. Smith, *Chem. Commun.*, 2006, 34-44.

232. R. Dong, Y. Zhou and X. Zhu, *Acc. Chem. Res.*, 2014, **47**, 2006-2016.

233. C.-M. Dong and G. Liu, *Polym. Chem.*, 2013, **4**, 46-52.

234. Y. Zhou, W. Huang, J. Liu, X. Zhu and D. Yan, *Adv. Mater.*, 2010, **22**, 4567-4590.

235. B. M. Rosen, C. J. Wilson, D. A. Wilson, M. Peterca, M. R. Imam and V. Percec, *Chem. Rev.*, 2009, **109**, 6275-6540.

236. Y. Zhou and D. Yan, *Chem. Commun.*, 2009, 1172-1188.

237. T. Emrick and J. M. J. Fréchet, *Curr. Opin. Colloid Interface Sci.*, 1999, **4**, 15-23.

238. K. Khanna, S. Varshney and A. Kakkar, *Polym. Chem.*, 2010, **1**, 1171-1185.

239. Z. Ge and S. Liu, *Macromol. Rapid Commun.*, 2009, **30**, 1523-1532.

240. G.-E. Yu, Z. Yang, D. Attwood, C. Price and C. Booth, *Macromolecules*, 1996, **29**, 8479-8486.

241. G.-E. Yu, C. A. Garrett, S.-M. Mai, H. Altinok, D. Attwood, C. Price and C. Booth, *Langmuir*, 1998, **14**, 2278-2285.

242. G.-E. Yu, Z.-K. Zhou, D. Attwood, C. Price, C. Booth, P. C. Griffiths and P. Stilbs, *J. Chem. Soc., Faraday Trans.*, 1996, **92**, 5021-5028.

243. Z. Ge, Y. Zhou, J. Xu, H. Liu, D. Chen and S. Liu, *J. Am. Chem. Soc.*, 2009, **131**, 1628-1629.

244. B. Zhang, H. Zhang, Y. Li, J. N. Hoskins and S. M. Grayson, *ACS Macro Lett.*, 2013, **2**, 845-848.

245. H. Iatrou, N. Hadjichristidis, G. Meier, H. Frielinghaus and M. Monkenbusch, *Macromolecules*, 2002, **35**, 5426-5437.

246. T. Isono, Y. Satoh, K. Miyachi, Y. Chen, S.-i. Sato, K. Tajima, T. Satoh and T. Kakuchi, *Macromolecules*, 2014, **47**, 2853-2863.

247. S. Honda, T. Yamamoto and Y. Tezuka, *J. Am. Chem. Soc.*, 2010, **132**, 10251-10253.

248. S. Honda, T. Yamamoto and Y. Tezuka, *Nature Commun.*, 2013, **4**, 1574.

249. K. Heo, Y. Y. Kim, Y. Kitazawa, M. Kim, K. S. Jin, T. Yamamoto and M. Ree, *ACS Macro Lett.*, 2014, **3**, 233-239.

250. R. Borsali, E. Minatti, J.-L. Putaux, M. Schappacher, A. Deffieux, P. Viville, R. Lazzaroni and T. Narayanan, *Langmuir*, 2002, **19**, 6-9.

251. E. Minatti, R. Borsali, M. Schappacher, A. Deffieux, V. Soldi, T. Narayanan and J.-L. Putaux, *Macromol. Rapid Commun.*, 2002, **23**, 978-982.

252. E. Minatti, P. Viville, R. Borsali, M. Schappacher, A. Deffieux and R. Lazzaroni, *Macromolecules*, 2003, **36**, 4125-4133.

253. N. Ouarti, P. Viville, R. Lazzaroni, E. Minatti, M. Schappacher, A. Deffieux and R. Borsali, *Langmuir*, 2005, **21**, 1180-1186.

254. N. Ouarti, P. Viville, R. Lazzaroni, E. Minatti, M. Schappacher, A. Deffieux, J.-L. Putaux and R. Borsali, *Langmuir*, 2005, **21**, 9085-9090.

255. J.-L. Putaux, E. Minatti, C. Lefebvre, R. Borsali, M. Schappacher and A. Deffieux, *Faraday Discuss.*, 2005, **128**, 163-178.

256. M. Schappacher and A. Deffieux, *Macromol. Chem. Phys.*, 2002, **203**, 2463-2469.

257. X. Wan, T. Liu and S. Liu, *Biomacromolecules*, 2011, **12**, 1146-1154.

258. Y.-Q. Dong, Y.-Y. Tong, B.-T. Dong, F.-S. Du and Z.-C. Li, *Macromolecules*, 2009, **42**, 2940-2948.

259. D. E. Lonsdale and M. J. Monteiro, *J. Polym. Sci., Part A: Polym. Chem.*, 2011, **49**, 4603-4612.

260. X. Fan, B. Huang, G. Wang and J. Huang, *Macromolecules*, 2012, **45**, 3779-3786.

261. T. Cai, W. J. Yang, K.-G. Neoh and E.-T. Kang, *Polym. Chem.*, 2012, **3**, 1061-1068.

262. O. Coulembier, S. b. Moins, J. De Winter, P. Gerbaux, P. Leclère, R. Lazzaroni and P. Dubois, *Macromolecules*, 2009, **43**, 575-579.

263. M. Schappacher and A. Deffieux, *Science*, 2008, **319**, 1512-1515.

2 Orthogonal Modification of Norbornene-Functional Polycarbonates

2.1 Introduction

The design and synthesis of highly functional polymers is essential to fulfill the demands of advanced applications in materials science. Functional polymers can be prepared *via* two approaches; the synthesis and polymerisation of specifically designed functional monomers or the post-polymerisation modification of a polymer scaffold containing reactive groups. The latter of these approaches is particularly attractive as it allows the incorporation of functionalities that may be difficult to polymerise or incompatible with the chosen polymerisation technique and can be used to prepare a library of functional polymers with relative ease, avoiding the need to optimise multiple monomer syntheses and polymerisation conditions. A variety of highly efficient chemistries including "click" reactions have successfully been applied to the preparation of functional polymers *via* a post-polymerisation route.[1-8] Recent work has seen the development of polymer scaffolds containing two or more reactive functionalities, allowing the preparation of multifunctional materials *via* orthogonal modifications and illustrating the utility of a post-polymerisation modification approach.[6, 8-13]

The development of a cyclic carbonate monomer scaffold based around 2,2'-bis(hydroxymethyl) propionic acid (bis-MPA) has enabled the preparation and subsequent polymerisation of a range of functional cyclic carbonate monomers.[14, 15] Methods to further functionalise such polymers allows facile access to a wider range of functional materials and the incorporation of functionalities that are incompatible with ROP or those of significant steric bulk, that would hinder polymerisation if incorporated into the monomer prior to ROP *via* reduction of monomer ring-strain. Recent work by the groups of Dove

and others has demonstrated the post-polymerisation modification of polycarbonates bearing pendent allyl,[16-19] maleimide,[20] (meth)acrylic,[21] vinyl-sulfone,[22] alkyne[23-25] and azide groups.[26, 27]

To expand the scope of post-polymerisation functionalisation strategies the work in this chapter aimed to design a polycarbonate scaffold containing a reactive functionality that could undergo multiple orthogonal modification reactions by simply varying reaction stimuli, such as temperature or UV irradiation. The norbornenyl group is an attractive reactive handle for such a purpose. As a consequence of their highly strained ring structure, norbornenes exhibit extremely high reactivity during thermal and UV initiated thiol-ene radical additions,[28-31] are excellent dienophiles in the inverse electron demand Diels-Alder reaction with tetrazines,[32-37] undergo reaction in 1,3-dipolar cycloadditions[38-42] and are the archetypal monomers for ring-opening metathesis polymerisations.[43, 44]

Hence, in this chapter, the synthesis and ROP of a novel norbornene-functional cyclic carbonate monomer for the preparation of multi-reactive polymer scaffolds and their subsequent post-polymerisation functionalisation *via* the heat promoted 1,3-dipolar cycloaddition reaction with azides, the inverse electron demand Diels-Alder reaction with tetrazines and the radical addition of thiols promoted by UV irradiation is reported, demonstrating the functionalisation chemistries both individually and in a sequential one-pot reaction. Furthermore, the norbornene-functional polycarbonates are utilised in the preparation of degradable graft copolymers *via* radical thiol-ene chemistry.

2.2 Results and Discussion

2.2.1 Monomer Synthesis

The norbornene-functional cyclic carbonate monomer, **4**, was prepared in three steps from the acetonide-protected analogue of 2,2'-bis(hydroxymethyl) propionic acid, **1**, that in turn was prepared according to the literature.[45] Coupling of **1** with an *endo*/*exo* mixture of 5-norbornene-2-methanol in the presence of *N*-(3-dimethyl-aminopropyl)-*N'*-ethylcarbodiimide hydrochloride (EDC.HCl) and 4-(dimethylamino)pyridine (DMAP), followed by hydrolysis of the acetyl groups of **2** with DOWEX 50W-X2 resin, yielded the norbornene-functional diol **3**. The norbornene-functional cyclic carbonate monomer **4** was subsequently formed by ring-closure using triphosgene and an excess of pyridine to trap hydrochloric acid. The product was isolated as a mixture of *endo* and *exo* isomers (*endo*:*exo* = 60:40) in 49% overall yield after recrystallisation from hot cyclohexane (Scheme 2.1).

Analysis of monomer **4** by ^{1}H NMR spectroscopy revealed signals that correspond to both norbornene and cyclic carbonate functionality, in particular,

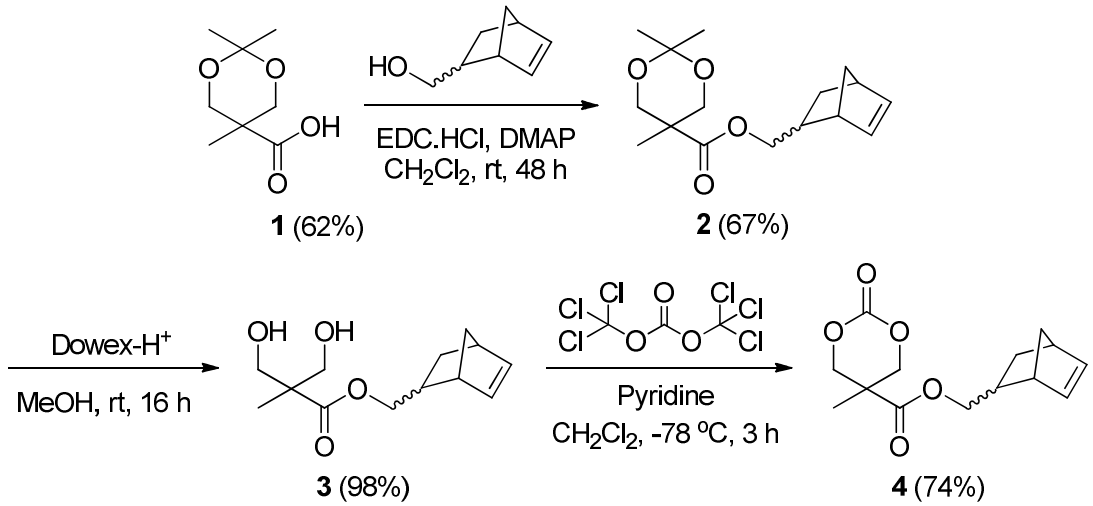

Scheme 2.1. Synthesis of norbornene-functional cyclic carbonate monomer, **4**.

the characteristic multiplet resonances at δ = 6.19 - 5.91 ppm that correspond to the norbornene alkene protons of both the *endo* and *exo* isomers and the signals at δ = 4.70 and 4.20 ppm that correspond to the inequivalent protons of the CH_2 groups of the carbonate ring (Figure 2.1). Resonances that correspond to the norbornene double bond were also observed in the ^{13}C NMR spectrum of the monomer, at δ = 137.8 – 131.9 ppm, as well as the resonance at δ = 147.6 ppm that corresponds to the carbonate carbonyl group of both *endo* and *exo* isomers (Figure 2.2). The expected structure of monomer **4** was further confirmed by elemental analysis and mass spectrometry.

2.2.2 Ring-Opening Polymerisation Studies

Initial studies of the ring-opening polymerisation of **4** were conducted in $CDCl_3$ or CH_2Cl_2 at room temperature (Scheme 2.2), using 1,8-diazabicycloundec-7-ene (DBU) and 1-(3,5-bis(trifluoromethyl)phenyl)-3-cyclohexylthiourea (**5**) as cocatalysts.[14, 46] Monomer conversion was followed by ^1H NMR spectroscopy by comparing the reduction of the CH_2 signals of the monomer carbonate ring at δ

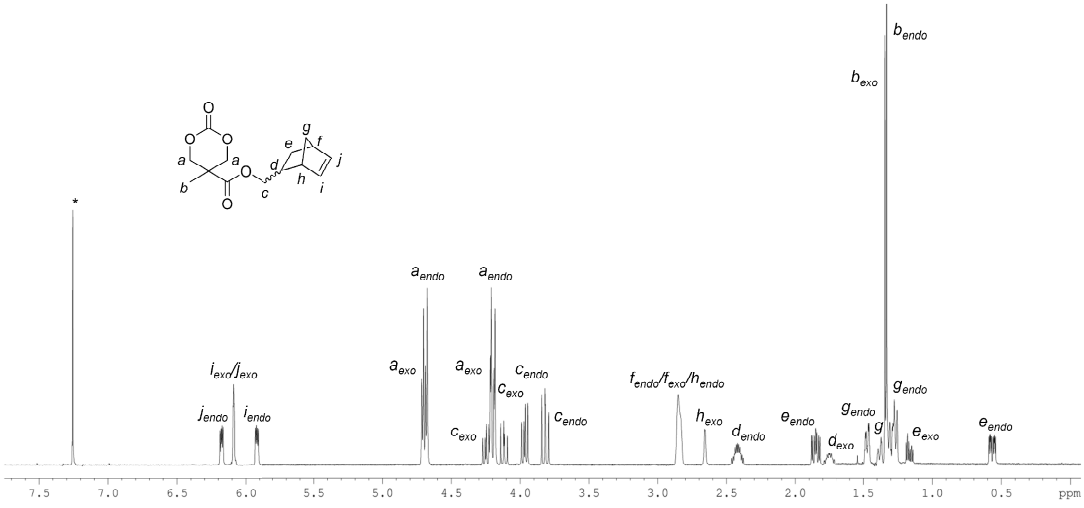

Figure 2.1. ^1H NMR spectrum (400 MHz; $CDCl_3$) of monomer **4** (*$CHCl_3$).

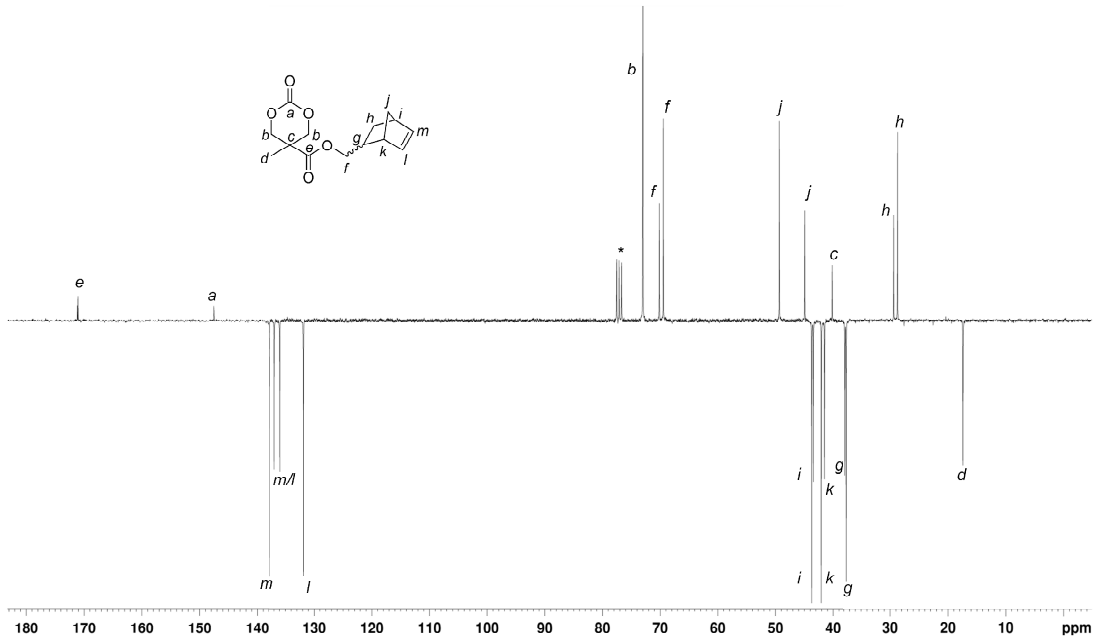

Figure 2.2. ^{13}C NMR spectrum (100 MHz; $CDCl_3$) of monomer **4** (*$CDCl_3$).

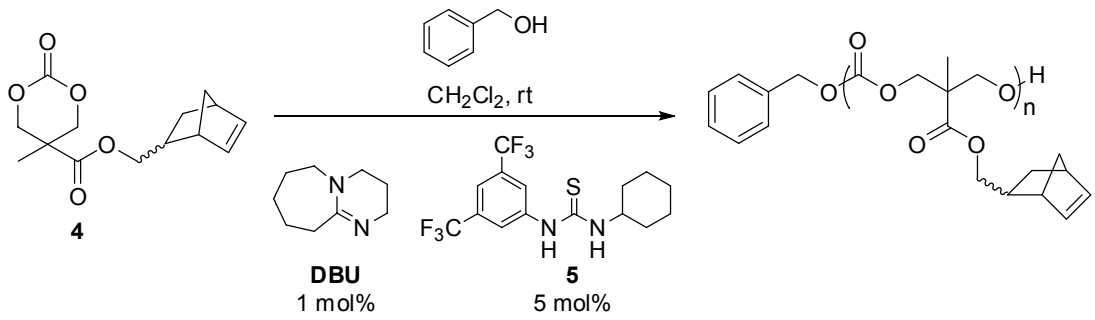

Scheme 2.2. Ring-opening polymerisation of monomer **4** to prepare norbornene-functional polycarbonates.

= 4.70 and 4.20 ppm, with the appearance of a broad signal at δ = 4.29 ppm that corresponds to the CH_2 groups of the polycarbonate backbone. Polymerisations were quenched at monomer conversions ≥ 90% with acidic Amberlyst resin, before purification by flash column chromatography (silica, 100% dichloromethane, then 100% ethyl acetate) to remove residual monomer and catalyst.

Application of 1 mol% of DBU and 5 mol% of cocatalyst **5**, with benzyl alcohol as the polymerisation initiator, an initial monomer-to-initiator ratio ($[M]_0/[I]_0$) of 20 and initial monomer concentration of 0.5 M, resulted in 90% monomer conversion after 7 h (Figure 2.3). Analysis of the resulting polymer by size exclusion chromatography (SEC) after purification revealed a monomodal trace with a low dispersity value, $Đ_M$, of 1.14 and number-average molecular weight, M_n, of 4.9 kDa (Figure 2.4). Further analysis of the polymer by ^{1}H NMR spectroscopy confirmed a degree of polymerisation (DP) of 19 by comparison of the integral of the aromatic protons of the benzyl carbonate polymer end-group, at δ = 7.36 ppm, against resonances of the CH_2 and CH_3 groups of the polycarbonate backbone at δ = 4.29 and 1.26 ppm respectively (Figure 2.5). The ^{1}H NMR spectra of the polymer also revealed complete preservation of the pendent norbornene groups at δ = 6.15 – 5.91 ppm, indicating no deleterious side reactions of the norbornene functionality occurred during polymerisation.

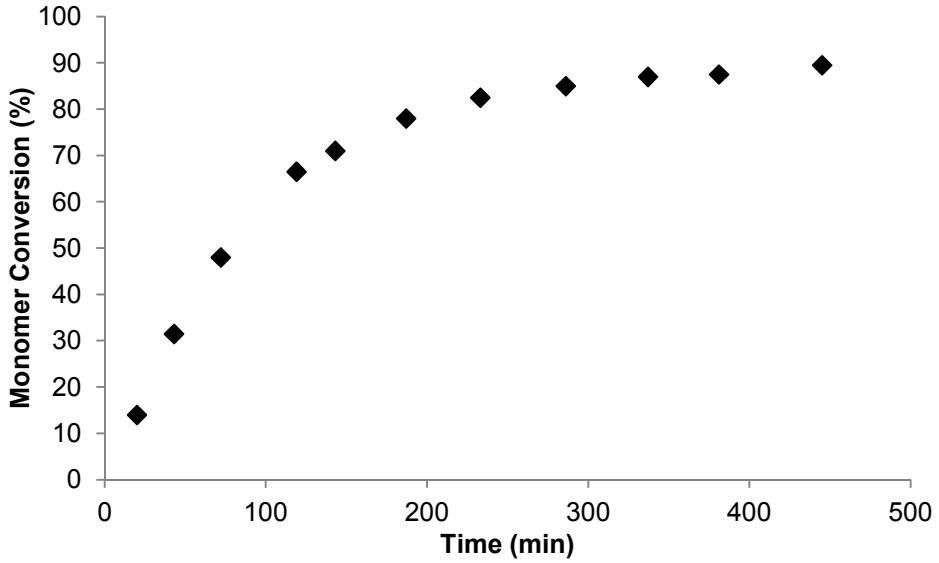

Figure 2.3. Plot of time (min) against monomer conversion (%) for the ring-opening polymerisation of **4**. Conditions: [**4**] = 0.5 M, $CDCl_3$ at 25 °C, [M]/[I] = 20 using benzyl alcohol as initiator and 1 mol% DBU and 5 mol% **5**.

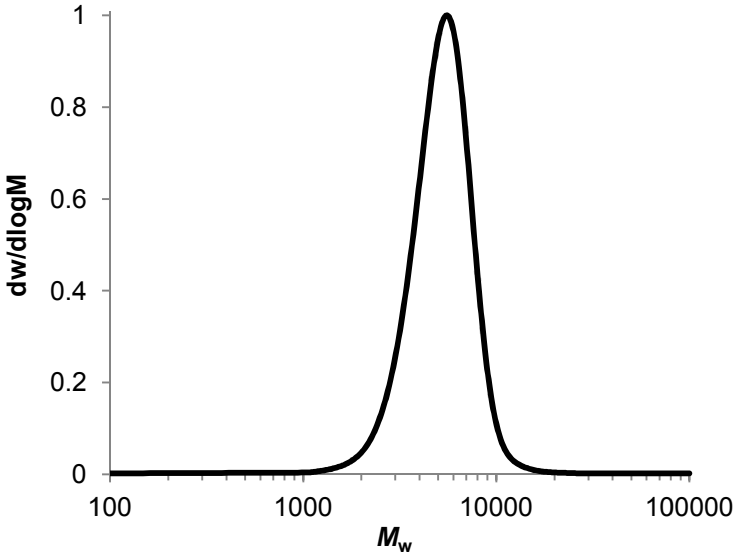

Figure 2.4. SEC chromatogram of norbornene-functional polycarbonate (M_n = 4.8 kDa, $Đ_M$ = 1.09). Conditions: [M]/[I] = 20, using benzyl alcohol as initiator and 1 mol% DBU and 5 mol% **5**.

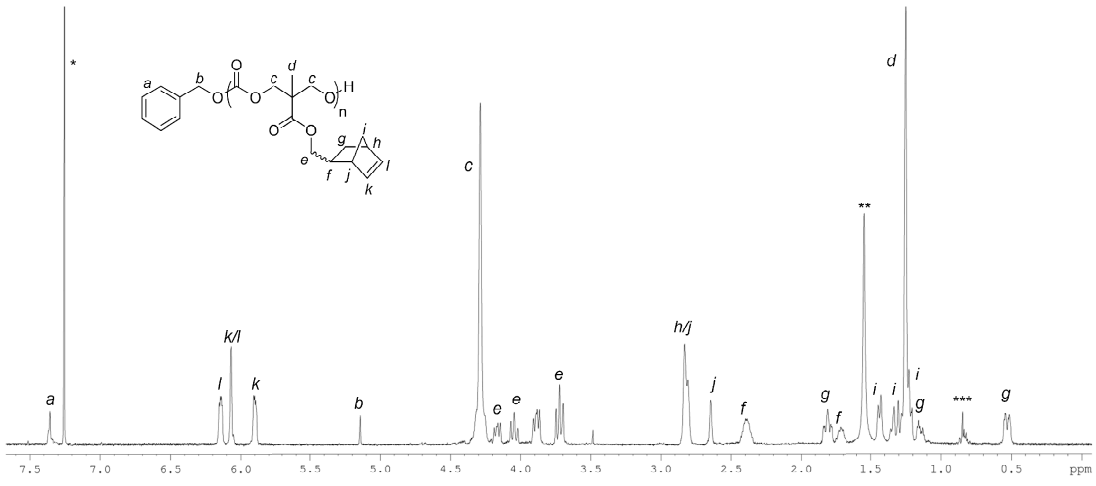

Figure 2.5. ^{1}H NMR spectrum (400 MHz; $CDCl_3$) of norbornene-functional polycarbonate, [M]/[I] = 20 (*$CHCl_3$, **H_2O, *** petroleum ether).

Matrix-assisted laser desorption ionisation time-of-flight mass spectrometry (MALDI-ToF MS) revealed a single sodium-charged distribution with regular spacings equal to the molecular weight of the monomer repeat unit (*m/z* = 266) and a benzyl alcohol end-group, demonstrating the extremely high end-group fidelity and controlled nature of the polymerisation (Figure 2.6 and Table 2.1).

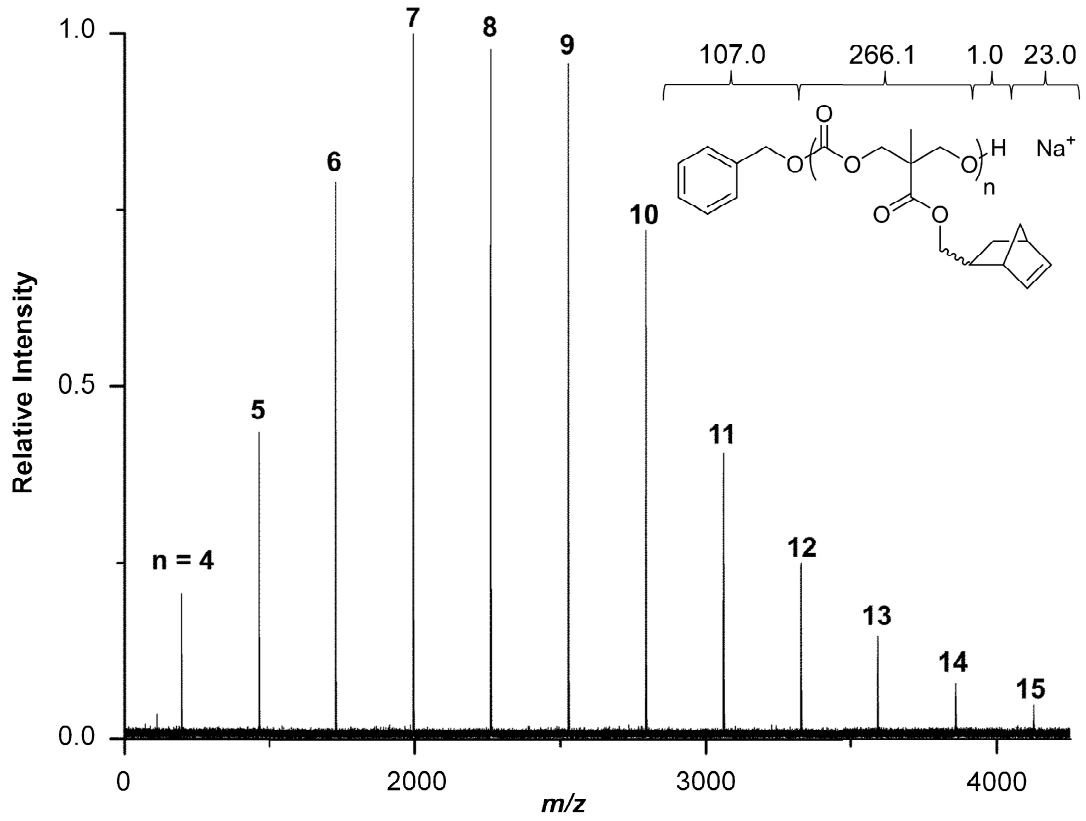

Figure 2.6. MALDI-TOF mass spectrum of norbornene-functional polycarbonate initiated from benzyl alcohol, [M]/[I] = 20.

Table 2.1. Theoretical and observed *m/z* values of norbornene-functional polycarbonate.

DP	Experimental *m/z*[a]	Calculated *m/z*
7	1993.997	1993.855
8	2260.119	2259.97
9	2526.272	2526.086
10	2792.437	2792.201

[a]Determined by MALDI-TOF MS analysis using trans-2-[3-(4-*tert*-butylphenyl)-2-methyl-2-propylidene]malonitrile (DCTB) as a matrix, sodium trifluoroacetate as the cationisation agent and PEG monomethyl ether 2k and 5k standards.

As a consequence of the controlled nature of the polymerisation of monomer **4**, using 1 mol% of DBU and 5 mol% of thiourea cocatalyst **5**, no further optimisation of the ROP conditions was undertaken.

Further investigation of the living characteristics of the polymerisation of **4** revealed a linear correlation between M_n(SEC) and monomer conversion (Figure 2.7), whilst also retaining low dispersity values ($Đ_M$ < 1.2) and monomodal SEC chromatograms throughout the polymerisation (Figure 2.8). A linear relationship was also observed between and M_n(SEC) and $[M]_0/[I]_0$ (Figure 2.9), highlighting the ability to prepare a range of norbornene-functional polycarbonates with targeted and predictable molecular weights (Figure 2.10). All observations suggest that the polymerisation of **4** proceeds in a controlled and living manner and highlights the orthogonality of the norbornene functionality with respect to the organocatalysed ROP of cyclic carbonates.

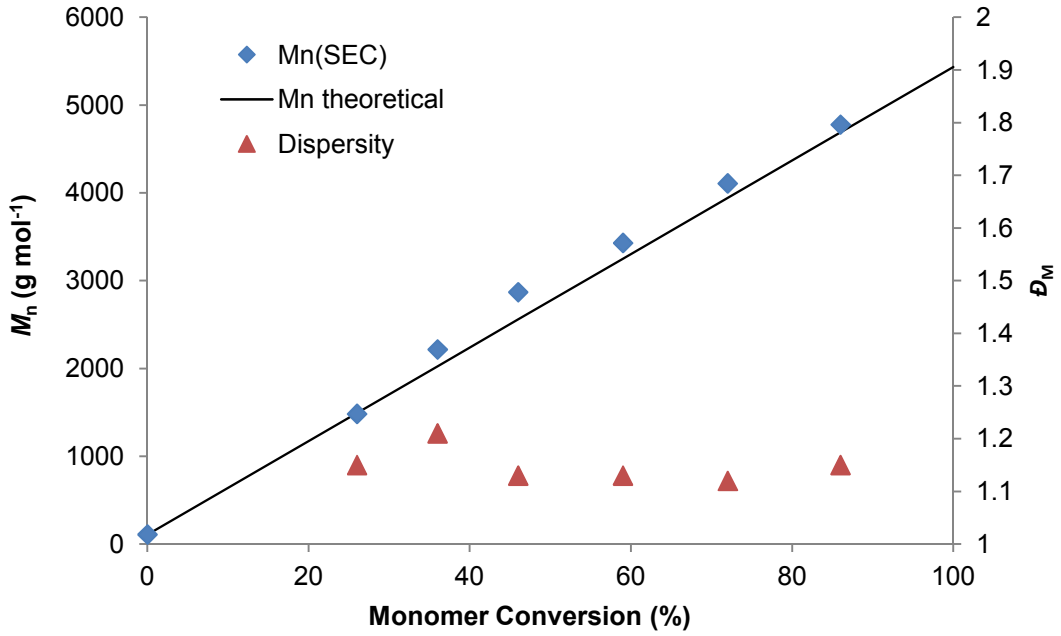

Figure 2.7. Plot of M_n(SEC) (kDa) against monomer conversion (%) and dispersity, $Đ_M$, against monomer conversion (%) for the ring-opening polymerisation of **4**. Conditions: [**4**] = 0.5 M, [M]/[I] = 20, using 1 mol% DBU and 5 mol% **5** and benzyl alcohol as the polymerisation initiator.

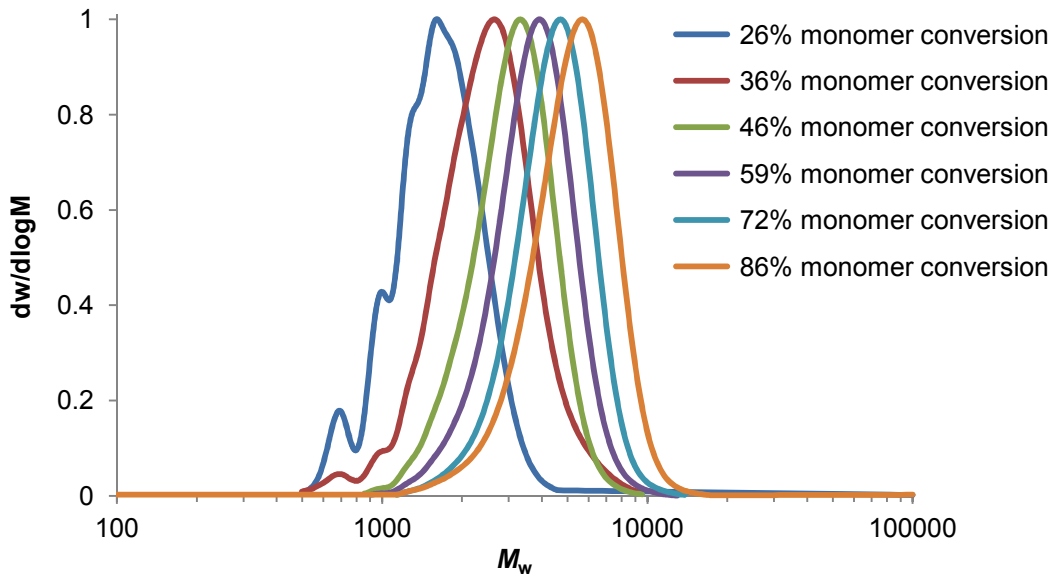

Figure 2.8. Evolution of SEC chromatograms for the ROP of **4**. Conditions: [**4**] = 0.5 M, [M]/[I] = 20, using 1 mol% DBU and 5 mol% **5** and benzyl alcohol as the polymerisation initiator.

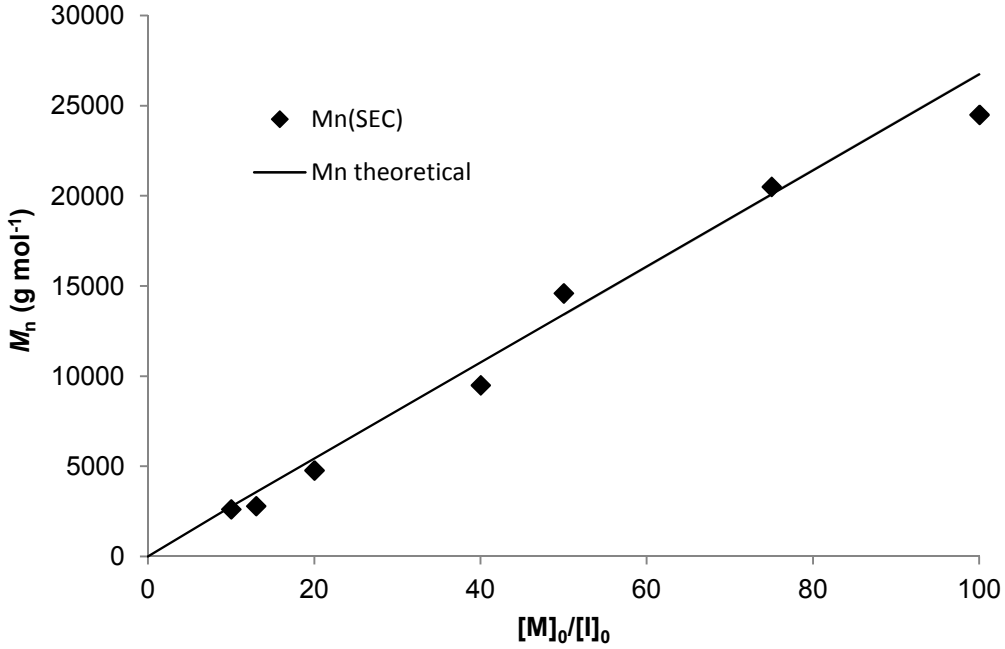

Figure 2.9. Plot of M_n(SEC) (kDa) against [M]/[I] for the ROP of **4**. Conditions: [**4**] = 0.5 M, using 1 mol% DBU and 5 mol% **5** and benzyl alcohol as the polymerisation initiator.

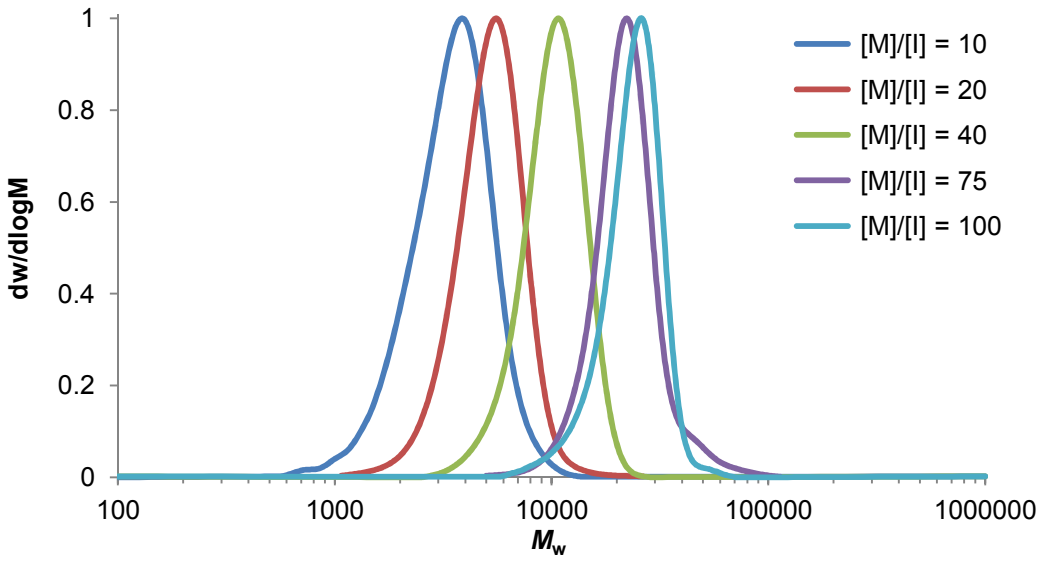

Figure 2.10. SEC chromatograms of norbornene-functional polycarbonates with varying [M]/[I]. Conditions: [**4**] = 0.5 M, using 1 mol% DBU, 5 mol% **5** and benzyl alcohol as initiator.

2.2.3 Post-Polymerisation Functionalisation of Norbornene-Functional Polycarbonates

Following the successful preparation of well-defined norbornene functionalised polycarbonates, a range of post-polymerisation modifications were investigated; namely the 1,3-dipolar cycloaddition of norbornenes and azides, the inverse electron demand Diels-Alder (DA_{inv}) reaction between norbornenes and tetrazines and the radical addition of thiols to norbornenes (Scheme 2.3). The polymer modifications were initially studied separately using a norbornene-functional polycarbonate with a DP of 100 (**6**, M_n = 24.5 kDa, $Đ_M$ = 1.11), as well as a lower molecular weight polycarbonate of DP 12 (**7**, M_n = 2.8 kDa, $Đ_M$ = 1.21) to assist with the ready characterisation of the modified polymers by MALDI-ToF MS. 1,4-Dioxane was chosen as the reaction solvent for all polymer modifications as it is an excellent solvent for polycarbonates and was found to be compatible with all three reactions.

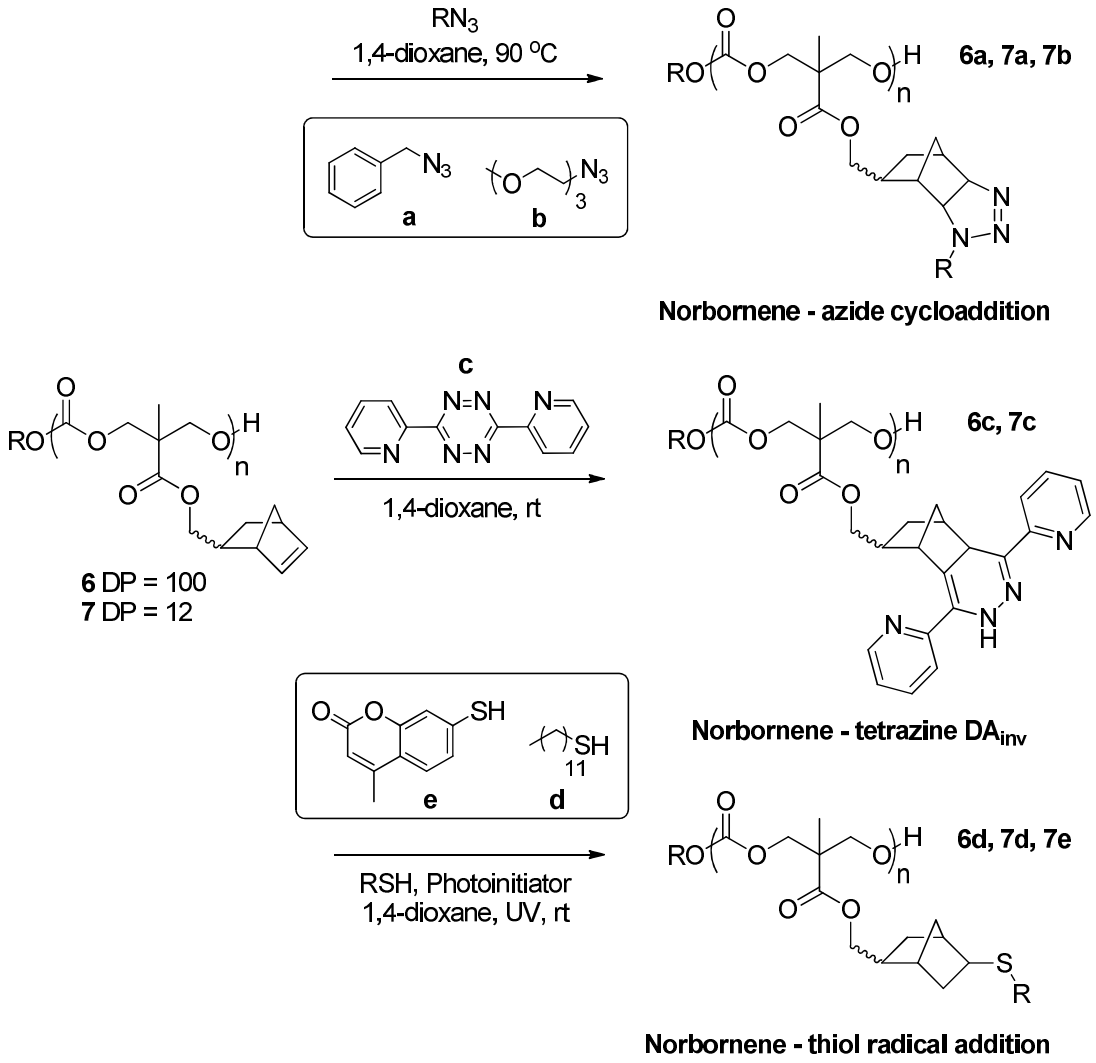

Scheme 2.3. Functionalisations of norbornene-functional polycarbonates.

2.2.3.1 Post-Polymerisation Functionalisation of Norbornene-Functional Polycarbonates: Norbornene-Azide 1,3-Dipolar Cycloaddition

As a consequence of the limited number of reports of norbornene-azide 1,3-dipolar cycloadditions in the literature,[42, 47, 48] a model reaction between benzyl azide and 5-norbornene-2-methanol was performed prior to polymer functionalisation (Scheme 2.4). Previous reports of norbornene-azide cycloadditions used elevated temperatures and/or extended reaction times, hence 1.05 equivalents of azide and 1 equivalent of small molecule norbornene

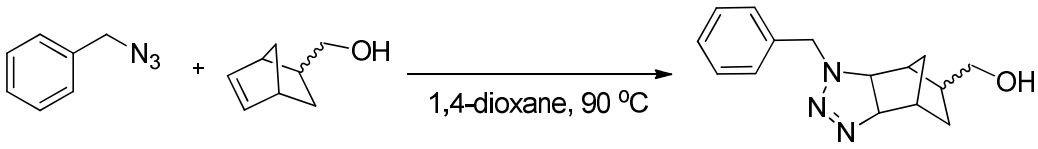

Scheme 2.4. Small molecule model reaction for the 1,3-dipolar norbornene-azide cycloaddition.

were heated at 90 °C in 1,4-dioxane and the reaction followed by ^{1}H NMR spectroscopy over several days. Monitoring the reduction of resonances that correspond to the norbornene double bond revealed a conversion of 63% after 14 h, increasing to 89% conversion after 2 days (Figure 2.11).

Based on these findings, a significantly larger excess of benzyl azide (10 equivalents) was used for polymer functionalisations, to drive the reaction to completion and also shorten reaction times as the occurrence of degradation was anticipated for the prolonged heating of the polymer in solution. Indeed, degradation of the polycarbonate backbone was observed after 36 h of heating at 90 °C in the presence of benzyl azide, as evidenced by the appearance of a low molecular weight tail during SEC analysis and broadening of molecular weight distribution ($Đ_M$ = 1.68) (Figure 2.12). However, monitoring the polymer functionalisations by ^{1}H NMR spectroscopy revealed that after only 14 h > 99% of the norbornene units had been consumed, as evidenced by the reduction of resonances at δ = 6.15 – 5.91 ppm that correspond to the norbornene double bond. The modified polymers were precipitated into cold methanol to remove excess benzyl azide before being further analysed. SEC analysis of the precipitated polymers after 14 h of heating at 90 °C in the presence of benzyl azide showed an increase in molecular weight, from M_n = 24.5 to 25.6 kDa (**6a**, DP = 100) and M_n = 2.8 to 4.9 kDa (**7a**, DP = 12), while the dispersities of the polymers remained low ($Đ_M$ = 1.16 and 1.10) (Figure 2.13).

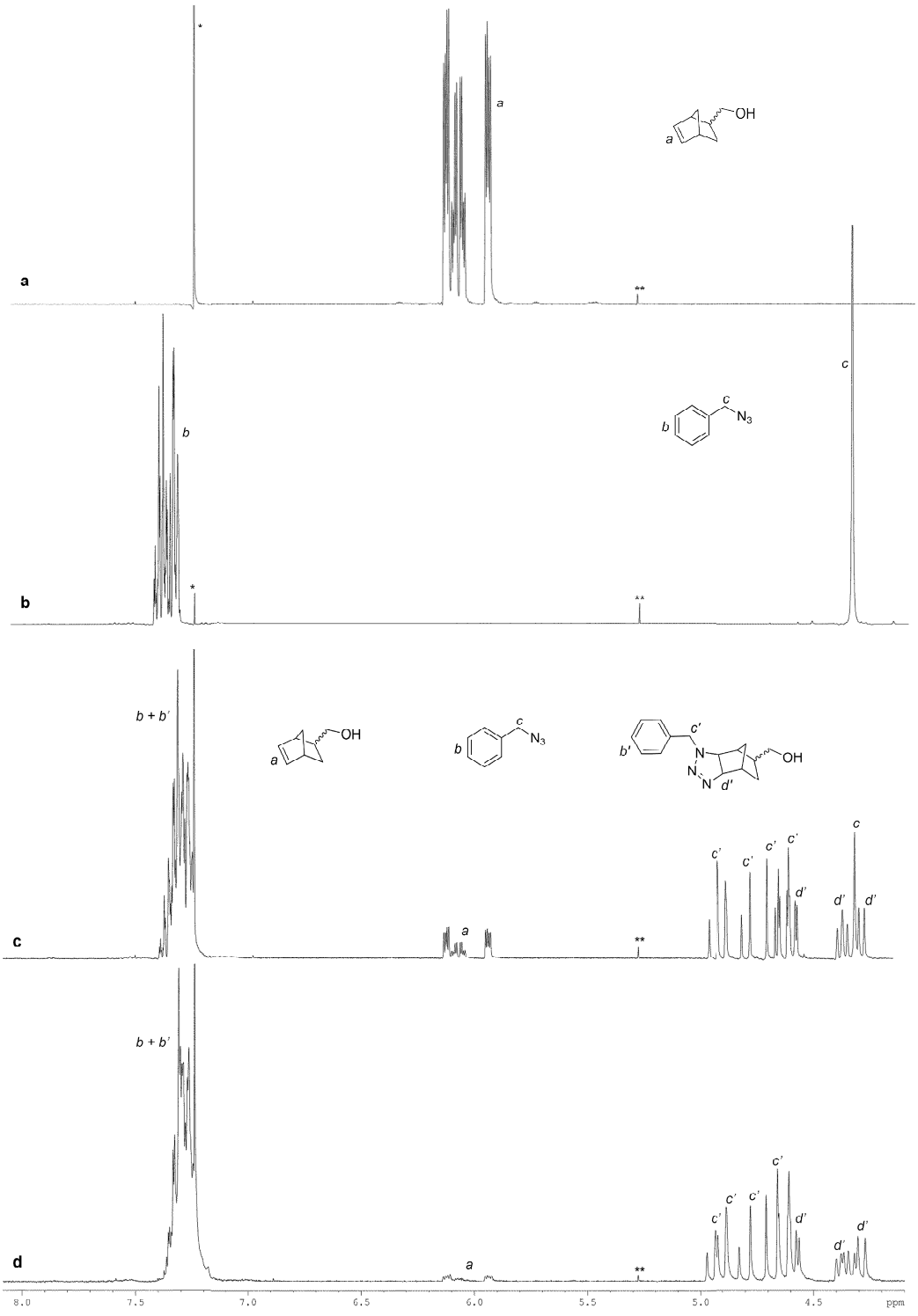

Figure 2.11. Expansion (δ = 6.15 – 5.91 ppm) of ^{1}H NMR spectra (400 MHz; $CDCl_3$) of (**a**) 5-norbornene-2-methanol, (**b**) benzyl azide, (**c**) crude reaction mixture after 14 h and (**d**) crude reaction mixture after 2 days (*$CHCl_3$, ** CH_2Cl_2).

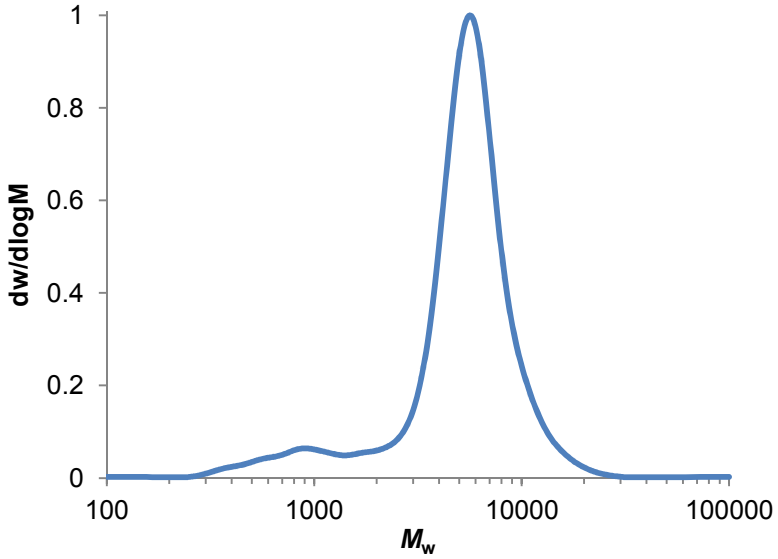

Figure 2.12. SEC chromatogram of DP 12 norbornene-functional polycarbonate after heating in the presence of benzyl azide for 36 h (M_n = 3.4 kDa, $Đ_M$ = 1.68).

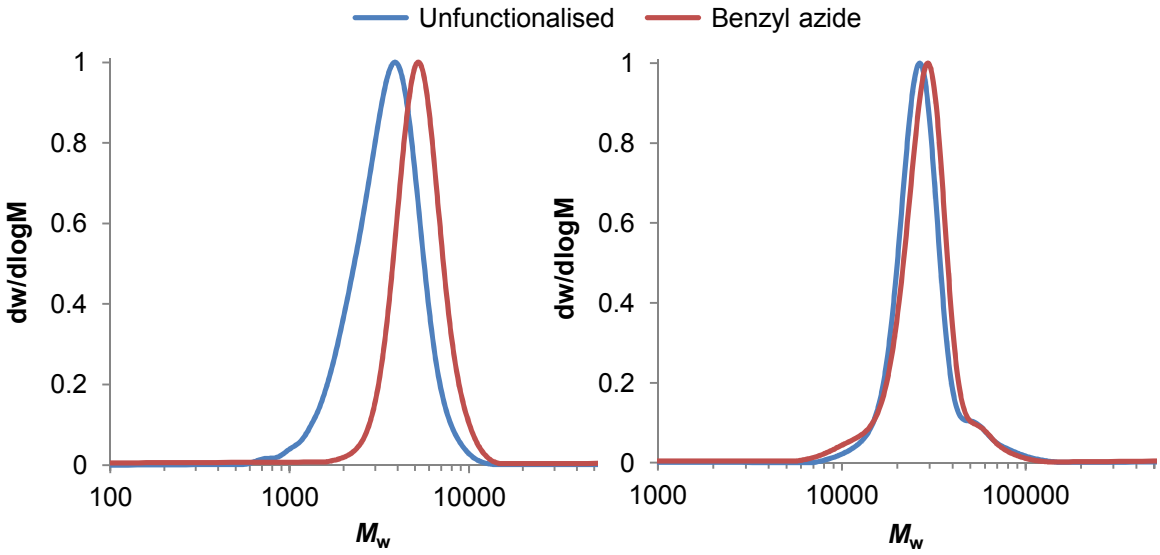

Figure 2.13. (Left) SEC chromatogram of DP 12 norbornene-functional polycarbonate before (**7**, M_n = 2.8 kDa, $Đ_M$ = 1.21) and after functionalisation with benzyl azide (**7a**, M_n = 4.9 kDa, $Đ_M$ = 1.10). (Right) SEC chromatogram of DP 100 norbornene-functional polycarbonate before (**6**, M_n = 24.5 kDa, $Đ_M$ = 1.14) and after functionalisation with benzyl azide (**6a**, M_n = 25.6 kDa, $Đ_M$ = 1.16).

The ^{1}H NMR spectra of the purified polymers show the appearance of new resonances that correspond to the aromatic and benzyl protons of the cycloaddition product at δ = 7.35 – 7.21 ppm and δ = 4.91 – 4.64 ppm

respectively and the two protons of the newly formed triazoline ring at δ = 4.68 – 4.33 ppm and δ = 3.05 – 3.38 ppm (Figure 2.14).

Analysis of the DP 12 polymer (**7a**) by MALDI-ToF MS revealed a new sodium-charged distribution consistent with the addition of benzyl azide to the pendent norbornene groups, forming the expected triazoline cycloadduct as observed by an increase of repeat unit from *m/z* = 266 to 399 (Figure 2.15). A second distribution of much lower intensity was also observed, which corresponds to the loss of molecular nitrogen from one pendent group per polymer chain. It was postulated that this loss of nitrogen occurs upon ionisation by the laser, forming the corresponding aziridine *via* photolysis (Scheme 2.5). In fact, the generation of aziridines from norbornene derived triazolines under photo-chemical conditions has been previously reported.[48, 49] Increasing the laser power used during MALDI-ToF MS analysis increased the intensity of this second distribution and revealed the appearance of other minor distributions that correspond to polymer chains with two or more aziridine groups.

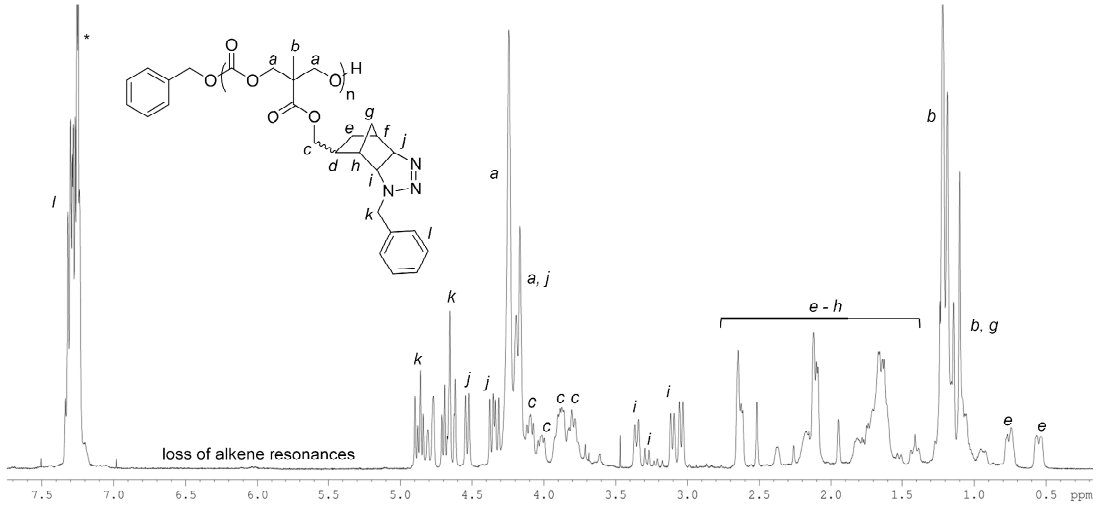

Figure 2.14. ^{1}H NMR spectrum (400 MHz; $CDCl_3$) of DP 100 norbornene-functional polycarbonate after functionalisation with benzyl azide **6a** (*$CHCl_3$).

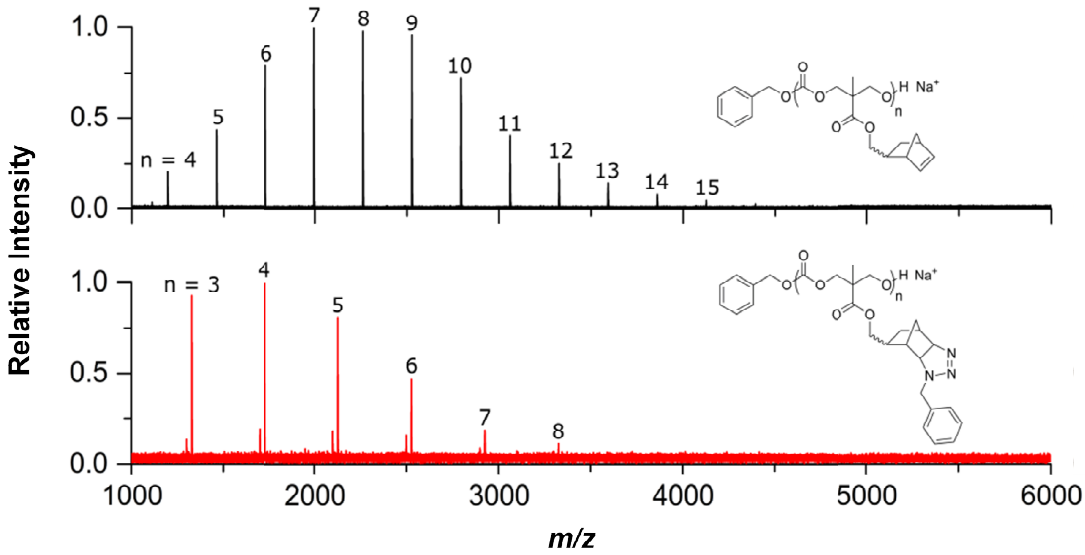

Figure 2.15. MALDI-TOF MS analysis (reflectron mode) of DP 12 norbornene-functional polycarbonate before (**7**) (top) and after (**7a**) (bottom) functionalisation with benzyl azide.

Table 2.2. Theoretical and observed *m/z* values of benzyl azide functionalisation.

DP	Experimental *m/z*[a]	Calculated *m/z*
4	1727.7	1727.8
5	2126.9	2126.9
6	2526.1	2526.1
7	2925.3	2925.3

[a]Determined by MALDI-TOF MS analysis using trans-2-[3-(4-*tert*-butylphenyl)-2-methyl-2-propylidene]malonitrile (DCTB) as a matrix, sodium trifluoroacetate as the cationisation agent and PEG monomethyl ether 2k and 5k standards.

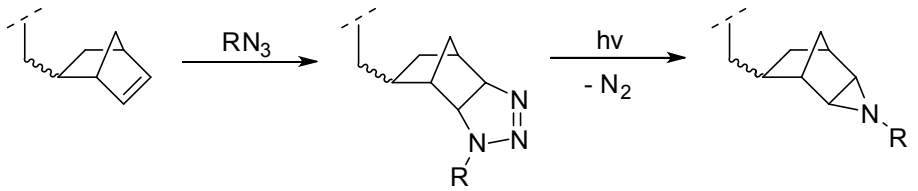

Scheme 2.5. Norbornene-azide 1,3-dipolar cycloaddition and photolysis of the triazoline product to an aziridine.

The norbornene-azide cycloaddition was further demonstrated using triethyleneglycol (TEG) monomethyl ether azide to functionalise norbornene-functional polycarbonate **7** (DP = 12). The successful functionalisation was confirmed by ^{1}H NMR spectroscopic analysis, evidenced by the > 99% reduction of the norbornene double bond resonances and the appearance of three resonances at δ = 3.65, 3.56 and 3.39 ppm that correspond to the TEG group (Figure 2.16). The molecular weight distribution of the polymer remained narrow after functionalisation ($Đ_M$ = 1.14), with an increase in molecular weight from M_n = 2.8 to 4.4 kDa observed by SEC analysis (Figure 2.17).

Similar to vinyl polymers composed of TEG (meth)acrylate, the TEG-functional polycarbonate, **7b**, was found to exhibit a cloud point in aqueous solution. The cloud point was determined using UV/vis spectroscopy, by measuring the turbidity of the solution (1 mg/mL) at various temperatures with a 1 °C/min heating/cooling cycle. A transition was observed in the plot of transmittance *versus* temperature corresponding to a cloud point of 17 °C (Figure 2.18) and

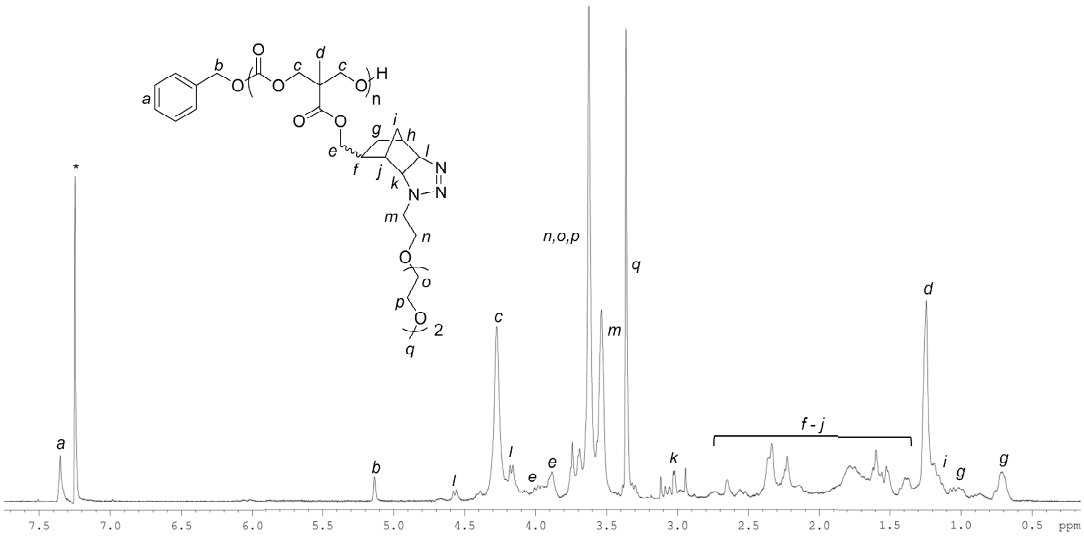

Figure 2.16. ^{1}H NMR spectrum (400 MHz; $CDCl_3$) of DP 12 norbornene-functional polycarbonate after functionalisation with TEG azide **7b** (*$CHCl_3$).

demonstrates how post-polymerisation functionalisation can provide access to thermoresponsive hydrophilic polycarbonates.

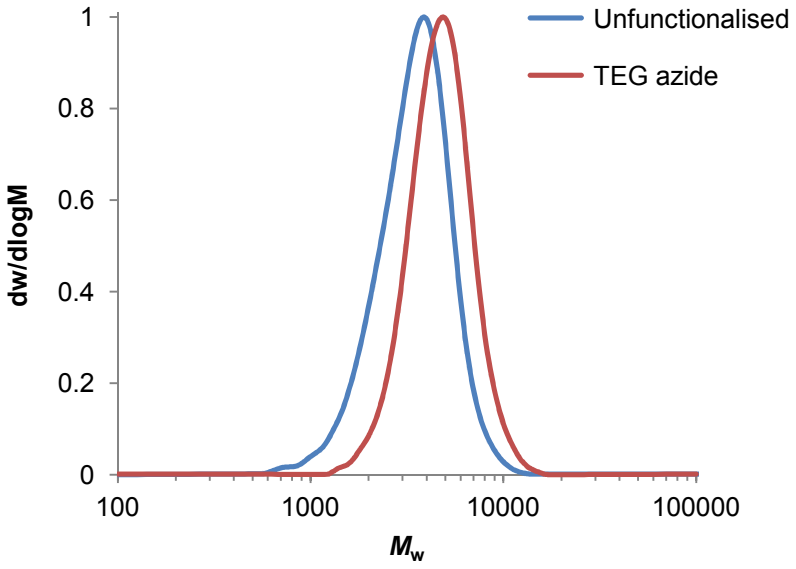

Figure 2.17. SEC chromatogram of DP 12 norbornene-functional polycarbonate before (**7**, M_n = 2.8 kDa, $Đ_M$ = 1.21) and after functionalisation with benzyl azide (**7b**, M_n = 4.4 kDa, $Đ_M$ = 1.14).

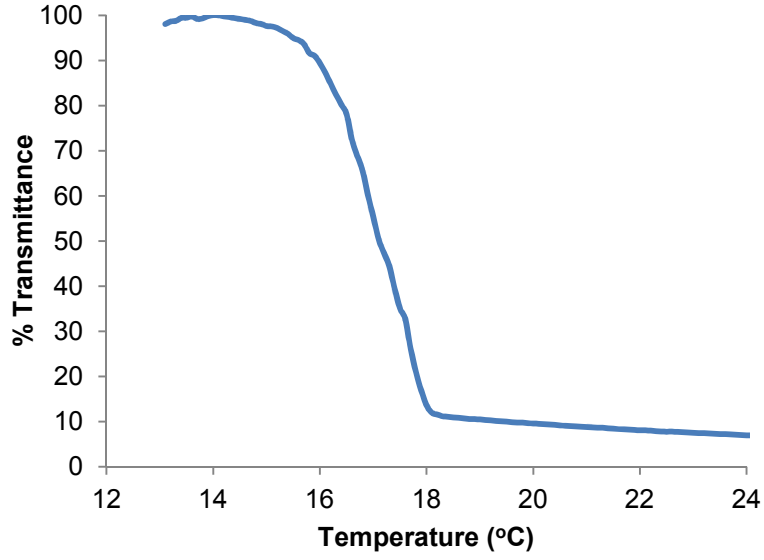

Figure 2.18. Plot of % transmittance against temperature (°C) for heating cycle of TEG-functional polycarbonate (**7b**) at 1 mg/mL in nanopure water, heating/cooling rate = 1 °C/min.

2.2.3.2 Post-Polymerisation Functionalisation of Norbornene-Functional Polycarbonates: Norbornene-Tetrazine Inverse Electron Demand Diels-Alder Reaction

The inverse electron demand Diels-Alder reaction between tetrazines and norbornenes has recently been shown to be quantitative for the side-chain and end-group functionalisation of polymers, in addition to polymer-polymer coupling reactions, where the reaction proceeds with excellent efficiency in a range of organic solvents and aqueous media at room temperature.[34, 50] Hence, in this study an equimolar amount of commercially available 3,6-di-2-pyridyl-1,2,4,5-tetrazine to pendent norbornene functionality was used and reaction mixtures were stirred for 10 h at room temperature in 1,4-dioxane. During this time, the characteristic colour change from pink to pale yellow as tetrazine is consumed indicated completion of the reaction, as was further confirmed by ^{1}H NMR spectroscopy that revealed a complete loss of the norbornene alkene resonances at δ = 6.15 – 5.91 ppm. After precipitation into hexane, the ^{1}H NMR

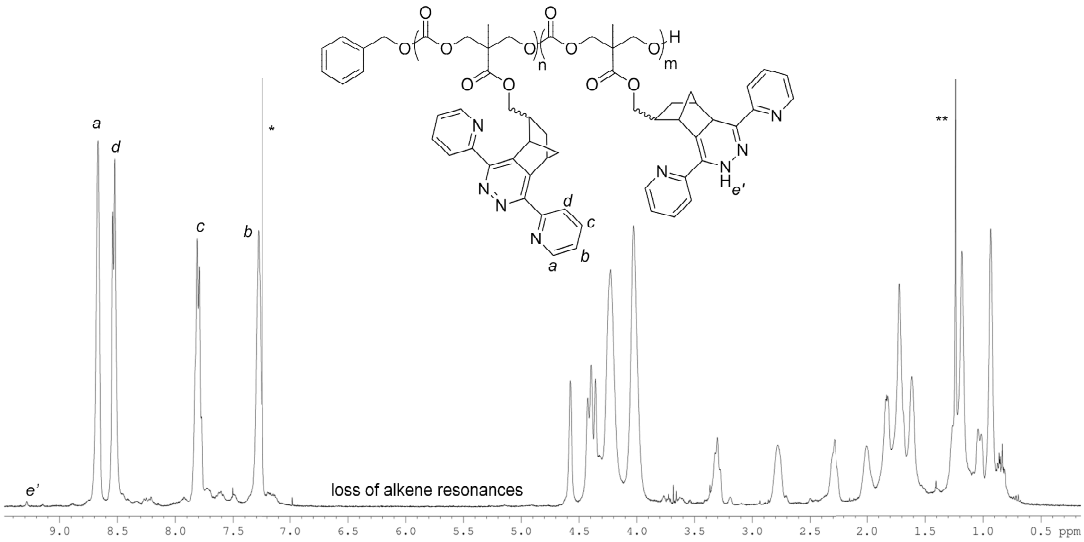

Figure 2.19. ^{1}H NMR spectrum (400 MHz; $CDCl_3$) of DP 100 norbornene-functional polycarbonate after functionalisation with 3,6-di-2-pyridyl-1,2,4,5-tetrazine (*$CHCl_3$, ** H_2O).

spectra of the isolated polymers show the appearance of new resonances, between δ = 8.68 and 7.18 ppm, that correspond to the aromatic protons of the norbornene-tetrazine cycloadduct (Figure 2.19). The major conjugation product was assigned to the fully aromatic pyradizine group, however a small amount of unoxidised dihydropyradizine was also observed, as evidenced by the characteristic NH resonance at δ = 9.31 ppm. The functionalised polymers exhibited narrow molecular weight distributions and low dispersity values by SEC analysis ($Đ_M$ = 1.08 and 1.23), indicating the cycloaddition between norbornenes and tetrazines is compatible with polycarbonates (Figure 2.20). Both the DP = 100 (**6c**) and DP = 12 (**7c**) modified polymers revealed little change in retention time and apparent molecular weight. This was attributed to a change in solubility of the functionalised polymers in the SEC eluent, hence the hydrodynamic volume of the polymers remained similar before and after

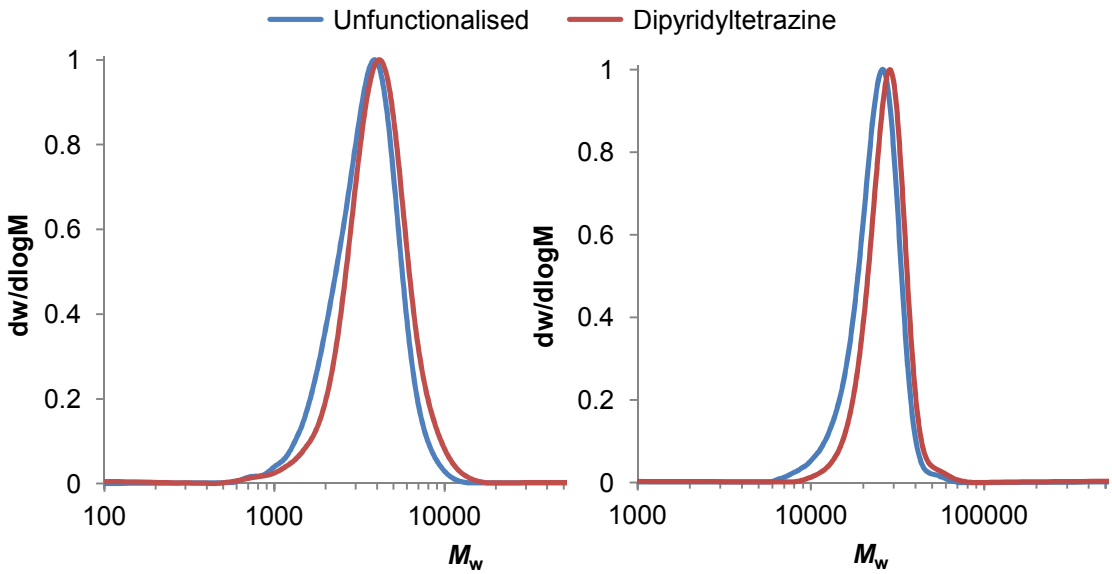

Figure 2.20. (Left) SEC chromatogram of DP 12 norbornene-functional polycarbonate before (**7**, M_n = 2.8 kDa, $Đ_M$ = 1.21) and after functionalisation with dipyridyltetrazine (**7c**, M_n = 3.5 kDa, $Đ_M$ = 1.23). (Right) SEC chromatogram of DP 100 norbornene-functional polycarbonate before (**6**, M_n = 24.5 kDa, $Đ_M$ = 1.11) and after functionalisation with dipyridyltetrazine (**6c**, M_n = 25.7 kDa, $Đ_M$ = 1.08).

functionalisation, despite the significant increase in molecular weight. MALDI-ToF MS analysis of the DP = 12 polymer (**7c**) revealed an increase in the molecular weight of the repeat unit from m/z = 266 to 474, which corresponds to the addition of dipyridyltetrazine to each repeat unit (Figure 2.21 and Table 2.3). In addition to the major sodium-charged distribution, a second distribution of much smaller intensity that corresponds to proton-charged polymer chains was also observed.

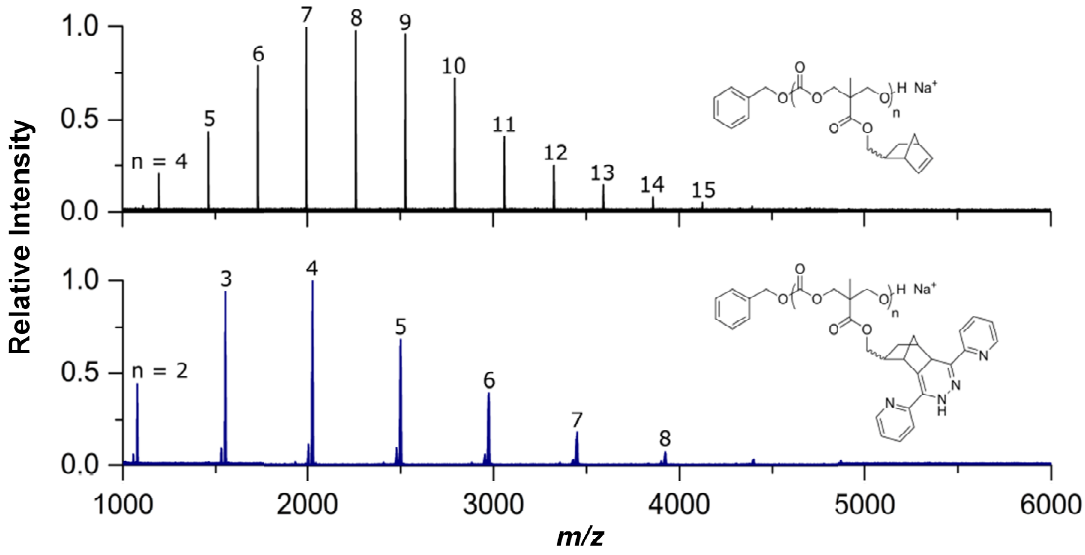

Figure 2.21. MALDI-ToF MS analysis (reflectron mode) of DP 12 norbornene-functional polycarbonate before (**7**) (top) and after (**7c**) (bottom) functionalisation with 3,6-di-2-pyridyl-1,2,4,5-tetrazine.

Table 2.3. Theoretical and observed *m/z* values of dipyridyltetrazine functionalisation.

DP	Experimental *m/z*[a]	Calculated *m/z*
4	2028.0	2027.8
5	2502.3	2502.0
6	2976.6	2976.2
7	3450.9	3450.4

[a]Determined by MALDI-TOF MS analysis using trans-2-[3-(4-*tert*-butylphenyl)-2-methyl-2-propylidene]malonitrile (DCTB) as a matrix, sodium trifluoroacetate as the cationisation agent and PEG monomethyl ether 2k and 5k standards.

2.2.3.3 Post-Polymerisation Functionalisation of Norbornene-Functional Polycarbonates: Norbornene -Thiol Radical Addition

For the radical addition of thiols to the norbornene-functional polycarbonates, a small molecule model reaction was undertaken prior to polymer functionalisation to ensure quantitative conversion of the norbornene groups. A slight excess of 1-dodecanethiol (1.2 equivalents) to 5-norbornene-2-methanol was stirred under UV irradiation (Metalight QX1 lightbox λ = 320 - 400 nm) in the presence of the radical photoinitiator, 2-benzyl-2-(dimethylamino)-4'-morpholinobutyrophenone (0.015 equivalents) (Scheme 2.6) and the reaction followed by ^{1}H NMR spectroscopy. Monitoring the reduction of resonances that correspond to the norbornene double bond at

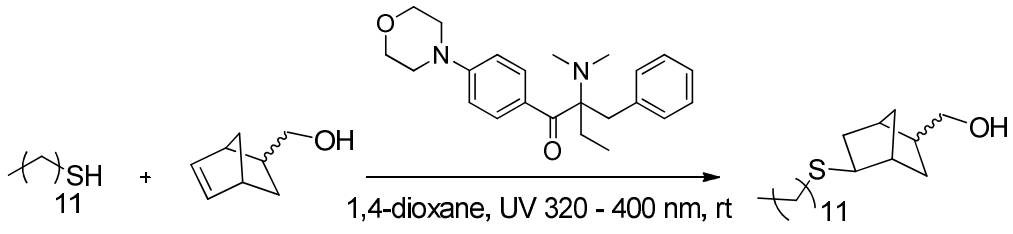

Scheme 2.6. Small molecule model reaction for the norbornene-thiol radical addition.

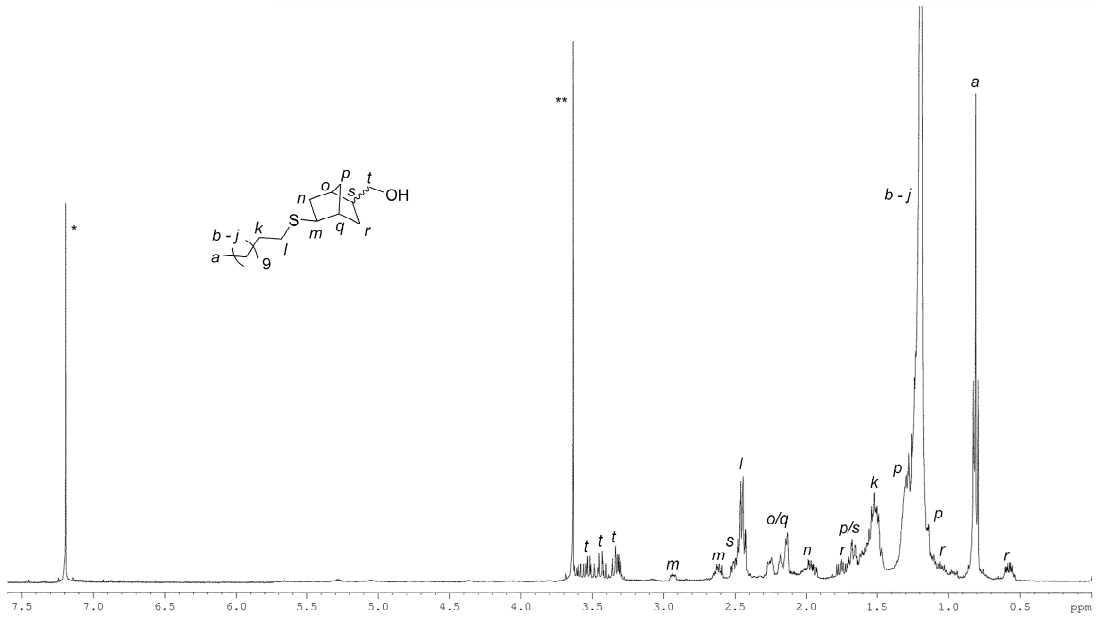

Figure 2.22. ^{1}H NMR spectrum (400 MHz; $CDCl_3$) of 5-norbornene-2-methanol and 1-dodecanethiol conjugation product (*$CHCl_3$, **1,4-dioxane).

δ = 6.11 – 5.91 ppm revealed a conversion of 89% after 30 min and quantitative conversion after 60 min (Figure 2.22).

Utilising these conditions for the analogous modification of norbornene-functional polycarbonates, quantitative conversion of the norbornene groups was confirmed by ^{1}H NMR spectroscopic analysis after 1.5 h of UV irradiation. The modified polymers (**6d** and **7d**) were subsequently precipitated into cold methanol to remove unreacted 1-dodecanethiol before further analysis by ^{1}H NMR spectroscopy, SEC and MALDI-ToF MS. The ^{1}H NMR spectra of the precipitated polymers showed the complete disappearance of the norbornene alkene signals and the appearance of signals that correspond to the addition of 1-dodecanethiol, notably the triplet resonance at δ = 0.88 ppm and quartet resonance at δ = 2.50 ppm arising from the dodecyl chain-end and CH_2 group adjacent to the thioether respectively, as well as additional resonances at δ = 1.26 ppm that correspond to 18 protons of the dodecyl chain (Figure 2.23).

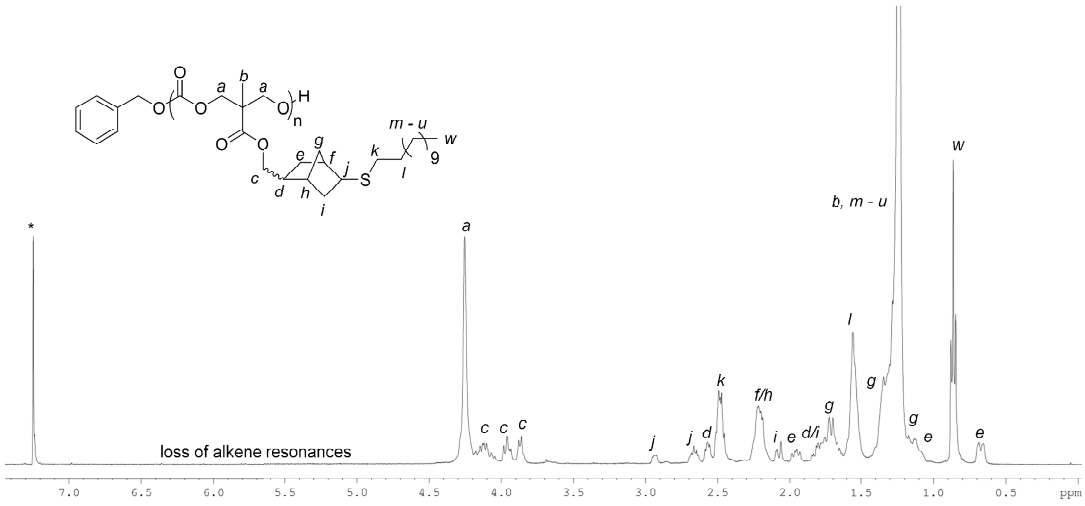

Figure 2.23. ^{1}H NMR spectrum (400 MHz; $CDCl_3$) of DP 100 norbornene-functional polycarbonate after functionalisation with 1-dodecanethiol **6d** (*$CHCl_3$).

MALDI-ToF MS analysis of the DP = 12 modified polymer (**7d**) revealed a single sodium-charged distribution with the expected increase in molecular weight of the repeat unit (m/z = 266 to 468) that corresponds to the addition of 1-dodecanethiol (Figure 2.24 and Table 2.4). SEC analysis of the thiol-ene modified polymers showed an increase in molecular weight from M_n = 24.5 to 39.6 kDa (**6d**, DP = 100) and M_n = 2.8 to 6.0 kDa (**7d**, DP = 12), while again retaining low dispersity values ($Đ_M$ = 1.18 and 1.13) (Figure 2.25).

Table 2.4. Theoretical and observed m/z values of 1-dodecanethiol functionalisation.

DP	Experimental m/z[a]	Calculated m/z
6	2940.9	2940.8
7	3409.4	3409.1
8	3877.6	3877.4
9	4346.2	4345.7

[a]Determined by MALDI-TOF MS analysis using trans-2-[3-(4-*tert*-butylphenyl)-2-methyl-2-propylidene]malonitrile (DCTB) as a matrix, sodium trifluoroacetate as the cationisation agent and PEG monomethyl ether 2k and 5k standards.

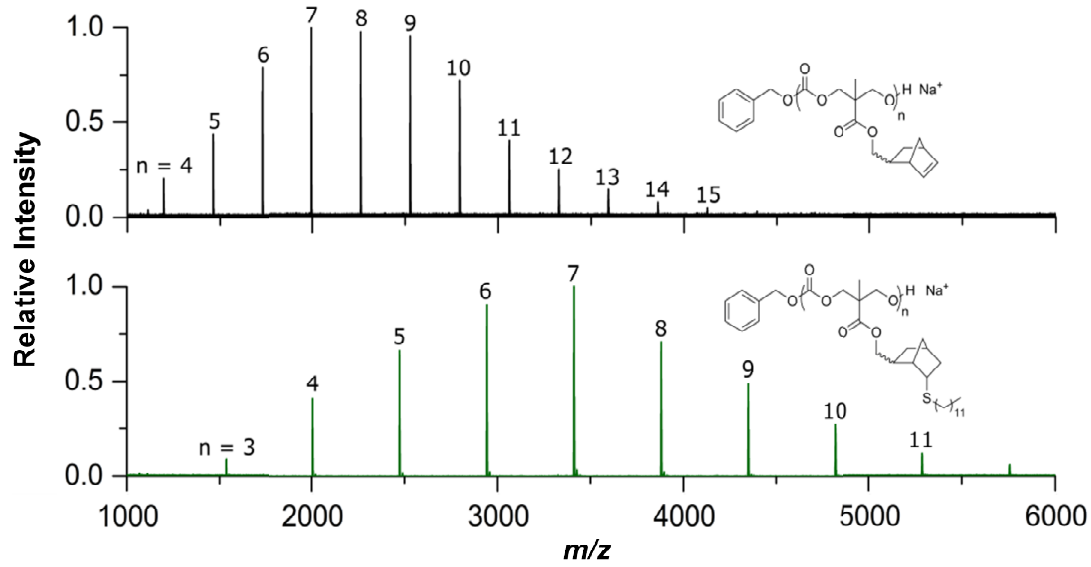

Figure 2.24. MALDI-ToF MS analysis (reflectron mode) of DP 12 norbornene-functional polycarbonate before (**7**) (top) and after (**7d**) (bottom) functionalisation with 1-dodecanethiol.

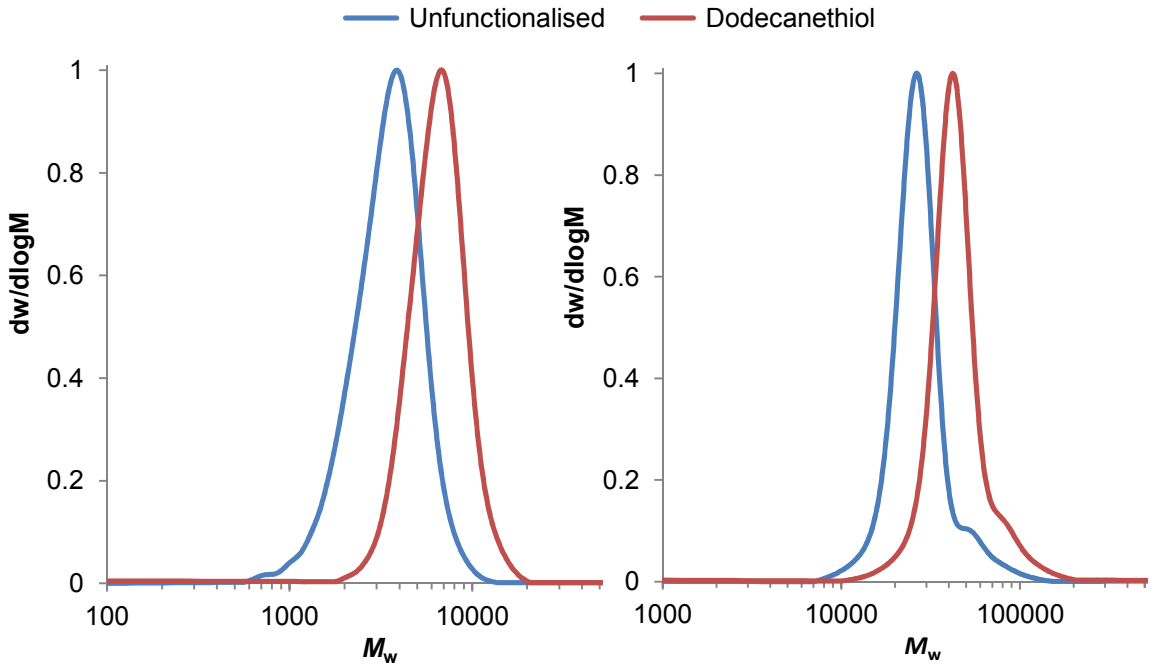

Figure 2.25. (Left) SEC chromatograms of DP 12 norbornene-functional polycarbonate before (**7**, M_n = 2.8 kDa, $Đ_M$ = 1.21) and after functionalisation with dodecanethiol (**7d**, M_n = 6.0 kDa, $Đ_M$ = 1.13). (Right) SEC chromatograms of DP 100 norbornene-functional polycarbonate before (**6**, M_n = 24.5 kDa, $Đ_M$ = 1.14) and after functionalisation with dodecanethiol (**6d**, M_n = 39.6 kDa, $Đ_M$ = 1.18).

The radical thiol-ene addition of the fluorescent thiol 7-mercapto-4-methylcoumarin to polycarbonate **7** (DP = 12) was also investigated. Quantitative conversion of the norbornene groups was achieved after 1.5 h of UV irradiation, as confirmed by ^{1}H NMR spectroscopic analysis which revealed the complete loss of norbornene double bond signals. The appearance of resonances that correspond to the coumarin moiety were also observed by ^{1}H NMR spectroscopy; namely the three aromatic resonances between δ = 7.69 – 7.09 ppm, the vinyl resonance at δ = 6.11 ppm and the methyl resonance at δ = 2.31 ppm (Figure 2.26). Comparison of the UV-vis spectra of the polymer before (**7**) and after (**7e**) modification showed the appearance of a peak with an absorbance maximum at 335 nm, consistent with the successful addition of the fluorescent thiol to the polymer chain (Figure 2.27). The molecular weight distribution of the polymer remained narrow after functionalisation ($Đ_M$ =1.30),

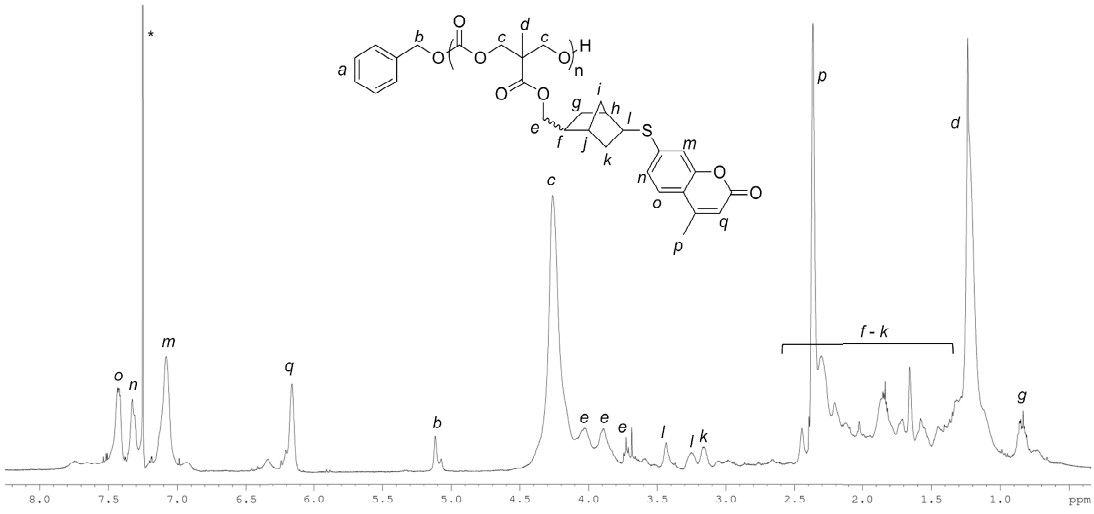

Figure 2.26. ^{1}H NMR spectrum (400 MHz; $CDCl_3$) of DP 12 norbornene-functional polycarbonate after functionalisation with 7-mercapto-4-methylcoumarin, **7e** (*$CHCl_3$).

with an increase in molecular weight from M_n = 2.8 to 4.7 kDa observed by SEC analysis (Figure 2.28).

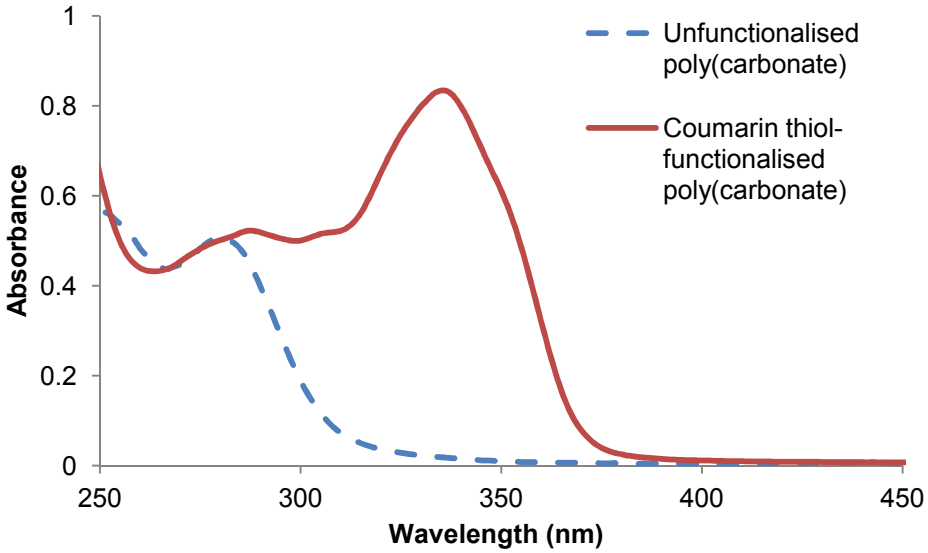

Figure 2.27. UV-vis spectra of norbornene-functional polycarbonate before (**7**) (blue dashed) and after (**7e**) (red solid) functionalisation with 7-mercapto-4-methylcoumarin (spectra recorded in dichloromethane).

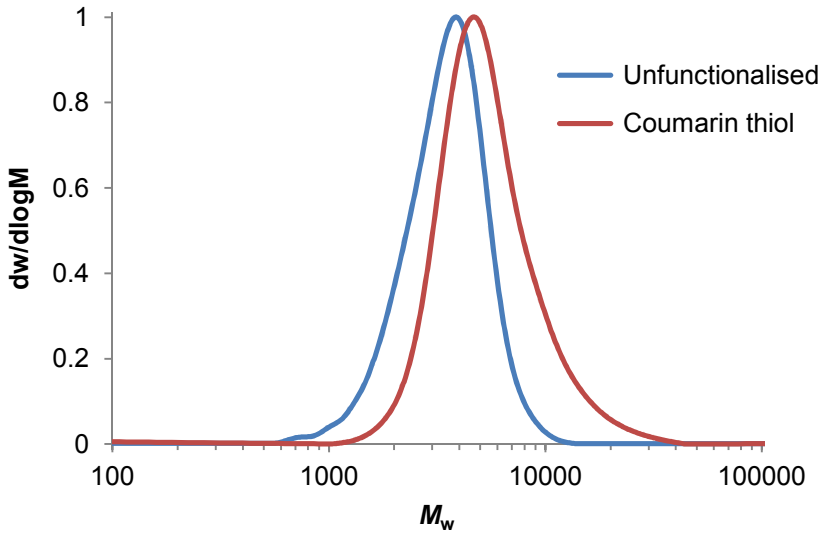

Figure 2.28. SEC chromatogram of DP 12 norbornene-functional polycarbonate before (**7**, M_n = 2.8 kDa, $Đ_M$ = 1.21) and after functionalisation with 7-mercapto-4-methylcoumarin (**7e**, M_n = 4.7 kDa, $Đ_M$ = 1.30).

2.2.4 One-Pot, Multi-Step, Orthogonal Functionalisation of Norbornene-Functional Polycarbonates

Following the success of the individual post-polymerisation functionalisation reactions, a sequential multi-step, one-pot triple functionalisation strategy was investigated (Scheme 2.7). Functional reagents were chosen that would be easily distinguishable by ^{1}H NMR spectroscopy, namely TEG azide, 3,6-di-2-pyridyl-1,2,4,5-tetrazine and 1-dodecanethiol. As the least efficient reaction, the norbornene-azide cycloaddition was undertaken first. A norbornene-functional polycarbonate of DP 35 (**8**, M_n = 9.5 kDa, $Đ_M$ = 1.12) was heated at 90 °C for 1 h in the presence of 10 equivalents of TEG azide, after which ^{1}H NMR spectroscopy revealed that *ca*. 30% of the norbornene groups had undergone reaction. The reaction was cooled to room temperature before the addition of 0.5 equivalents of dipyridyltetrazine per remaining norbornene group. The reaction was then stirred at room temperature for 4 h until the solution lost its pink colour, indicating the complete consumption of tetrazine units. Finally, an excess of 1-dodecanethiol (3 equivalents per remaining norbornene group) and

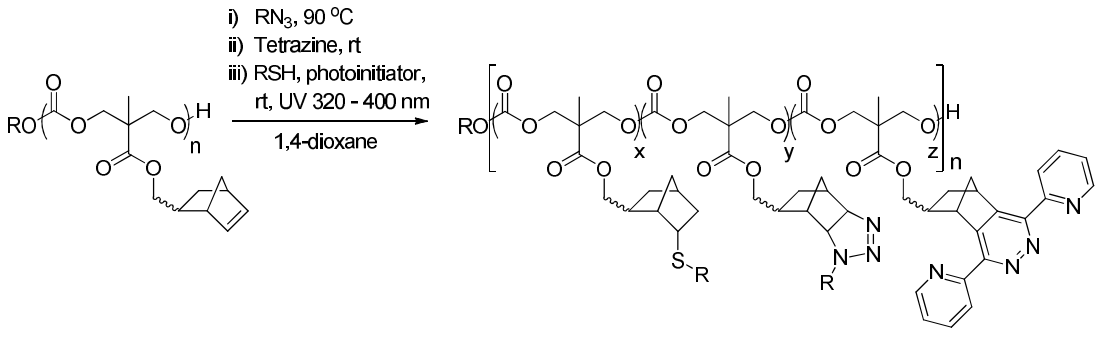

Scheme 2.7. One-pot functionalisation of norbornene-functional polycarbonates.

the radical photoinitiator, 2-benzyl-2-(dimethylamino)-4'-morpholinobutyrophenone, were added to the reaction mixture which was subsequently irradiated with UV light for 2 h. Control experiments in which the tetrazine-norbornene and thiol-norbornene functionalisations were performed in the presence of an excess of TEG azide, confirmed that the presence of unreacted TEG azide did not interfere with subsequent functionalisations, in the one-pot multi-functionalisation reaction. SEC analysis of the crude reaction mixture after each functionalisation step revealed that the molecular weight distribution of the polymer remained narrow and monomodal throughout the reaction, with an overall increase in molecular weight from 9.5 to 12.2 kDa and final $Đ_M$ value of 1.14 (Figure 2.29).

The one-pot orthogonally functionalised polymer was purified by precipitation into hexane. The ^{1}H NMR spectrum of the precipitated polymer showed resonances that correspond to all three functional groups, specifically the aromatic resonances between δ = 9.32 – 7.21 ppm from reaction with

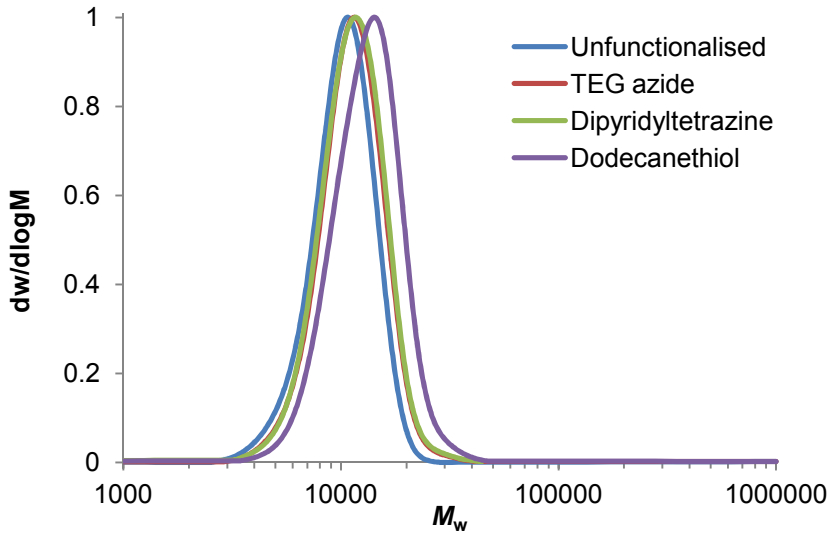

Figure 2.29. SEC chromatograms of DP 35 norbornene-functional polycarbonate after sequential modification with TEG azide, 3,6-di-2-pyridyl-1,2,4,5-tetrazine and 1-dodecanethiol.

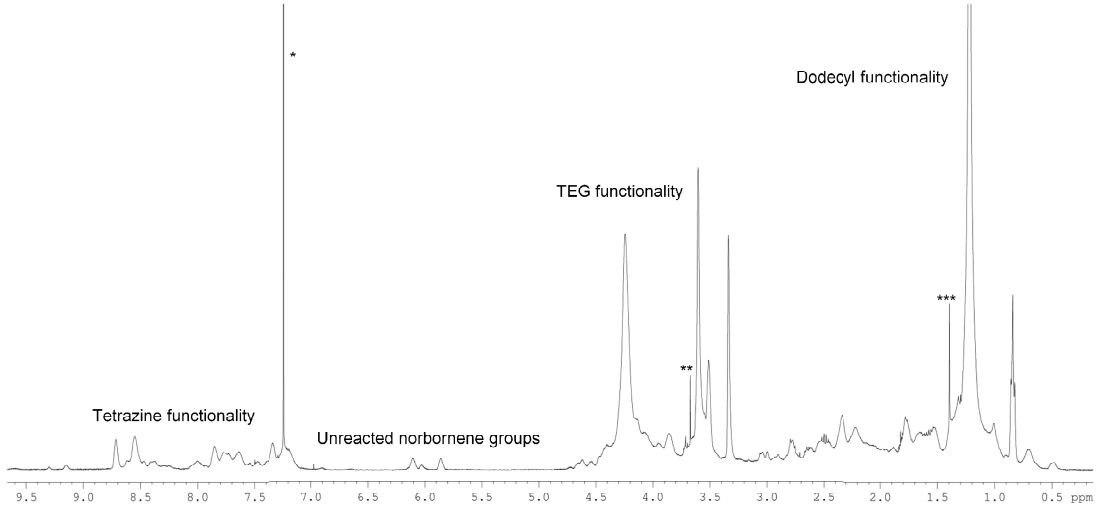

Figure 2.30. ^{1}H NMR spectrum (400 MHz; $CDCl_3$) of DP 35 multi-functionalised polycarbonate after sequential modification with TEG azide, 3,6-di-2-pyridyl-1,2,4,5-tetrazine and 1-dodecanethiol (*$CHCl_3$, **1,4-dioxane ***H_2O).

dipyridyltetrazine, the three resonances at δ = 3.62, 3.53 and 3.36 ppm that correspond to the TEG functionality and the significant increase in integral of the peak at δ = 1.24 ppm and the appearance of a triplet resonance at δ = 0.86 ppm as a consequence of the incorporation of 1-dodecanethiol (Figure 2.30). Despite using an excess of 1-dodecanethiol in the final thiol-ene step, ^{1}H NMR spectroscopic analysis also revealed a small proportion of unmodified norbornene groups (*ca*. 9%). This was thought to be caused by the reduced accessibility of the norbornene groups, as a consequence of the introduction of multiple functionalities preventing complete functionalisation. Increasing the equivalents of 1-dodecanethiol employed and extending the period of UV irradiation did not lead to an increase in norbornene conversion. The final purified polymer consisted of 30% TEG functionality, 35% tetrazine functionality, 26% dodecyl functionality and 9% unreacted norbornene functionality, as determined by ^{1}H NMR spectroscopy.

To demonstrate the versatility of the one-pot multi-functionalisation reaction, the order of functionalisation of a shorter DP 12 (**7**) norbornene-functional polycarbonate was changed to 3,6-di-2-pyridyl-1,2,4,5-tetrazine, 1-dodecanethiol and TEG azide. Again, ^{1}H NMR spectroscopic analysis of the resulting multi-functional polymer confirmed the successful incorporation of all three functionalities, however, for this order of functionalisation a higher proportion of norbornene functionality, *ca.* 20%, remained unreacted. This reduced reactivity was attributed to performing the least efficient functionalisation reaction last. SEC analysis of the crude polymer after each functionalisation step revealed that the molecular weight distribution of the polymer remained narrow and monomodal at each stage of the reaction giving a final dispersity value of 1.24 (Figure 2.31). The versatility of the one-pot functionalisation was further demonstrated by changing the thiol and azide to 7-mercapto-4-methylcoumarin and benzyl azide respectively (Figure 2.32).

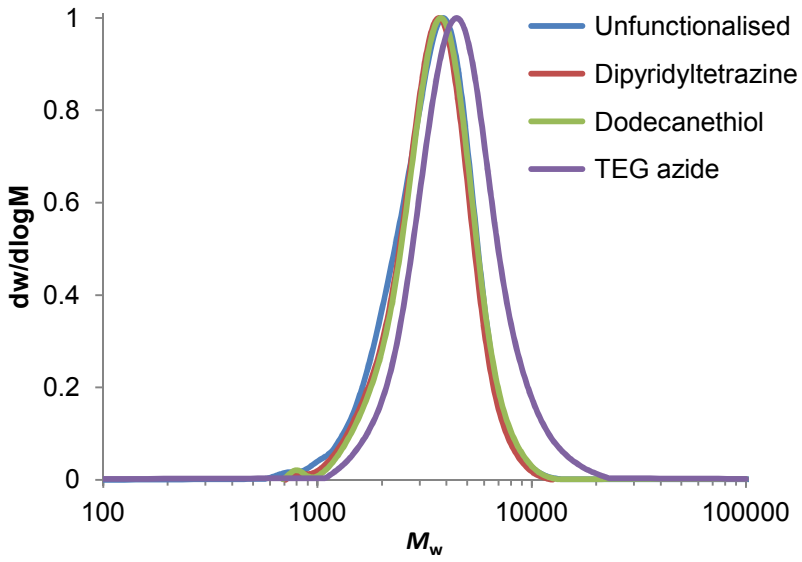

Figure 2.31. SEC chromatograms of a DP 12 norbornene-functional polycarbonate after sequential modification with 3,6-di-2-pyridyl-1,2,4,5-tetrazine, 1-dodecanethiol and TEG azide.

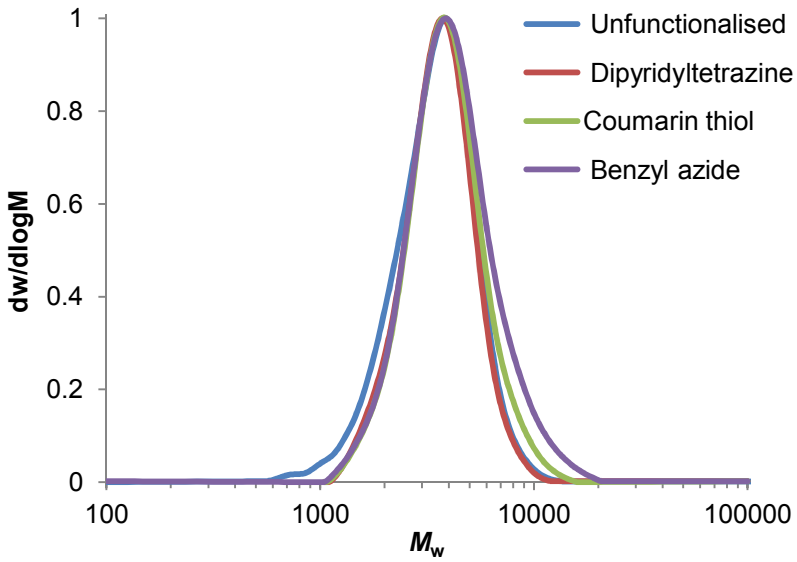

Figure 2.32. SEC chromatograms of a DP 12 norbornene-functional polycarbonate after sequential modification with 3,6-di-2-pyridyl-1,2,4,5-tetrazine, 7-mercapto-4-methylcoumarin and benzyl azide.

2.2.5 Graft Copolymer Synthesis

To further demonstrate the potential utility of the norbornene-functional polycarbonates, the preparation of graft copolymers *via* radical thiol-ene chemistry was investigated. Thiol-terminated poly(*N*-isopropylacrylamide) (poly(NiPAm)) was synthesised in two steps *via* reversible addition-fragmentation chain transfer (RAFT) polymerisation and subsequent reduction of the RAFT CTA end-group to a thiol, before grafting to a norbornene-functional polycarbonate.

2.2.5.1 Graft Copolymer Synthesis: Poly(NiPAm) Synthesis

RAFT polymerisations of NiPAm were conducted at 65 °C in 1,4-dioxane, where 1-dodecyl-S'-(α,α'-dimethyl-α''-acetic acid) trithiocarbonate (DDMAT) was employed as the RAFT chain transfer agent (CTA) and [CTA]:[AIBN] = 1:0.1.

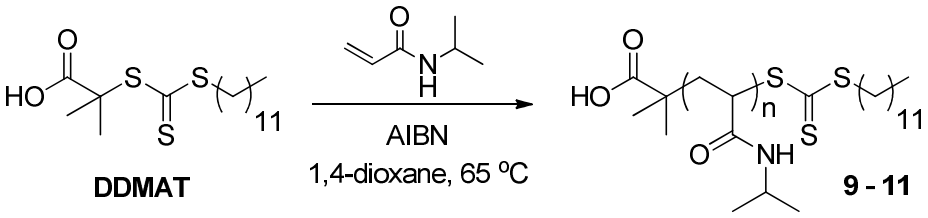

Scheme 2.8. RAFT polymerisation of *N*-isopropylacrylamide.

Polymerisations were terminated at *ca.* 80% monomer conversion to ensure high RAFT end-group fidelity and precipitated twice in cold diethyl ether to remove unreacted NiPAm. The DP of the polymers was determined by ^{1}H NMR spectroscopy, by comparing the integrals of the resonances arising from the RAFT end-group, notably the quartet resonance at δ = 3.32 ppm and triplet resonance at δ = 0.86 ppm that correspond to the CH_3 group of the dodecyl chain-end and CH_2 group adjacent to the trithiocarbonate, with the resonances of the isopropyl group of the NiPAm repeat unit at δ = 3.99 and 1.12 ppm (Figure 2.33). The ^{1}H NMR spectra of the precipitated polymers also showed resonances that correspond to the NH amide proton at δ = 7.2 – 5.8 ppm and poly(NiPAm) backbone at δ = 2.4 - 1.5 ppm. Poly(NiPAm) with a range of molecular weights was prepared by varying the CTA-to-monomer ratio and a strong correlation was found between DP and theoretical values of DP based on NiPAm conversion, indicating the polymerisations were well controlled. This control was further confirmed by SEC analysis, which revealed narrow, monomodal molecular weight distributions with low dispersity values ($Đ_M$ < 1.1) (Figure 2.34 and Table 2.5). SEC analysis with UV detection at 309 nm exhibited a strong response further confirming the presence of the trithiocarbonate RAFT end-groups.

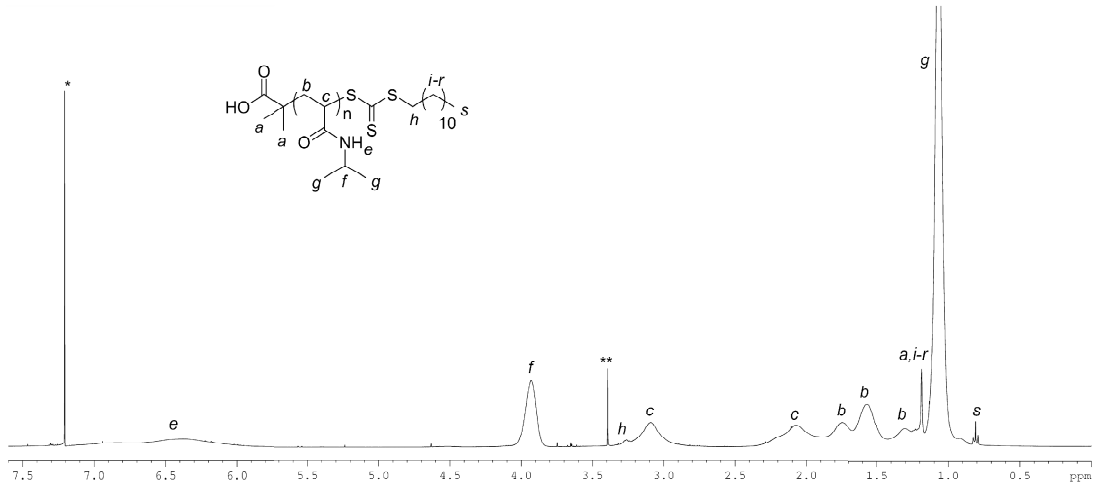

Figure 2.33. ^{1}H NMR spectrum (400 MHz; $CDCl_3$) of poly(NiPAm)$_{78}$, **10**, (*$CHCl_3$, **1,4-dioxane).

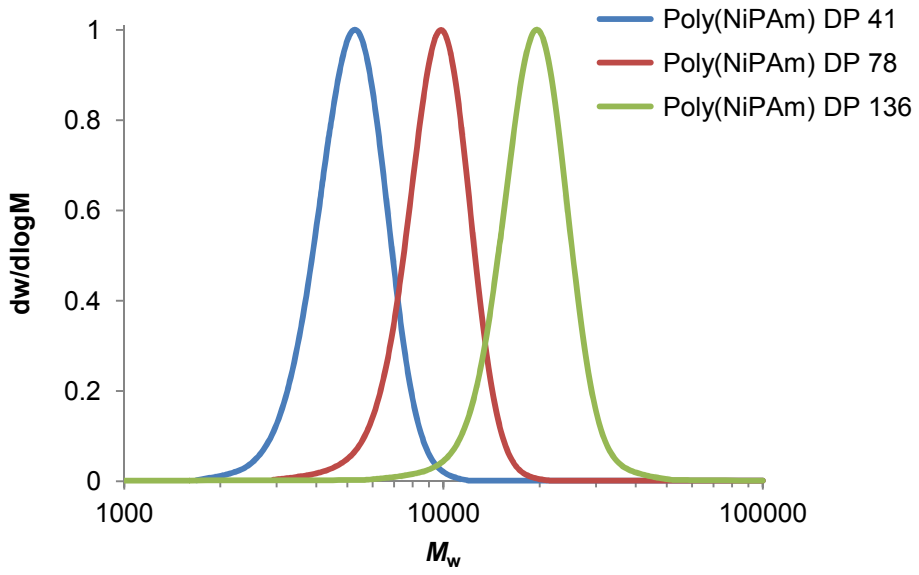

Figure 2.34. SEC chromatograms of poly(NiPAm) (**9**, DP = 41, M_n = 4.9 kDa, $Đ_M$ = 1.07), (**10**, DP = 78, M_n = 9.1 kDa, $Đ_M$ = 1.07), (**11**, DP = 136, M_n = 18.4, $Đ_M$ = 1.07).

Table 2.5. Characterisation of poly(NiPAm).

Polymer	DP[a]	M_n(NMR) (kDa)[a]	M_n(SEC) (kDa)[b]	$Đ_M$[b]
9	41	5.0	4.9	1.07
10	78	9.2	9.1	1.07
11	136	15.8	18.4	1.07

[a]Determined by ^{1}H NMR spectroscopy. [b]Determined by SEC analysis in DMF using PMMA standards.

2.2.5.2 Graft Copolymer Synthesis: End-Group Modification of Poly(NiPAm)

The thiocarbonyl end-group of polymers prepared by RAFT polymerisation is inherently reactive and provides the opportunity for ready modification, in particular; end-group thermolysis, radical induced reduction, reaction with nucleophiles and hetero-Diels-Alder reactions.[51, 52] The transformation of the thiocarbonyl end-group to a thiol, by reaction with excess amine or other reducing agents, is well-known and has been utilised for the preparation of cyclic,[53] multi-block[53] and star polymers,[54] polymer stabilised metal particles[55] and polymer bio-conjugates,[56, 57] among other applications.

Reduction of the poly(NiPAm) trithiocarbonate end-groups was achieved using an excess of hydrazine (20 equivalents per RAFT CTA group), under a nitrogen

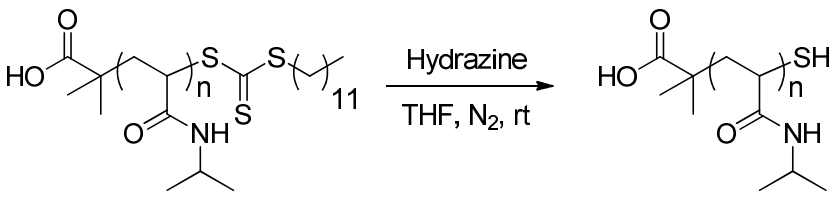

Scheme 2.9. Reduction of the trithiocarbonate end-group of poly(NiPAm) to a thiol.

atmosphere to minimise the occurrence of disulfide coupling (Scheme 2.9).[58] A degassed solution of hydrazine in THF was added to a degassed solution of poly(NiPAm) and stirred at room temperature for 2 h, during which time the solution lost the characteristic yellow colour of the trithiocarbonate end-group. SEC analysis of the thiol-terminated polymers using UV detection at 309 nm revealed no signal suggesting quantitative reduction of the RAFT end-groups (Figure 2.35). SEC analysis with refractive index detection, however, showed a slight broadening of dispersity ($Đ_M$ = 1.10) and the appearance of a small high molecular weight shoulder suggesting that a small proportion of polymer chains had undergone disulfide coupling (Figure 2.36). The ^{1}H NMR spectra of thiol-terminated poly(NiPAm) revealed the reduction of resonances that correspond to the RAFT end-group, most notably the triplet resonance at δ = 0.86 ppm that arises from the CH_3 protons of the dodecyl chain-end and the multiplet at δ = 1.25 ppm that corresponds to resonances from the dodecyl chain (Figure 2.37).

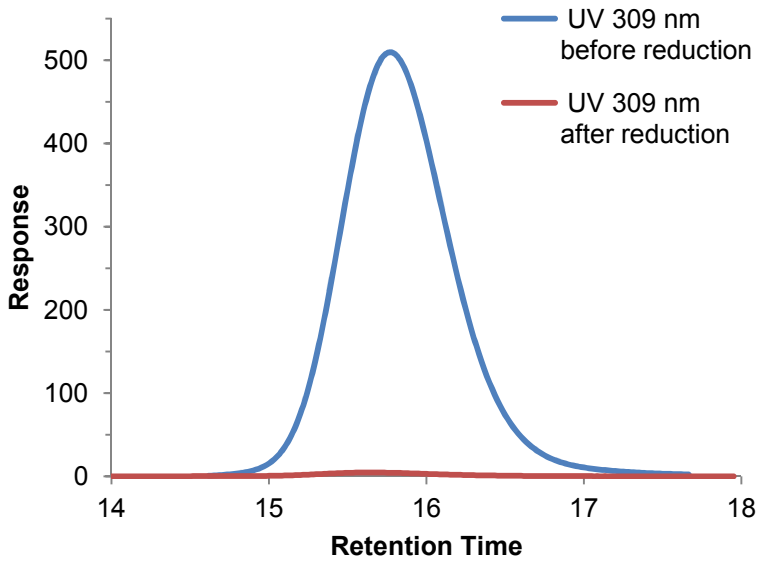

Figure 2.35. SEC chromatograms with UV detection at 309 nm showing poly(NiPAm)$_{78}$ before (**10**) and after reduction (**10**$_{\text{-SH}}$) with hydrazine.

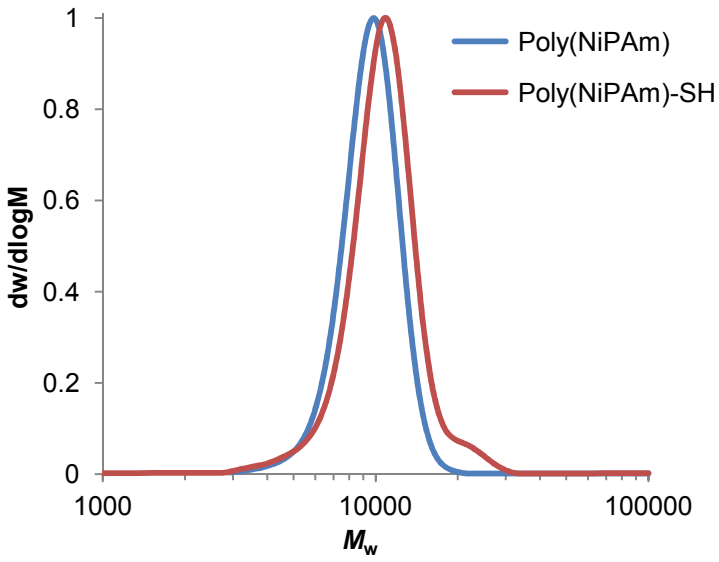

Figure 2.36. SEC chromatograms showing poly(NiPAm)$_{78}$ before (**10**, M_n = 9.1 kDa, $Đ_M$ = 1.07) and after (**10**$_{\mathbf{SH}}$, M_n = 10.0 kDa, $Đ_M$ = 1.10) reduction with hydrazine.

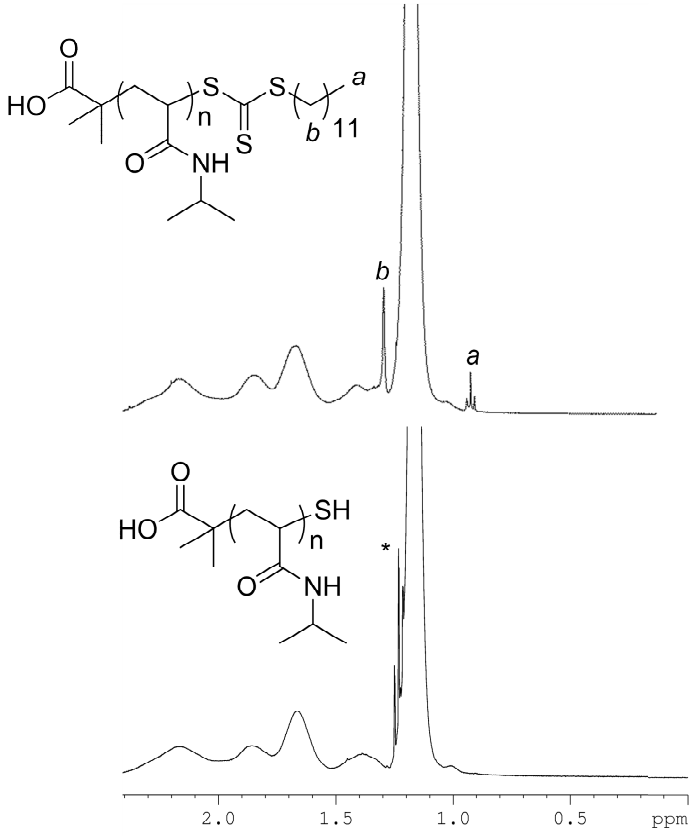

Figure 2.37. Expansion (δ = 2.4 – 0.0 ppm) of ^{1}H NMR spectra (400 MHz; $CDCl_3$) of poly(NiPAm)$_{78}$ (**10**) before and after reduction with hydrazine (*diethyl ether).

2.2.5.3 Graft Copolymer Synthesis: Thiol-Ene Polymer Grafting

Initial studies of the radical thiol-ene coupling of thiol-terminated poly(NiPAm) to a norbornene-functional polycarbonate (DP = 35) (**8**, M_n = 9.5 kDa, $Đ_M$ = 1.12) were undertaken using the same conditions employed for the analogous small molecule radical thiol-ene functionalisations; namely 1.2 equivalents of thiol end-group per pendent norbornene and 0.015 equivalents of radical photoinitiator, stirred under UV irradiation (Scheme 2.10). The reaction solvent was changed from 1,4-dioxane to tetrahydrofuran to increase the solubility of poly(NiPAm) and reactions were performed at a concentration of 10 mg of polycarbonate per 1 mL of THF. Aliquots of the reaction solution were taken periodically and analysed by ^{1}H NMR spectroscopy and SEC. For the grafting of the lowest molecular weight poly(NiPAm) (**9**$_{\text{-SH}}$, M_n = 4.9 kDa, DP = 41) to the norbornene-functional polycarbonate, SEC analysis of the reaction mixture after 9 h of UV irradiation showed no change suggesting either no or minimal grafting had occurred. The ^{1}H NMR spectrum at this time still clearly showed the norbornene double bond signals at δ = 6.15 – 5.91 ppm, however it was not possible to integrate these peaks to determine conversion as the

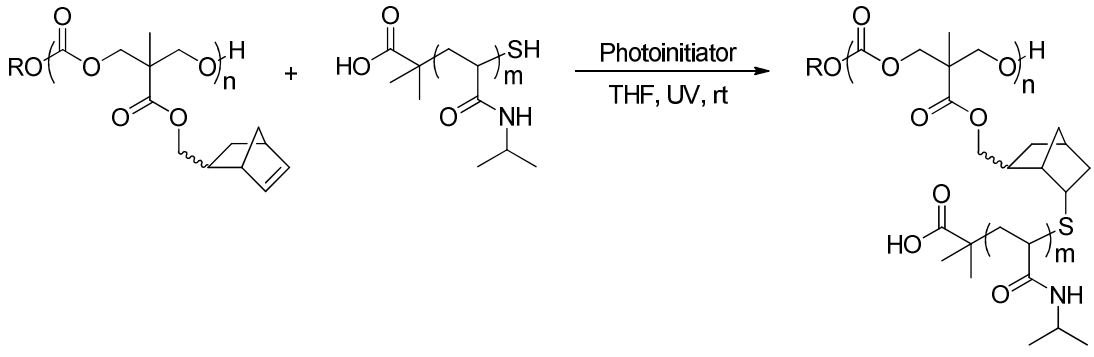

Scheme 2.10. Polycarbonate-*g*-poly(NiPAm) synthesis by radical thiol-ene chemistry.

resonances were obscured by those of much greater intensity that correspond to the NH group of poly(NiPAm) at δ = 7.2 – 5.8 ppm.

In an attempt to improve the grafting reaction, the amount of radical photoinitiator used was increased to 0.05 equivalents, however, no improvement in grafting was observed by SEC analysis. Finally, the equivalents of thiol-terminated poly(NiPAm) were increased to 5 polymer chains per norbornene group. After 9 h of UV irradiation, SEC analysis revealed the appearance of a new polymer distribution at higher molecular weight (M_n = 23.4 kDa) that may correspond to graft copolymer (Figure 2.38). A large excess of unreacted poly(NiPAm) was also observed, as well as a slight increase in the proportion of disulfide coupled polymer chains. Again, the grafting efficiency could not be determined by ^{1}H NMR spectroscopy as a consequence of the significant overlap of resonances that correspond to norbornene double bond and poly(NiPAm) NH functionality. However, as a large proportion of the

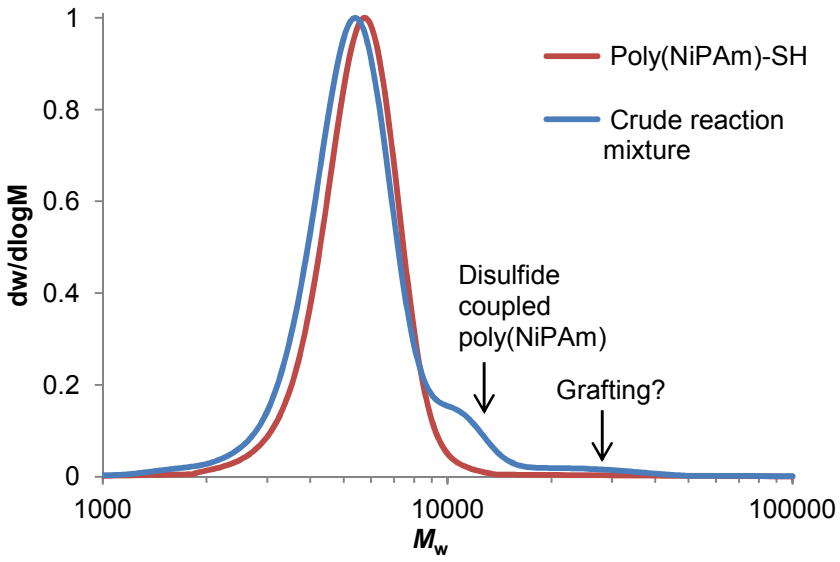

Figure 2.38. SEC chromatogram of crude reaction sample of norbornene-functional polycarbonate and thiol terminated poly(NiPAm) grafting by radical thiol-ene chemistry and SEC chromatogram of polyNiPAm$_{41}$-SH (**9-$_{SH}$**)before reaction.

norbornene peaks remained present in the ^{1}H NMR spectra, it was concluded that only a low grafting efficiency was achieved.

The limited success of graft copolymer synthesis through thiol-ene coupling compared to the highly successful small molecule polymer functionalisations is not surprising. A slower rate of coupling and lower coupling yields are expected for polymer grafting as a consequence of the use of bulky polymeric thiols, where access to the thiol end-group maybe obstructed by the surrounding polymer or where successful polymer coupling may prevent further grafting reactions through the blocking of unreacted norbornene groups. As a consequence of lower conjugation efficiency in polymeric systems, side reactions become more significant, notably disulfide formation between two polymeric thiol groups, through oxidation or coupling of thiyl radicals, as well as other bimolecular termination reactions. Increasing the concentration of photoinitiator, hence increasing the radical flux, may in fact increase the occurrence of such radical termination side reactions. In combination with the added difficulty of removing unreacted excess polymer, increasing the equivalents of polymeric thiol may also increase the likelihood of disulfide coupling. Based on these findings it was concluded that the use of radical thiol-ene coupling to prepare graft copolymers is not a viable approach. Similar findings have been previously reported by Du Prez and Van Camp on the use of radical thiol-ene polymer-polymer coupling to prepare poly(styrene)-poly(vinyl acetate) block copolymers.[59] Thiol-terminated poly(styrene) was prepared by sequential RAFT polymerisation and aminolysis, whereas allyl-terminated poly(vinyl acetate) was prepared from an allyl-functional RAFT chain transfer agent. Thiol-ene polymer-polymer coupling reactions were performed under

UV irradiation in the presence of the radical photoinitiator, 2,2-dimethoxy-2-phenylacetophenone. When the poly(styrene) and poly(vinyl acetate) were reacted in equimolar quantities a low coupling efficiency of approximately 25% was found by ^{1}H NMR spectroscopy and elemental analysis. Increasing the equivalents of either thiol-terminated poly(styrene) or allyl-terminated poly(vinyl acetate) to a fivefold excess did not improve the coupling efficiency and evidence of competitive side reactions, namely bimolecular termination reactions, were also reported.

2.3 Conclusions

In conclusion, a novel cyclic carbonate monomer bearing a norbornene pendent group has been synthesised and its controlled ring-opening polymerisation demonstrated using an organocatalyst system, comprised of 1 mol% 1,8-diazabicycloundec-7-ene (DBU) and 5 mol% 1-(3,5-bis(trifluoromethyl)phenyl) -3-cyclohexylthiourea. The resulting polymers were well-defined and exhibited low dispersity values and monomodal molecular weight distributions. Subsequently, the norbornene-functional polycarbonates were utilised in a new approach for the synthesis of multi-functionalised polymers, where a single polymeric scaffold containing a reactive handle, in this case norbornene functionality, can undergo multiple post-polymerisation modifications both individually and sequentially in an orthogonal one-pot process. Quantitative polymer functionalisation was demonstrated for the 1,3-dipolar cycloaddition between norbornenes and azides, the inverse electron demand Diels-Alder reaction between norbornenes and tetrazines and the radical addition of thiols to norbornenes when the functionalisations were performed individually. Up to 90% functionalisation was achieved when functionalisations were undertaken sequentially on the same polycarbonate backbone, where the versatility of the one-pot multi-functionalisation reaction was shown through variation of functionalisation order. This approach creates a new platform for the preparation of complex multifunctional materials, where an extensive library of functionalised polymers can be prepared by simply varying the combinations and relative proportions of functional reactants, in an undemanding one-pot multi-step process. For example, the physical properties of a polymer may be changed by the introduction of hydrophilic and responsive functionalities,

whilst also tagging polymers with fluorescent or biologically relevant molecules. The norbornene-functional polycarbonates were also employed in the preparation of graft copolymers through radical thiol-ene coupling with thiol terminated poly(NiPAm), however this grafting onto approach showed only limited success.

2.4 References

1. P. L. Golas and K. Matyjaszewski, *Chem. Soc. Rev.*, 2010, **39**, 1338-1354.
2. C. E. Hoyle, A. B. Lowe and C. N. Bowman, *Chem. Soc. Rev.*, 2010, **39**, 1355-1387.
3. R. K. Iha, K. L. Wooley, A. M. Nyström, D. J. Burke, M. J. Kade and C. J. Hawker, *Chem. Rev.*, 2009, **109**, 5620-5686.
4. M. A. Gauthier, M. I. Gibson and H.-A. Klok, *Angew. Chem. Int. Ed.*, 2009, **48**, 48-58.
5. W. H. Binder and R. Sachsenhofer, *Macromol. Rapid Commun.*, 2007, **28**, 15-54.
6. A. S. Goldmann, M. Glassner, A. J. Inglis and C. Barner-Kowollik, *Macromol. Rapid Commun.*, 2013, **34**, 810-849.
7. K. A. Günay, P. Theato and H.-A. Klok, *J. Polym. Sci., Part A: Polym. Chem.*, 2012, **51**, 1-28.
8. C.-H. Wong and S. C. Zimmerman, *Chem. Commun.*, 2013, **49**, 1679-1695.
9. M. Malkoch, R. J. Thibault, E. Drockenmuller, M. Messerschmidt, B. Voit, T. P. Russell and C. J. Hawker, *J. Am. Chem. Soc.*, 2005, **127**, 14942-14949.
10. K. Nilles and P. Theato, *J. Polym. Sci., Part A: Polym. Chem.*, 2010, **48**, 3683-3692.
11. M. Schaefer, N. Hanik and A. F. M. Kilbinger, *Macromolecules*, 2012, **45**, 6807-6818.
12. J. M. Spruell, M. Wolffs, F. A. Leibfarth, B. C. Stahl, J. Heo, L. A. Connal, J. Hu and C. J. Hawker, *J. Am. Chem. Soc.*, 2011, **133**, 16698-16706.
13. S. K. Yang and M. Weck, *Macromolecules*, 2007, **41**, 346-351.

14. R. C. Pratt, F. Nederberg, R. M. Waymouth and J. L. Hedrick, *Chem. Commun.*, 2008, 114-116.

15. D. P. Sanders, K. Fukushima, D. J. Coady, A. Nelson, M. Fujiwara, M. Yasumoto and J. L. Hedrick, *J. Am. Chem. Soc.*, 2010, **132**, 14724-14726.

16. X. Hu, X. Chen, S. Liu, Q. Shi and X. Jing, *J. Polym. Sci., Part A: Polym. Chem.*, 2008, **46**, 1852-1861.

17. S. Tempelaar, L. Mespouille, P. Dubois and A. P. Dove, *Macromolecules*, 2011, **44**, 2084-2091.

18. C.-F. Wang, Y.-X. Lin, T. Jiang, F. He and R.-X. Zhuo, *Biomaterials*, 2009, **30**, 4824-4832.

19. D. M. Stevens, S. Tempelaar, A. P. Dove and E. Harth, *ACS Macro Lett.*, 2012, **1**, 915-918.

20. S. Onbulak, S. Tempelaar, R. J. Pounder, O. Gok, R. Sanyal, A. P. Dove and A. Sanyal, *Macromolecules*, 2012, **45**, 1715-1722.

21. W. Chen, H. Yang, R. Wang, R. Cheng, F. Meng, W. Wei and Z. Zhong, *Macromolecules*, 2009, **43**, 201-207.

22. R. Wang, W. Chen, F. Meng, R. Cheng, C. Deng, J. Feijen and Z. Zhong, *Macromolecules*, 2011, **44**, 6009-6016.

23. C. Lu, Q. Shi, X. Chen, T. Lu, Z. Xie, X. Hu, J. Ma and X. Jing, *J. Polym. Sci., Part A: Polym. Chem.*, 2007, **45**, 3204-3217.

24. Q. Shi, X. Chen, T. Lu and X. Jing, *Biomaterials*, 2008, **29**, 1118-1126.

25. S. Tempelaar, I. A. Barker, V. X. Truong, D. J. Hall, L. Mespouille, P. Dubois and A. P. Dove, *Polym. Chem.*, 2013, **4**, 174-183.

26. J. Xu, F. Prifti and J. Song, *Macromolecules*, 2011, **44**, 2660-2667.

27. X. Zhang, Z. Zhong and R. Zhuo, *Macromolecules*, 2011, **44**, 1755-1759.

28. N. B. Cramer, S. K. Reddy, A. K. O'Brien and C. N. Bowman, *Macromolecules*, 2003, **36**, 7964-7969.

29. C. E. Hoyle and C. N. Bowman, *Angew. Chem. Int. Ed.*, 2010, **49**, 1540-1573.

30. T. M. Roper, C. A. Guymon, E. S. Jönsson and C. E. Hoyle, *J. Polym. Sci., Part A: Polym. Chem.*, 2004, **42**, 6283-6298.

31. A. Dondoni, *Angew. Chem. Int. Ed.*, 2008, **47**, 8995-8997.

32. R. A. Carboni and R. V. Lindsey, *J. Am. Chem. Soc.*, 1959, **81**, 4342-4346.

33. N. K. Devaraj, R. Weissleder and S. A. Hilderbrand, *Bioconjugate Chem.*, 2008, **19**, 2297-2299.

34. C. F. Hansell, P. Espeel, M. M. Stamenović, I. A. Barker, A. P. Dove, F. E. Du Prez and R. K. O'Reilly, *J. Am. Chem. Soc.*, 2011, **133**, 13828-13831.

35. J. Schoch, M. Wiessler and A. Jäschke, *J. Am. Chem. Soc.*, 2010, **132**, 8846-8847.

36. C. F. Hansell and R. K. O'Reilly, *ACS Macro Lett.*, 2012, **1**, 896-901.

37. A.-C. Knall and C. Slugovc, *Chem. Soc. Rev.*, 2013, **42**, 5131-5142.

38. K. Gutsmiedl, C. T. Wirges, V. Ehmke and T. Carell, *Org. Lett.*, 2009, **11**, 2405-2408.

39. R. Huisgen, *Angew. Chem. Int. Ed.*, 1963, **2**, 565-598.

40. R. Huisgen, P. H. J. Ooms, M. Mingin and N. L. Allinger, *J. Am. Chem. Soc.*, 1980, **102**, 3951-3953.

41. E. Kaya, M. Vrabel, C. Deiml, S. Prill, V. S. Fluxa and T. Carell, *Angew. Chem. Int. Ed.*, 2012, **51**, 4466-4469.

42. T. Sasaki, S. Eguchi, M. Yamaguchi and T. Esaki, *J. Org. Chem.*, 1981, **46**, 1800-1804.

43. C. W. Bielawski and R. H. Grubbs, *Prog. Polym. Sci.*, 2007, **32**, 1-29.

44. M. R. Buchmeiser, in *Ring-opening metathesis polymerization*, Wiley-VCH Verlag GmbH & Co. KGaA, 2009, pp. 197-225.

45. H. Ihre, A. Hult, J. M. J. Fréchet and I. Gitsov, *Macromolecules*, 1998, **31**, 4061-4068.

46. B. G. G. Lohmeijer, R. C. Pratt, F. Leibfarth, J. W. Logan, D. A. Long, A. P. Dove, F. Nederberg, J. Choi, C. Wade, R. M. Waymouth and J. L. Hedrick, *Macromolecules*, 2006, **39**, 8574-8583.

47. J. A. Castillo, D. E. Borchmann, A. Y. Cheng, Y. Wang, C. Hu, A. J. García and M. Weck, *Macromolecules*, 2011, **45**, 62-69.

48. R. Huisgen, L. Möbius, G. Müller, H. Stangl, G. Szeimies and J. M. Vernon, *Chem. Ber.*, 1965, **98**, 3992-4013.

49. K. J. Shea and J. S. Kim, *J. Am. Chem. Soc.*, 1992, **114**, 4846-4855.

50. I. A. Barker, D. J. Hall, C. F. Hansell, F. E. Du Prez, R. K. O'Reilly and A. P. Dove, *Macromol. Rapid Commun.*, 2011, **32**, 1362-1366.

51. G. Moad, E. Rizzardo and S. H. Thang, *Polym. Int.*, 2011, **60**, 9-25.

52. H. Willcock and R. K. O'Reilly, *Polym. Chem.*, 2010, **1**, 149-157.

53. M. R. Whittaker, Y.-K. Goh, H. Gemici, T. M. Legge, S. Perrier and M. J. Monteiro, *Macromolecules*, 2006, **39**, 9028-9034.

54. J. W. Chan, B. Yu, C. E. Hoyle and A. B. Lowe, *Chem. Commun.*, 2008, 4959-4961.

55. A. B. Lowe, B. S. Sumerlin, M. S. Donovan and C. L. McCormick, *J. Am. Chem. Soc.*, 2002, **124**, 11562-11563.

56. C. Boyer, A. Granville, T. P. Davis and V. Bulmus, *J. Polym. Sci., Part A: Polym. Chem.*, 2009, **47**, 3773-3794.

57. G. N. Grover, S. N. S. Alconcel, N. M. Matsumoto and H. D. Maynard, *Macromolecules*, 2009, **42**, 7657-7663.

58. W. Shen, Q. Qiu, Y. Wang, M. Miao, B. Li, T. Zhang, A. Cao and Z. An, *Macromol. Rapid Commun.*, 2010, **31**, 1444-1448.

59. S. P. S. Koo, M. M. Stamenović, R. A. Prasath, A. J. Inglis, F. E. Du Prez, C. Barner-Kowollik, W. Van Camp and T. Junkers, *J. Polym. Sci., Part A: Polym. Chem.*, 2010, **48**, 1699-1713.

3 Polycarbonate Graft Copolymers by Ring-Opening and Reversible Addition-Fragmentation Chain Transfer Polymerisation

3.1 Introduction

Polymers with a diverse range of properties and applications can be prepared by tailoring polymer topology and composition. Major developments in "controlled" and "living" polymerisation techniques have enabled the preparation of well-defined complex polymer architectures,[1, 2] including block, star,[3-5] cyclic,[6-8] branched[9, 10] and dendritic[11, 12] polymer topologies.

Among these polymer architectures, the preparation of graft copolymers has been intensely investigated.[13-18] Three main strategies exist for their synthesis: "grafting-to", "grafting-through" and "grafting-from" (Figure 3.1). In a "grafting-to" approach, end-group-functionalised polymer chains are coupled to a polymer backbone containing multiple complimentary functionalities. While this approach allows the polymer backbone and side arms to be separately

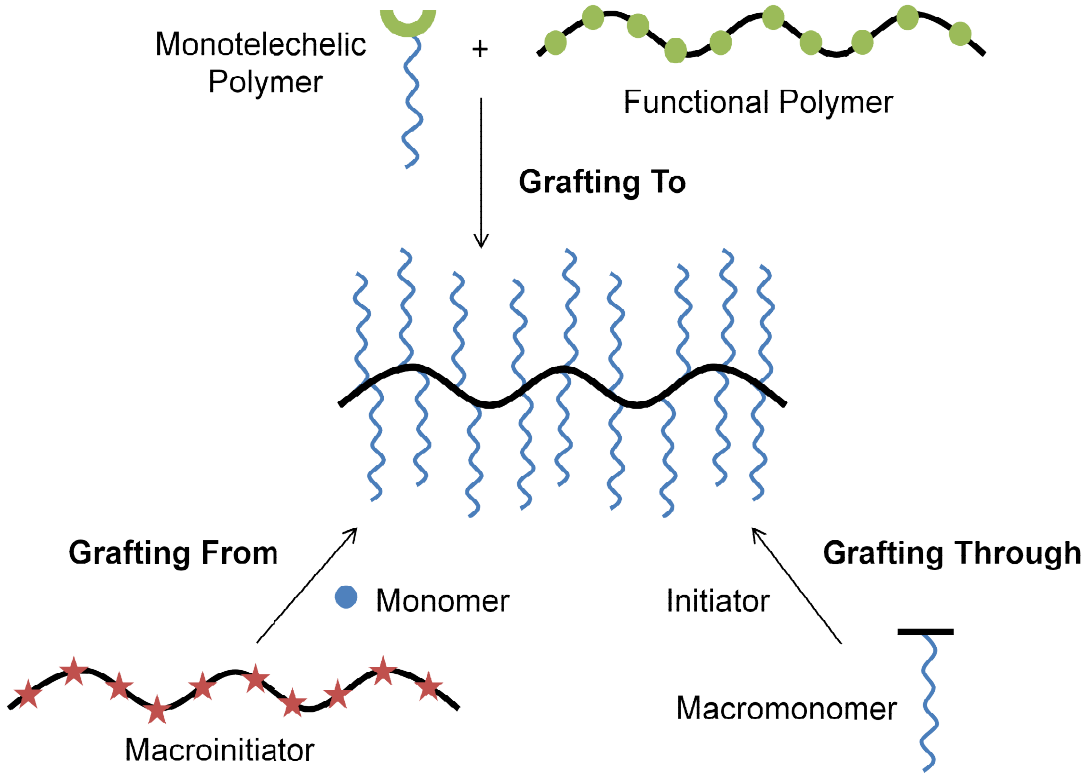

Figure 3.1. Preparation of graft copolymers *via* "grafting-to", "grafting-from" and "grafting-through" approaches.

prepared and characterised prior to coupling, grafting density is commonly limited as a consequence of steric repulsion between the bulky side arms. This limitation can be overcome by a "grafting-through" approach in which graft copolymers are prepared by the polymerisation of macromonomers. Here however, the bulky nature of the macromonomers can result in polymerisations being slow and limited to low monomer conversions and chain lengths. The "grafting from" approach in which polymer chains are grown from a polymer with multiple initiation sites located along its backbone can lead to inherently less control over the length of the polymer grafts, however, greater control of the overall length of the graft copolymer, as well as access to higher graft densities can be achieved. Careful choice of synthetic method, grafting density, composition and length of the polymer backbone and side-arms, allows graft copolymers with unique structural characteristics and a range of functionalities to be prepared.[13-16]

Recent advances in the incorporation of functionality into cyclic ester and carbonate monomers have enabled the synthesis of polyester and polycarbonate materials with a wide array of functionality incorporated throughout the polymer backbone.[19-23] In turn, these advances in monomer synthesis have opened routes for the preparation of graft copolymers with degradable backbones. The development of highly efficient "click" reactions and the incorporation of suitable reactive groups onto cyclic ester and carbonate monomers has enabled the synthesis of graft copolymers by the "grafting-to" approach.[24-39] Limited success has also been reported in the ROP of poly(ethylene glycol) functionalised monomers in a "grafting-through" approach, although this method is unattractive as a consequence of the ring-

chain equilibrium associated with sterically hindered cyclic ester and carbonate monomers.[40-45] Only a handful of examples have been reported using a "grafting-from" strategy *via* the attachment of initiating groups and protected initiating groups to cyclic ester and carbonate monomers prior to ROP. The incorporation of protected hydroxyl groups into the polymer backbone has allowed for the preparation of graft copolymers by consecutive ROP reactions.[46-48] Alternatively, Hedrick and co-workers prepared graft copolymers *via* a combination of ROP and atom transfer radical polymerisation (ATRP), by the synthesis and subsequent polymerisation of a novel derivative of ε-caprolactone with a pendent ATRP initiator group.[49]

As a consequence of its high functional group tolerance and ability to control the polymerisation of a wide range of monomers, reversible addition-fragmentation chain transfer (RAFT) polymerisation in combination with ROP offers a particularly promising route to prepare novel degradable graft copolymers.[50-56] "Grafting-from" *via* RAFT polymerisation can be achieved *via* either a Z-group approach, in which the RAFT CTA is attached to the polymer backbone *via* the Z-group or an R-group approach where the RAFT CTA is attached *via* the R-group (Figure 3.2). The reactive thiocarbonyl groups of the CTA can either remain close to the polymer backbone (Z-group) or be located at the graft polymer chain termini (R-group), which can allow subsequent post-polymerisation modification at the surface of the graft copolymer.[57] Furthermore, in a Z-group approach grafting density is limited as a consequence of the addition/fragmentation of the growing polymer chains from the RAFT CTA groups located along the polycarbonate backbone during polymerisation. Therefore, disadvantages similar to those of a "grafting-to" approach are

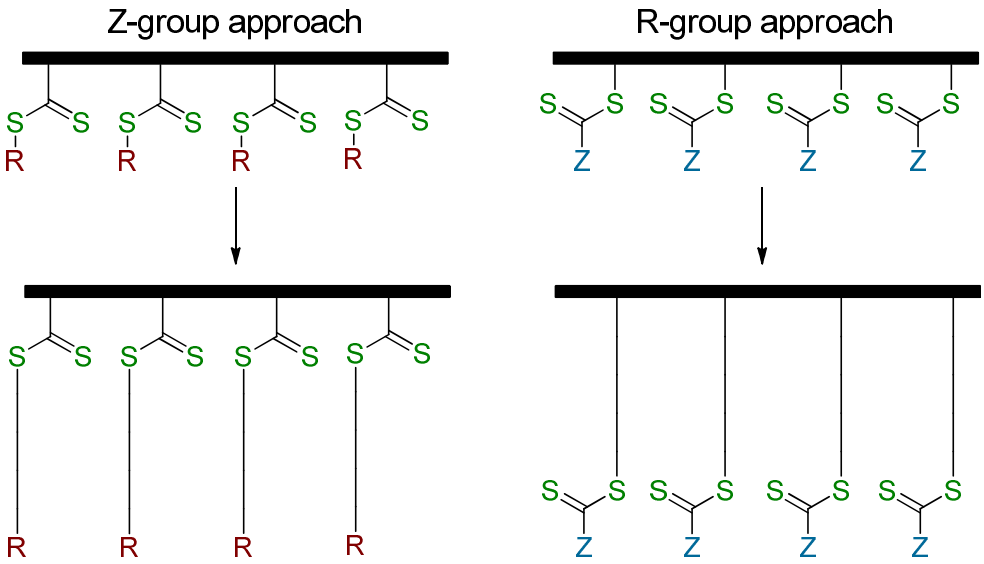

Figure 3.2. Preparation of graft copolymers by RAFT polymerisation *via* a Z-group approach or R-group approach.

encountered in a Z-group RAFT approach. Mespouille *et al*. have recently reported the preparation of graft copolymers *via* a combination of ROP and a Z-group RAFT approach.[58] A novel RAFT CTA-functional cyclic carbonate, where the RAFT CTA functionality was attached *via* the Z-group was copolymerised with an ethyl-functional cyclic carbonate monomer and *N*-isopropylacrylamide was subsequently grown from the resulting polycarbonate backbone *via* RAFT polymerisation. Despite the success of this initial report, only low grafting densities were targeted (10% RAFT CTA incorporation), as a consequence of employing a Z-group approach, and only graft copolymers with a target poly(*N*-isopropylacrylamide) arm length of DP 40 were prepared.

In this chapter, graft copolymers with significantly higher grafting densities are prepared *via* a combination of ROP and an R-group RAFT approach. A novel RAFT CTA-functional cyclic carbonate monomer with RAFT CTA functionality attached *via* the R-group is synthesised and polymerised through ROP and the

resulting polycarbonates utilised in the preparation of well-defined graft copolymers with a degradable backbone.

3.2 Results and Discussion

3.2.1 Monomer Synthesis

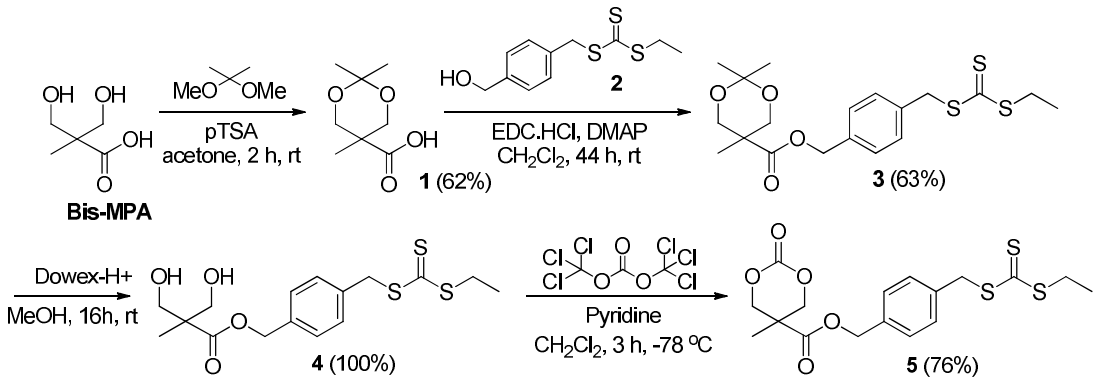

Scheme 3.1. Synthesis of RAFT CTA-functional cyclic carbonate monomer, **5**.

The RAFT CTA-functional cyclic carbonate monomer, **5**, was synthesised in 4 steps from commercially available 2,2'-bis(hydroxymethyl) propionic acid (bis-MPA), (Scheme 3.1). Reaction of bis-MPA with 2,2-dimethoxypropane, in the presence of a catalytic amount of *p*-toluenesulfonic acid, resulted in the formation of an acetonide-protected bis-MPA analogue, **1**.[59] The incorporation of RAFT CTA functionality was achieved *via* the esterification of **1** with the hydroxyl containing CTA, **2**, that in turn was prepared in a one-pot synthesis according to adapted literature procedures.[60, 61] Ethanethiol and carbon disulfide were added to a suspension of potassium phosphate in acetone, 4-(chloromethyl)benzyl alcohol was added and the reaction mixture was stirred for 3 days (Scheme 3.2). Subsequent coupling of **1** and the CTA **2** in the presence of *N*-(3-dimethyl-aminopropyl)-*N*'-ethylcarbodiimide hydrochloride (EDC.HCl) and 4-(dimethylamino)pyridine (DMAP), followed by hydrolysis of the acetonide protecting group of **3** with DOWEX 50W-X2 resin, yielded the CTA-functionalised diol, **4**. The RAFT CTA-functional cyclic carbonate monomer **5** was subsequently formed by ring-closure using triphosgene in the presence of

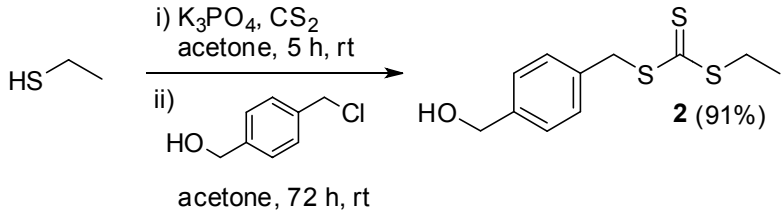

Scheme 3.2. One-pot synthesis of RAFT CTA **2**.

pyridine to trap hydrochloric acid. The product was isolated in 27% overall yield after recrystallisation, *via* the sequential addition of hot tetrahydrofuran and diethyl ether.

Analysis of the ^{1}H NMR spectrum of monomer **5** revealed resonances that correspond to both CTA and cyclic carbonate functionality (Figure 3.3). Most notably, a quartet and triplet resonance at δ = 3.38 and 1.36 ppm respectively, that arise from the ethyl group of the RAFT CTA moiety, in addition to a pair of doublets at δ = 4.70 and 4.20 ppm that correspond to the inequivalent CH_2 protons on the carbonate ring. The appearance of a resonance at δ = 147.5 ppm in the ^{13}C NMR spectrum, that corresponds to the carbonate carbonyl group of **5** and the resonance at δ = 223.3 ppm that corresponds to the thiocarbonyl carbon of the RAFT CTA moiety, provides further evidence of the monomer

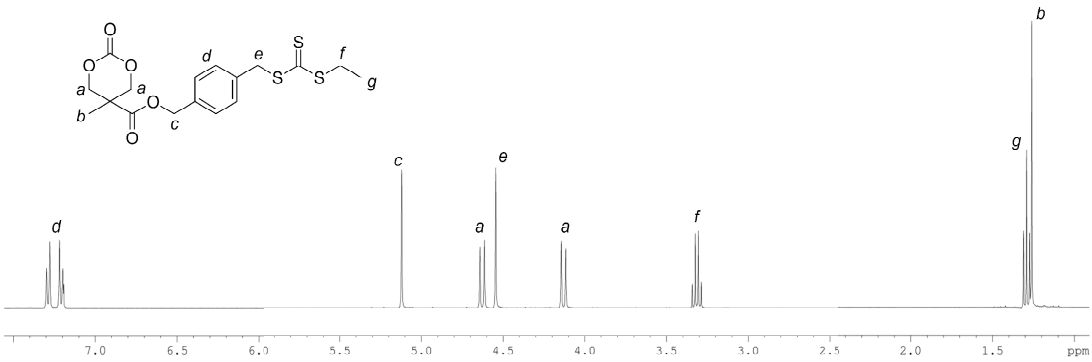

Figure 3.3. ^{1}H NMR spectrum (400 MHz; $CDCl_3$) of monomer **5**.

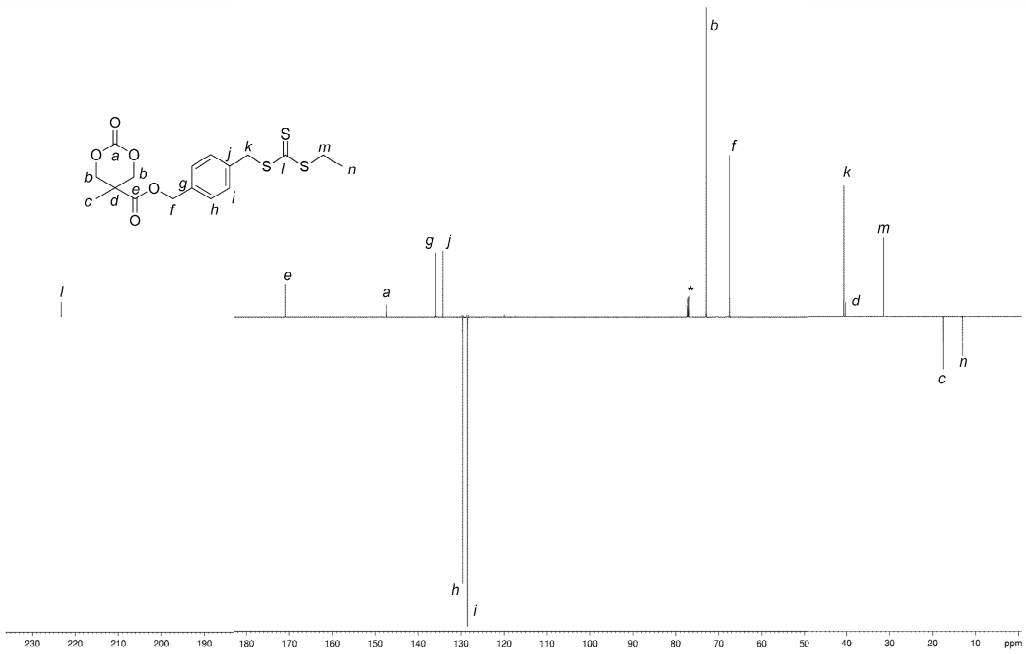

Figure 3.4. ^{13}C NMR spectrum (175 MHz; $CDCl_3$) of monomer **5** (*$CDCl_3$).

structure (Figure 3.4). The structure of monomer **5** was further confirmed by elemental analysis and mass spectrometry.

3.2.2 Ring-Opening Polymerisation Studies

Initial studies into the ring-opening polymerisation of **5** were conducted in $CDCl_3$ at room temperature (Scheme 3.3), where $[\mathbf{5}]_0$ = 0.25 M, with the initial monomer-to-initiator ratio, $[M]_0/[I]_0$ = 20, using benzyl alcohol as the initiator. Monomer conversion was monitored by ^1H NMR spectroscopy by comparing the reduction of the doublet resonances from **5** at δ = 4.70 and 4.20 ppm with the appearance of a broad multiplet resonance at δ = 4.28 ppm, attributed to the polycarbonate backbone. After the allotted time, polymerisations were quenched by the addition of acidic Amberlyst resin and purified by column chromatography to remove residual monomer and catalyst (100% CH_2Cl_2, then 100% ethyl acetate).

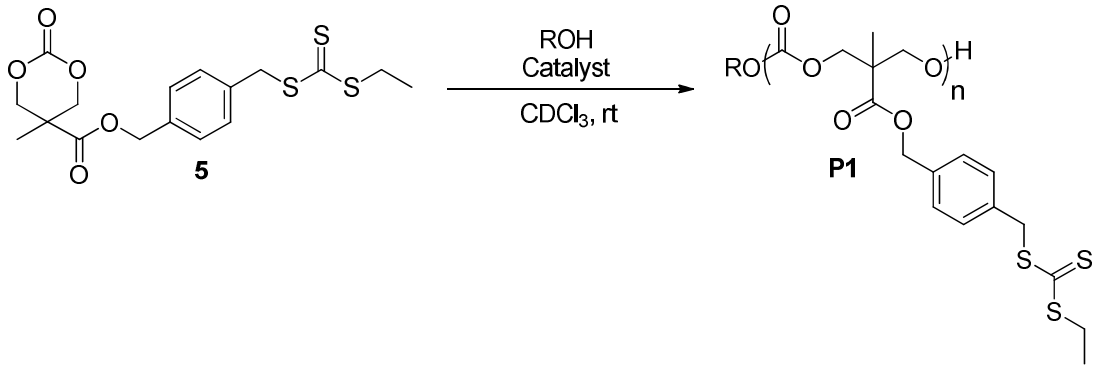

Scheme 3.3. Ring-opening polymerisation of monomer **5** to prepare RAFT CTA-functional polycarbonates.

3.2.2.1 Ring-Opening Polymerisation Studies: Choice of Catalyst

A range of organocatalyst systems were tested for the controlled polymerisation of **5** (Figure 3.5), starting with the highly active amidine base 1,8-diazabicyclo[5.4.0]undec-7-ene (DBU) which has successfully catalysed the ROP of trimethylene carbonate and functional cyclic carbonate monomers exhibiting excellent control.[31, 43, 62] As trithiocarbonate groups are known to react with primary and secondary amines, the stability of the trithiocarbonate moiety of RAFT CTA **2** in the presence of DBU was investigated. CTA **2** and DBU were dissolved in $CDCl_3$ and monitored by ^1H NMR spectroscopy over 48 h. During this time no alteration in the ^1H NMR spectra of **2** was observed and the solution retained the characteristic yellow colour of the trithiocarbonate group.

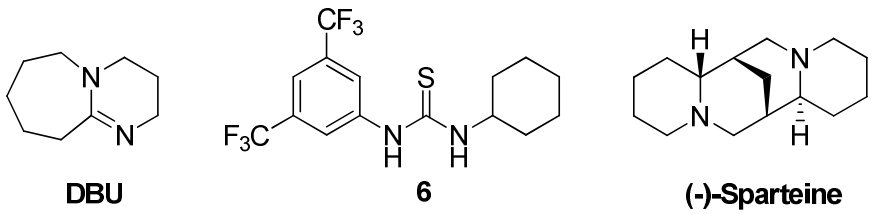

Figure 3.5. Organic catalysts screened for the ring-opening polymerisation of **5**.

For the ROP of **5** catalysed by DBU (5 mol%) size exclusion chromatography (SEC) analysis indicated the polymerisation was well controlled with a dispersity ($Đ_M$) of 1.17. Monitoring the polymerisation by ^{1}H NMR spectroscopy however revealed significant retardation of polymerisation rate occurred when monomer conversions > 70% were attained; indeed no further polymerisation was observed above *ca*. 80% monomer conversion (Figure 3.6). This observation is consistent with the decreased polymerisability of the monomer resulting from a low ring-chain equilibrium attributed to the sterically hindered nature of **5** as a consequence of the bulky RAFT CTA substituent.[31, 43, 63] Prolonged reaction times did not result in additional monomer conversion and instead led to a broadening of the molecular weight distribution of the polymer ($Đ_M$ > 1.70) consistent with the occurrence of transesterification side reactions as a consequence of the strong basicity of DBU.

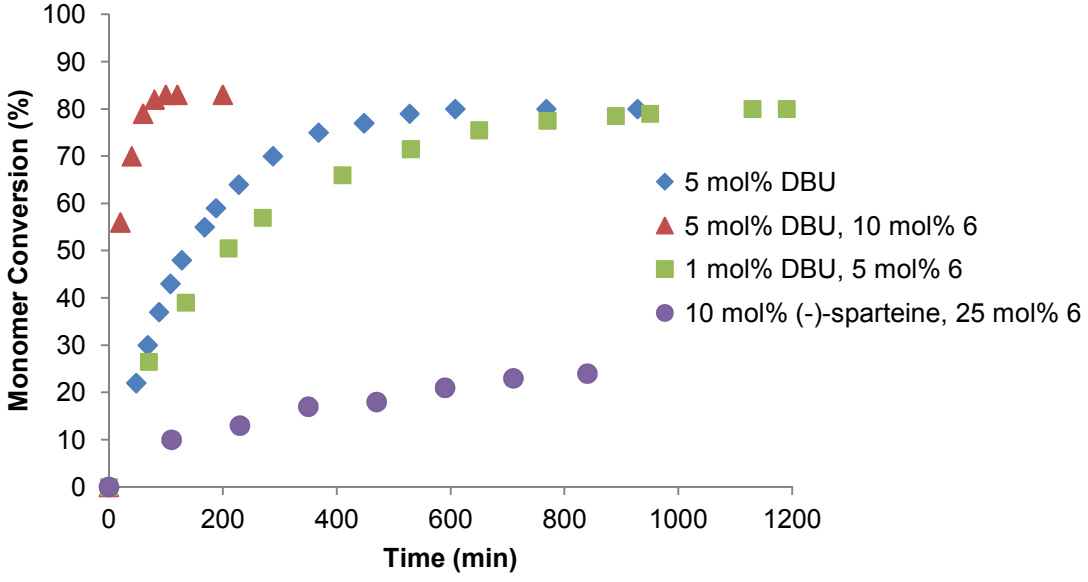

Figure 3.6. Plot of time (min) against monomer conversion (%) for the ring-opening polymerisation of **5** using different catalyst systems. Conditions: [**5**] = 0.25 M, $CDCl_3$ at 25 °C, [M]/[I] = 20 using benzyl alcohol as initiator.

In an attempt to achieve higher monomer conversions the addition of a cocatalyst, 1-(3,5-bis(trifluoromethyl)phenyl)-3-cyclohexylthiourea (**6**), was investigated. Cocatalyst **6** activates the monomer through hydrogen bonding to the carbonate carbonyl, showing a preference for activating cyclic carbonates and esters over their linear counterparts and indeed has been shown to promote polymerisation in systems where the application of only DBU has resulted in no polymerisation.[64] At catalyst loadings of 5 mol% DBU and 10 mol% cocatalyst **6** significantly accelerated polymerisation rates were observed, achieving 83% monomer conversion after only 100 minutes, but at the cost of polymerisation control as evidenced by the broad molecular weight distribution (Table 3.1). SEC analysis also revealed the presence of low molecular weight oligomeric species, in addition to the main molecular weight distribution, which suggested the occurrence of significant transesterification and scrambling of polymer chains. Reducing catalyst loading to 1 mol% DBU

Table 3.1. Organic catalyst systems for the ring-opening polymerisation of **5**.

Catalyst	Time (h)	Monomer conversion (%)[a]	M_n (SEC) (kDa)[b]	$Đ_M$[b]
5 mol% **DBU**	10	80	5.9	1.17
5 mol% **DBU** + 10 mol% **6**	1.7	83	4.4	1.48
1 mol% **DBU** + 5 mol% **6**	16	80	5.0	1.16
10 mol% **(-)-sparteine** + 25 mol% **6**	290	84	4.1	1.35

[a]Determined by ^{1}H NMR spectroscopy. [b]Determined by SEC analysis in $CHCl_3$ using poly(styrene) standards. Conditions: [**5**] = 0.25 M, $CDCl_3$ at 25 °C, [M]/[I] = 20 using benzyl alcohol as initiator.

and 5 mol% cocatalyst **6** resulted in a higher level of polymerisation control ($Đ_M$ = 1.16), however monomer conversion did not increase above 80%.

The dual catalyst system of (-)-sparteine and thiourea cocatalyst **6** was also investigated for the ROP of monomer **5**. At catalyst loadings of 5 and 10 mol% of (-)-sparteine and cocatalyst **6** respectively, the polymerisation rate was considerably slower than both the DBU and DBU/thiourea catalyst systems, reaching only 6% monomer conversion after 13 h. This was attributed to the less basic nature of (-)-sparteine (pK_a = 17.5) compared to DBU (pK_a = 23.4). Increasing the loading of (-)-sparteine to 10 mol% and cocatalyst **6** to 25 mol% increased polymerisation activity; however a monomer conversion of only 24% was achieved after 14 h, reaching a maximum conversion of 84% after 12 days. Of the organic catalyst systems investigated, DBU (5 mol%) exhibited the best combination of control and activity and was therefore chosen as the catalyst for all subsequent polymerisations of **5**.

3.2.2.2 Ring-Opening Polymerisation Studies: Choice of Initiator

Initial polymerisation studies utilised benzyl alcohol as the initiator, however, the resonances attributed to the benzyl carbonate end group in the ^{1}H NMR spectrum of the resultant polymer overlapped with the aromatic and benzyl signals of the polymer repeat unit at δ = 7.27 and 5.10 ppm respectively. This prevented the determination of number-average molecular weight (M_n(NMR)) and degree of polymerisation (DP) by ^{1}H NMR spectroscopy. To overcome this problem alternative polymerisation initiators were investigated. The *tert*-butyl groups of *neo*-pentanol were expected to give an unobscured resonance at δ <1.00 ppm when used as the initiating alcohol. Indeed, the ^{1}H NMR spectrum of

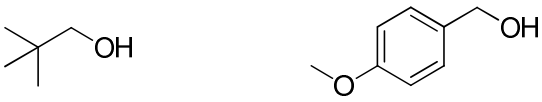

***neo*-Pentanol** **4-Methoxybenzyl alcohol**

Figure 3.7. Alternative initiators used in the ring-opening polymerisation of **5**.

a purified polymer with a *neo*-pentyl carbonate end group clearly shows the *tert*-butyl resonance at δ = 0.93 ppm, however calculation of the DP using this peak gave a value approximately double the theoretical DP calculated from [M]/[I] and monomer conversion (Table 3.2). Inspection of the ^{1}H NMR spectra obtained during the polymerisation showed two resonances below δ = 1.00 ppm; a slightly broadened signal at δ = 0.93 ppm that corresponds to the *tert*-butyl groups of the polymer chain end and a more defined peak at δ = 0.91 ppm that corresponds to unreacted *neo*-pentanol (Figure 3.8). Comparison of the integrals of these resonances revealed for example, that at 70% monomer conversion, 31% of n*eo*-pentanol remained unreacted. These data suggested that the rate of initiation by *neo*-pentanol was considerably slower than the rate of propagation, resulting in the DP of the isolated polymer being significantly higher than expected, as well as a broadening of dispersity ($Đ_M$ = 1.26) (Figure 3.9).

Table 3.2. Alternative initiators used for the ring-opening polymerisation of **5**.

Initiating alcohol	**[M]/[I]**	**Monomer conversion(%)[a]**	**DP**	**M_n(NMR) (kDa)[b]**	**M_n(SEC) (kDa)[b]**	**$Đ_M$[b]**
neo-pentanol	20	85	31	12.5	6.8	1.26
4-methoxybenzyl alcohol	20	80	16	6.5	4.8	1.09

[a]Determined by ^{1}H NMR spectroscopy. [b]Determined by SEC analysis in $CHCl_3$ using poly(styrene) standards. Conditions: [**5**] = 0.25 M, $CDCl_3$ at 25 °C, using 5 mol% DBU.

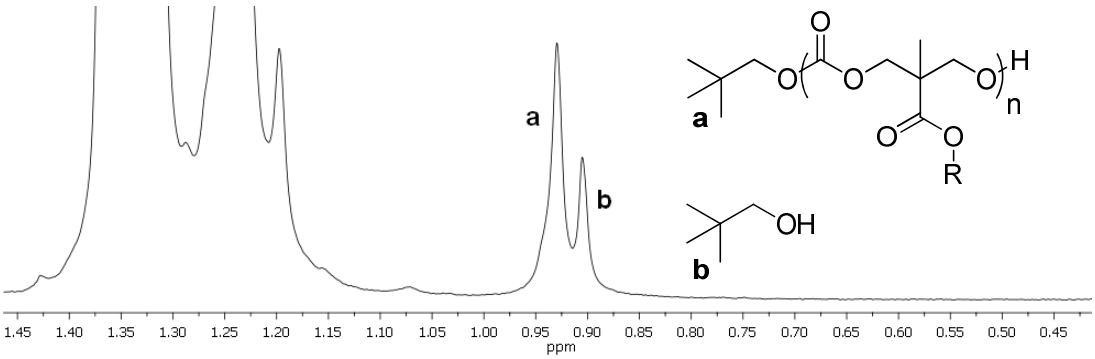

Figure 3.8. Expansion of the δ = 1.45 – 0.45 ppm region of ^{1}H NMR spectrum (400 MHz; $CDCl_3$) showing the *tert*-butyl resonances during the ring-opening polymerisation of **5** at 70% monomer conversion.

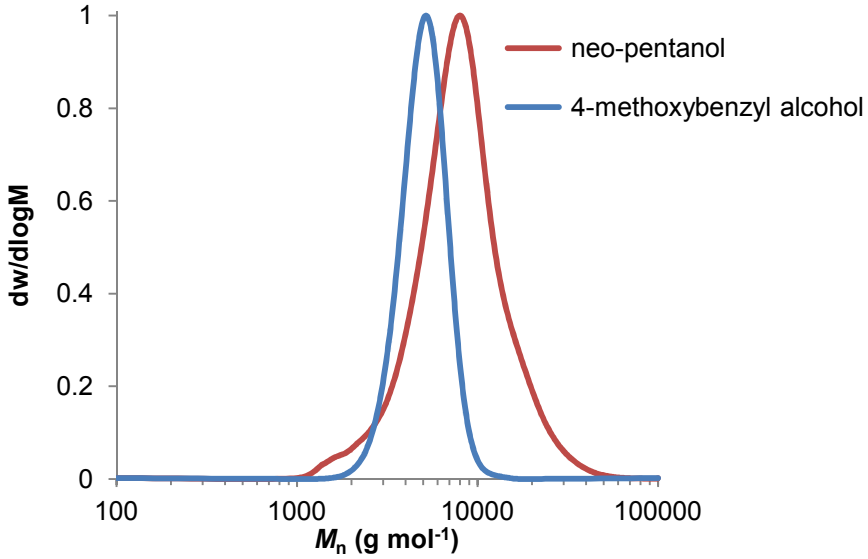

Figure 3.9. SEC chromatograms of **P1** initiated by *neo*-pentanol (M_n = 6.8 kDa, = $Đ_M$ 1.26) and 4-methoxybenzyl alcohol (M_n = 4.8 kDa, = $Đ_M$ 1.09).

This poor initiator efficiency is thought to occur as a consequence of the electron rich nature of *neo*-pentanol. In order to improve initiator efficiency and provide a functional group for end-group analysis by ^{1}H NMR spectroscopy, the use of 4-methoxybenzyl alcohol as the polymerisation initiator was investigated. The benzyl functionality of 4-methoxybenzyl alcohol was expected to be less electron donating than the *tert*-butyl group of *neo*-pentanol. Therefore, the hydroxyl proton of 4-methoxybenzyl alcohol is expected to have

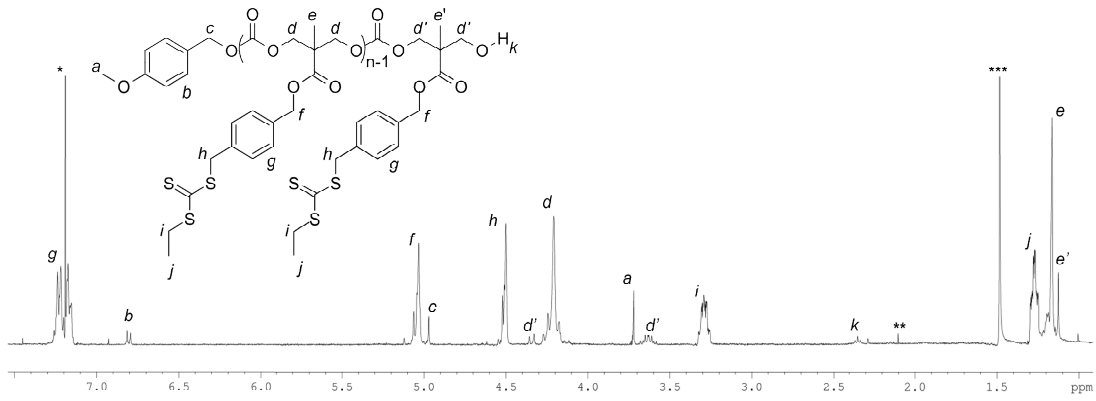

Figure 3.10. ^{1}H NMR spectrum (400 MHz; $CDCl_3$) of **P1** using 4-methoxybenzyl alcohol as the polymerisation initiator (*$CHCl_3$, **acetone, ***H_2O).

a lower pKa value than the hydroxyl proton of *neo*-pentanol, resulting in improved initiation and affording polymers with narrow molecular weight distributions. The singlet resonances at δ = 3.79 and 5.04 ppm of the methoxy and benzylic protons in addition to the downfield shifted doublet at δ = 6.87 ppm which arises from the aromatic protons, remained clearly visible in the ^{1}H NMR spectra of the resultant polymers allowing the determination of M_n(NMR) and DP and demonstrating the end-group fidelity of the polymerisation (Figure 3.10). SEC analysis indicated the polymerisation was well controlled, with $Đ_M$ = 1.09, and a strong agreement was found between theoretical and calculated DP. As such, 4-methoxybenzyl alcohol was chosen as the initiator for all subsequent polymerisations of monomer **5**.

3.2.2.3 Ring-Opening Polymerisation Studies: Polymerisation Control

Further investigation of the controlled nature of the homopolymerisation of **5** revealed a linear relationship between M_n(SEC) and monomer conversion, as well as, M_n(SEC) and theoretical DP (Figure 3.11 and 3.12), while retaining low dispersity values and monomodal SEC chromatograms throughout the

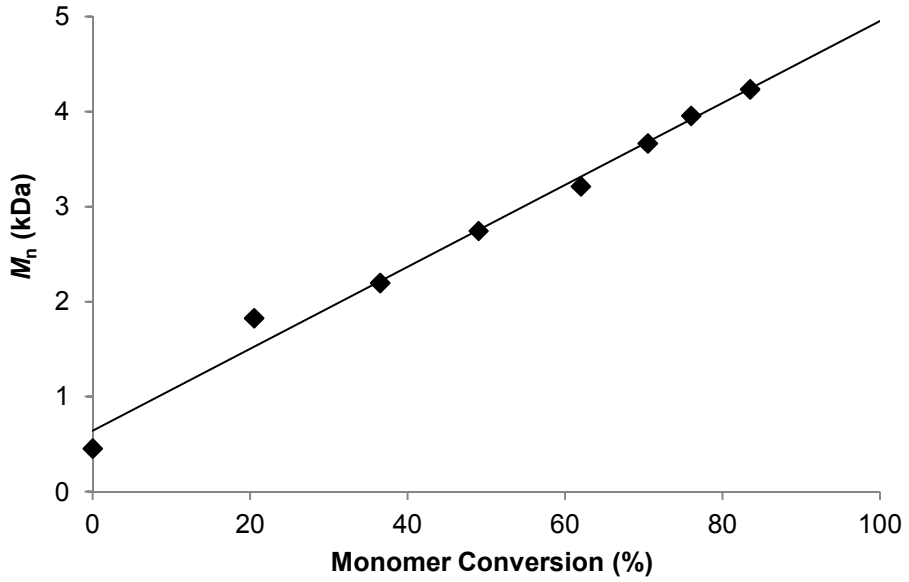

Figure 3.11. Plot of M_n(SEC) (kDa) against monomer conversion (%) for the ring-opening polymerisation of **5**. Conditions: [**5**] = 0.25 M, [M]/[I] = 20, using 5 mol% DBU and 4-methoxybenzyl alcohol as the polymerisation initiator.

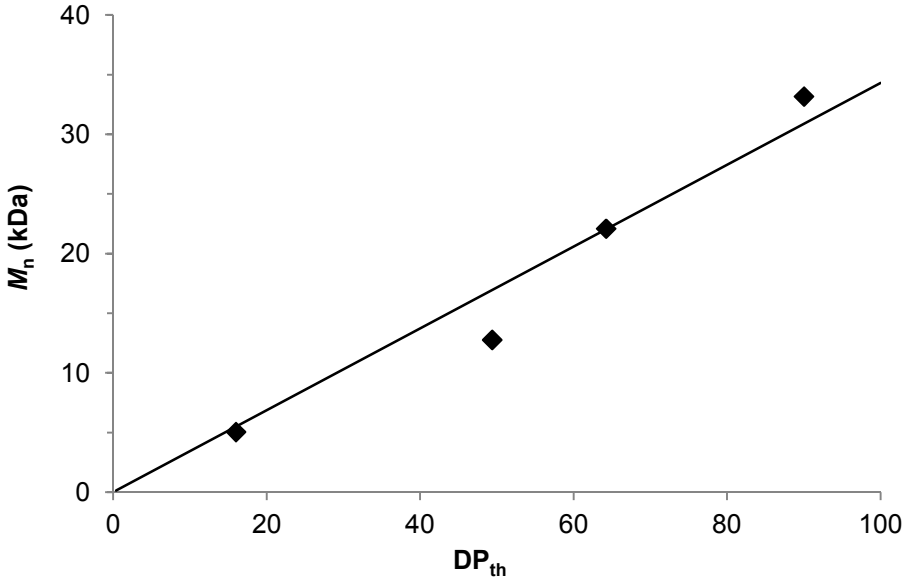

Figure 3.12. Plot of M_n(SEC) (kDa) against theoretical DP for the ROP of **5**. Conditions: [**5**] = 0.25 M, using 5 mol% DBU and 4-methoxybenzyl alcohol as the polymerisation initiator.

polymerisation. During this study, large differences were observed between values of M_n determined by SEC analysis and values of M_n determined by ^{1}H NMR spectroscopy, with values of M_n(SEC) consistently lower than predicted.

This is attributed to a significant difference in hydrodynamic volume between poly(styrene) SEC standards and the RAFT CTA- functionalised polycarbonates (Table 3.3).

Analysis of polymers by matrix-assisted laser desorption ionisation time-of-flight mass spectrometry (MALDI-ToF MS) revealed a sodium-charged main distribution with regular spacings equal to the molecular weight of the monomer repeat unit (*m/z* = 400 Da) and a 4-methoxybenzyl alcohol end group (Table 3.4 and Figure 3.13), demonstrating the end group fidelity and living nature of the polymerisation. Closer examination of the isotope pattern of a DP 7 polymer chain (Figure 3.14), revealed excellent agreement between the observed and theoretical pattern, providing further evidence of the desired repeat unit.

Table 3.3. Variation of [M]/[I] for the ring-opening polymerisation of **5**.

[M]/[I]	DP_{th}[a]	$M_{n,th}$ (kDa)[a]	M_n(NMR) (kDa)[a]	M_n(SEC) (kDa)[b]	$Đ_M$[b]
20	16	6.5	6.8	4.8	1.09
65	49	19.8	16.8	12.8	1.16
95	64	25.9	27.4	22.1	1.09
125	90	36.2	39.0	33.2	1.11

[a]Determined by ^{1}H NMR spectroscopy. [b]Determined by SEC analysis in $CHCl_3$ using poly(styrene) standards. Conditions: [**5**] = 0.25 M, $CDCl_3$ at 25 °C, using 5 mol% DBU and 4-methoxybenzyl alcohol as the polymerisation initiator.

Table 3.4. Theoretical and observed *m/z* values of **P1**.

DP	Experimental *m/z*[a]	Calculated *m/z*
3	1361.0	1361.2
4	1761.6	1761.2
5	2162.1	2161.3
6	2562.5	2561.3
7	2962.9	2961.4

[a]Determined by MALDI-TOF MS analysis using trans-2-[3-(4-*tert*-butylphenyl)-2-methyl-2-propylidene]malonitrile (DCTB) as a matrix, sodium trifluoroacetate as the cationisation agent and PEG monomethyl ether 2k and 5k standards.

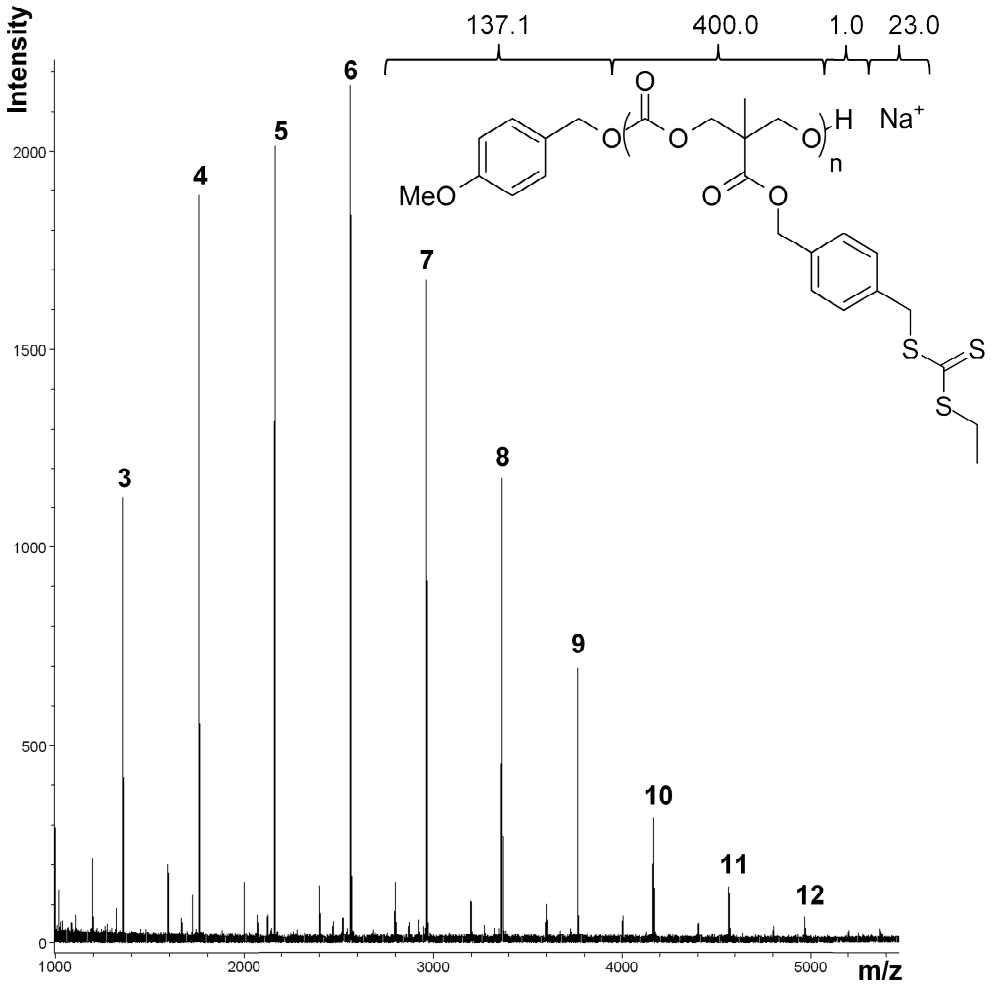

Figure 3.13. MALDI-ToF MS analysis of **P1** ([M]/[I] = 20) initiated from 4-methoxybenzyl alcohol.

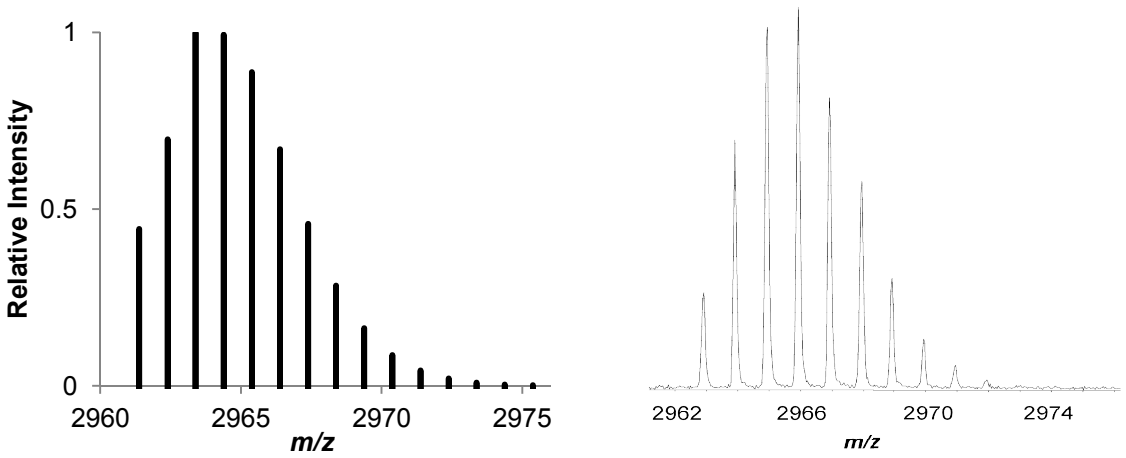

Figure 3.14. Predicted (left) and observed (right) isotope patterns for DP 7 peak of polymer **P1** initiated for 4-methoxybenzyl alcohol.

3.2.3 Copolymerisation Studies

In order to tune the incorporation of RAFT CTA functionality along the polycarbonate backbone and subsequently tune the grafting density of the graft copolymers, monomer **5** was copolymerised with 5-methyl-5-ethoxycarbonyl-1,3-dioxan-2-one (**7**). Monomer **7** was prepared in two steps according to adapted literature procedures (Scheme 3.4).[47, 65] Bis-MPA was esterified with ethanol in the presence of acidic Amberlyst resin acting as a heterogeneous catalyst. The resulting ethyl ester analogue of bis-MPA was cyclised with ethyl chloroformate in the presence of triethylamine and recrystallised from toluene to afford the monomer **7** in 50% overall yield. The ^{1}H NMR (Figure 3.15) and

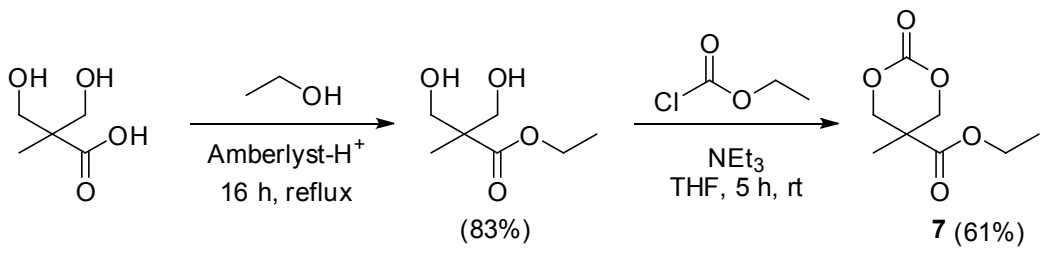

Scheme 3.4. Synthesis of 5-methyl-5-ethoxycarbonyl-1,3-dioxan-2-one (**7**).

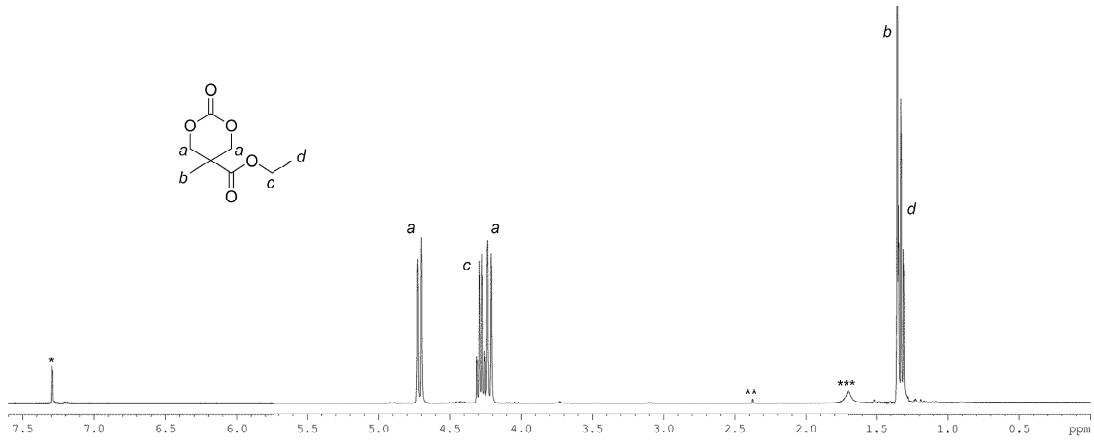

Figure 3.15. ^{1}H NMR spectrum (400 MHz; $CDCl_3$) of monomer **7** (*$CHCl_3$, **Toluene, ***H_2O).

^{13}C NMR spectra of monomer **7** were found to be in accordance with those previously reported.[65]

Copolymerisations of **5** and **7** were conducted in dichloromethane ([total monomer] = 0.25 M) at room temperature, with 5 mol% of DBU and 4-methoxybenzyl alcohol as the initiator (Scheme 3.5). Copolymers were prepared with a range of RAFT CTA incorporations by varying the comonomer feed ratio from 1:1 to 1:4 (**5**:**7**). Monitoring the conversion of both **5** and **7** by ^{1}H NMR spectroscopy during copolymerisation, showed that the two monomers

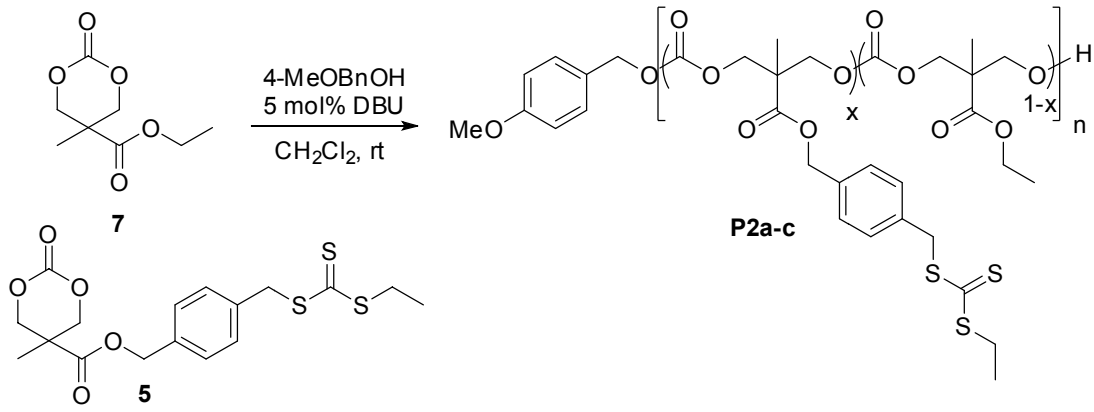

Scheme 3.5. Synthesis of RAFT CTA- and ethyl-functional polycarbonate copolymers *via* the ring-opening polymerisation of **5** and **7**.

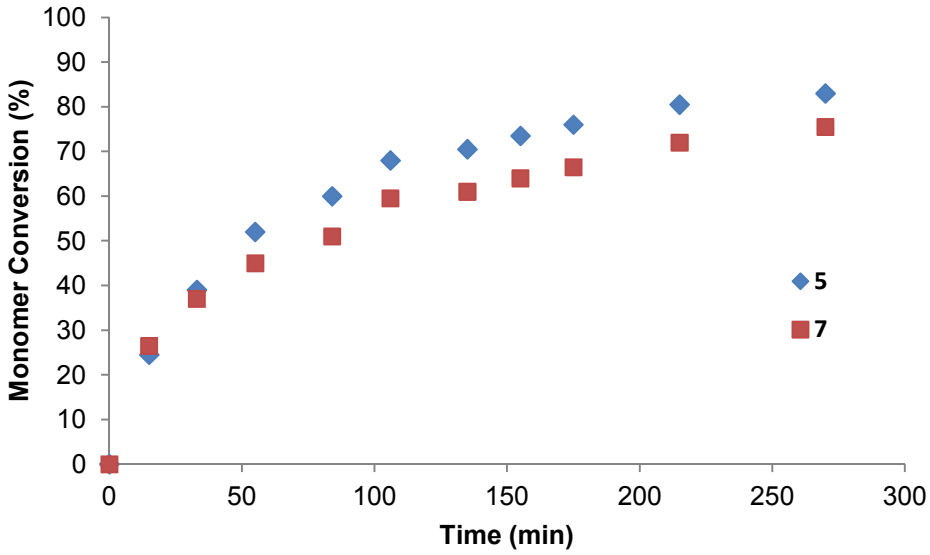

Figure 3.16. Plot of monomer conversion (%) against time (min) for the 1:1 copolymerisation of monomers **5** and **7**. Conditions: [monomer] = 0.25 M in CH_2Cl_2, using 5 mol% DBU and 4-methoxybenzyl alcohol as the polymerisation initiator.

were polymerised at a similar rate, with **5** being consumed slightly faster than **7** (Figure 3.16). These data suggested the formation of statistical copolymers, with RAFT CTA functionality distributed throughout the polymer backbone, rather than the formation of blocky or gradient copolymers.

Analysis of the copolymers by ^{1}H NMR spectroscopy, after purification by column chromatography to remove residual monomer and catalyst, revealed that the composition of the copolymers was in good agreement with the monomer feed ratios and that copolymers with 52% (**P2a**), 35% (**P2b**) and 24% (**P2c**) incorporations of **5** were obtained (Table 3.5). The ^{1}H NMR spectra of the copolymers show the appearance of a quartet resonance that corresponds to the CH_2 group of the ethyl ester functionality at δ = 4.18 ppm, whereas the triplet resonance of the adjacent CH_3 group is obscured by the methyl groups of the polycarbonate backbone at δ = 1.24 ppm (Figure 3.17). The ^{1}H NMR spectra of the copolymers also reveal distinct resonances that

Table 3.5. Characterisation and composition of copolymers.

Polymer	Monomer ratio (5 : 7)	Polymer composition[a]	Incorporation of 5 (%)[a]	M_n(NMR) (kDa)[a]	M_n(SEC) (kDa)[b]	$Đ_M$[b]
P2a	1 : 1	1 : 0.91	52	6.4	3.6	1.21
P2b	1 : 2	1 : 1.86	35	5.4	4.5	1.14
P2c	1 : 4	1 : 3.23	24	6.0	6.1	1.11

[a]Determined by ^{1}H NMR spectroscopy. [b]Determined by SEC analysis in $CHCl_3$ using poly(styrene) standards. Conditions: [monomer] = 0.25 M in CH_2Cl_2, using 5 mol% DBU and 4-methoxybenzyl alcohol as the polymerisation initiator.

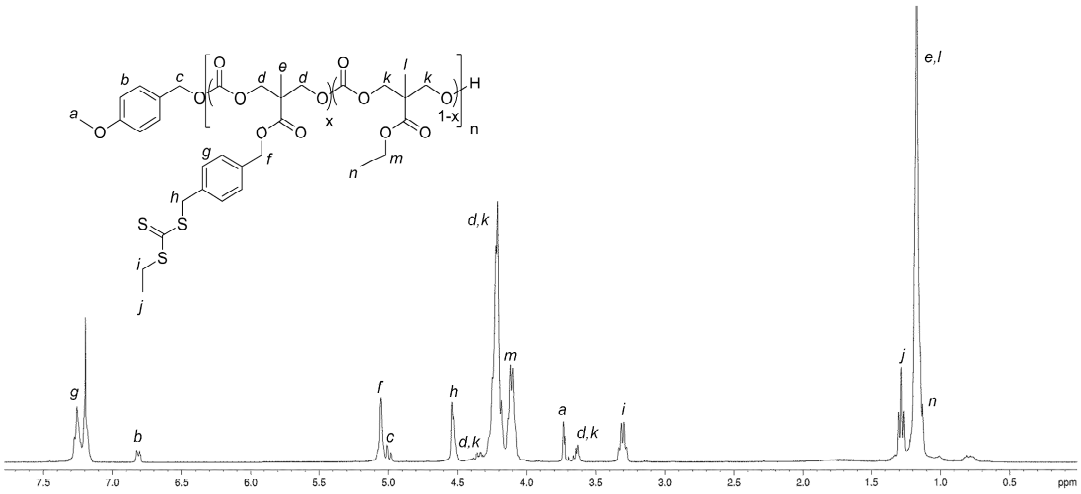

Figure 3.17. ^{1}H NMR spectrum (400 MHz; $CDCl_3$) of RAFT- and ethyl-functional polycarbonate copolymer **P2c** (*$CHCl_3$).

correspond to the methoxybenzyl carbonate end-groups adjacent to units of both **5** and **7**; namely the two singlets of the benzylic protons at δ = 5.08 and 5.05 ppm and the two singlets of the methoxy protons at δ = 3.80 and 3.79 ppm. Analysis of the ^{13}C NMR spectra of the purified copolymers revealed three distinct carbonyl resonances around δ = 154.5 ppm that correspond to carbonate carbon atoms in slightly different environments in the polymer backbone (Figure 3.18). These resonances indicate the resolution of diad level sensitivity within the backbone with each signal arising from either two

adjacent units of **5** (AA), two adjacent units of **7** (BB) or a unit of **5** adjacent to a unit of **7** (AB or BA). Comparison of the ^{13}C NMR spectra of the copolymers with those of the homopolymers of **5** and **7** enabled assignment of the carbonyl peaks to the corresponding diads. The occurrence of three distinct carbonyl resonances of similar intensities is expected for the analysis of statistical copolymers and provides further evidence for the even distribution of RAFT CTA functionality along the carbonate backbone.

SEC analysis of the copolymers revealed the $Đ_M$ values of polymers **P2a-c** were low (≤ 1.2) (Figure 3.19), which in combination with degrees of polymerisation being in line with those predicted from [M]/[I], indicates that the copolymerisations were well controlled. Interestingly, as the incorporation of RAFT CTA groups was reduced, the values of M_n(SEC) became closer to the values of M_n(NMR), which suggests that the hydrodynamic volume of polymers comprised of **7** were more comparable to that of poly(styrene), compared to the RAFT CTA-functionalised homopolymers.

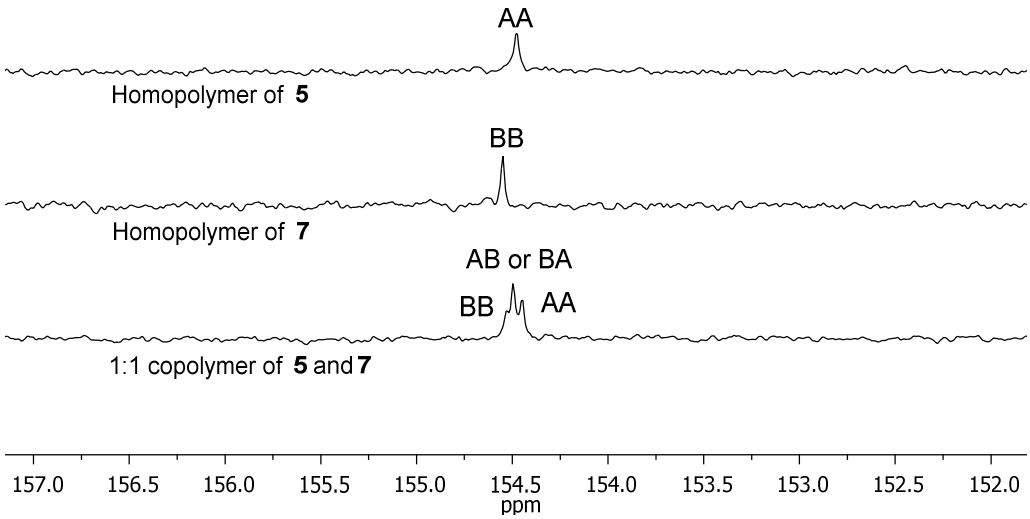

Figure 3.18. Expansion of the δ = 152 – 157 ppm region of ^{13}C NMR spectra showing the carbonyl carbonate resonances of homopolymer **5**, homopolymer **7** and the 1:1 copolymerisation of **5** and **7**.

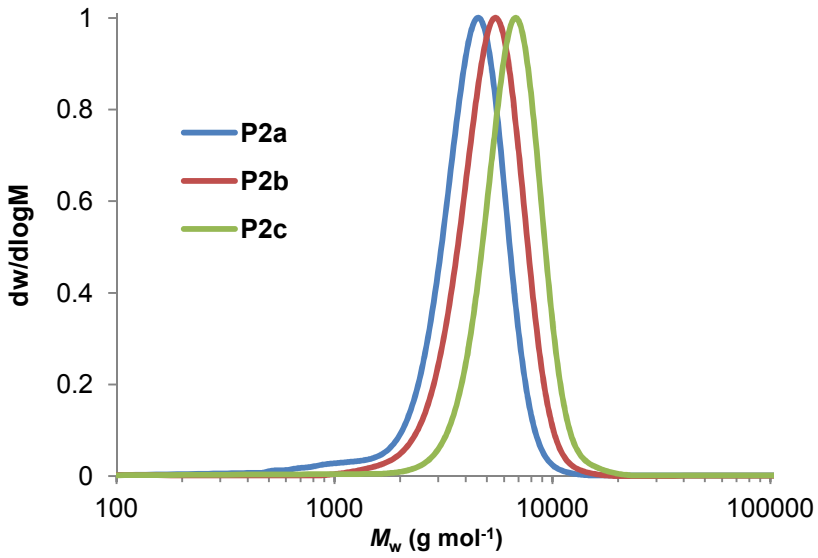

Figure 3.19. SEC chromatograms of copolymers **P2a** (52% incorporation of **5**, M_n = 3.6 kDa, $Đ_M$ = 1.21), **P2b** (35% incorporation of **5**, M_n = 4.5 kDa, $Đ_M$ = 1.14) and **P2c** (24% incorporation of **5**, M_n = 6.1 kDa, $Đ_M$ = 1.11).

3.2.4 Synthesis of Graft Copolymers by RAFT Polymerisation

Initial studies to prepare graft copolymers focused on growing styrene arms from the RAFT CTA groups located along the polycarbonate backbone of polymers **P1** and **P2a-c** (Scheme 3.6). Polymerisations were conducted at 65 °C, in 10 mM solutions of starting polymer in chloroform, using 2,2'-azobis(isobutyronitrile) (AIBN) as the radical initiator. A ratio of

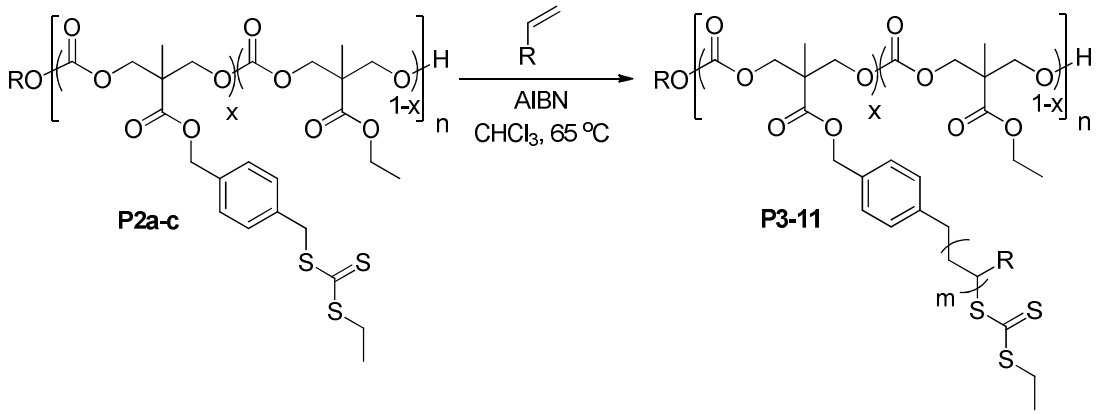

Scheme 3.6. Synthesis of graft copolymers *via* RAFT polymerisation.

[CTA]:[AIBN]:[monomer] of 1:0.1:50 was used for the polymerisations based on the average number of CTA groups per polymer chain as determined by ^{1}H NMR spectroscopy. Polymerisations were stopped after 24 h at approximately 60% styrene conversion. SEC analysis of the crude polymer samples showed multimodal traces with broad dispersities ($Đ_M$ > 3.0) (Figure 3.20) which is consistent with the occurrence of side reactions and intermolecular termination during polymerisation.

In the synthesis of graft copolymers by an R-group approach two propagating species are formed after the initial pre-equilibrium stage; radicals attached to the arms of the graft copolymer and linear macroradicals resulting from initiation by AIBN (Scheme 3.7). Both these species are in equilibrium between dormant thiocarbonyl groups and active propagating radicals resulting in the observation of bimodal molecular weight distributions by SEC analysis; where the main distribution corresponds to the graft copolymers and the low

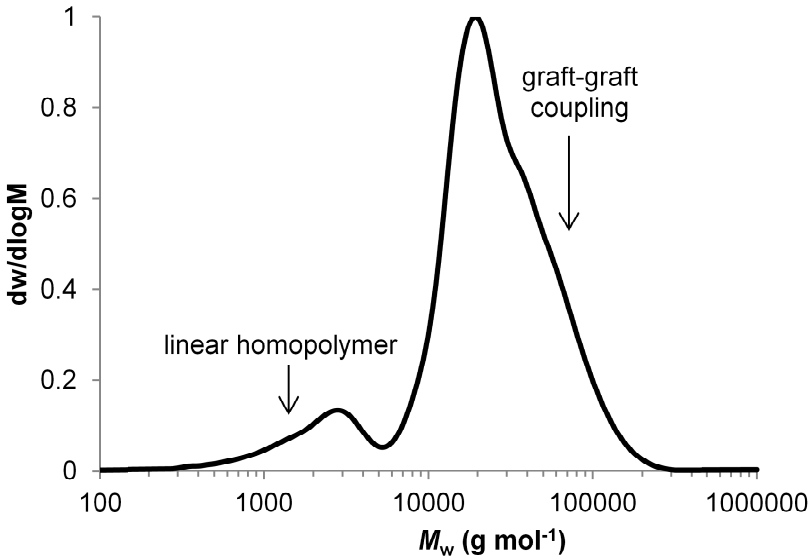

Figure 3.20. SEC chromatogram of poly(**7**-*co*-**5**-*g*-styrene) (M_n = 9.6 kDa, $Đ_M$ = 3.28). Conditions: [CTA]:[AIBN]:[styrene] = 1:0.1:50, [starting polymer] = 0.01 M in $CHCl_3$ at 65 °C.

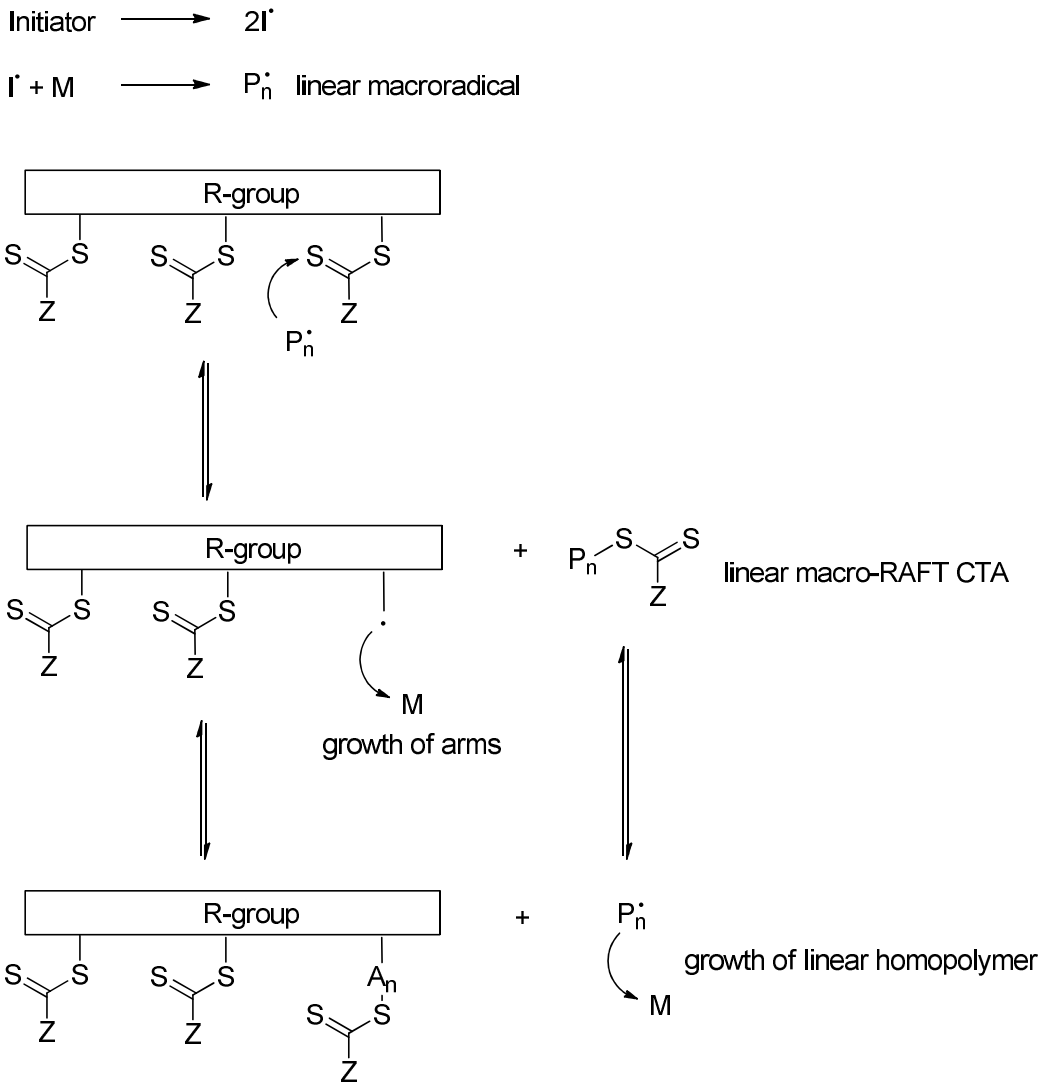

Scheme 3.7. Synthesis of graft copolymers by a RAFT R-group approach.

molecular weight second distribution corresponds to linear polymer chains. Termination of these propagating species by radical-radical coupling can occur in several ways. Intramolecular arm-arm coupling and coupling with linear polymer chains leads to the formation of dead arms. Intermolecular arm-arm coupling, leading to graft-graft coupling, results in the formation of higher molecular weight species, which can be seen as high molecular weight shoulders of the main polymer distribution by SEC analysis and become more pronounced as monomer conversion increases. The SEC chromatogram in

Figure 3.20 clearly shows the occurrence of graft-graft coupling and the presence of low molecular weight linear poly(styrene). Similar findings have been previously reported for the preparation of star and graft copolymers through RAFT R-group approaches with a range of monomers.[66, 67]

3.2.4.1 Synthesis of Graft Copolymers by RAFT Polymerisation: Optimisation of Conditions

In order to reduce the amount of graft-graft coupling, polymerisations were conducted under more dilute conditions (3.0 mM of starting polymer in chloroform). A decrease in high molecular weight shoulder and $Đ_M$ (~ 2.5) was observed, however, as a consequence of the slow propagation rate of styrene and longer polymerisation times at lower concentrations, a significant amount of graft-graft coupling was still observed. Monitoring the change in molecular weight distribution with respect to time revealed that even at monomer conversions of *ca.* 10% graft-graft coupling was still present (Figure 3.21).

In order to prepare well-defined graft copolymers, further studies focused on the preparation of graft copolymers with a faster propagating monomer. This would provide shortened polymerisation times, that in turn would reduce the number of radicals generated during polymerisation and reduce the likelihood of termination by radical-radical coupling. To this end, methyl acrylate, MA, was grafted from polymer **P2c** (24% incorporation of **5**, the lowest incorporation of **5**), using a ratio of 1:0.1:50 ([CTA]:[AIBN]:[monomer]) and 3.0 mM starting polymer solution. The polymerisation was stopped after 7 h and ^{1}H NMR spectroscopic analysis of the solution revealed that 73% monomer conversion had been obtained. Monitoring the change in molecular weight

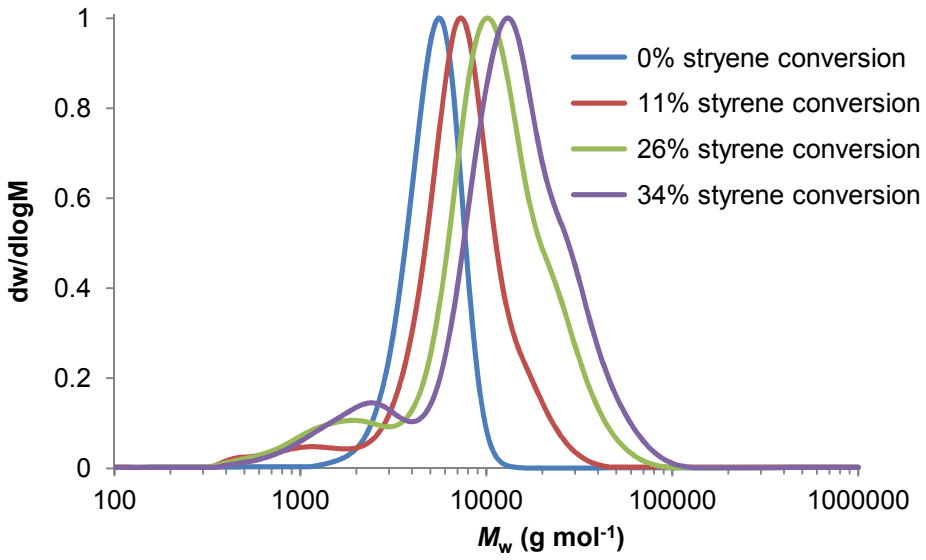

Figure 3.21. Evolution of SEC chromatograms during preparation of poly(**7**-*co*-**5**-*g*-styrene) Conditions:, [CTA]:[AIBN]:[styrene] = 1:0.1:50, [starting polymer] = 0.003 M in $CHCl_3$ at 65 °C.

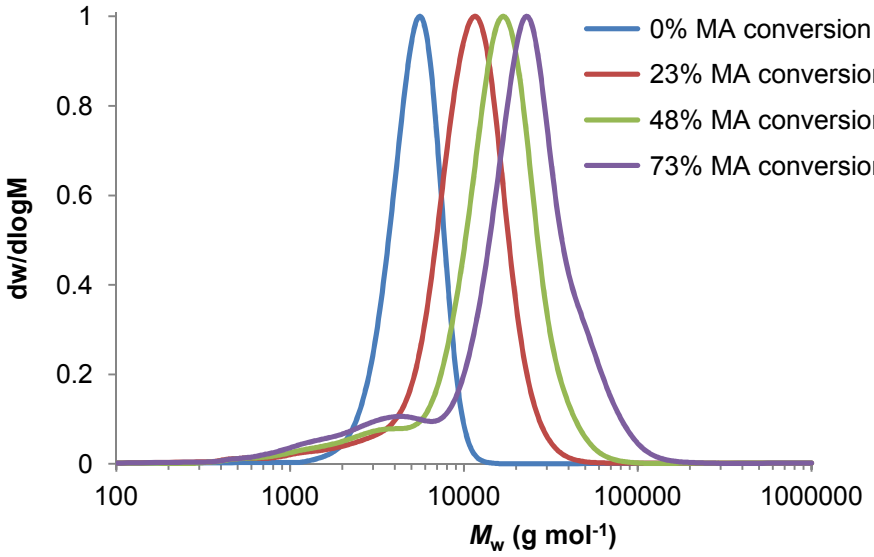

Figure 3.22. Evolution of SEC chromatograms during preparation of poly(**7**-*co*-**5**-*g*-MA) Conditions: [CTA]:[AIBN]:[MA] = 1:0.1:50, [starting polymer] = 0.003 M in $CHCl_3$ at 65 °C.

distribution with respect to time revealed that for polymerisations of MA, graft-graft coupling was not observed until > 50% monomer conversion (Figure 3.22) and the final polymer showed significantly reduced graft-graft coupling compared to analogous poly(styrene) polymerisations as judged by SEC analysis.

The amount of linear homopolymer and termination by graft-graft coupling is proportional to the number of radicals generated during polymerisation; therefore reducing the concentration of radicals in the polymerisation system should prevent such undesirable side reactions. In practice however, it was found that halving the concentration of AIBN led to longer polymerisation times, which in turn increased the total number of radicals generated during the polymerisation. Thus no significant difference was observed in the amount of graft-graft coupling and linear PMA between polymerisations with 0.1 and 0.05 equivalents of AIBN with respect to RAFT CTA concentration (Figure 3.23). Consequently, to prepare graft copolymers in the absence of termination by graft-graft coupling, polymerisations were terminated at low MA conversions (*ca.* 30%). After precipitation into methanol, to remove linear PMA homopolymer impurities, well-defined graft copolymers with monomodal SEC chromatograms and narrow dispersities ($Đ_M \leq 1.2$) were isolated (Figure 3.24).

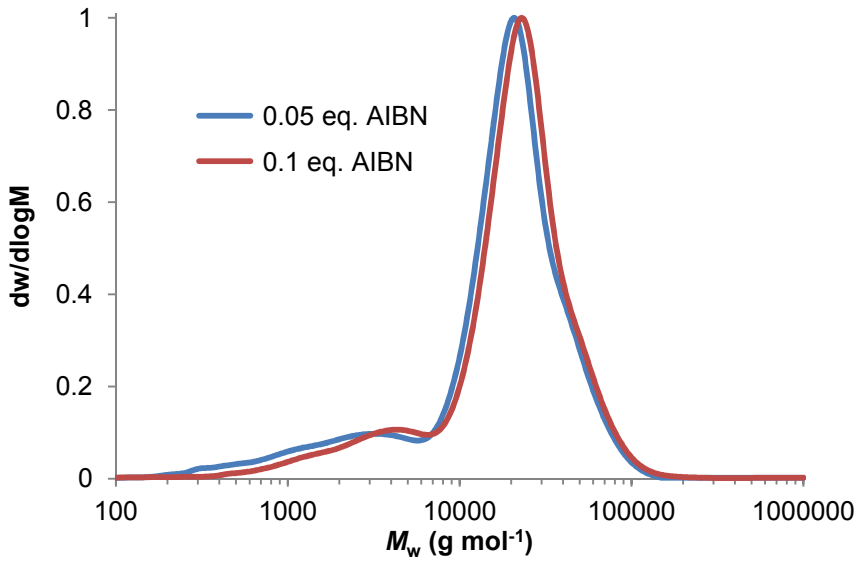

Figure 3.23. SEC chromatograms of poly(**7**-*co*-**5**-*g*-MA) with varying equivalents of AIBN. 0.05 eq. of AIBN (M_n = 6.4 kDa, $Đ_M$ = 3.54), 0.1 eq. of AIBN (M_n = 9.4 kDa, $Đ_M$ = 2.68). Conditions: [CTA]:[MA] = 1:50, [starting polymer] = 0.003 M in $CHCl_3$ at 65 °C.

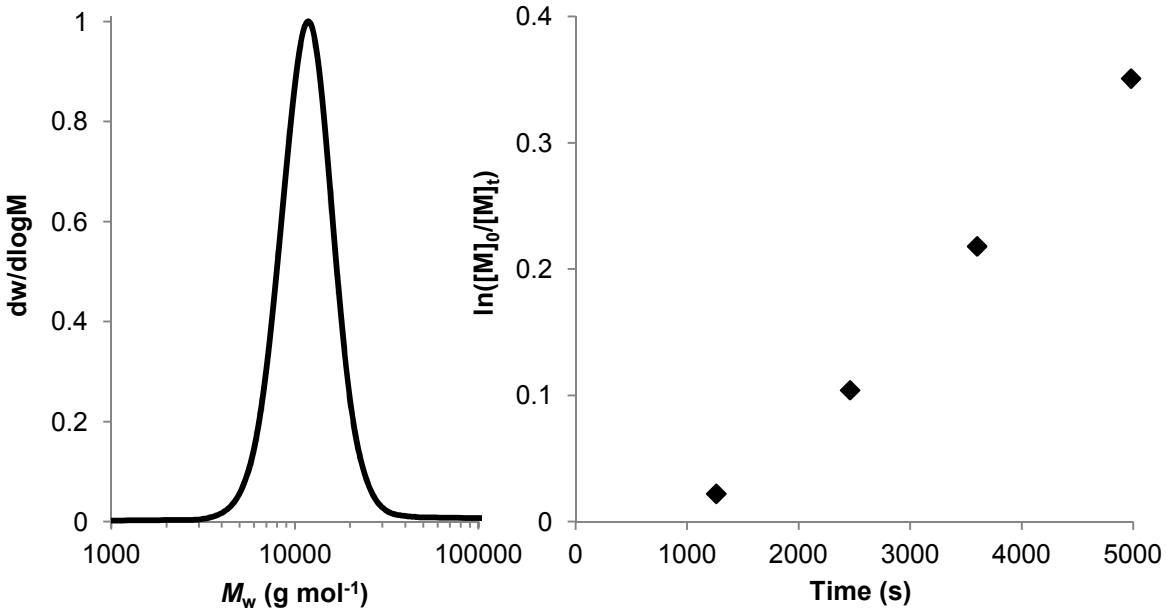

Figure 3.24. (Left) SEC chromatogram of graft copolymer **P3** poly(**7**$_{13}$-*co*-**5**$_4$-*g*-MA$_{15}$) (M_n = 10.9 kDa, $Đ_M$ = 1.14). Conditions: [CTA]:[AIBN]:[MA]) = 1:0.1:50, in $CHCl_3$ at 65 °C. (Right) *Pseudo*-first-order kinetic plot up to 30% MA conversion. Conditions: [CTA]:[AIBN]:[MA] = 1:0.1:500, in $CHCl_3$ at 65 °C.

The linear behaviour of the *pseudo*-first-order kinetic plot up to 30% monomer conversion after a short inhibition period, demonstrates that the concentration of radicals in the polymerisation system is constant and provides further evidence that no significant termination by graft-graft coupling or other mechanisms is occurring .

3.2.4.2 Synthesis of Graft Copolymers by RAFT Polymerisation: Varying Arm Length and Grafting Density

Variation of the equivalents of methyl acrylate used during polymerisation enabled the synthesis of polymers **P3-6**, with different arm lengths ranging from DP 15 to DP 120. Again, well-defined graft copolymers with monomodal SEC traces and narrow molecular weight distributions were obtained after

precipitation by terminating the polymerisations at low monomer conversion (Figure 3.25).

PMA graft copolymers with higher grafting densities were prepared by growing PMA arms from polycarbonates with greater incorporations of monomer **5**; **P1**, **P2a** and **P2b** (100%, 52% and 34% incorporation of monomer **5** respectively). For polymers with 52% and 34% RAFT CTA incorporation well-defined graft copolymers were isolated after precipitation (**P7** and **P8** Table 3.6). However, some graft-graft coupling was observed when grafting from the polymer with the highest incorporation of RAFT CTA functionality, **P1**, even at lower monomer conversions (*ca.* 20%). This was attributed to the greater concentration and close proximity of the RAFT CTA sites in polymer **P1** leading to an increased likelihood of graft-graft coupling. Termination of the polymerisation below 15% monomer conversion allowed this limitation to be

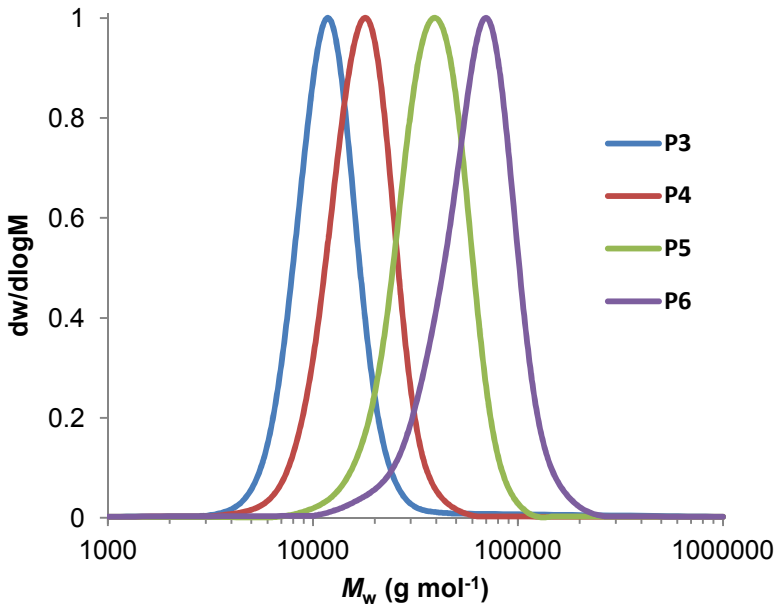

Figure 3.25. SEC chromatograms of graft copolymers **P3** (poly(**7**$_{13}$-*co*-**5**$_4$-*g*-MA$_{15}$), M_n = 10.9 kDa, $Đ_M$ = 1.14), **P4** (poly(**7**$_{13}$-*co*-**5**$_4$-*g*-MA$_{31}$), M_n = 15.6 kDa, $Đ_M$ = 1.15), **P5** (poly(**7**$_{13}$-*co*-**5**$_4$-*g*-MA$_{59}$), M_n = 33.9 kDa, $Đ_M$ = 1.18) and **P6** (poly(**7**$_{13}$-*co*-**5**$_4$-*g*-MA$_{120}$), M_n = 55.4 kDa, $Đ_M$ = 1.23).

overcome and hence provides access to well-defined highly dense graft copolymer structures (**P9** Table 3.6 and Figure 3.26).

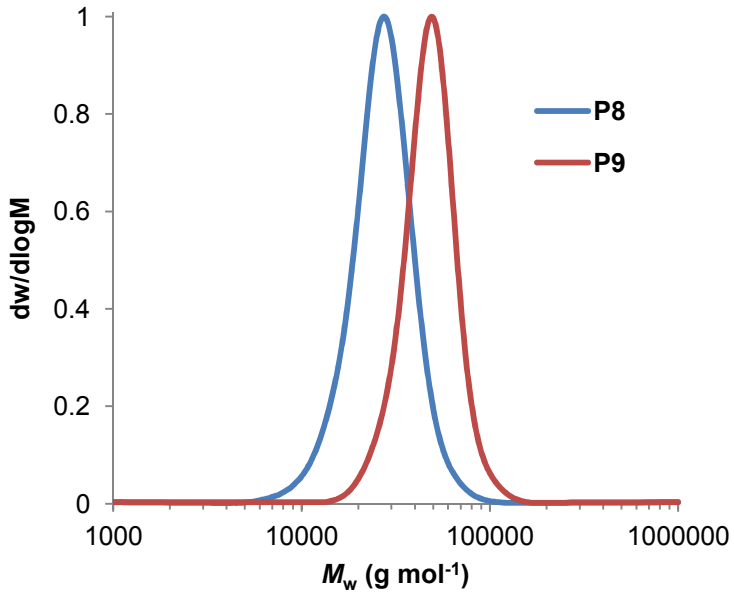

Figure 3.26. SEC chromatograms of graft copolymers **P8** poly($\mathbf{7}_{10}$-*co*-$\mathbf{5}_{11}$-*g*-MA$_{36}$) (M_n = 24.4 kDa, $Đ_M$ = 1.17) and **P9** poly($\mathbf{5}_{20}$-*g*-MA$_{48}$) (M_n = 44.7 kDa, $Đ_M$ = 1.12).

Table 3.6. Characterisation of PMA graft copolymers **P3-P9**.

Polymer	Structure	Monomer conversion (%)[e]	M_n(NMR) (kDa)[e]	M_n(SEC) (kDa)[f]	$Đ_M$[f]
P3[a]	Poly($\mathbf{7}_{13}$-*co*-$\mathbf{5}_{4}$-*g*-MA$_{15}$)	24	9.2	10.9	1.14
P4[b]	Poly($\mathbf{7}_{13}$-*co*-$\mathbf{5}_{4}$-*g*-MA$_{31}$)	23	14.7	15.6	1.15
P5[c]	Poly($\mathbf{7}_{13}$-*co*-$\mathbf{5}_{4}$-*g*-MA$_{59}$)	30	24.3	33.9	1.18
P6[d]	Poly($\mathbf{7}_{13}$-*co*-$\mathbf{5}_{4}$-*g*-MA$_{120}$)	27	45.4	55.4	1.23
P7[b]	Poly($\mathbf{7}_{13}$-*co*-$\mathbf{5}_{7}$-*g*-MA$_{39}$)	30	28.9	23.9	1.17
P8[b]	Poly($\mathbf{7}_{10}$-*co*-$\mathbf{5}_{11}$-*g*-MA$_{36}$)	21	40.0	24.4	1.17
P9[c]	Poly($\mathbf{5}_{20}$-*g*-MA$_{48}$)	14	89.6	44.7	1.12

[a]50 eq. of MA. [b]100 eq. of MA. [c]250 eq. of MA. [d]500 eq. of MA. [e]Determined by ^{1}H NMR spectroscopy. [f]Determined by SEC analysis in $CHCl_3$ using PMMA standards. Conditions: [CTA]:[AIBN] = 1:0.1 in $CHCl_3$ at 65 °C.

^{1}H NMR spectroscopic analysis of polymers **P3-9** reveals the appearance of a singlet at δ = 3.66 ppm and multiple resonances at δ = 1.00 – 2.50 ppm that correspond to the methyl group of the PMA repeat unit and the PMA backbone respectively (Figure 3.27). Resonances at δ = 4.27 and 1.23 ppm that result from the polycarbonate backbone were also observed. The RAFT CTA end group fidelity of the PMA arms was confirmed by the retention of the quartet and triplet resonances at δ = 3.37 and 1.35 ppm respectively, that correspond to the ethyl group of the RAFT CTA moiety. By comparison of the integral of the PMA repeat unit and the integrals corresponding to the ethyl group of the RAFT CTA moiety, the average DP of the PMA arms was determined and found to be in excellent agreement with theoretical values of DP based on monomer conversion. Furthermore, the complete loss of resonance at δ = 4.73 ppm, that corresponds to the benzyl protons adjacent to the trithiocarbonate group, confirms quantitative "grafting from" all RAFT CTA groups located along the polycarbonate backbone .

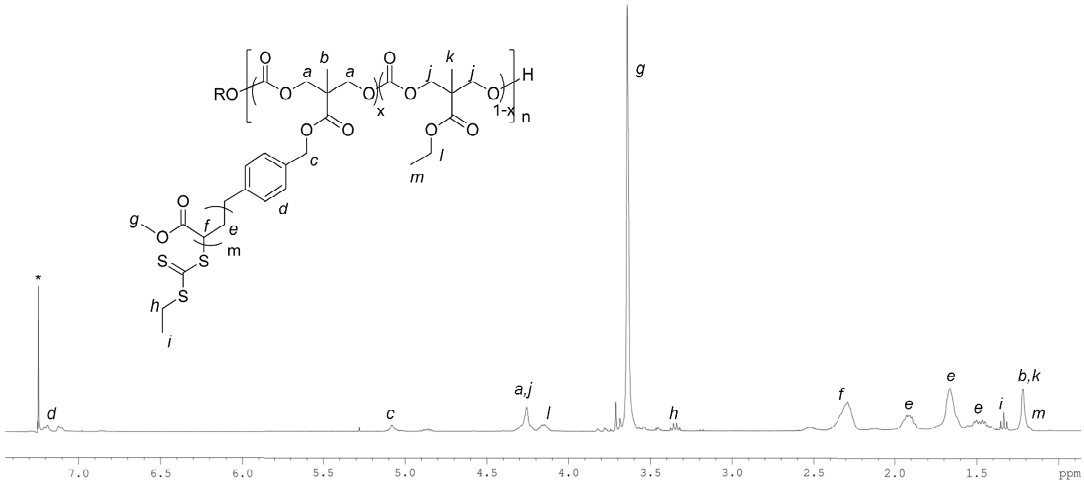

Figure 3.27. ^{1}H NMR spectrum (400 MHz; $CDCl_3$) of graft copolymer **P7** poly(**7**$_{13}$-*co*-**5**$_7$-*g*-MA$_{39}$) (*$CHCl_3$).

Analysis of the graft copolymers by diffusion-ordered NMR spectroscopy (DOSY) revealed that resonances that correspond to the polycarbonate repeat unit (δ = 4.27 and 1.23 ppm) and PMA repeat unit (δ = 1.00 – 2.50 and 3.66 ppm) possess a single diffusion coefficient, indicating that the PMA arms are indeed attached to the polycarbonate backbone (Figure 3.28). The DOSY spectra also showed no evidence of residual PMA homopolymer impurities present in the precipitated samples.

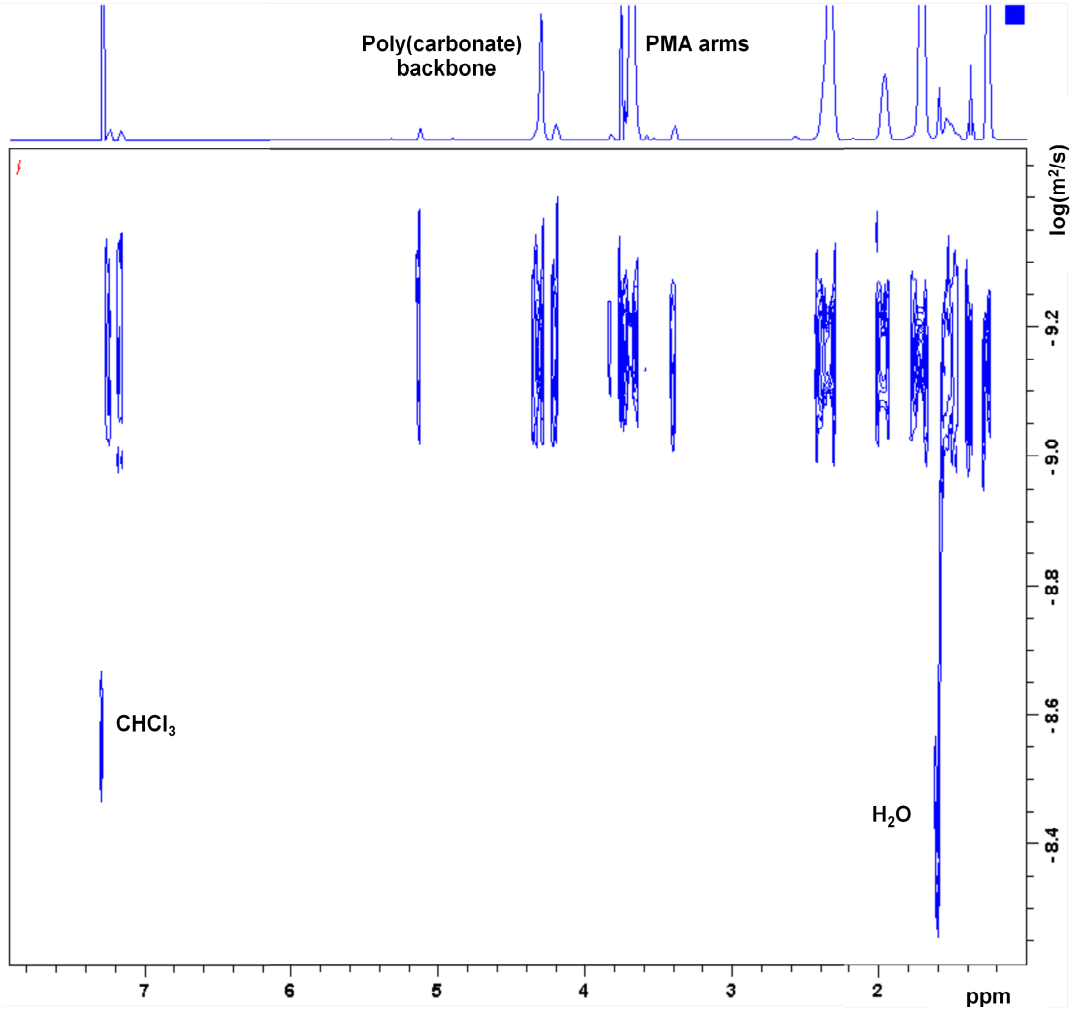

Figure 3.28. ^{1}H NMR DOSY spectrum (500MHz; $CDCl_3$) of graft copolymer **P7** poly(**7**$_{13}$-*co*-**5**$_{7}$-*g*-MA$_{39}$).

3.2.4.3 Synthesis of Graft Copolymers by RAFT Polymerisation: Growth of Hydrophilic Monomers

To further demonstrate the versatility of this method, graft copolymers were prepared using the thermoresponsive monomer *N*-isopropylacrylamide (NiPAm) and the pro-hydrophilic monomer tetrahydropyran acrylate (THPA) (Figure 3.29), where poly(THPA) can be deprotected to afford poly(acrylic acid). Poly(NiPAm) and poly(THPA) arms were grown from polymer **P2c** (24% incorporation of **5**), with either 100 or 250 equivalents of monomer per CTA unit and [starting polymer] = 3.0 mM in chloroform. Similar to the grafting of methyl acrylate, following the polymerisations by SEC analysis with respect to time revealed the presence of linear homopolymer impurities and occurrence of graft-graft coupling at higher monomer conversions (Figure 3.30).

Linear poly(NiPAm) impurities could be removed by precipitation in diethyl ether, whereas linear poly(THPA) impurities were removed by precipitation in petroleum ether 40-60 °C. When polymerisations were terminated at *ca*. 35% monomer conversion and subsequently precipitated, the resulting polycarbonate-*graft*-poly(NiPAm) (**P10**) and polycarbonate-*graft*- poly(THPA) (**P11**) copolymers showed narrow molecular weight distributions by SEC analysis (Figure 3.31 and Table 3.7).

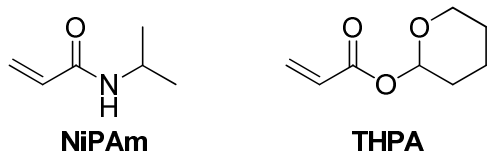

Figure 3.29. Monomers used to prepare hydrophilic graft copolymers.

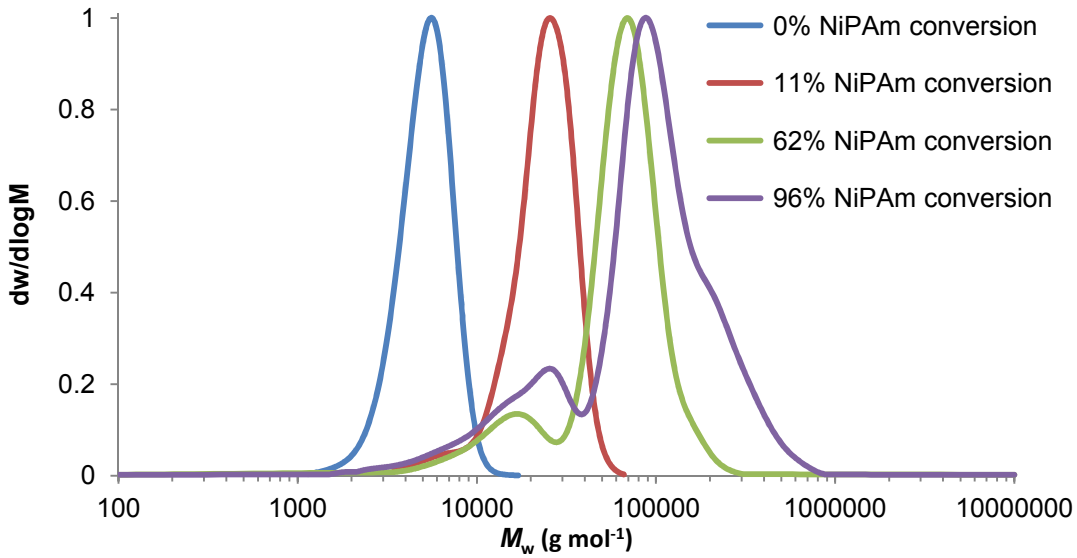

Figure 3.30. Evolution of SEC chromatograms during preparation of poly(**7**-*co*-**5**-*g*-NiPAm) Conditions: [CTA]:[AIBN]:[NiPAm] = 1:0.1:250, [starting polymer] = 0.003 M in $CHCl_3$ at 65 °C.

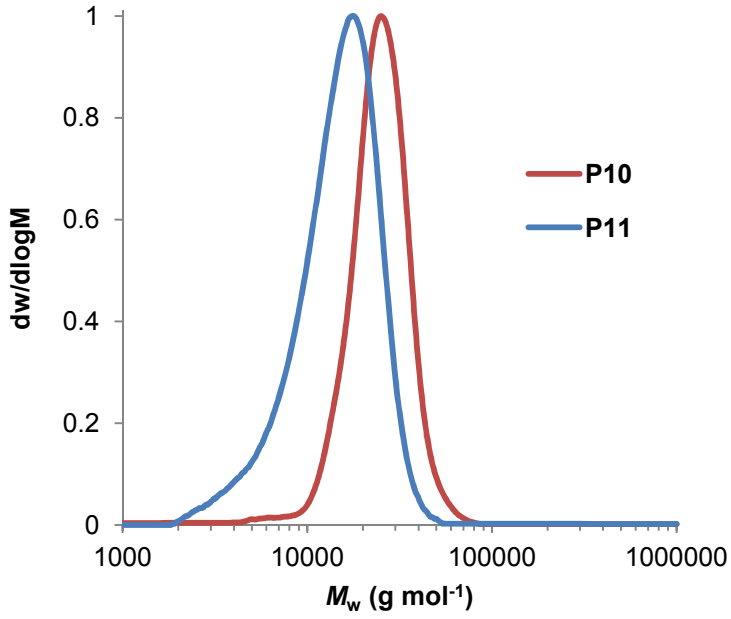

Figure 3.31. SEC chromatograms of graft copolymers **P10** poly($\mathbf{7}_{13}$-*co*-$\mathbf{5}_4$-*g*-NiPAm$_{40}$) (M_n = 22.3 kDa, $Đ_M$ = 1.15) and **P11** poly($\mathbf{7}_{13}$-*co*-$\mathbf{5}_4$-*g*-THPA$_{32}$) (M_n = 12.2 kDa, $Đ_M$ = 1.32).

Table 3.7. Characterisation of graft copolymers **P10** and **P11**.

Polymer	Structure	Monomer conversion (%)	M_n(NMR) (kDa)[a]	M_n(SEC) (kDa)	$Đ_M$
P10	Poly(**7**$_{13}$-*co*-**5**$_4$-*g*-NiPAm$_{40}$)	35	23.0	22.3[b]	1.15[b]
P11	Poly(**7**$_{13}$-*co*-**5**$_4$-*g*-THPA$_{32}$)	35	26.1	12.2[c]	1.32[c]

[a]Determined by ^{1}H NMR spectroscopy. [b]Determined by SEC analysis in DMF using PMMA standards. [c]Determined by SEC analysis in $CHCl_3$ using PMMA standards. Conditions: [CTA]:[AIBN]:[monomer] = 1:0.1:100 in $CHCl_3$ at 65 °C.

3.2.4.4 Synthesis of Graft Copolymers by RAFT Polymerisation: Thermal Properties

Analysis of the PMA and poly(NiPAm) graft copolymers by differential scanning calorimetry was performed to investigate the effect of chemical structure on the thermal properties of the polymers. The growth of PMA arms from the polycarbonate backbone decreased the glass transition temperature (T_g) of the graft copolymers compared to the polymer prior to RAFT polymerisation (Table 3.8). For example, polymer **P2c** displayed a T_g of 21.6 °C before RAFT polymerisation, decreasing to 18.0 °C when PMA arms of DP 31 (**P4**) were

Table 3.8. Glass transition temperatures of PMA and poly(NiPAm) graft copolymers.

Polymer	Structure	T_g (°C)[a]
P2c	Poly(**7**$_{13}$-*co*-**5**$_4$)	21.6
P4	Poly(**7**$_{13}$-*co*-**5**$_4$-*g*-MA$_{31}$)	18.0
P5	Poly(**7**$_{13}$-*co*-**5**$_4$-*g*-MA$_{59}$)	20.0
P6	Poly(**7**$_{13}$-*co*-**5**$_4$-*g*-MA$_{120}$)	21.5
P10	Poly(**7**$_{13}$-*co*-**5**$_4$-*g*-NiPAm$_{40}$)	125.4

[a]Determined by DSC analysis at the second scan.

grown from the backbone. A slight increase in T_g was observed as PMA arm length was increased. As expected the poly(NiPAm) graft copolymer **P10** displayed a significantly higher T_g (125.4 °C) than that of the PMA graft copolymers.

3.2.5 Self-Assembly of Polycarbonate-*g*-Poly(*N*-isopropylacrylamide)

The hydrophobic nature of the polycarbonate backbone and thermoresponsive hydrophilic behaviour of the poly(NiPAm) arms of graft copolymer **P10** provided the opportunity to form self-assembled nanostructures in water, possessing a polycarbonate core and poly(NiPAm) shell (Scheme 3.8).

3.2.5.1 Self-Assembly of Polycarbonate-*g*-Poly(*N*-isopropylacrylamide): Particle Formation and Characterisation

Initial investigations into the self-assembly behaviour of **P10** found the polymer was insoluble in water at room temperature, but was found to solubilise when the temperature of the solution was reduced to 4 °C. Consequently, the self-

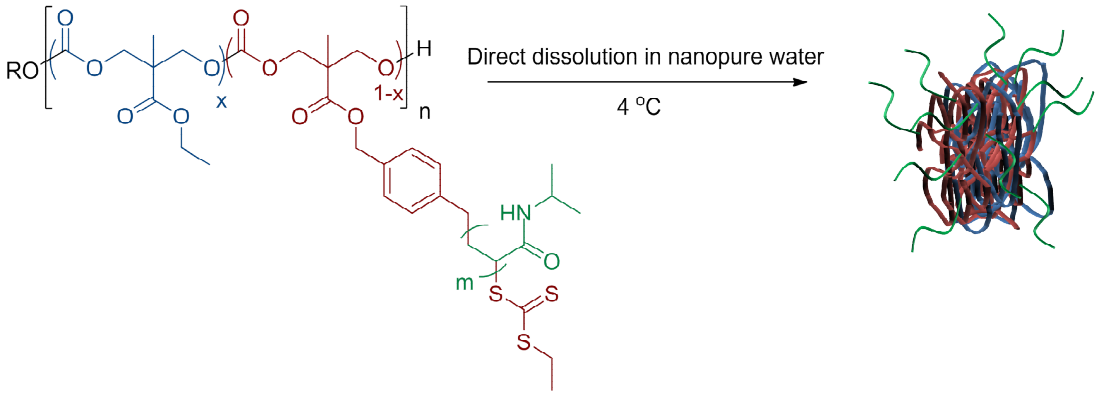

Scheme 3.8. Self-assembly of graft copolymer **P10** (poly(**7**$_{13}$-*co*-**5**$_4$-*g*-NiPAm$_{40}$)).

assembly of **P10** could be induced by direct dissolution, where the polymer was dissolved in nanopure water (18.2 mΩ·cm) at 4 °C, at a concentration of 1 mg/mL. Analysis of the resulting solution by dynamic light scattering (DLS) confirmed the presence of nanostructures with a number-average solution hydrodynamic diameter, D_h, of 12 ± 0.4 nm (Figure 3.32). A slightly broad dispersity of 0.331 was observed for the particles as a consequence of larger aggregated species as observed in the intensity profile and thought to be caused by favourable interactions between poly(NiPAm) corona. Attempts to optimise the self-assembly conditions by preparing solutions at lower concentrations (0.25 mg/mL) and utilising a solvent switch method, from THF to nanopure water, did not reduce the formation of these aggregates. DLS analysis of **P10** in nanopure water was compared with DLS analysis of **P10** in THF, a good solvent for both the polycarbonate backbone and poly(NiPAm) arms. The polymer THF solution gave a lower number-average solution hydrodynamic diameter of

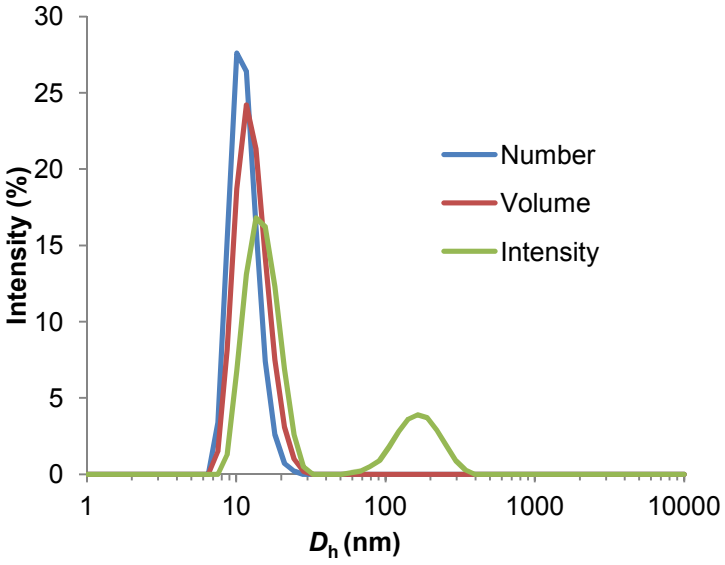

Figure 3.32. DLS analysis of particles prepared from **P10** poly($\mathbf{7}_{13}$-*co*-$\mathbf{5}_{4}$-*g*-NiPAm$_{40}$) at 1 mg/mL in nanopure water at 4 °C.

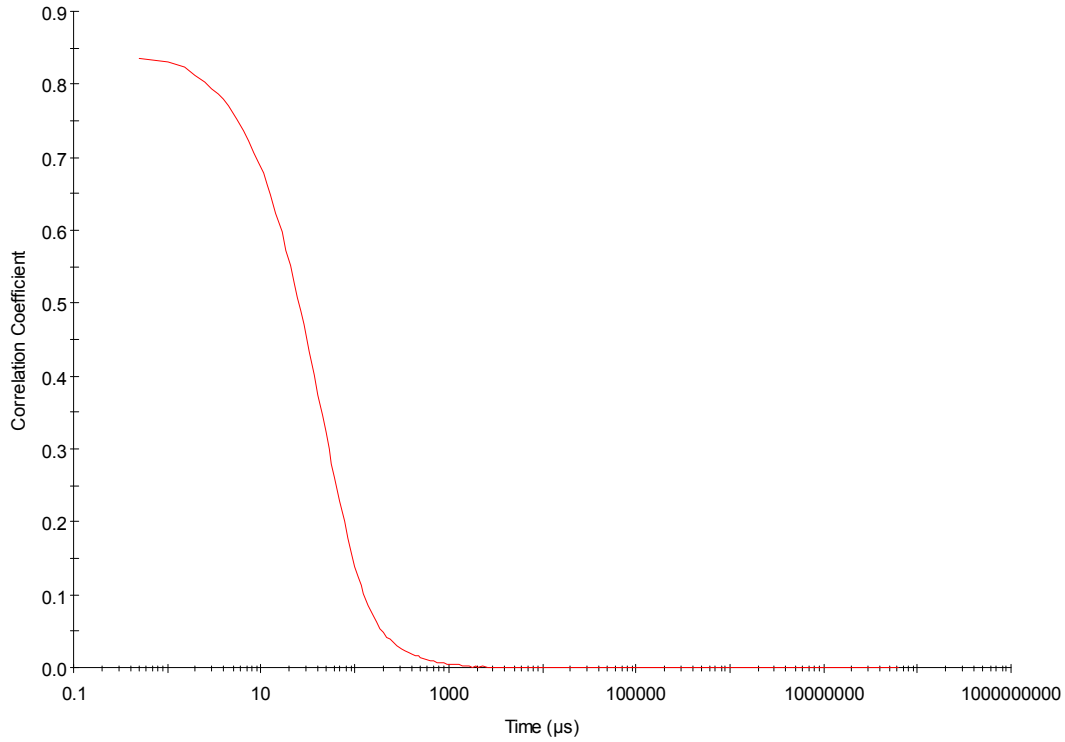

Figure 3.33. Correlation function for poly($\mathbf{7}_{13}$-*co*-$\mathbf{5}_{4}$-*g*-NiPAm$_{40}$) particles at 1 mg/mL in nanopure water at 4 °C.

7.5 ± 0.4 nm, indicating the presence of unimers in THF in contrast to the assembled structures observed in nanopure water.

The size and morphology of the self-assembled nanostructures was further investigated by dry-state transmission electron microscopy (TEM). TEM samples were prepared by drop deposition onto a copper/carbon grid previously deposited with a thin film of graphene oxide. The grids were cooled to 4 °C prior to sample deposition and kept at this temperature until all water had evaporated. The use of a nearly electron transparent graphene oxide film results in excellent image contrast without the use of staining.[68] Well-defined spherical micellar structures were observed by TEM with an average diameter of 12 ± 2 nm (Figure 3.34).

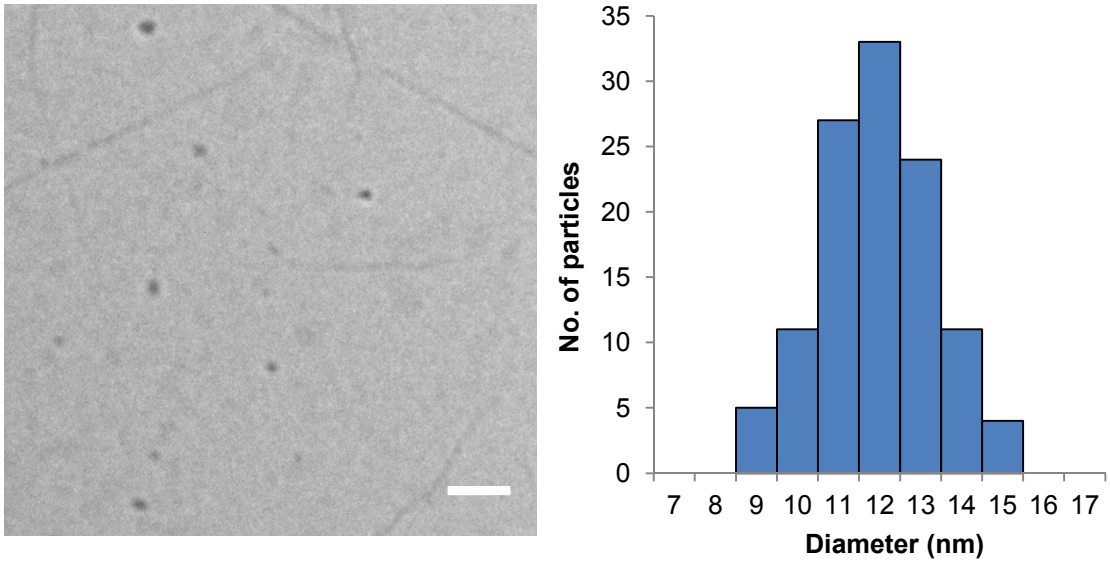

Figure 3.34. TEM analysis of particles prepared from **P10** poly($\mathbf{7}_{13}$-*co*-$\mathbf{5}_{4}$-*g*-NiPAm$_{40}$). (Left) TEM image, scale bar = 100 nm. (Right) TEM size distribution histogram.

3.2.5.2 Self-Assembly of Polycarbonate-*g*-Poly(*N*-isopropylacrylamide): Thermoresponsive Behaviour

The lower critical solution temperature (LCST) of the micelles in nanopure water was determined spectrophotometrically by measuring the turbidity of the solution (1 mg/mL) at various temperatures (6 – 30 °C), with a 1 °C/min heating/cooling cycle. A sharp transition was observed in the plot of transmittance *versus* temperature corresponding to an LCST of 20 °C (Figure 3.35), 12 °C lower than the LSCT reported for poly(NiPAm) homopolymer.[69] This decrease in LCST was attributed to the close proximity of the poly(NiPAm) arms to the hydrophobic polycarbonate backbone, as a consequence of the grafted structure of the copolymer, therefore increasing the overall hydrophobicity of the polymer. Similar findings have previously been reported for amphiphilic poly(NiPAm) block copolymers.[70] The heating and cooling traces for the transition overlaid well indicating minimal hysteresis occurred

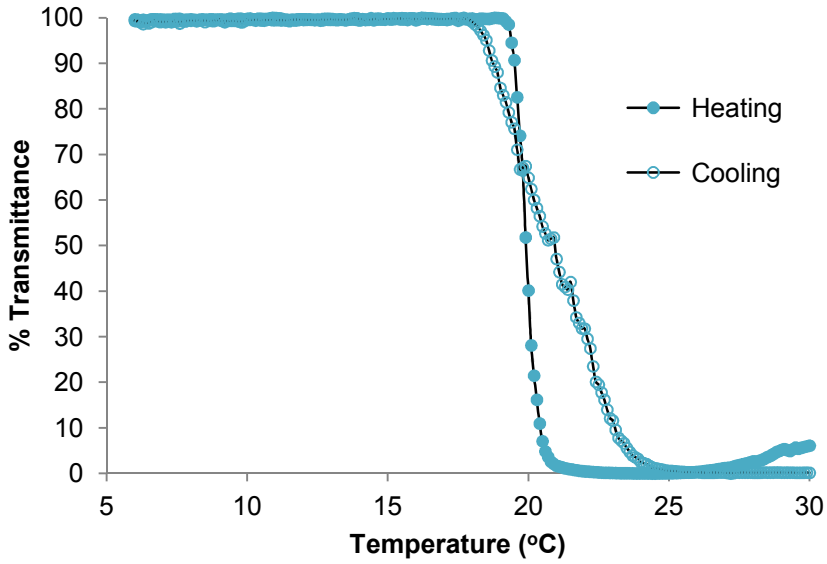

Figure 3.35. Plot of percentage transmittance against temperature (°C) for graft copolymer **P10** poly(**7**$_{13}$-*co*-**5**$_{4}$-*g*-NiPAm$_{40}$) at 1 mg/mL in nanopure water, heating/cooling rate = 1 °C/min.

during the phase transition. Micelles readily reformed upon cooling, as determined by DLS analysis, indicating the transition was indeed reversible (Figure 3.36).

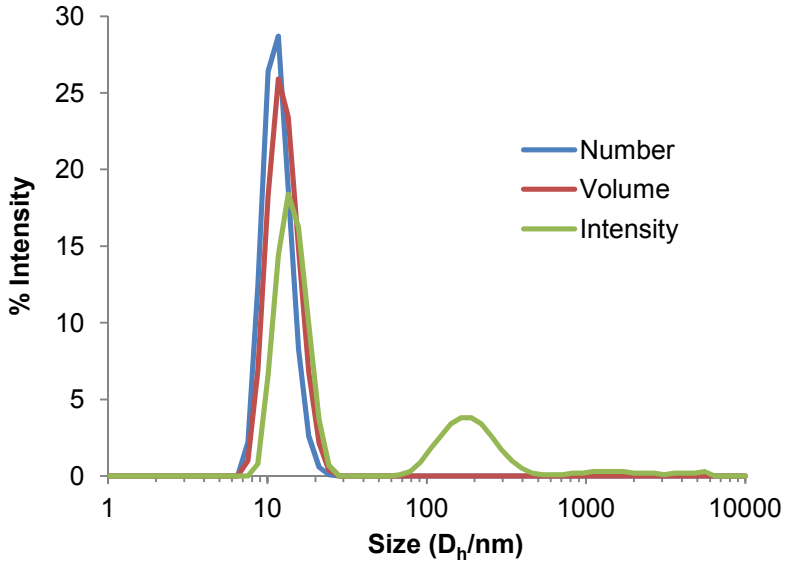

Figure 3.36. DLS analysis of particles formed after a heating/cooling cycle from **P10** poly(**7**$_{13}$-*co*-**5**$_{4}$-*g*-NiPAm$_{40}$) at 1 mg/mL in nanopure water at 4 °C.

3.3 Conclusions

In conclusion, a novel cyclic carbonate monomer bearing a RAFT CTA pendent group has been synthesised and its ring-opening polymerisation demonstrated using a range of organocatalyst systems. The optimum catalyst system, 5 mol% 1,8-diazabicycloundec-7-ene (DBU), exhibited excellent control and activity and yielded well-defined polycarbonates with low dispersity values and monomodal molecular weight distributions. The incorporation of RAFT CTA functionality into the polycarbonate backbone was varied through copolymerisation of the RAFT-functional cyclic carbonate monomer with an ethyl-functional cyclic carbonate monomer. Subsequent RAFT polymerisations allowed the preparation of graft copolymers with a degradable polycarbonate backbone, by an R-group RAFT approach. Optimisation of the RAFT polymerisation conditions; specifically polymerising fast propagating monomers and terminating polymerisations at low conversions, enabled the synthesis of well-defined graft copolymers with narrow molecular weight distributions and predictable arm lengths. Control of the solution and thermal properties of the graft copolymers was achieved through variation of graft length, grafting density and grafting monomer. The growth of poly(NiPAm) from the polycarbonate backbone afforded thermoresponsive amphiphilic graft copolymers, that were found to self-assemble in nanopure water at 4 °C, providing a convenient route to novel thermoresponsive biodegradable micelles. This work demonstrates how combining disparate polymerisation techniques, namely ROP and RAFT, provides a versatile methodology to incorporate functionality into polycarbonates.

3.4 References

1. N. Hadjichristidis, H. Iatrou, M. Pitsikalis and J. Mays, *Prog. Polym. Sci.*, 2006, **31**, 1068-1132.
2. N. Hadjichristidis, M. Pitsikalis, S. Pispas and H. Iatrou, *Chem. Rev.*, 2001, **101**, 3747-3792.
3. A. Blencowe, J. F. Tan, T. K. Goh and G. G. Qiao, *Polymer*, 2009, **50**, 5-32.
4. K. Khanna, S. Varshney and A. Kakkar, *Polym. Chem.*, 2010, **1**, 1171-1185.
5. H. Gao and K. Matyjaszewski, *Prog. Polym. Sci.*, 2009, **34**, 317-350.
6. H. R. Kricheldorf, *J. Polym. Sci., Part A: Polym. Chem.*, 2010, **48**, 251-284.
7. Z. Jia and M. J. Monteiro, *J. Polym. Sci., Part A: Polym. Chem.*, 2012, **50**, 2085-2097.
8. B. A. Laurent and S. M. Grayson, *Chem. Soc. Rev.*, 2009, **38**, 2202-2213.
9. R. M. England and S. Rimmer, *Polym. Chem.*, 2010, **1**, 1533-1544.
10. B. I. Voit and A. Lederer, *Chem. Rev.*, 2009, **109**, 5924-5973.
11. A. Carlmark, C. Hawker, A. Hult and M. Malkoch, *Chem. Soc. Rev.*, 2009, **38**, 352-362.
12. K. Inoue, *Prog. Polym. Sci.*, 2000, **25**, 453-571.
13. C. Feng, Y. Li, D. Yang, J. Hu, X. Zhang and X. Huang, *Chem. Soc. Rev.*, 2011, **40**, 1282-1295.
14. H.-i. Lee, J. Pietrasik, S. S. Sheiko and K. Matyjaszewski, *Prog. Polym. Sci.*, 2010, **35**, 24-44.
15. S. S. Sheiko, B. S. Sumerlin and K. Matyjaszewski, *Prog. Polym. Sci.*, 2008, **33**, 759-785.
16. M. Zhang and A. H. E. Müller, *J. Polym. Sci., Part A: Polym. Chem.*, 2005, **43**, 3461-3481.

17. O. Azzaroni, *J. Polym. Sci., Part A: Polym. Chem.*, 2012, **50**, 3225-3258.

18. D. Uhrig and J. Mays, *Polym. Chem.*, 2011, **2**, 69-76.

19. H. Keul, in *Handbook of Ring-Opening Polymerization*, Wiley-VCH Verlag GmbH & Co. KGaA, 2009, pp. 307-327.

20. X. Lou, C. Detrembleur and R. Jérôme, *Macromol. Rapid Commun.*, 2003, **24**, 161-172.

21. R. J. Pounder and A. P. Dove, *Polym. Chem.*, 2010, **1**, 260-271.

22. G. Rokicki, *Prog. Polym. Sci.*, 2000, **25**, 259-342.

23. C. K. Williams, *Chem. Soc. Rev.*, 2007, **36**, 1573-1580.

24. W. Chen, H. Yang, R. Wang, R. Cheng, F. Meng, W. Wei and Z. Zhong, *Macromolecules*, 2009, **43**, 201-207.

25. V. Darcos, S. El Habnouni, B. Nottelet, A. El Ghzaoui and J. Coudane, *Polym. Chem.*, 2010, **1**, 280-282.

26. H. Freichels, V. Pourcelle, C. S. Le Duff, J. Marchand-Brynaert and C. Jérôme, *Macromol. Rapid Commun.*, 2011, **32**, 616-621.

27. R. K. Iha, B. A. van Horn and K. L. Wooley, *J. Polym. Sci., Part A: Polym. Chem.*, 2010, **48**, 3553-3563.

28. X. Jiang, E. B. Vogel, M. R. Smith and G. L. Baker, *Macromolecules*, 2008, **41**, 1937-1944.

29. R.-S. Lee and Y.-T. Huang, *J. Polym. Sci., Part A: Polym. Chem.*, 2008, **46**, 4320-4331.

30. M. Leemhuis, N. Akeroyd, J. A. W. Kruijtzer, C. F. van Nostrum and W. E. Hennink, *Eur. Polym. J.*, 2008, **44**, 308-317.

31. S. Onbulak, S. Tempelaar, R. J. Pounder, O. Gok, R. Sanyal, A. P. Dove and A. Sanyal, *Macromolecules*, 2012, **45**, 1715-1722.

32. B. Parrish, R. B. Breitenkamp and T. Emrick, *J. Am. Chem. Soc.*, 2005, **127**, 7404-7410.

33. J. Rieger, K. Van Butsele, P. Lecomte, C. Detrembleur, R. Jérôme and C. Jérôme, *Chem. Commun.*, 2005, 274-276.

34. R. Riva, S. Schmeits, C. Jérôme, R. Jérôme and P. Lecomte, *Macromolecules*, 2007, **40**, 796-803.

35. R. Riva, S. Schmeits, F. Stoffelbach, C. Jérôme, R. Jérôme and P. Lecomte, *Chem. Commun.*, 2005, 5334-5336.

36. S. Tempelaar, L. Mespouille, P. Dubois and A. P. Dove, *Macromolecules*, 2011, **44**, 2084-2091.

37. R. Wang, W. Chen, F. Meng, R. Cheng, C. Deng, J. Feijen and Z. Zhong, *Macromolecules*, 2011, **44**, 6009-6016.

38. Y. Yu, J. Zou, L. Yu, W. Ji, Y. Li, W.-C. Law and C. Cheng, *Macromolecules*, 2011, **44**, 4793-4800.

39. X. Zhang, Z. Zhong and R. Zhuo, *Macromolecules*, 2011, **44**, 1755-1759.

40. J.-Z. Du, D.-P. Chen, Y.-C. Wang, C.-S. Xiao, Y.-J. Lu, J. Wang and G.-Z. Zhang, *Biomacromolecules*, 2006, **7**, 1898-1903.

41. X. Jiang, M. R. Smith and G. L. Baker, *Macromolecules*, 2007, **41**, 318-324.

42. X. Jiang, E. B. Vogel, M. R. Smith and G. L. Baker, *J.Polym. Sci., Part A: Polym. Chem.*, 2007, **45**, 5227-5236.

43. F. Nederberg, B. G. G. Lohmeijer, F. Leibfarth, R. C. Pratt, J. Choi, A. P. Dove, R. M. Waymouth and J. L. Hedrick, *Biomacromolecules*, 2006, **8**, 153-160.

44. J. Rieger, K. V. Bernaerts, F. E. Du Prez, R. Jérôme and C. Jérôme, *Macromolecules*, 2004, **37**, 9738-9745.

45. X. Zhang, F. Chen, Z. Zhong and R. Zhuo, *Macromol. Rapid Commun.*, 2010, **31**, 2155-2159.

46. W. Dai, J. Zhu, A. Shangguan and M. Lang, *Eur. Polym. J.*, 2009, **45**, 1659-1667.

47. K. Fukushima, R. C. Pratt, F. Nederberg, J. P. K. Tan, Y. Y. Yang, R. M. Waymouth and J. L. Hedrick, *Biomacromolecules*, 2008, **9**, 3051-3056.

48. F. Tasaka, Y. Ohya and T. Ouchi, *Macromolecules*, 2001, **34**, 5494-5500.

49. D. Mecerreyes, B. Atthoff, K. A. Boduch, M. Trollsås and J. L. Hedrick, *Macromolecules*, 1999, **32**, 5175-5182.

50. C. Barner-Kowollik and S. Perrier, *J.Polym. Sci., Part A: Polym. Chem.*, 2008, **46**, 5715-5723.

51. A. P. Dove, *Chem. Commun.*, 2008, 6446-6470.

52. G. Moad, E. Rizzardo and S. H. Thang, *Aust. J. Chem.*, 2005, **58**, 379-410.

53. G. Moad, E. Rizzardo and S. H. Thang, *Aust. J. Chem.*, 2006, **59**, 669-692.

54. G. Moad, E. Rizzardo and S. H. Thang, *Polymer*, 2008, **49**, 1079-1131.

55. G. Moad, E. Rizzardo and S. H. Thang, *Aust. J. Chem.*, 2009, **62**, 1402-1472.

56. S. Perrier and P. Takolpuckdee, *J. Polym. Sci., Part A: Polym. Chem.*, 2005, **43**, 5347-5393.

57. H. Willcock and R. K. O'Reilly, *Polym. Chem.*, 2010, **1**, 149-157.

58. L. Mespouille, F. Nederberg, J. L. Hedrick and P. Dubois, *Macromolecules*, 2009, **42**, 6319-6321.

59. H. Ihre, A. Hult, J. M. J. Fréchet and I. Gitsov, *Macromolecules*, 1998, **31**, 4061-4068.

60. N. Petzetakis, A. P. Dove and R. K. O'Reilly, *Chem. Sci.*, 2011, **2**, 955-960.

61. J. Skey and R. K. O'Reilly, *Chem. Commun.*, 2008, 4183-4185.

62. R. C. Pratt, F. Nederberg, R. M. Waymouth and J. L. Hedrick, *Chem. Commun.*, 2008, 114-116.

63. H. Keul, R. Bächer and H. Höcker, *Makromol. Chem.*, 1986, **187**, 2579-2589.

64. B. G. G. Lohmeijer, R. C. Pratt, F. Leibfarth, J. W. Logan, D. A. Long, A. P. Dove, F. Nederberg, J. Choi, C. Wade, R. M. Waymouth and J. L. Hedrick, *Macromolecules*, 2006, **39**, 8574-8583.

65. Z.-L. Liu, Y. Zhou and R.-X. Zhuo, *J. Polym. Sci., Part A: Polym. Chem.*, 2003, **41**, 4001-4006.

66. C. Barner-Kowollik, T. P. Davis and M. H. Stenzel, *Aust. J. Chem.*, 2006, **59**, 719-727.

67. M. H. Stenzel, in *Handbook Of RAFT Polymerisation*, Wiley-VCH, Wenheim, 2008, pp. 315-372.

68. J. P. Patterson, A. M. Sanchez, N. Petzetakis, T. P. Smart, T. H. Epps III, I. Portman, N. R. Wilson and R. K. O'Reilly, *Soft Matter*, 2012, **8**, 3322-3328.

69. X. Wang, X. Qiu and C. Wu, *Macromolecules*, 1998, **31**, 2972-2976.

70. P. Cotanda, A. Lu, J. P. Patterson, N. Petzetakis and R. K. O'Reilly, *Macromolecules*, 2012, **45**, 2377-2384.

4 Cyclic Graft Copolymers by Ring-Opening and Reversible-Addition Fragmentation Chain Transfer Polymerisation

4.1 Introduction

The properties of polymers are inherently linked to their structure. Aided by advancements in controlled polymerisation techniques,[1-5] polymers with a diverse range of topologies have been prepared, including well-defined block, star,[6-8] cyclic,[9-13] graft,[14-17] branched[18-21] and dendritic[22, 23] polymers. However, as our ability to access different polymer architectures increases, so does the desire to explore increasingly complex and unusual polymer structures, including mikto-arm star polymers,[24] multi-cyclic topologies[25, 26] or hybrid architectures.[27] Consequently, the preparation of cyclic graft copolymers has attracted increasing attention in order to elucidate the effect of their unusual architecture on polymer properties. Cyclic polymers and graft copolymers are known to exhibit unique behaviour in comparison to linear polymers and therefore the combination of these two architectures is expected to impart unique physical properties on the resulting materials.[9, 12, 14, 15, 28]

Similar to the preparation of linear graft copolymers, cyclic graft copolymers can be prepared by either a "grafting-from", "grafting-to" or "grafting-through" approach and cyclisation can be achieved *via* ring-closure or ring-expansion techniques. For the preparation of cyclic graft copolymers *via* a ring-closure approach cyclisation is performed before "grafting-to" or "grafting-from" the cyclic backbone, to prevent a decrease in cyclisation yield as a consequence of steric crowding. Similarly, the combination of "grafting-through" and ring-closure techniques is not favored.

Schappacher and Deffieux first reported the preparation of cyclic graft copolymers in 1999 *via* a ring-closure/"grafting-to" approach to yield cyclic poly(chloroethyl vinyl ether)-*g*-poly(styrene) (PCEVE-*g*-PS), where the PCEVE

backbone and PS arms were prepared *via* living cationic and anionic polymerisations respectively.[29] In a later report, the same group pioneered the use of atomic force microscopy (AFM) to visualise high molecular weight cyclic graft copolymers (Figure 4.1).[30] Chen *et al*. also used a combination of ring-closure and "grafting-to" in the synthesis of cyclic poly(acrylic acid)-*g*-poly(ethylene glycol) (PAA-*g*-PEG), where the cyclic PAA backbone was prepared *via* the atom transfer radical polymerisation (ATRP), ring-closure and deprotection of *tert*-butyl acrylate.[31] Amine-functional PEG was subsequently grafted to the cyclic PAA backbone *via* amidation.

Huang and coworkers have investigated the preparation of cyclic graft copolymers *via* a combination of ring-closure and "grafting-from" techniques. A series of cyclic graft copolymers with poly(ethylene oxide) (PEO) backbones were prepared *via* the anionic ring-opening polymerisation (ROP) of ethylene

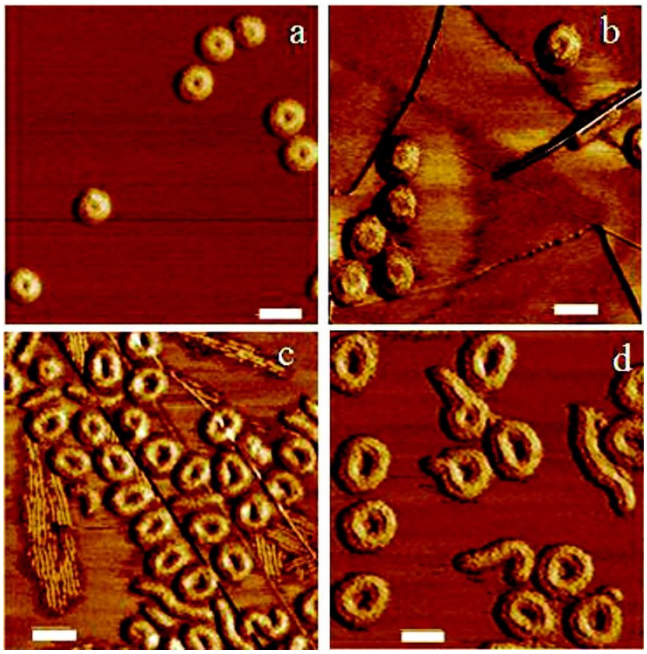

Figure 4.1. AFM phase images of cyclic polystyrene combs with increasing cyclic DP and/or with different PS graft lengths (scale bars = 100 nm).

oxide and functional epoxide monomers, allowing the introduction of initiation groups into the PEO backbone.[32-34] Poly(ethylene oxide)-*g*-poly(styrene) (PEO-*g*-PS) was prepared by two methods; in the first approach PS was grown by nitroxide mediated polymerisation (NMP), from pendent 2,2,6,6-tetramethylpiperdine-1-oxyl (TEMPO) groups located on the backbone,[32] whereas in the second approach, PS was grown by atom transfer radical polymerisation (ATRP) from 2-bromoisobutyryl bromide groups located on the cyclic PEO backbone.[34] Similarly, cyclic poly(ethylene oxide)-*g*-poly(ε-caprolactone) (PEO-*g*-PCL) was prepared *via* the ROP of ε-CL from pendent hydroxyl groups on the cyclic PEO backbone.[33] Huang and coworkers have also reported the combination of "grafting-from" and "grafting-to" approaches to prepare cyclic poly(2-hydroxyethyl methacrylate)-*g*-(poly(stryrene)-*b*-poly(ethylene oxide)) (PHEMA-*g*-(PS-*b*-PEO)) *via* ATRP and single-electron transfer nitroxide radical coupling.[35]

The use of ring-expansion techniques to prepare cyclic graft copolymers has been reported in combination with "grafting-to", "grafting-from" and "grafting-through" approaches. Grubbs and coworkers prepared high molecular weight cyclic graft copolymers *via* the ring-expansion metathesis polymerisation (REMP) of PS- and poly(lactic acid) (PLA)-functional norbornene macromonomers, demonstrating a "grafting-through" approach.[36] While Tew and coworkers have utilised both "grafting-from" and "grafting-to" techniques in combination with REMP to prepare cyclic graft copolymers.[37-39] A range of cyclic poly(norbornene)-*g*-poly(ester) copolymers were synthesised *via* the REMP of hydroxyl-functional norbornenes and subsequent ROP from the resulting hydroxyl initiation sites located on the cyclic poly(norbornene)

backbone.[38] In a "grafting-to" approach, cyclic poly(norbornene)-*g*-poly(ethylene glycol) (PNb-*g*-PEG) was prepared by the nucleophilic substitution of pentafluorophenyl (PFP) functionalised cyclic poly(norbornene), with amine-functional PEG.[37] Alternatively, cyclic PNb-*g*-PS and cyclic PNb-*g*-PEG were prepared *via* the nucleophilic substitution of the PFP groups with propargylamine, followed by the copper-catalysed azide-alkyne cycloaddition (CuAAC) with azide-functional PEG or PS.[37] In another example, cyclic PNb-*g*-PS and cyclic PNb-*g*-PEG were prepared through supramolecular metal-ligand interactions between ruthenium, terpyridine functionalised cyclic poly(norbornene) and terpyridine functionalised PS or PEG.[39] The resulting metallo-supramolecular cyclic graft copolymers could be visualised by transmission electron microscopy (TEM) and represents the first time TEM has been used to image an individual polymer of cyclic topology.

Li *et al*. reported the use of ring-expansion ROP to prepare hydroxyl-functional cyclic PCL, where subsequent "grafting-to" *via* esterification with carboxylic

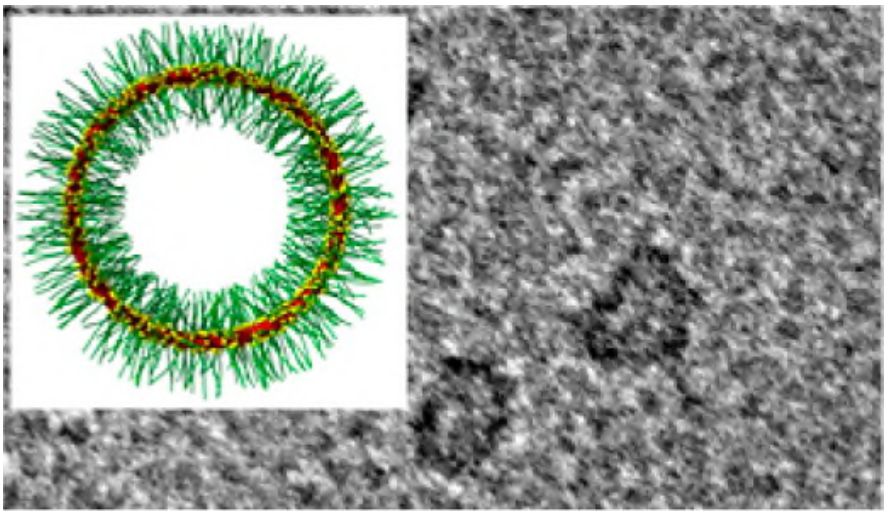

Figure 4.2. TEM image of metallo-supramolecular cyclic brush polymers with PEG side chains.

acid-functional PEG yielded cyclic PCL-*g*-PEG.[40] Nasongkla *et al*. used the same approach to prepare cyclic PCL-*g*-PEG, however, higher grafting densities were reported as a result of employing the highly efficient CuAAC reaction during PEGylation.[41] More recently, Zhang and coworkers prepared cyclic poly(*N*-carboxyanhydride)-*g*-PEG copolymers through the *N*-heterocyclic carbene (NHC) mediated zwitterionic ring-expansion ROP of propagyl-functional *N*-carboxyanhydride and subsequent grafting of azide-functional PEG *via* the CuAAC reaction.[42]

Although these current methods have allowed access to a range of cyclic graft copolymers, the preparation of cyclic graft copolymers with hydrophilic arms is extremely limited, with PEG arms being the only reported example. Furthermore, the introduction of PEG side arms is limited to a "grafting-to" approach which can suffer from limited grafting density as a consequence of steric repulsion between side arms. To prepare cyclic graft copolymers with a high grafting density "grafting-from" techniques are favoured, however there are no reports of the grafting of hydrophilic monomers using this approach.

The reversible addition-fragmentation chain transfer (RAFT) polymerisation technique is extremely versatile and has controlled the polymerisation of a wide range of monomers, including many hydrophilic monomers.[43-46] In this chapter the use of RAFT polymerisation to prepare cyclic graft copolymers *via* a "grafting-from" approach is reported and applied to the preparation of cyclic graft copolymers with hydrophilic side arms, greatly expanding the range of accessible graft compositions. Cyclic polymers with RAFT chain transfer agent (CTA) functionality located on the polymer backbone were prepared *via* the ring-closure of RAFT CTA-functional polycarbonates, which in turn were

prepared using procedures developed in the previous chapter. Subsequent RAFT polymerisations were also performed using the optimised conditions reported in Chapter 3 for the preparation of linear graft copolymers.

4.2 Results and Discussion

4.2.1 Synthetic Strategy

Cyclic graft copolymers with a degradable polycarbonate backbone were prepared through a combination of ring-closure and "grafting-from" approaches (Scheme 4.1). Linear precursor polycarbonates were prepared *via* ring-opening polymerisation (ROP) and subsequently end-group modified, before ring-closure *via* copper catalysed azide-alkyne cycloaddition (CuAAC).

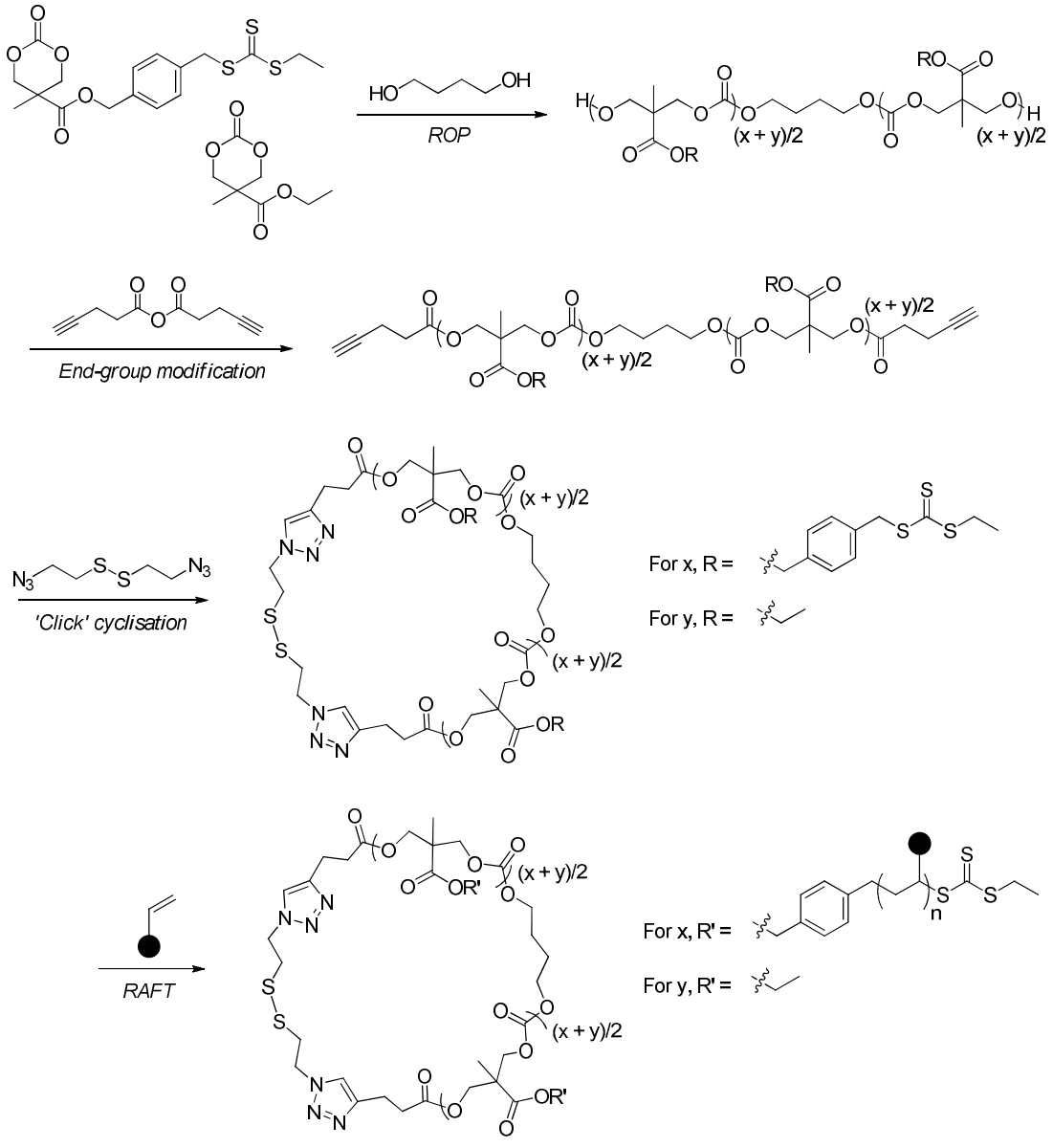

Scheme 4.1. Synthetic strategy for the preparation of cyclic graft copolymers.

RAFT polymerisation from RAFT CTA groups located on the polymer backbone of the resulting cyclic polycarbonates yielded cyclic graft copolymers. The ability to selectively cleave these cyclic graft copolymers into linear graft copolymers was also desired, and to this end a bimolecular ring-closure mechanism was utilised, where the small molecule linking agent contained a cleavable moiety. Disulfide functionality was chosen as the cleavable group, however this method provides the opportunity to incorporate a wide array of other responsive functionalities.[47]

4.2.1.1 Synthesis of Homodifunctional Linear Polycarbonates: Ring-Opening Polymerisations

RAFT CTA-functional polycarbonates were prepared using the same ROP procedure as specified in Chapter 3, however, for this work 1,4-butanediol was used as the polymerisation initiator to install hydroxyl functionality at both chain-ends (Scheme 4.2). Copolymerisations of a RAFT CTA-functional cyclic carbonate monomer, **1**, and an ethyl-functional cyclic carbonate monomer, 5-methyl-5-ethoxycarbonyl-1,3-dioxan-2-one, **2**, were conducted in dichloromethane ([total monomer] = 0.25 M) at room temperature, using 5 mol% of 1,8-diazabicycloundec-7-ene (DBU) as the polymerisation catalyst (Scheme 4.2). Polymerisations were quenched at total monomer conversions ≥ 80% with acidic Amberlyst resin, before purification by flash column chromatography (silica, 100% dichloromethane, then 100% ethyl acetate) to remove unreacted monomer and residual DBU. The proportion of RAFT CTA functionality and subsequent grafting density of the cyclic graft copolymers was tailored by varying the ratio of RAFT CTA-functional and ethyl-functional

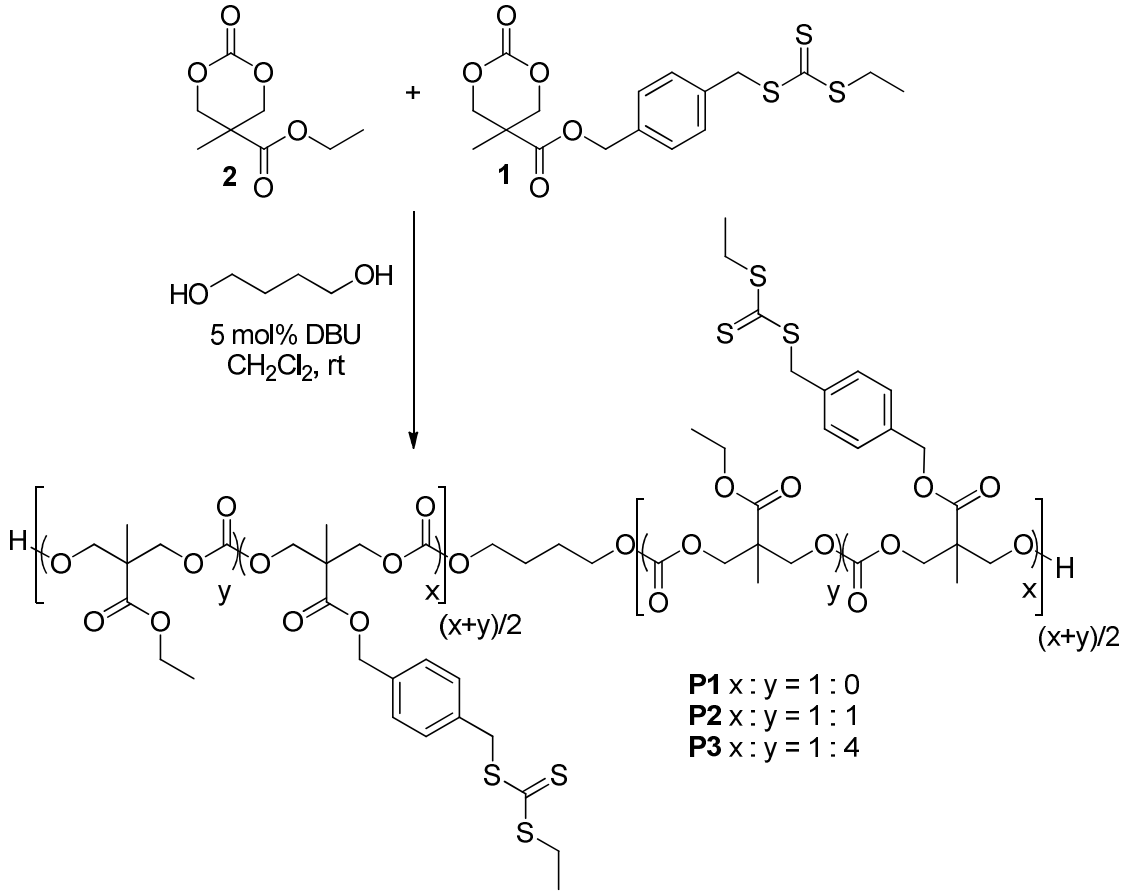

Scheme 4.2. Ring-opening copolymerisations of RAFT CTA-functional (**1**) and ethyl-functional (**2**) cyclic carbonate monomers.

monomers. An initial ratio of 1:1 RAFT CTA to ethyl functionality was targeted and a range of copolymers with different molecular weights were obtained through variation of the initial monomer-to-initiator ratio ([M]/[I]). SEC analysis of the resulting polycarbonate copolymers revealed monomodal molecular weight distributions with low dispersity values ($Đ_M \leq 1.2$), which indicates the controlled nature of the copolymerisations (Figure 4.3 and Table 4.1).

The comonomer feed ratio of the polymerisations was also varied to target polycarbonates with 100% and 20% RAFT CTA functionality. Again, the polymers exhibited well-defined molecular weight distributions and low values of $Đ_M$ (Figure 4.4). ^{1}H NMR spectroscopic analysis of the copolymers

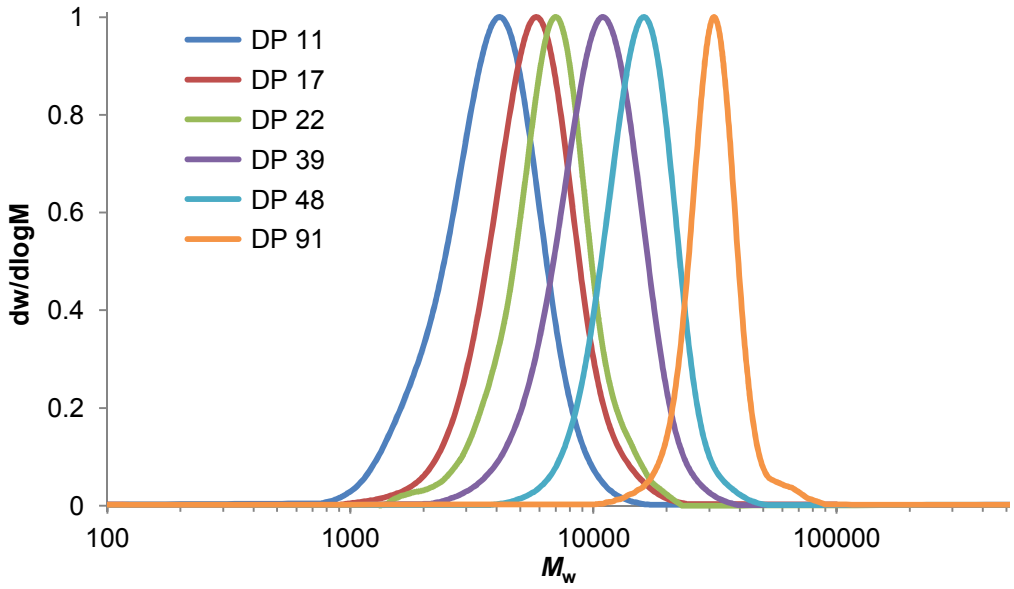

Figure 4.3. SEC chromatograms of RAFT CTA-functional polycarbonate copolymers with a 1:1 (**1**:**2**) comonomer feed ratio and varying degrees of polymerisation (**P2a-f**). Conditions: [monomer] = 0.25 M, using 5 mol% DBU and 1,4-butanediol as initiator.

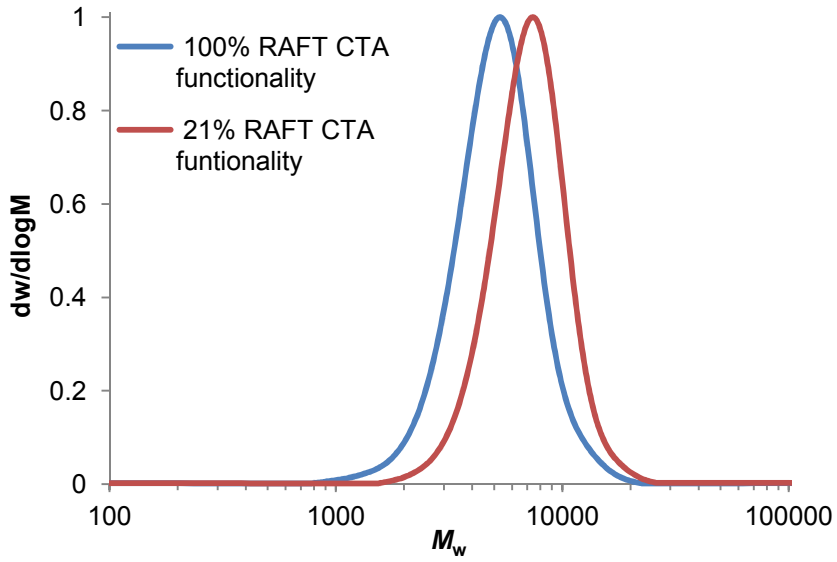

Figure 4.4. SEC chromatograms of polymers **P1** (100% incorporation of **1**, M_n = 4.6 kDa, $Đ_M$ = 1.21) and **P3** (21% incorporation of **1**, M_n = 6.5 kDa, $Đ_M$ = 1.16).

after purification revealed resonances that correspond to both RAFT CTA and ethyl functionality (Figure 4.5). Integration of these resonances allowed determination of the obtained incorporation of RAFT CTA functionality and revealed a strong agreement between the monomer feed ratio and the final

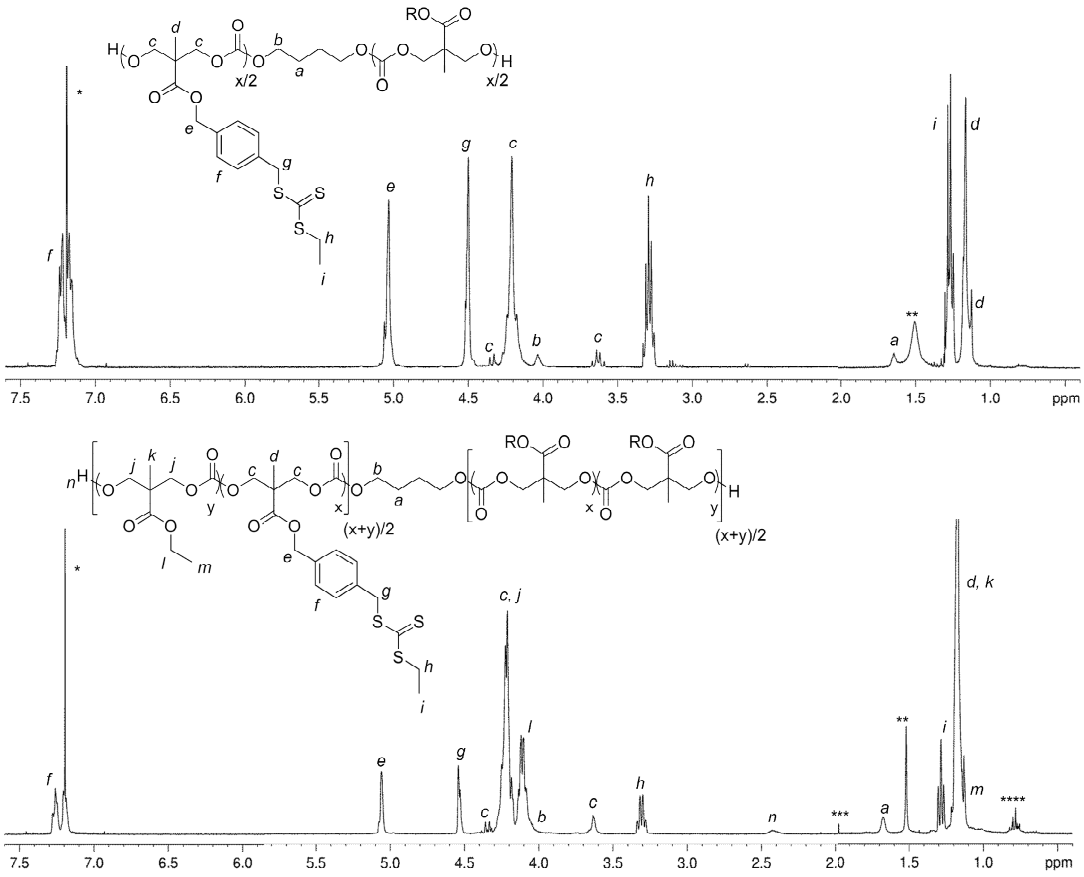

Figure 4.5. ^{1}H NMR spectra (400 MHz; $CDCl_3$) of (top) RAFT CTA-functional polycarbonate homopolymer (**P1**) and (bottom) RAFT CTA- and ethyl-functional polycarbonate copolymer (**P3**), 21% RAFT CTA functionality (*$CHCl_3$, **H_2O, ***acetone, ****petroleum ether).

composition of the copolymers (Table 4.1). Resonances that correspond to the CH_2 groups of the 1,4-butanediol initiating group at δ = 4.10 and 1.71 ppm were also observed by ^{1}H NMR spectroscopy and confirm the successful incorporation of the difunctional initiator.

Matrix-assisted laser desorption ionisation time-of-flight mass spectrometry (MALDI-ToF MS) of polymer **P1** with 100% RAFT CTA-functionality, revealed a single sodium-charged distribution with regular spacing equal to the molecular weight of the RAFT CTA- functional monomer repeat unit (m/z = 400) and a 1,4-butanediol initiating group, confirming the extremely high end-group fidelity of

the polycarbonates and controlled nature of the polymerisation (Table 4.2 and Figure 4.6).

Table 4.1. Characterisation and composition of RAFT CTA- and ethyl-functional copolymers.

Polymer	Monomer ratio (1 : 2)	Polymer composition[a]	DP[a]	M_n(NMR)[a] (kDa)	M_n(SEC)[b] (kDa)	$Đ_M$[b]
P1	1 : 0	-	17	6.8	4.6	1.21
P2a	1 : 1	1 : 0.95	11	3.4	3.4	1.24
P2b	1 : 1	1 : 0.98	17	5.0	5.0	1.21
P2c	1 : 1	1 : 0.96	22	6.7	6.0	1.18
P2d	1 : 1	1 : 0.85	39	12.0	9.4	1.19
P2e	1 : 1	1 : 0.92	48	14.3	14.4	1.13
P2f	1 : 1	1 : 0.86	91	27.5	31.4	1.07
P3	1 : 4	1 : 3.81	23	5.6	6.5	1.16

[a]Determined by ^{1}H NMR spectroscopy. [b]Determined by SEC analysis in $CHCl_3$ using poly(styrene) standards. Conditions: [monomer] = 0.25 M in CH_2Cl_2, using 5 mol% DBU and 1,4-butanediol as the polymerisation initiator.

Table 4.2. Theoretical and observed *m/z* values of **P1**.

DP	Experimental *m/z*[a]	Calculated *m/z*
4	1713.3	1713.2
5	2113.4	2113.3
6	2513.5	2513.3
7	2914.6	2913.4
8	3314.7	3313.4

[a]Determined by MALDI-TOF MS analysis using trans-2-[3-(4-*tert*-butylphenyl)-2-methyl-2-propylidene]malonitrile (DCTB) as a matrix, sodium trifluoroacetate as the cationisation agent and PEG monomethyl ether 2k and 5k standards.

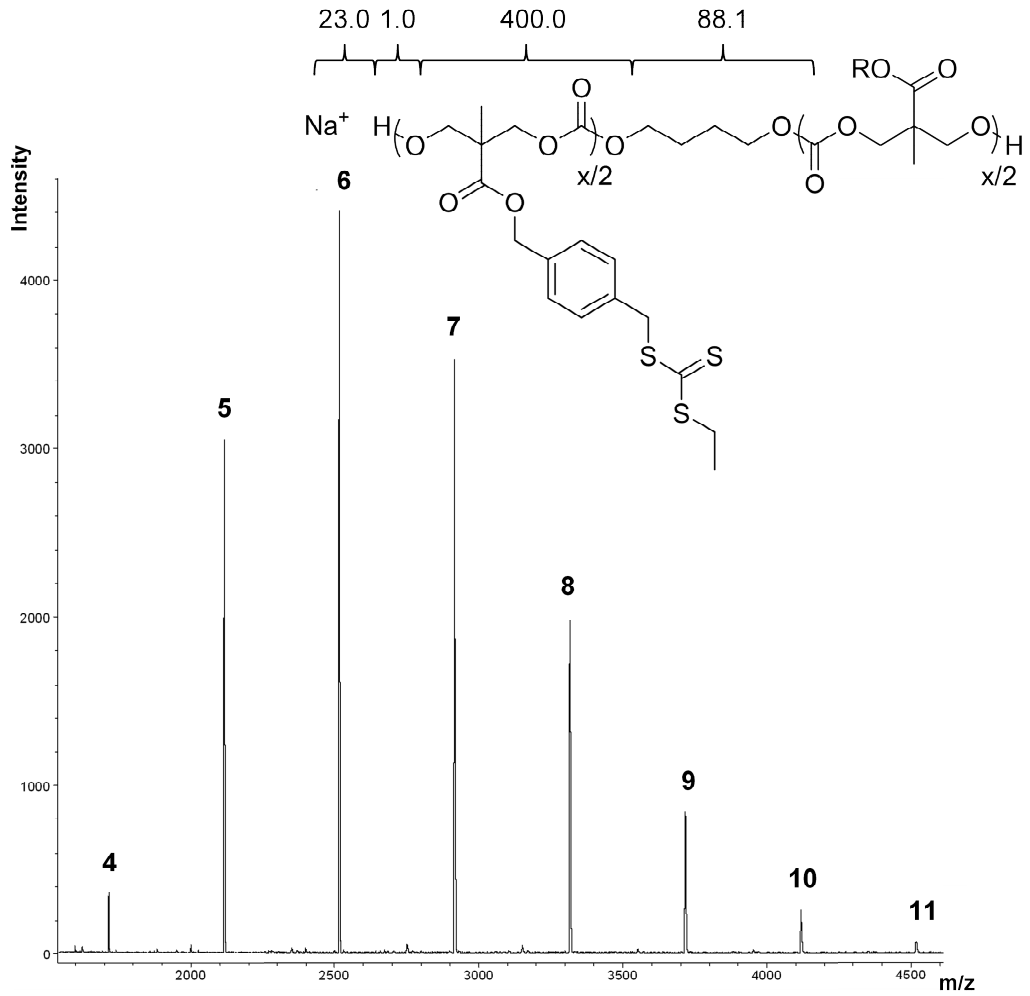

Figure 4.6. MALDI-ToF MS analysis of **P1** (DP = 17) initiated from 1,4-butanediol.

4.2.1.2 Synthesis of Homodifunctional Linear Polycarbonates: End-Group Modification

To incorporate alkyne functionality onto the chain–ends of the RAFT CTA-functional copolymers, the hydroxyl end-groups were esterified by reaction with a 30 eq. excess of 4-pentynoic anhydride, in the presence of a catalytic amount of 4-(dimethylamino)pyridine (DMAP) and a 300 eq. excess of pyridine (Scheme 4.3). The quantitative conversion of hydroxyl-functional end-groups to alkyne-functional end-groups was confirmed by ^{1}H NMR spectroscopy, IR

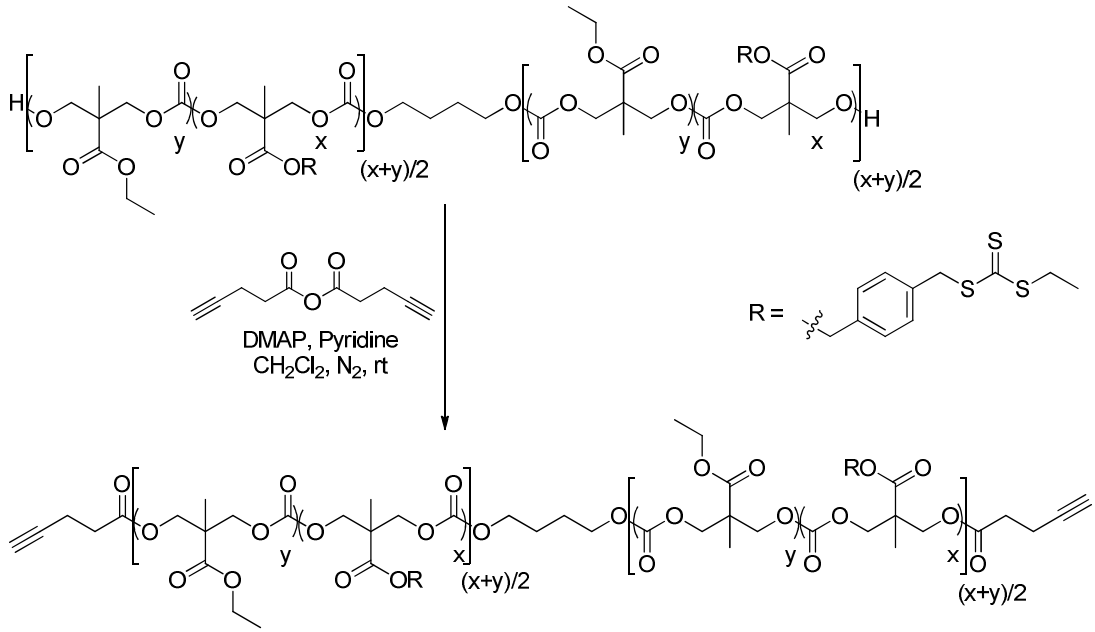

Scheme 4.3. End-group modification of RAFT-CTA functional polycarbonate copolymers.

spectroscopy and MALDI-ToF mass spectrometry. Comparison of the ^{1}H NMR spectra of the telechelic polycarbonates before and after functionalisation revealed the appearance of a triplet resonance at δ = 1.97 ppm, that corresponds to the terminal proton of the alkyne functionality, and new resonances at δ = 2.58 – 2.37 ppm that correspond to the CH_2 groups adjacent to the alkyne moiety (Figure 4.7). The complete downfield shift of the resonance at δ = 3.70 ppm, that corresponds to the CH_2 groups adjacent to the terminal hydroxyl functionalities was also observed. Examination of the IR spectra of the alkyne-functional telechelic polycarbonates showed the complete loss of the broad peak at 3540 cm^{-1} that corresponds to the OH stretch of the hydroxyl end-groups and the appearance of a new signal at 3290 cm^{-1} that corresponds to the CH stretch of the alkyne functionality (Figure 4.8).

MALDI-ToF MS analysis of polymer **P1$_{alkyne}$**, with 100% RAFT-CTA functionality, further confirmed the quantitative functionalisation of end-groups, revealing a single sodium charged distribution consistent with the

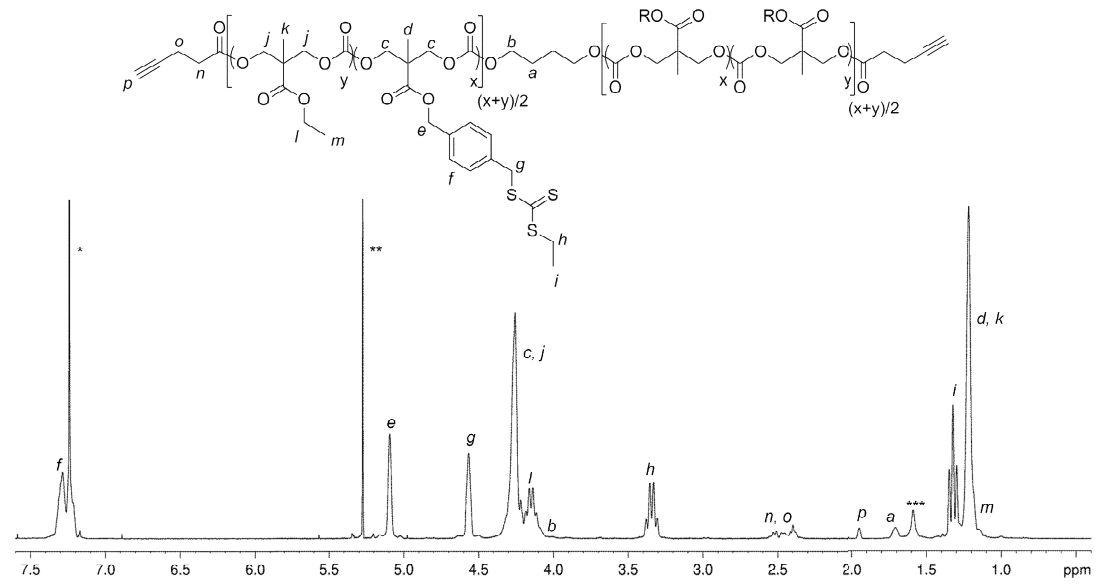

Figure 4.7. ^{1}H NMR spectrum (400 MHz; $CDCl_3$) of alkyne-terminated RAFT CTA-functional polycarbonate copolymer **P2c$_{alkyne}$** (*$CHCl_3$, **CH_2Cl_2, ***H_2O).

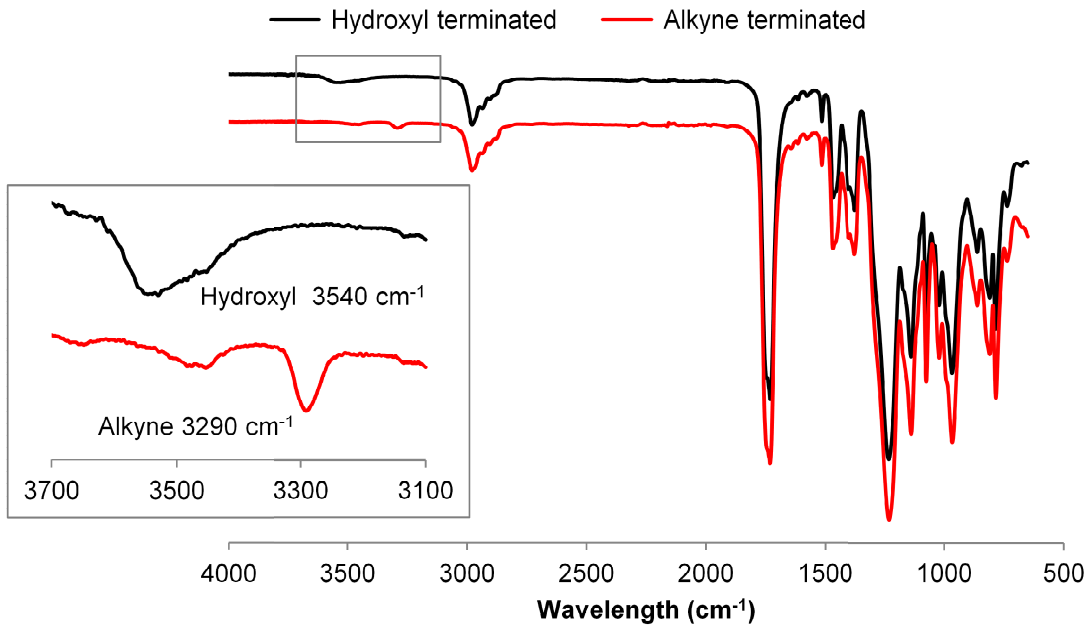

Figure 4.8. IR spectra of hydroxyl-terminated and alkyne-terminated RAFT CTA-functional polycarbonate copolymers. (Inset) Expansion of IR spectra (3700 – 3100 cm^{-1}) highlighting peaks that correspond to hydroxyl and alkyne functionalities.

successful esterification of both hydroxyl groups, observed as an increase in molecular weight of m/z = 161 kDa for each polymer chain (Figure 4.9 and Table 4.3). Furthermore, SEC analysis revealed that the molecular weight

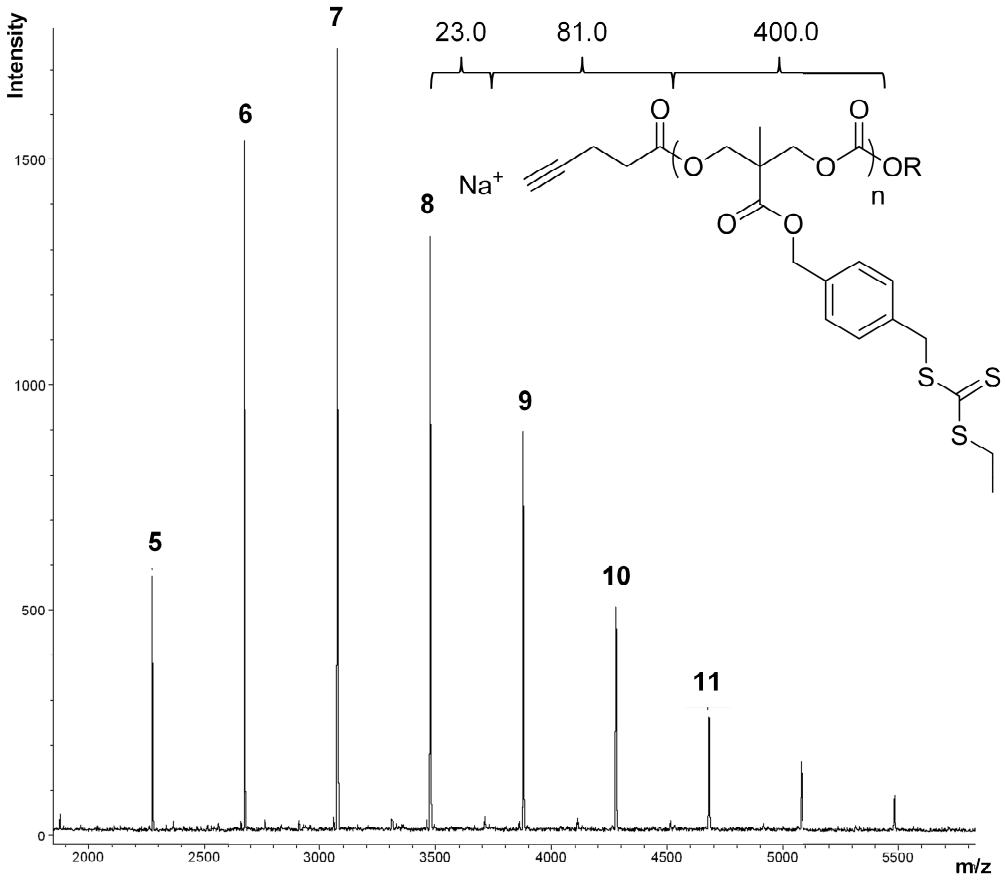

Figure 4.9. MALDI-ToF MS analysis of $\mathbf{P1_{alkyne}}$ (DP = 17) after alkyne end-group functionalisation.

Table 4.3. Theoretical and observed *m/z* values of alkyne-terminated polycarbonate, $\mathbf{P1_{alkyne}}$.

DP	Experimental *m/z*[a]	Calculated *m/z*
5	2273.5	2273.3
6	2673.6	2673.4
7	3073.7	3073.4
8	3473.9	3473.5
9	3874.2	3873.5

[a]Determined by MALDI-TOF MS analysis using trans-2-[3-(4-*tert*-butylphenyl)-2-methyl-2-propylidene]malonitrile (DCTB) as a matrix, sodium trifluoroacetate as the cationisation agent and PEG monomethyl ether 2k and 5k standards.

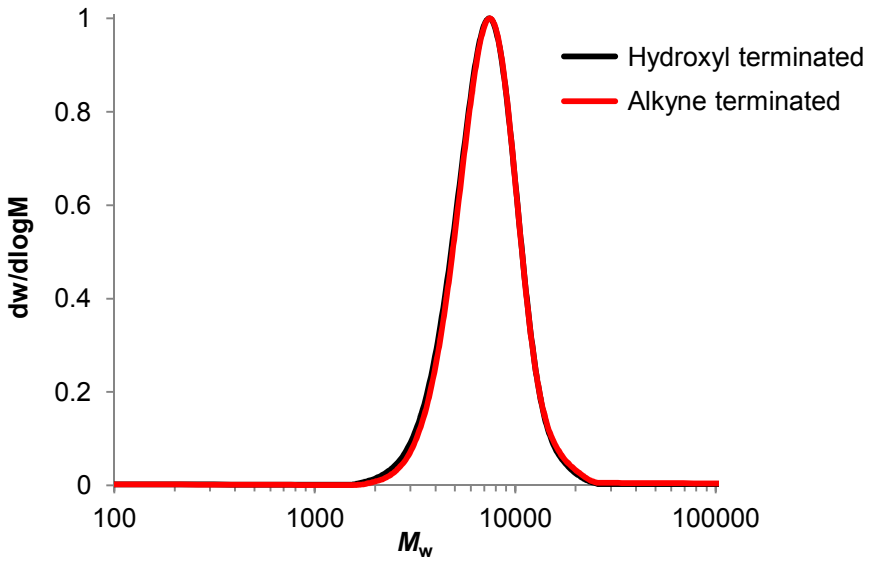

Figure 4.10. SEC chromatograms of hydroxyl-terminated (**P3**, M_n = 6.5 kDa, $Đ_M$ = 1.16) and alkyne-terminated (**P3$_{alkyne}$**, M_n = 6.7 kDa, $Đ_M$ = 1.15) polycarbonate copolymers.

distribution of the polycarbonate copolymers remained narrow after end-group functionalisation (Figure 4.10).

4.2.2 Cyclisation of Homodifunctional Linear Polycarbonates

To successfully prepare high purity cyclic polymers *via* a ring-closure approach, high dilution is critical to ensure cyclisation is preferred over condensation. Furthermore, an extremely efficient cyclisation reaction is required to eliminate the need for purification to remove linear polymer contaminants. The copper catalysed azide-alkyne cycloaddition is a highly efficient coupling reaction that exhibits high functional group tolerance and selectivity and has consequently found extensive use in synthetic polymer chemistry.[48, 49] Laurent and Grayson reported the use of the azide-alkyne cycloaddition to prepare near-quantitative cyclic poly(styrene) and poly(ε-caprolactone).[50, 51] To ensure the concentration of the cyclisation reaction remained low, but also reduce the quantity of solvent required, a *pseudo*-high dilution approach was used whereby the linear polymer

was slowly added to the reaction *via* a syringe pump. As a consequence of the rapid nature of the azide-alkyne cycloaddition, the concentration of unreacted linear polymer remained infinitesimal throughout the reaction. The copper catalysed azide-alkyne cycloaddition has also been shown to be compatible with RAFT CTA functionality[52, 53] and degradable polymers, including polycarbonates.[54-58] In this work, cyclic RAFT CTA-functional polycarbonates were prepared through bimolecular ring-closure *via* the copper catalysed cycloaddition of alkyne-terminated telechelic polymers and a disulfide containing diazide linker.

4.2.2.1 Cyclisation of Homodifunctional Linear Polycarbonates: Synthesis of Diazide Linker

The disulfide containing diazide linker, bis-(azidoethyl)disulfide, **4**, was prepared according to adapted literature procedures (Scheme 4.4).[59, 60] Bis-(hydroxyethyl)disulfide was reacted with methanesulfonyl chloride, in the presence of an excess of triethylamine, to afford bis-(mesylate ethyl)disulfide (**3**). Subsequent nucleophilic substitution with sodium azide gave the desired product in 89% overall yield after purification by flash column chromatography (silica, 1:5 ethyl acetate: petroleum ether 40-60 °C). The structure of **4** was confirmed by ^{1}H NMR, ^{13}C NMR and IR spectroscopy (Figure 4.11).

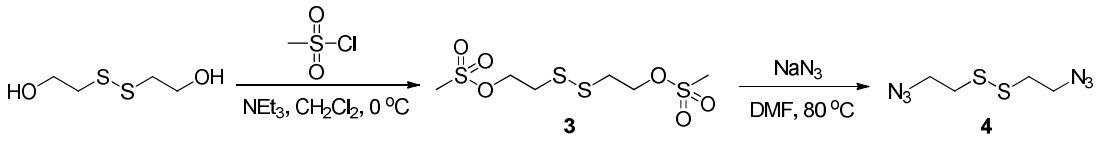

Scheme 4.4. Synthesis of the disulfide containing diazide linker **4**.

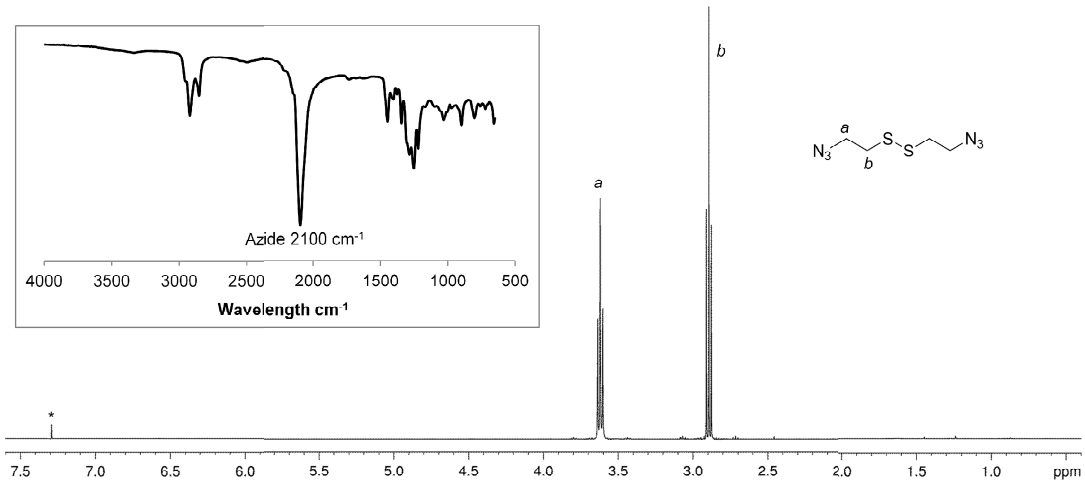

Figure 4.11. ^{1}H NMR spectrum (400 MHz; $CDCl_3$) of the disulfide containing diazide linker **4**. (*$CHCl_3$). (Inset) IR spectrum of **4**.

4.2.2.2 Cyclisation of Homodifunctional Linear Polycarbonates: Optimisation of Cyclisation Conditions

The initial conditions studied for cyclisation were based on the literature procedures reported by Grayson and coworkers,[50] as well as similar procedures reported for the successful cyclisation of poly(ester)s[51, 61] and poly(phosphoester)s.[62] An equimolar solution of difunctional alkyne-terminated polycarbonate $\mathbf{P2b_{alkyne}}$ (1.0 mM) and diazide linker, **4**, were added *via* syringe pump to a stirred solution of Cu(I)Br (0.05 mM) and *N,N.N',N''*-pentamethyldiethylenetriamine (PMDETA) (0.05 mM) at room temperature, at a rate of 0.3 mL h^{-1}. A 100 mole excess of Cu(I) catalyst per mole of polymer was used for initial cyclisation studies and dichloromethane was chosen as the cyclisation solvent. After complete addition of the polymer and diazide solution, the reaction was allowed to stir for a further 3 h. The copper catalyst was removed *via* washing with brine, before the polymer solution was stirred in

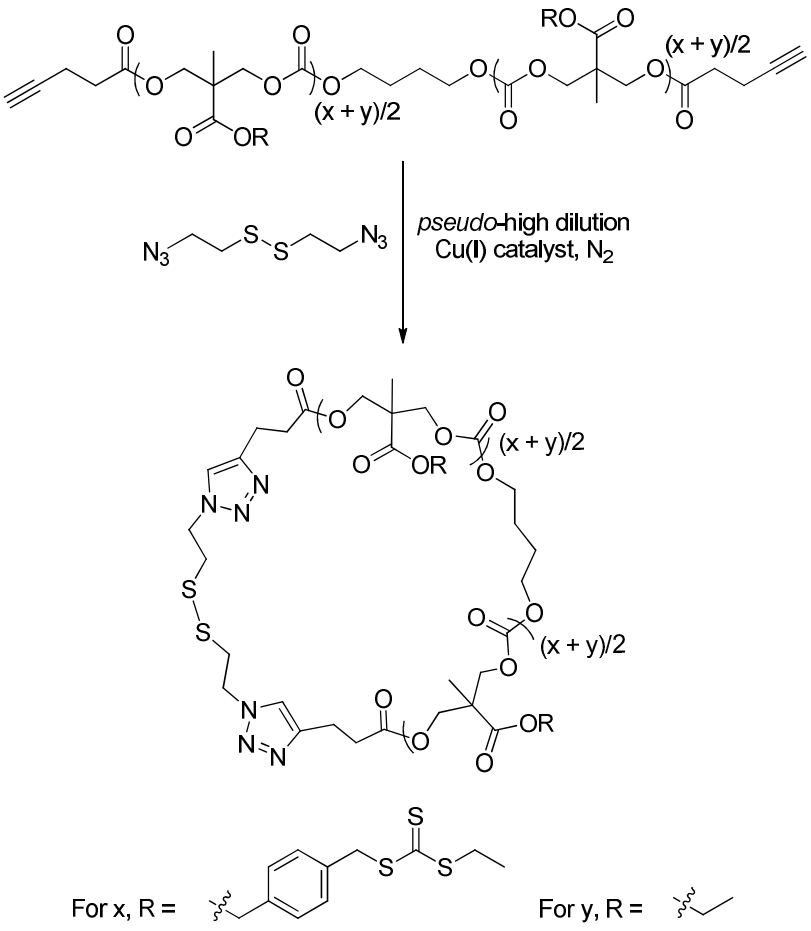

Scheme 4.5. Cyclisation of RAFT CTA-functional polycarbonate copolymers.

the presence of Cuprisorb beads, filtered and finally precipitated into petroleum ether 40-60 °C.

^{1}H NMR spectroscopy was used to determine the proportion of alkyne end-groups that had undergone reaction by integration of the CH_2 groups adjacent to the alkyne moiety at δ = 2.58 – 2.37 ppm. Examination of the ^{1}H NMR spectra of the precipitated polymer revealed that only 14% of the alkyne groups had undergone reaction. To establish whether these alkyne groups had ring-closed to form cyclic polycarbonates or undergone polycondensation to form higher molecular weight polycarbonates, the precipitated polymer was further analysed by SEC. As a result of the reduced conformational freedom of cyclic

polymers in comparison to linear polymers, cyclic polymers possess a smaller hydrodynamic volume than their linear counterparts.[63] Consequently, upon ring-closure cyclic polymers will exhibit a shift to an apparent lower molecular weight than the corresponding linear precursor polymer when analysed by SEC. Examination of the SEC chromatogram of the precipitated polymer revealed the appearance of a second polymer distribution at lower molecular weight consistent with the occurrence of incomplete cyclisation (Figure 4.12). The absence of an additional polymer distribution at higher molecular weight confirmed that minimal polycondensation had occurred.

In an attempt to increase the yield of cyclic polymer the amount of Cu(I)Br and PMDETA was increased, however, at both 200 and 500 molar excess of catalyst per polymer chain no improvement in cyclisation yield was observed (Table 4.4).

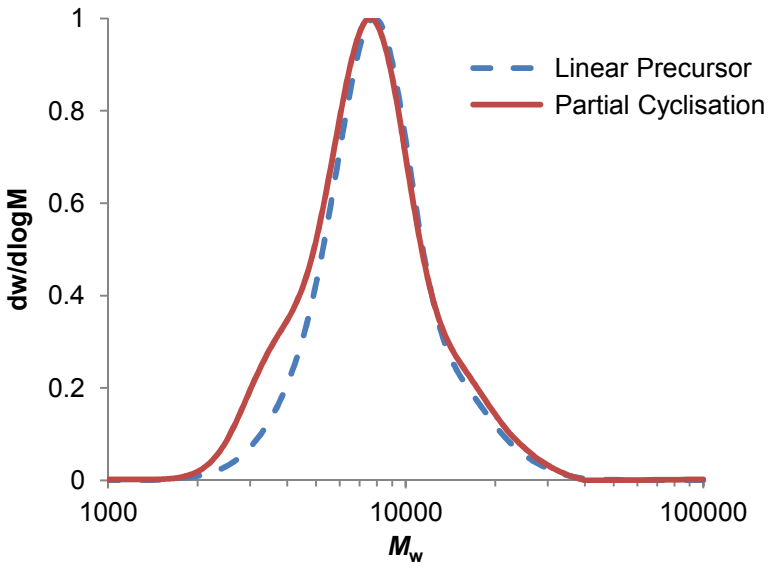

Figure 4.12. SEC chromatograms of alkyne-terminated polycarbonate **P2b$_{alkyne}$** (M_n = 7.2 kDa, $Đ_M$ = 1.22) and partially cyclised polycarbonate (M_n = 6.6 kDa, $Đ_M$ = 1.29).

Table 4.4 Optimisation of cyclisation conditions.

Catalyst system	Cu(I) eq.	Solvent	Conversion of alkyne groups (%)[a]
Cu(I)Br, PMDETA	100	CH_2Cl_2	14
Cu(I)Br, PMDETA	200	CH_2Cl_2	14
Cu(I)Br, PMDETA	500	CH_2Cl_2	16
Cu(I)Br, PMDETA	100	Toluene	>99
CuI.P(OEt)$_3$	100	CH_2Cl_2	9

[a]Determined by ^{1}H NMR spectroscopy.

The use of an alternative Cu(I) catalyst was also investigated, namely the pre-complexed catalyst copper iodide triethylphosphite (CuI.P(OEt)$_3$). However, ^{1}H NMR spectroscopy showed a decrease in activity; only 9% of alkyne groups underwent reaction. Finally, the effect of varying the reaction solvent was studied. Upon changing the reaction solvent from dichloromethane to toluene, quantitative reaction of the alkyne end-groups was observed by ^{1}H NMR spectroscopy. This dramatic increase in reactivity was thought to occur as a consequence of switching from a halogenated to a non-halogenated solvent that still maintained good solubility for both the polycarbonate and Cu(I) catalyst. Having optimised the conditions for successful ring-closure, the same cyclisation procedure was applied to the ring-closure of polycarbonates with 100% (**P1**$_{\mathbf{alkyne}}$) and approximately 20% (**P3**$_{\mathbf{alkyne}}$) RAFT CTA functionality, as well as varying degrees of polymerisation.

4.2.2.3 Cyclisation of Alkyne-Functional Telechelic Polycarbonates: Characterisation

A combination of characterisation techniques were used to confirm the successful cyclisation of the RAFT CTA-functional polycarbonates. ^{1}H NMR spectroscopic analysis of the polymers after precipitation was used to verify the end-group transformation of the polymers upon cyclisation (Figure 4.13). Complete disappearance of the resonances attributed to the terminal proton of the alkyne functionality at δ = 1.97 ppm was observed, as well as a shift in the resonances that correspond to the adjacent CH_2 groups from δ = 2.58 – 2.37 ppm to δ = 3.06 – 2.58 ppm. The appearance of resonances that correspond to the successful incorporation of the diazide disulfide linker were also observed, specifically the resonance at δ = 3.15 ppm that corresponds to the CH_2 groups adjacent to the disulfide moiety. The preservation of the quartet and triplet resonances at δ = 3.36 and 1.34 ppm respectively, that correspond to the ethyl group of the RAFT CTA functionality, confirm that the RAFT CTA functionality was successfully retained during the CuAAC cyclisation reaction.

The ^{1}H NMR spectra of the cyclised RAFT CTA-functional polycarbonates did not however show the appearance of a resonance that corresponds to the proton of the triazole ring. It was hypothesised that this resonance was obscured by the aromatic signals at δ = 7.41 – 7.19 ppm. To confirm this hypothesis and determine the chemical shift of the triazole proton, a small molecule reaction was undertaken whereby the diazide disulfide linker, **4**, was reacted with ethyl pent-4-ynoate under similar CuAAC reaction conditions. Ethyl pent-4-ynoate was prepared according to the literature[64] and subsequently reacted with **4** in the presence of a catalytic amount of Cu(I)Br

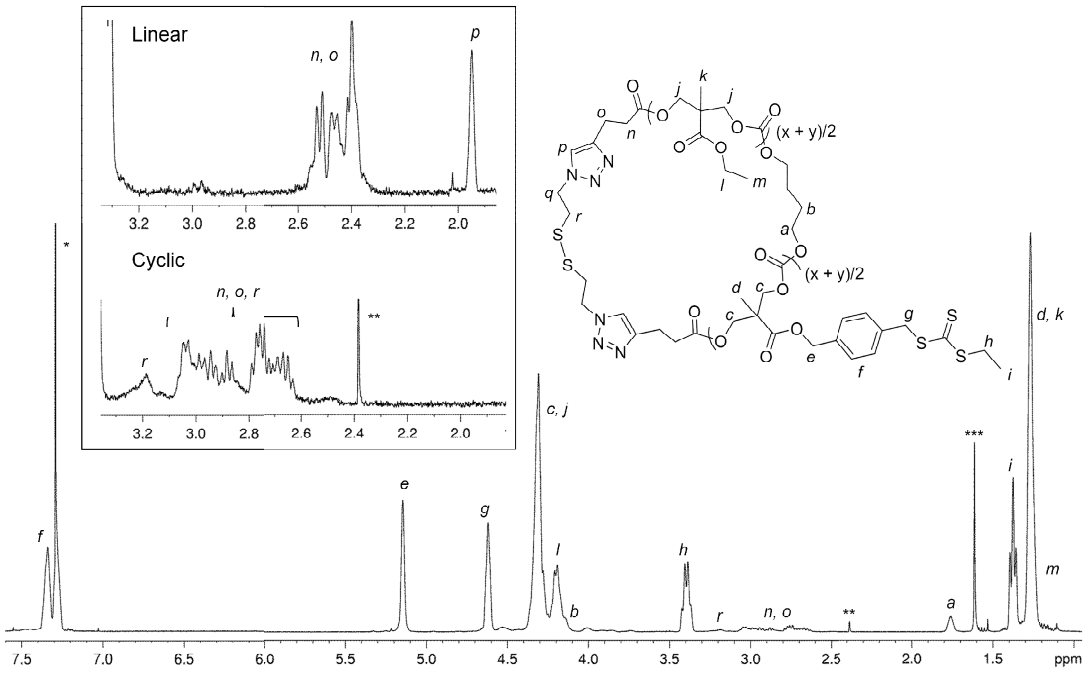

Figure 4.13. ^{1}H NMR spectrum (400 MHz; $CDCl_3$) of cyclised RAFT CTA-functional polycarbonate **P2b$_{cyclic}$**. (Inset) Expansion of ^{1}H NMR spectra (δ = 3.4 – 1.8 ppm) of alkyne terminated linear polymer (**P2b$_{alkyne}$**) and cyclic polymer (**P2b$_{cyclic}$**) (*$CHCl_3$, ** toluene, ***H_2O).

and PMDETA in toluene (Scheme 4.6). The ^{1}H NMR spectrum of the resulting product, **5**, showed the resonance of the triazole proton at δ = 7.43 ppm (Figure 4.14).

To provide further evidence of the successful formation of the triazole ring during ring-closure, an alkyne-functional telechelic polycarbonate comprised of only ethyl-functional carbonate repeat units was prepared and subsequently cyclised using the optimised cyclisation conditions. ^{1}H NMR spectroscopic analysis of the resulting polymer after purification, revealed the appearance of a

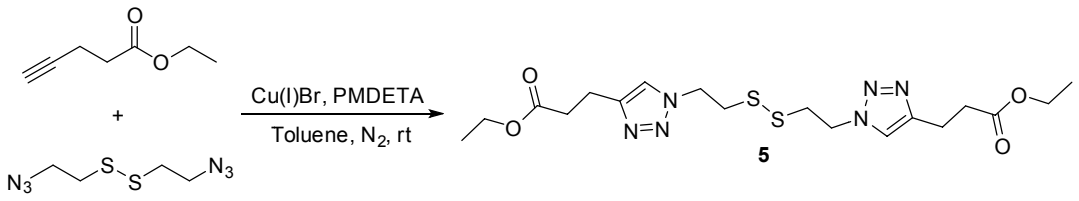

Scheme 4.6. Small molecule model reaction for CuAAC with disulfide containing diazide **4**.

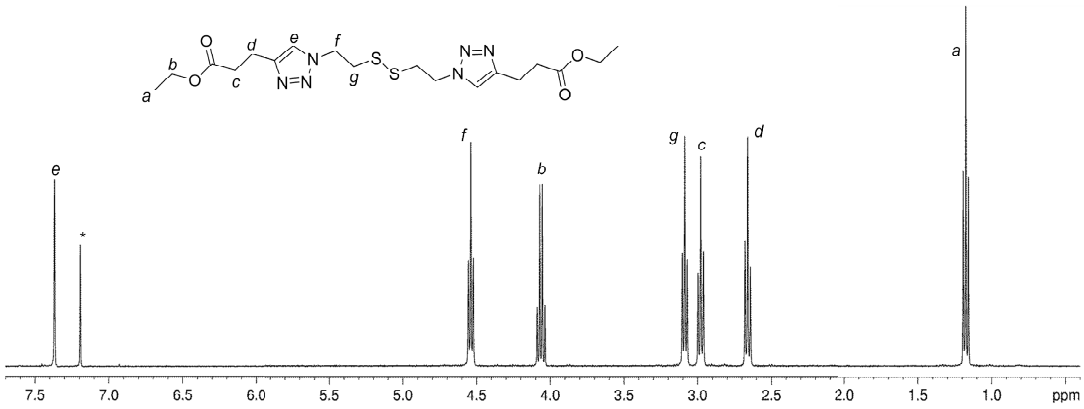

Figure 4.14. ^{1}H NMR spectrum (400 MHz; $CDCl_3$) of **5**, small molecule model CuAAC reaction (*$CHCl_3$).

resonance at δ = 7.46 ppm that was attributed to the proton of the triazole ring (Figure 4.15). The ^{1}H NMR spectrum of the polymer also revealed another resonance at δ = 4.62 ppm that corresponds to the CH_2 groups of the disulfide linker molecule adjacent to the triazole ring, that was previously obscured by resonances ascribed to the RAFT CTA functionality.

Analysis of the cyclised polymers by IR spectroscopy also provided evidence to support the successful end-group transformation of the polymers upon cyclisation, specifically the complete loss of the signal at 3290 cm^{-1} that corresponds to the CH stretch of the terminal alkyne groups (Figure 4.16).

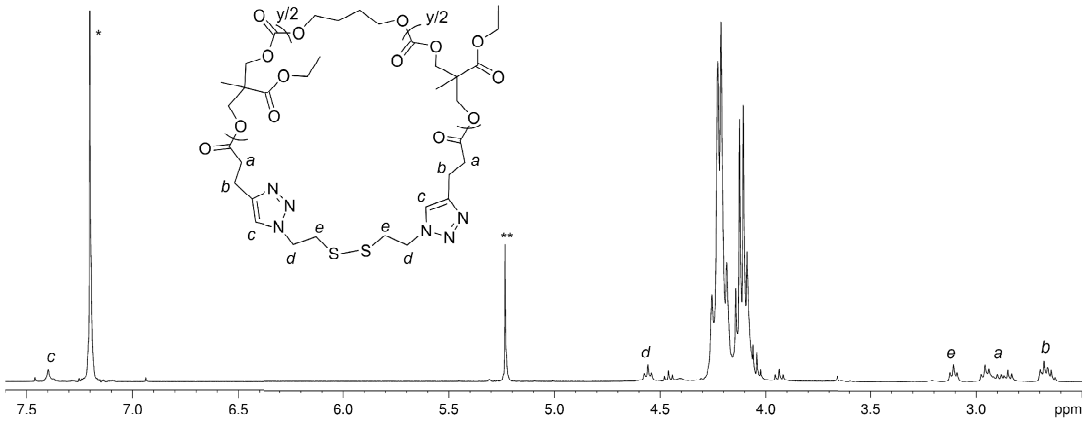

Figure 4.15. ^{1}H NMR spectrum (400 MHz; $CDCl_3$) of cyclised ethyl-functional polycarbonate (*$CHCl_3$, **CH_2Cl_2).

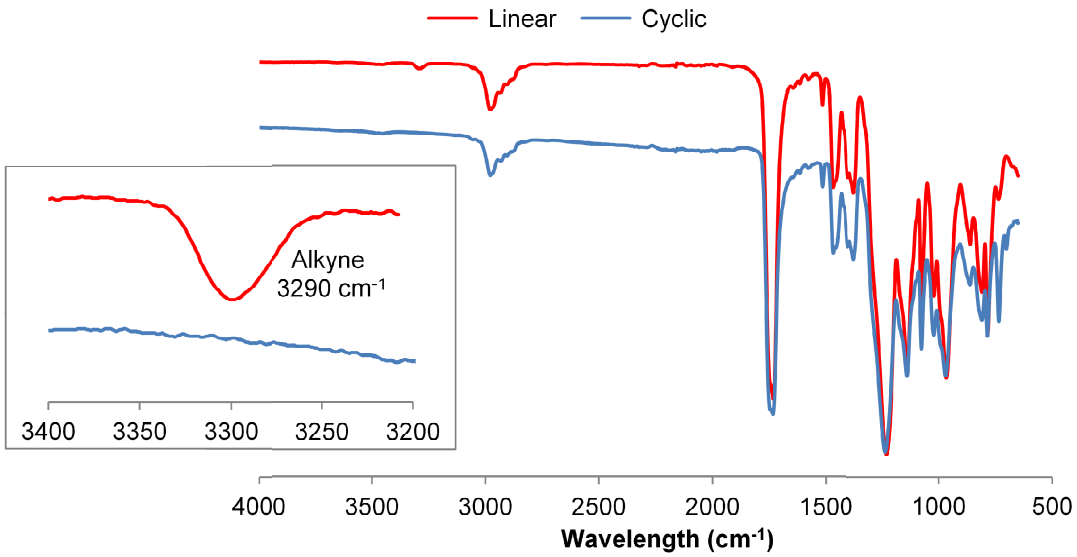

Figure 4.16. IR spectra of alkyne terminated linear polymer **P2b**$_{alkyne}$ and cyclic polymer **P2b**$_{cyclic}$. (Inset) Expansion of IR spectra (3400 – 3200 cm^{-1}) highlighting loss of alkyne functionality.

Analysis of polymers **P1**$_{cyclic}$, **P2a-c**$_{cyclic}$ and **P3**$_{cyclic}$ by SEC in comparison to the alkyne-functional linear precursor polymers, revealed an increase in retention time and therefore a reduction in apparent molecular weight, providing further evidence of successful cyclisation (Table 4.5 and Figure 4.17). Narrow molecular weight distributions and low dispersity values were also retained

Table 4.5. SEC analysis of cyclic polycarbonates, **P1**$_{cyclic}$, **P2a-c**$_{cyclic}$ and **P3**$_{cyclic}$.

Polymer	M_n(SEC)$_{linear}$ (kDa)[a]	$Đ_{M\ linear}$[a]	M_n(SEC)$_{cyclic}$ (kDa)[a]	$Đ_{M\ cyclic}$[a]	$M_{n\ cyclic}$ / $M_{n\ linear}$[a]
P1$_{cyclic}$	7.1	1.26	6.5	1.19	0.9
P2a$_{cyclic}$	3.8	1.20	3.6	1.18	0.9
P2b$_{cyclic}$	7.2	1.22	5.8	1.14	0.8
P2c$_{cyclic}$	7.4	1.17	6.2	1.16	0.8
P3$_{cyclic}$	6.7	1.15	6.0	1.16	0.9

[a]Determined by SEC analysis in $CHCl_3$ using poly(styrene) standards.

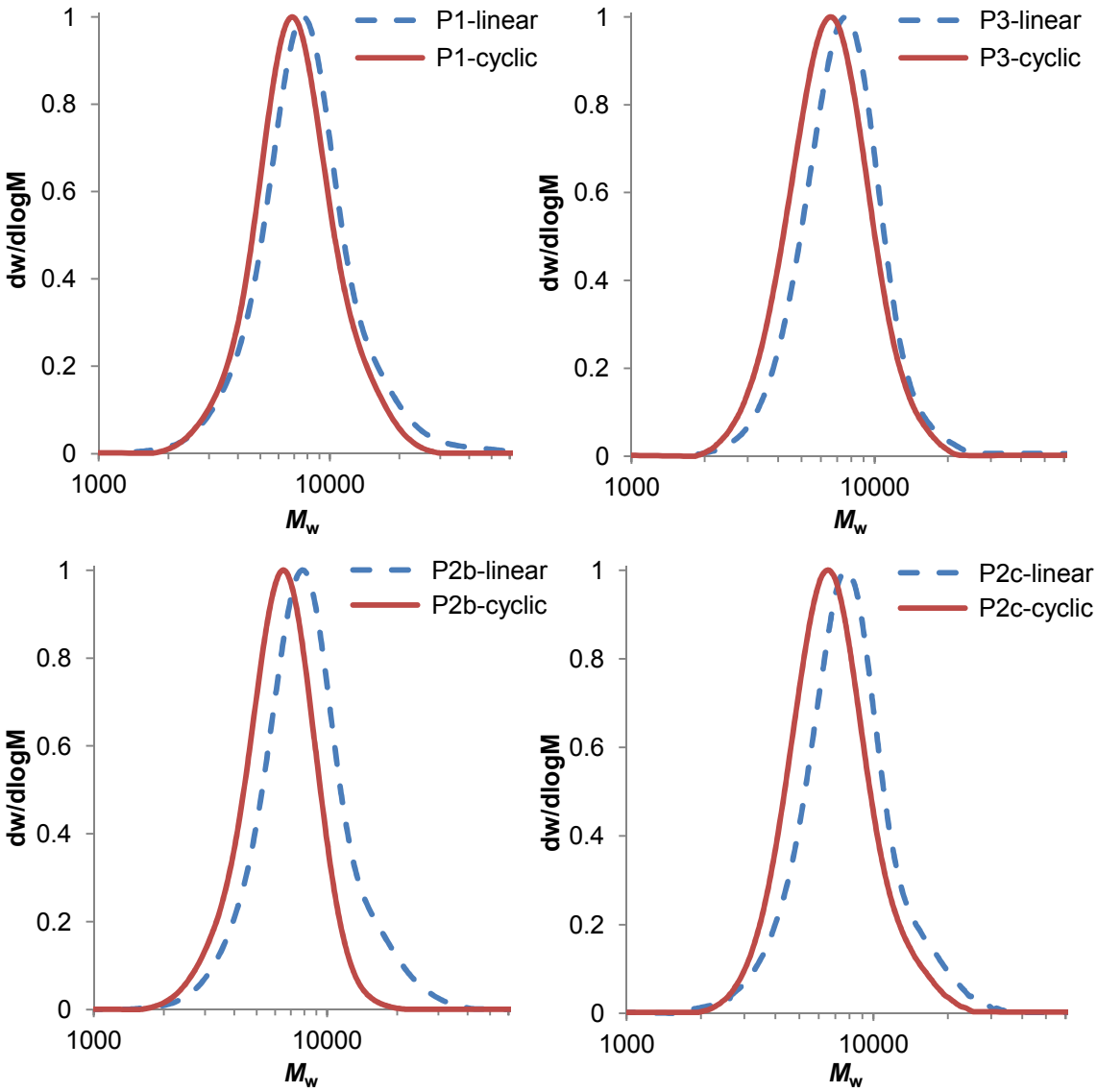

Figure 4.17. SEC chromatograms of RAFT CTA-functional cyclic polycarbonates and alkyne-terminated linear precursor polymers; (top left) **P1** 100% RAFT CTA incorporation, (top right) **P3** 21% RAFT CTA incorporation, (bottom left) **P2b** 51% RAFT CTA incorporation, DP = 17, (bottom right) **P2c** 51% RAFT CTA incorporation, DP = 22.

during ring-closure and the absence of any high molecular weight polymer impurities confirmed that polycondensation had not occurred.

Examination of the MALDI-ToF mass spectrum of polymer $\mathbf{P1}_{\mathbf{cyclic}}$ provided further evidence of successful cyclisation. An increase in molecular weight of 204 Da was observed after cyclisation, consistent with the addition of one equivalent of the diazide disulfide linker, **4**, per polymer chain (Figure 4.18). In

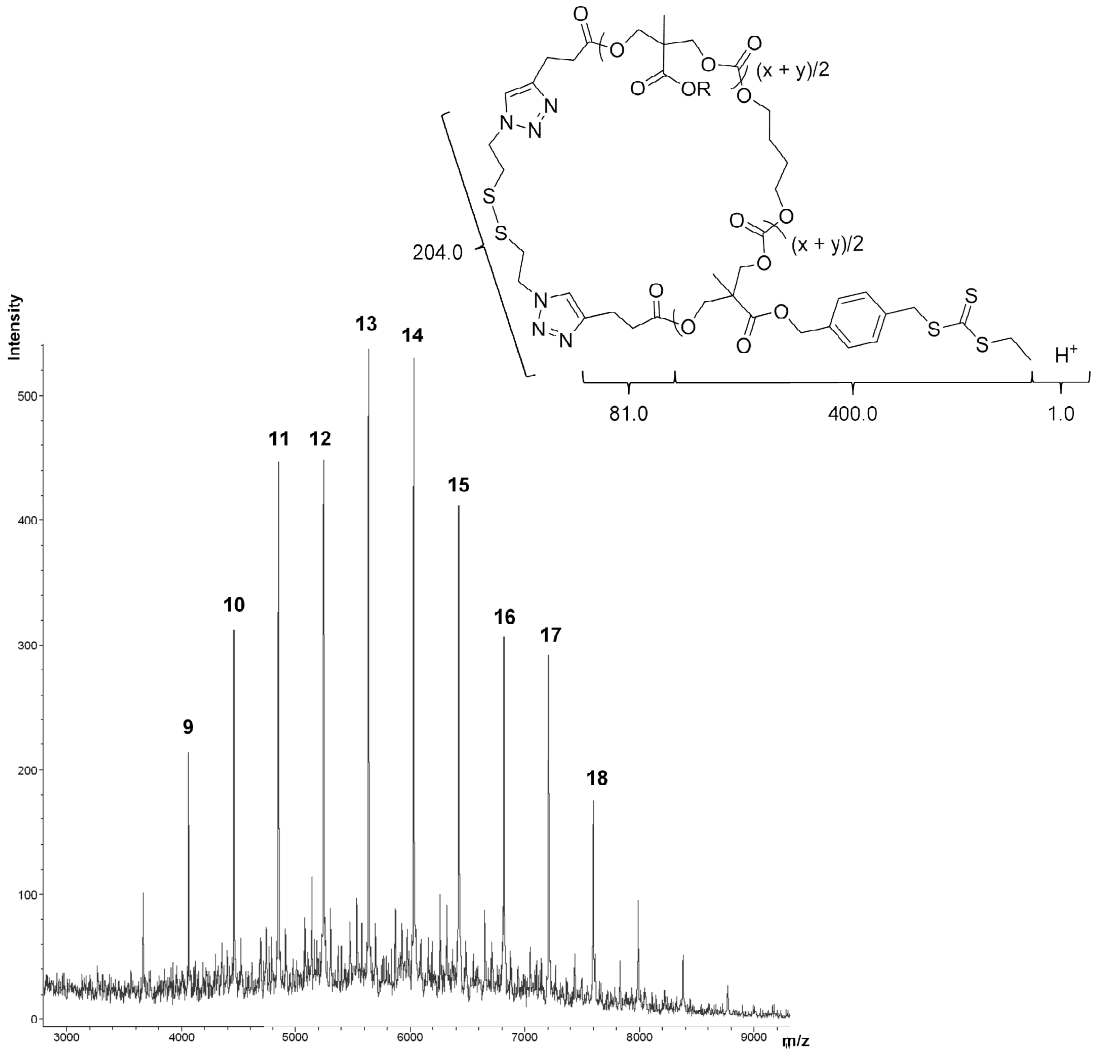

Figure 4.18. MALDI-ToF MS analysis of RAFT CTA- functional cyclic polycarbonate $\mathbf{P1_{cyclic}}$ (DP = 17).

addition to the main proton-charged distribution, a second distribution of much smaller intensity that corresponds to copper-charged polymer chains was also observed and again no high molecular weight impurities were detected.

The combination of evidence from a range of different characterisation techniques strongly supports the successful cyclisation of the RAFT CTA-functional polycarbonates without detrimental effect towards either the polycarbonate or RAFT CTA functionalities.

4.2.3 Synthesis of Cyclic Graft Copolymers by RAFT Polymerisation

To prepare cyclic graft copolymers, polymer arms were grown from the RAFT CTA groups located on the cyclic polycarbonate backbone using the optimised conditions developed in Chapter 3, for the preparation of linear graft copolymers. RAFT polymerisations were conducted at 65 °C in chloroform, with [starting polymer] = 3.0 mM and using 2,2'-azobis(isobutyronitrile) (AIBN) as the radical initiator (Scheme 4.7). A ratio of [CTA]:[AIBN] = 1:0.1 was used, where the average number of CTA groups per polymer chain was determined by ^{1}H NMR spectroscopy. The growth of poly(methyl acrylate) (PMA) arms was initially investigated to provide comparison with the synthesis of *linear-*

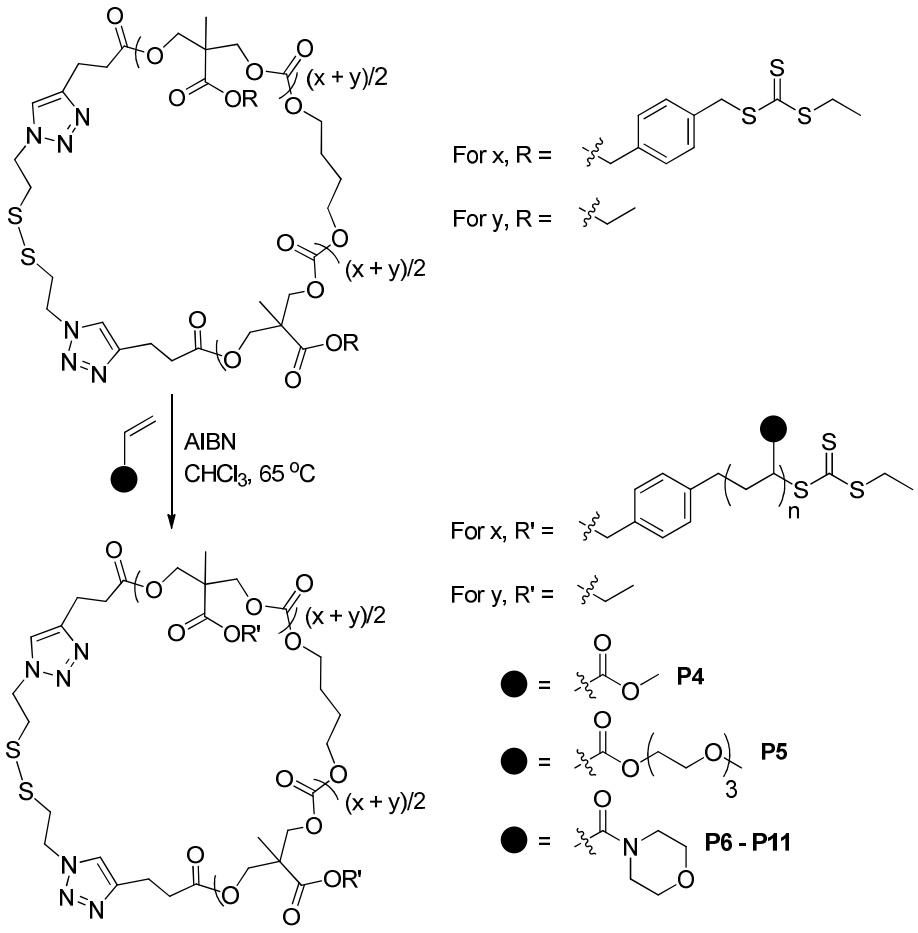

Scheme 4.7. Synthesis of cyclic graft copolymers *via* RAFT polymerisation.

polycarbonate-*g*-PMA copolymers in Chapter 3. The polymerisation of the hydrophilic monomers, *N*-acryloylmorpholine (NAM) and triethylene glycol methyl ether acrylate (TEGA), was subsequently investigated to enable the preparation of a series of water soluble cyclic graft copolymers.

4.2.3.1 Synthesis of Cyclic Graft Copolymers by RAFT Polymerisation: Polymerisation of Methyl Acrylate

Initial studies focused on the growth of PMA from polymer **P2c**$_{\text{cyclic}}$ (51% incorporation of RAFT CTA-functionality) using 100 equivalents of methyl acrylate per CTA unit. Following the polymerisation by SEC analysis revealed the presence of linear homopolymer impurities and the occurrence of graft-graft coupling at higher monomer conversions (Figure 4.19), as was previously observed in Chapter 3 for the preparation of *linear*-polycarbonate-*g*-PMA. Using the optimised conditions developed in Chapter 3, well-defined *cyclic*-

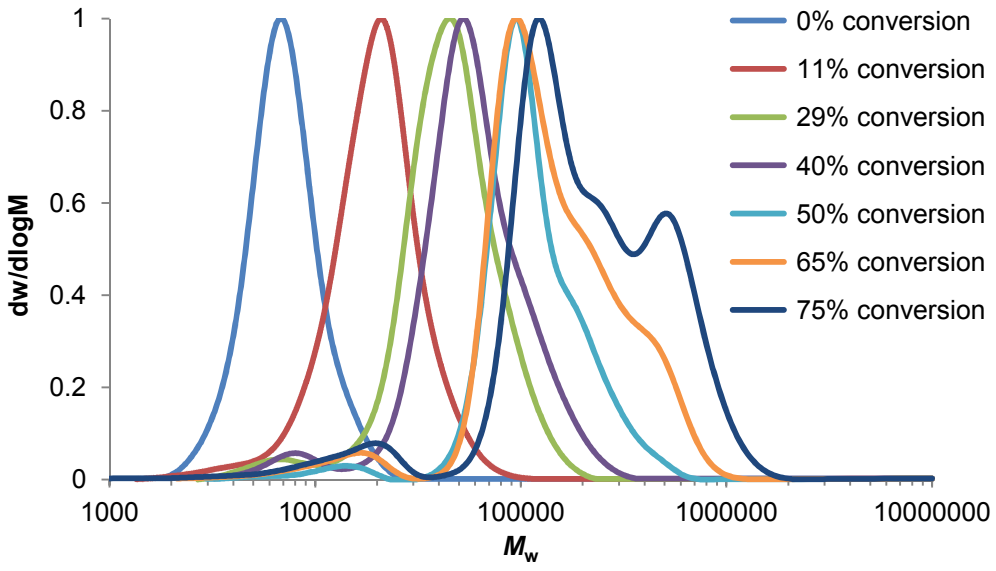

Figure 4.19. Evolution of SEC chromatograms during preparation of *cyclic*-poly(**2**$_{11}$-*co*-**1**$_{11}$-*g*-MA$_{19}$) Conditions: [CTA]:[AIBN]:[MA] = 1:0.1:100, [starting polymer] = 0.003 M in $CHCl_3$ at 65 °C.

polycarbonate-*g*-PMA was prepared (**P4**, M_n = 24.3 kDa, $Đ_M$ = 1.16). The occurrence of graft-graft coupling was prevented *via* termination of the polymerisation at low monomer conversion and linear PMA homopolymer impurities were removed from the crude polymer by precipitation in methanol (Figure 4.20).

^{1}H NMR spectroscopic analysis of the precipitated *cyclic*-polycarbonate-*g*-PMA copolymer revealed the appearance of resonances that correspond to the PMA repeat unit; namely the singlet resonance at δ = 3.66 ppm that corresponds to the methyl group of PMA and the multiple resonances at δ = 1.00 – 2.50 ppm that correspond to protons from the PMA backbone (Figure 4.21). The RAFT CTA end group fidelity of the PMA arms was confirmed by the retention of the quartet and triplet resonances, at δ = 3.37 and 1.35 ppm respectively, that correspond to the ethyl group of the RAFT CTA moiety. By comparison of the integral of the PMA repeat unit against the integrals that correspond to the

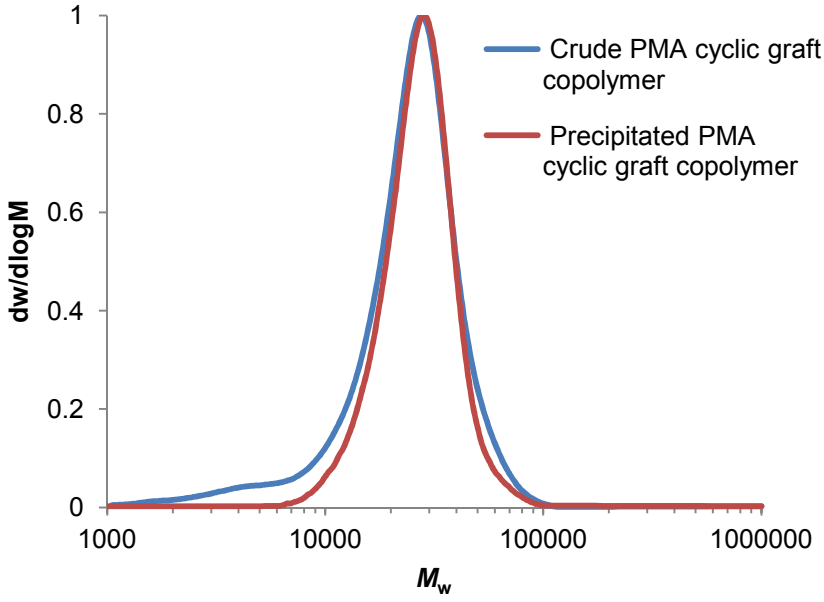

Figure 4.20. SEC chromatograms of optimised *cyclic*-poly(**2**-*co*-**1**-*g*-MA) **P4** before (M_n = 17.7 kDa, $Đ_M$ = 1.52) and after (M_n = 24.3 kDa, $Đ_M$ = 1.16) precipitation.

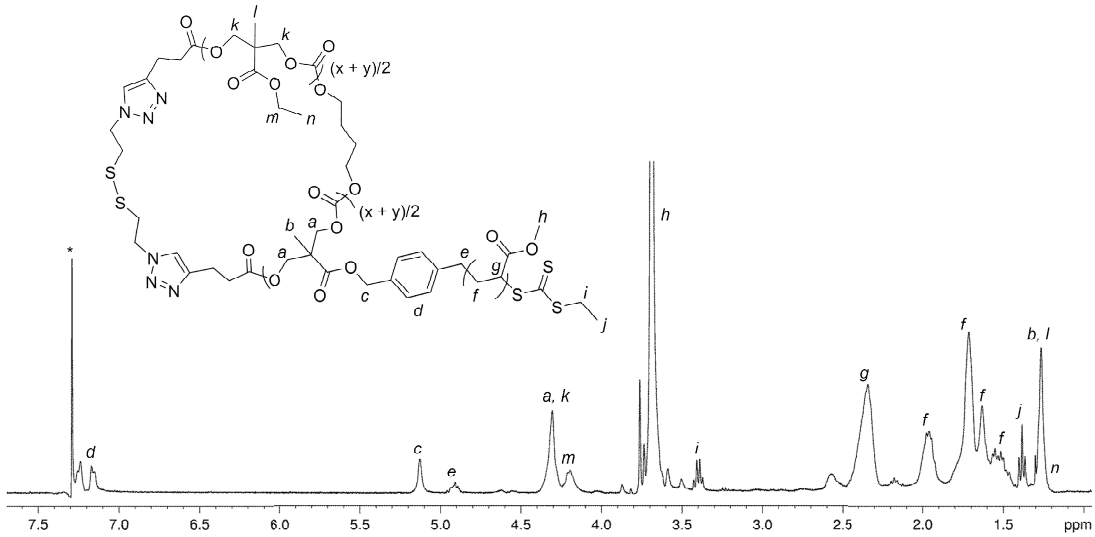

Figure 4.21. ^{1}H NMR spectrum (400 MHz; $CDCl_3$) of *cyclic*-polycarbonate-*g*-PMA copolymer **P4** (*$CHCl_3$).

RAFT CTA moiety, the average DP of the PMA arms was determined and found to be in excellent agreement with the expected value based on monomer conversion. Resonances that correspond to the polycarbonate backbone were also observed at δ = 4.27 and 1.23 ppm.

4.2.3.2 Synthesis of Cyclic Graft Copolymers by RAFT Polymerisation: Polymerisation of Hydrophilic Monomers

To exploit this method for the preparation of water soluble cyclic graft copolymers, the growth of hydrophilic poly(triethylene glycol methyl ether acrylate) (poly(TEGA)) and poly(*N*-acryloylmorpholine) (poly(NAM)) arms was also investigated. Again, polymerisations were conducted at 65 °C, with 100 equivalents of monomer per CTA unit, [starting polymer] = 3.0 mM in chloroform and AIBN as the radical initiator. Similar to the grafting of methyl acrylate, following the polymerisations of both monomers over time by SEC analysis revealed the presence of linear homopolymer impurities and

occurrence of graft-graft coupling at higher monomer conversions, leading to multimodal molecular weight distributions and large values of $Đ_M$ (Figures 2.22 and 2.23).

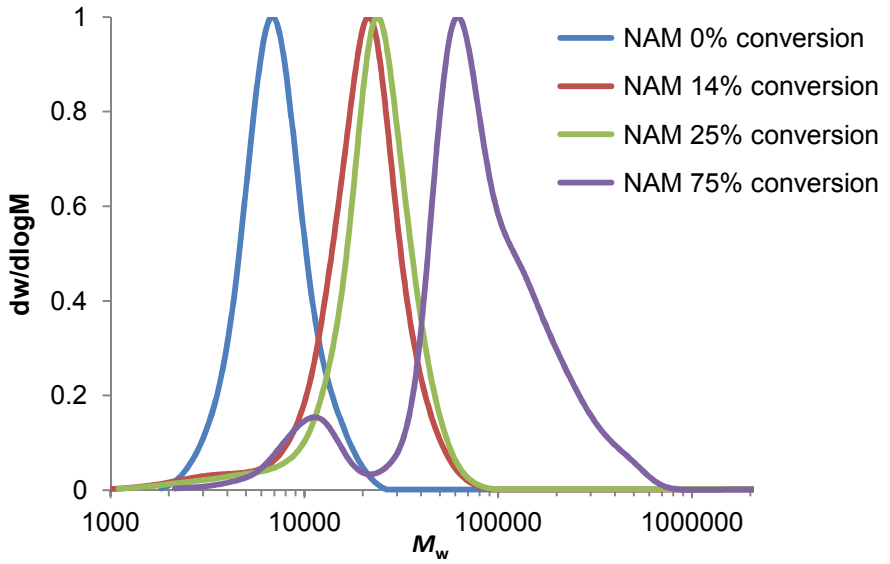

Figure 4.22. Evolution of SEC chromatograms during preparation of *cyclic*-poly($\mathbf{2_{11}}$-*co*-$\mathbf{1_{11}}$-*g*-NAM) Conditions: [CTA]:[AIBN]:[MA] = 1:0.1:100, [starting polymer] = 0.003 M in $CHCl_3$ at 65 °C.

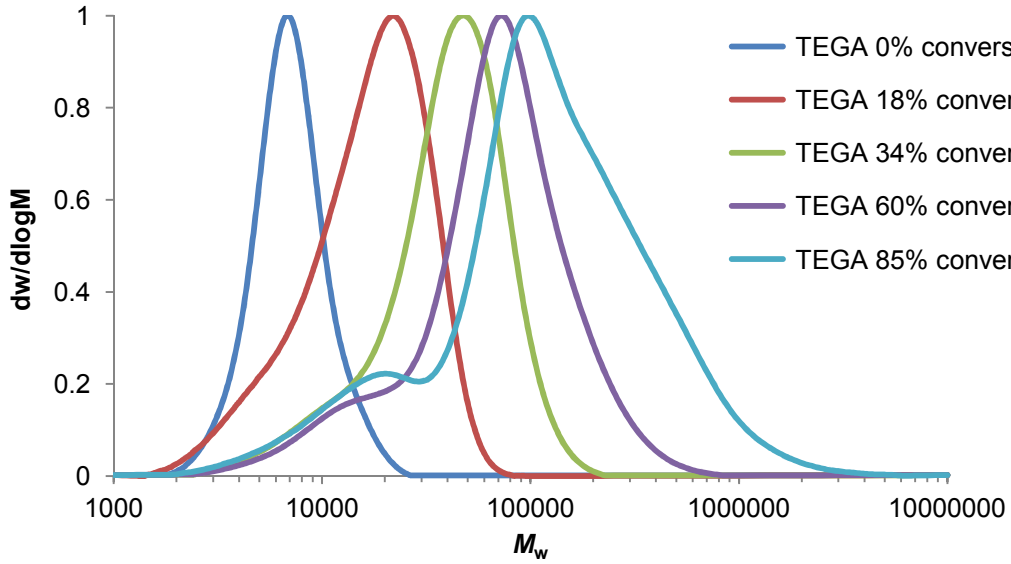

Figure 4.23. Evolution of SEC chromatograms during preparation of *cyclic*-poly($\mathbf{2_{11}}$-*co*-$\mathbf{1_{11}}$-*g*-TEGA) Conditions: [CTA]:[AIBN]:[MA] = 1:0.1:100, [starting polymer] = 0.003 M in $CHCl_3$ at 65 °C.

Graft-graft coupling could be eliminated by stopping polymerisations at low monomer conversion, however, in contrast to the preparation of polycarbonate-*g*-PMA copolymers, precipitation did not prove an effective method to remove linear poly(NAM) and poly(TEGA) homopolymer contaminants. Dialysis of the cyclic graft copolymers against distilled water to remove the linear homopolymer impurities was therefore attempted. SEC analysis of the graft copolymers after dialysis revealed a reduction in the amount of poly(TEGA) homopolymer (Figure 4.24), however no reduction in the amount poly(NAM) homopolymer was observed.

A range of *cyclic*-polycarbonate-*g*-poly(NAM) copolymers with different poly(NAM) arm lengths, from DP 19 to DP 112, were prepared by varying the equivalents of *N*-acryloylmorpholine used during polymerisation (Figure 4.25 and Table 4.6). *Cyclic*-polycarbonate-*g*-poly(NAM) copolymers with a lower grafting density were also prepared by growing poly(NAM) from cyclic

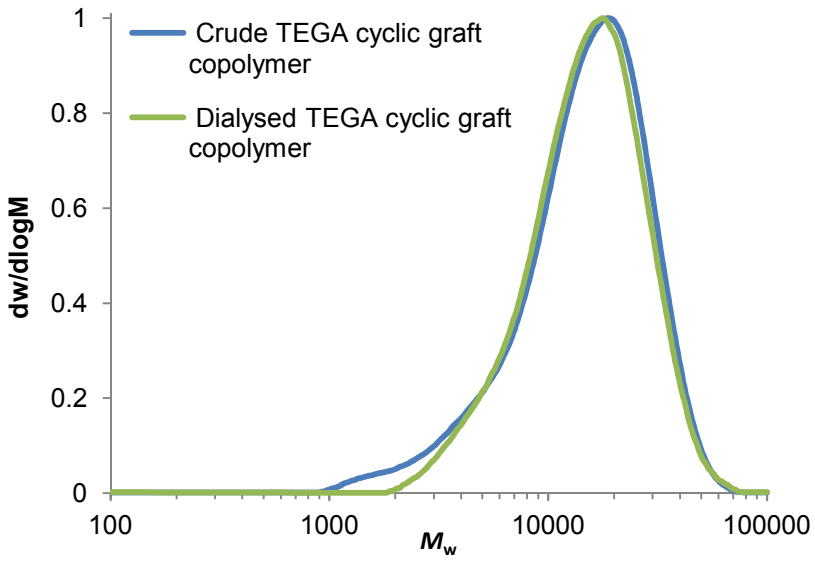

Figure 4.24. SEC chromatograms of optimised *cyclic*-poly(**2**$_{11}$-*co*-**1**$_{11}$-*g*-TEGA$_{12}$) **P5** before (M_n = 10.6 kDa, $Đ_M$ = 1.64) and after (M_n = 12.0 kDa, $Đ_M$ = 1.44) dialysis.

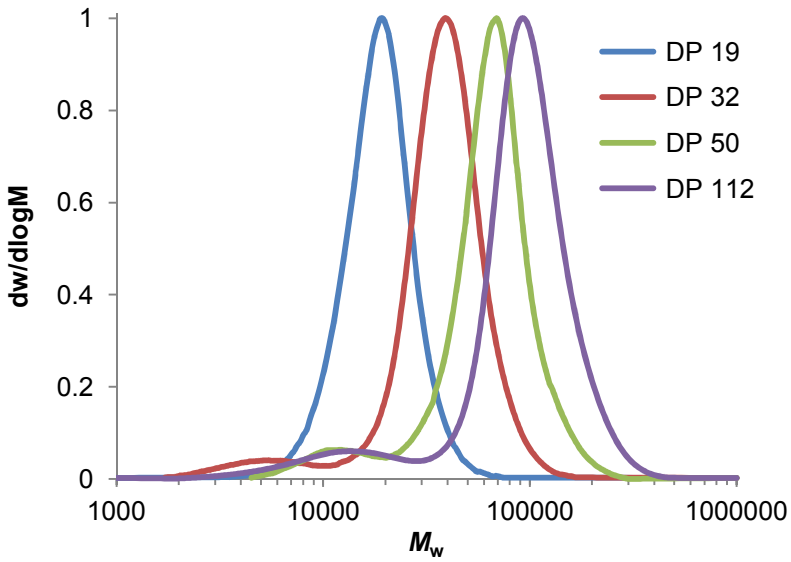

Figure 4.25. SEC chromatograms of cyclic graft copolymers **P6** (*cyclic*-poly(**2**$_{11}$-*co*-**1**$_{11}$-*g*-NAM$_{19}$), M_n = 16.1 kDa, $Đ_M$ = 1.50), **P7** (*cyclic*-poly(**2**$_{11}$-*co*-**1**$_{11}$-*g*-NAM$_{32}$), M_n = 26.6 kDa, $Đ_M$ = 1.51), **P8** (*cyclic*-poly(**2**$_{11}$-*co*-**1**$_{11}$-*g*-NAM$_{50}$), M_n = 45.3 kDa, $Đ_M$ = 1.47) and **P9** (*cyclic*-poly(**2**$_{11}$-*co*-**1**$_{11}$-*g*-NAM$_{112}$), M_n = 60.5 kDa, $Đ_M$ = 1.66).

polycarbonate **P3** with 21% RAFT CTA functionality (**P10** and **P11** Table 4.6). Analysis of the *cyclic*-polycarbonate-*g*-poly(NAM) copolymers by ^{1}H NMR spectroscopy revealed resonances that correspond to both the poly(NAM) arms and cyclic polycarbonate backbone (Figure 4.26); most notably the resonances at δ = 3.63 and 3.31 ppm attributed to the CH_2 groups of the morpholine ring and the resonances at δ = 4.27 and 1.24 ppm that correspond to CH_2 and CH_3 groups of the polycarbonate backbone respectively. Again, the presence of the quartet and triplet resonances at δ = 3.37 and 1.36 ppm that correspond to the ethyl group of the RAFT CTA moiety, confirm the retention of the RAFT CTA end groups during polymerisation.

Table 4.6 Characterisation of cyclic polycarbonate graft copolymers.

Polymer	Structure	DP[a]	M_n(NMR) (kDa)[a]	M_n(SEC) (kDa)[b]	$Đ_M$[b]
P4	poly(**2$_{11}$**-*co*-**1$_{11}$**-*g*-MA$_{19}$)	19	24.9	24.3	1.16
P5	poly(**2$_{11}$**-*co*-**1$_{11}$**-*g*-TEGA$_{11}$)	13	39.1	12.0	1.44
P6	poly(**2$_{11}$**-*co*-**1$_{11}$**-*g*-NAM$_{19}$)	19	37.3	16.1	1.50
P7	poly(**2$_{11}$**-*co*-**1$_{11}$**-*g*-NAM$_{32}$)	32	58.1	26.6	1.51
P8	poly(**2$_{11}$**-*co*-**1$_{11}$**-*g*-NAM$_{50}$)	50	86.8	45.3	1.47
P9	poly(**2$_{11}$**-*co*-**1$_{11}$**-*g*-NAM$_{112}$)	112	186	60.5	1.66
P10	poly(**2$_{18}$**-*co*-**1$_{5}$**-*g*-NAM$_{31}$)	31	27.7	20.4	1.52
P11	poly(**2$_{18}$**-*co*-**1$_{5}$**-*g*-NAM$_{56}$)	56	45.4	29.7	1.56

[a]Determined by ^{1}H NMR spectroscopy. [b]Determined by SEC analysis in $CHCl_3$ using poly(styrene) standards. Conditions: [CTA]:[AIBN] = 1:0.1 in $CHCl_3$ at 65 °C.

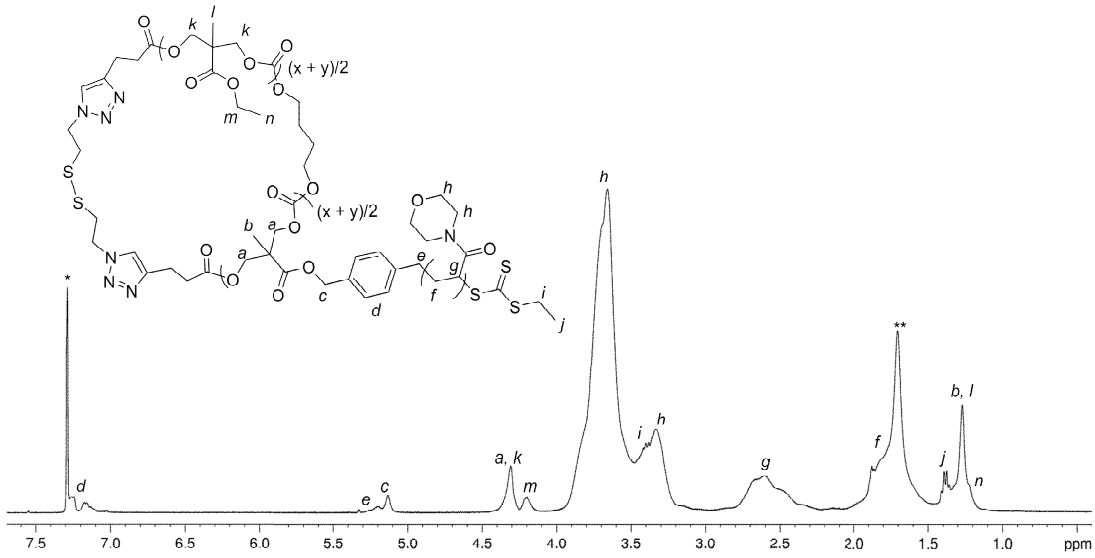

Figure 4.26. ^{1}H NMR spectrum (400 MHz; $CDCl_3$) of *cyclic*-polycarbonate-*g*-poly(NAM) copolymer **P7** (*$CHCl_3$, **H_2O).

4.3 Conclusions

In conclusion, a new approach for the preparation of cyclic graft copolymers with a degradable polycarbonate backbone has been developed through combination of ROP and a "grafting-from" approach, demonstrating for the first time the use of the RAFT polymerisation technique to prepare cyclic graft copolymers. In this approach, difunctional hydroxyl-terminated RAFT CTA-functional polycarbonates were prepared *via* the ring-opening copolymerisation of RAFT CTA- and ethyl- functional cyclic carbonate monomers initiated from the difunctional initiator, 1,4-butanediol. Esterification of the hydroxyl groups yielded difunctional alkyne-terminated polycarbonates, which were subsequently ring-closed *via* reaction with a diazide linker under *pseudo*-high dilution cyclisation conditions. Cyclic graft copolymers were prepared *via* RAFT mediated polymerisation from the CTA groups located along the polycarbonate backbone, where variation of the identity and equivalents of the grafting monomer allowed the preparation of a range of cyclic graft copolymers with different compositions. Particular attention was given to the grafting of hydrophilic monomers to prepare water soluble cyclic graft copolymers and demonstrates for the first time the preparation of water soluble graft copolymers *via* a "grafting from" approach, greatly expanding the range of accessible hydrophilic cyclic graft copolymers.

4.4 References

1. W. A. Braunecker and K. Matyjaszewski, *Prog. Polym. Sci.*, 2007, **32**, 93-146.
2. A. Gregory and M. H. Stenzel, *Prog. Polym. Sci.*, 2012, **37**, 38-105.
3. N. Hadjichristidis, H. Iatrou, M. Pitsikalis and J. Mays, *Prog. Polym. Sci.*, 2006, **31**, 1068-1132.
4. N. Hadjichristidis, M. Pitsikalis, S. Pispas and H. Iatrou, *Chem. Rev.*, 2001, **101**, 3747-3792.
5. A. Hirao, R. Goseki and T. Ishizone, *Macromolecules*, 2014, **47**, 1883-1905.
6. A. Blencowe, J. F. Tan, T. K. Goh and G. G. Qiao, *Polymer*, 2009, **50**, 5-32.
7. H. Gao and K. Matyjaszewski, *Prog. Polym. Sci.*, 2009, **34**, 317-350.
8. D. Kuckling and A. Wycisk, *J. Polym. Sci., Part A: Polym. Chem.*, 2013, **51**, 2980-2994.
9. K. Endo, in *New Frontiers in Polymer Synthesis*, ed. S. Kobayashi, Springer Berlin Heidelberg, 2008, vol. 217, pp. 121-183.
10. J. N. Hoskins and S. M. Grayson, *Polym. Chem.*, 2011, **2**, 289-299.
11. Z. Jia and M. J. Monteiro, *J. Polym. Sci., Part A: Polym. Chem.*, 2012, **50**, 2085-2097.
12. H. R. Kricheldorf, *J. Polym. Sci., Part A: Polym. Chem.*, 2010, **48**, 251-284.
13. B. A. Laurent and S. M. Grayson, *Chem. Soc. Rev.*, 2009, **38**, 2202-2213.
14. C. Feng, Y. Li, D. Yang, J. Hu, X. Zhang and X. Huang, *Chem. Soc. Rev.*, 2011, **40**, 1282-1295.
15. S. S. Sheiko, B. S. Sumerlin and K. Matyjaszewski, *Prog. Polym. Sci.*, 2008, **33**, 759-785.

16. D. Uhrig and J. Mays, *Polym. Chem.*, 2011, **2**, 69-76.

17. M. Zhang and A. H. E. Müller, *J. Polym. Sci., Part A: Polym. Chem.*, 2005, **43**, 3461-3481.

18. R. M. England and S. Rimmer, *Polym. Chem.*, 2010, **1**, 1533-1544.

19. K. Inoue, *Prog. Polym. Sci.*, 2000, **25**, 453-571.

20. X. Zhu, Y. Zhou and D. Yan, *J. Polym. Sci., Part B: Polym. Phys.*, 2011, **49**, 1277-1286.

21. B. I. Voit and A. Lederer, *Chem. Rev.*, 2009, **109**, 5924-5973.

22. A. Carlmark, C. Hawker, A. Hult and M. Malkoch, *Chem. Soc. Rev.*, 2009, **38**, 352-362.

23. R. Dong, Y. Zhou and X. Zhu, *Acc. Chem. Res.*, 2014.

24. K. Khanna, S. Varshney and A. Kakkar, *Polym. Chem.*, 2010, **1**, 1171-1185.

25. N. Sugai, H. Heguri, K. Ohta, Q. Meng, T. Yamamoto and Y. Tezuka, *J. Am. Chem. Soc.*, 2010, **132**, 14790-14802.

26. N. Sugai, H. Heguri, T. Yamamoto and Y. Tezuka, *J. Am. Chem. Soc.*, 2011, **133**, 19694-19697.

27. Y. Deng, S. Zhang, G. Lu and X. Huang, *Polym. Chem.*, 2013, **4**, 1289-1299.

28. T. Yamamoto and Y. Tezuka, *Polym. Chem.*, 2011, **2**, 1930-1941.

29. M. Schappacher, C. Billaud, C. Paulo and A. Deffieux, *Macromol. Chem. Phys.*, 1999, **200**, 2377-2386.

30. M. Schappacher and A. Deffieux, *J. Am. Chem. Soc.*, 2008, **130**, 14684-14689.

31. B. Chen, K. Jerger, J. M. J. Fréchet and F. C. Szoka Jr, *J. Controlled Release*, 2009, **140**, 203-209.

32. Z. Jia, Q. Fu and J. Huang, *Macromolecules*, 2006, **39**, 5190-5193.

33. X. Pang, R. Jing and J. Huang, *Polymer*, 2008, **49**, 893-900.

34. X. Pang, G. Wang, Z. Jia, C. Liu and J. Huang, *J. Polym. Sci., Part A: Polym. Chem.*, 2007, **45**, 5824-5837.

35. X. Fan, G. Wang and J. Huang, *J. Polym. Sci., Part A: Polym. Chem.*, 2011, **49**, 1361-1367.

36. Y. Xia, A. J. Boydston and R. H. Grubbs, *Angew. Chem. Int. Ed.*, 2011, **50**, 5882-5885.

37. K. Zhang, M. A. Lackey, Y. Wu and G. N. Tew, *J. Am. Chem. Soc.*, 2011, **133**, 6906-6909.

38. K. Zhang and G. N. Tew, *ACS Macro Lett.*, 2012, **1**, 574-579.

39. K. Zhang, Y. Zha, B. Peng, Y. Chen and G. N. Tew, *J. Am. Chem. Soc.*, 2013, **135**, 15994-15997.

40. H. Li, R. Jérôme and P. Lecomte, *Macromolecules*, 2008, **41**, 650-654.

41. N. Nasongkla, B. Chen, N. Macaraeg, M. E. Fox, J. M. J. Fréchet and F. C. Szoka, *J. Am. Chem. Soc.*, 2009, **131**, 3842-3843.

42. S. H. Lahasky, W. K. Serem, L. Guo, J. C. Garno and D. Zhang, *Macromolecules*, 2011, **44**, 9063-9074.

43. G. Moad, E. Rizzardo and S. H. Thang, *Aust. J. Chem.*, 2005, **58**, 379-410.

44. G. Moad, E. Rizzardo and S. H. Thang, *Aust. J. Chem.*, 2006, **59**, 669-692.

45. G. Moad, E. Rizzardo and S. H. Thang, *Aust. J. Chem.*, 2009, **62**, 1402-1472.

46. S. Perrier and P. Takolpuckdee, *J. Polym. Sci., Part A: Polym. Chem.*, 2005, **43**, 5347-5393.

47. S. Zhang and Y. Zhao, *J. Am. Chem. Soc.*, 2010, **132**, 10642-10644.

48. W. H. Binder and R. Sachsenhofer, *Macromol. Rapid Commun.*, 2007, **28**, 15-54.

49. P. L. Golas and K. Matyjaszewski, *Chem. Soc. Rev.*, 2010, **39**, 1338-1354.

50. B. A. Laurent and S. M. Grayson, *J. Am. Chem. Soc.*, 2006, **128**, 4238-4239.

51. J. N. Hoskins and S. M. Grayson, *Macromolecules*, 2009, **42**, 6406-6413.

52. M. A. Harvison and A. B. Lowe, *Macromol. Rapid Commun.*, 2011, **32**, 779-800.

53. D. Quemener, T. P. Davis, C. Barner-Kowollik and M. H. Stenzel, *Chem. Commun.*, 2006, 5051-5053.

54. C. Lu, Q. Shi, X. Chen, T. Lu, Z. Xie, X. Hu, J. Ma and X. Jing, *J. Polym. Sci., Part A: Polym. Chem.*, 2007, **45**, 3204-3217.

55. Q. Shi, X. Chen, T. Lu and X. Jing, *Biomaterials*, 2008, **29**, 1118-1126.

56. S. Tempelaar, I. A. Barker, V. X. Truong, D. J. Hall, L. Mespouille, P. Dubois and A. P. Dove, *Polym. Chem.*, 2013, **4**, 174-183.

57. J. Xu, F. Prifti and J. Song, *Macromolecules*, 2011, **44**, 2660-2667.

58. X. Zhang, Z. Zhong and R. Zhuo, *Macromolecules*, 2011, **44**, 1755-1759.

59. Y. Wang, R. Zhang, N. Xu, F.-S. Du, Y.-L. Wang, Y.-X. Tan, S.-P. Ji, D.-H. Liang and Z.-C. Li, *Biomacromolecules*, 2010, **12**, 66-74.

60. A. B. J. Withey, G. Chen, T. L. U. Nguyen and M. H. Stenzel, *Biomacromolecules*, 2009, **10**, 3215-3226.

61. H. Misaka, R. Kakuchi, C. Zhang, R. Sakai, T. Satoh and T. Kakuchi, *Macromolecules*, 2009, **42**, 5091-5096.

62. Y.-Y. Yuan, J.-Z. Du and J. Wang, *Chem. Commun.*, 2012, **48**, 570-572.

63. G. Hadziioannou, P. M. Cotts, G. ten Brinke, C. C. Han, P. Lutz, C. Strazielle, P. Rempp and A. J. Kovacs, *Macromolecules*, 1987, **20**, 493-497.

64. I. Tellitu, S. Serna, M. T. Herrero, I. Moreno, E. Domínguez and R. SanMartin, *J. Org. Chem.*, 2007, **72**, 1526-1529.

5 Comparison of the Solution Properties and Self-Assembly of Linear and Cyclic Graft Copolymers

5.1 Introduction

As a consequence of their grafted structure, graft copolymers display unique physical properties in comparison to linear polymers.[1, 2] For example, graft copolymers exhibit improved rheological properties compared to analogous linear polymers and have consequently been employed to improve the mechanical properties of commodity plastics such as poly(propylene)[3] and poly(styrene)/poly(diene)[4] systems. Furthermore, the properties of graft copolymers can be tailored *via* the systematic variation of arm length, backbone length and grafting density and to this end, an extremely versatile range of materials can be prepared from graft copolymers.

Recent significant interest has been given to the preparation of graft copolymers with high grafting density, commonly termed "molecular bottlebrushes", where steric crowding between arms causes elongation of the polymer backbone, resulting in a transition from a flexible coil to a rigid worm-like conformation.[5, 6] Amphiphilic "molecular brushes" have been found to exhibit unique self-assembly behaviour, providing access to significantly larger domain spacings compared to the phase separation of conventional amphiphilic block copolymers.[7-10]

Graft copolymers with lower grafting densities have also been found to exhibit distinct self-assembly behaviour in comparison to the self-assembly of linear polymers.[11-15] Graft copolymers comprised of a hydrophobic backbone and hydrophilic side arms are reported to form either unimolecular or multi-molecular micelles upon dissolution in water. In a unimolecular micelle, the hydrophobic backbone is adequately protected from unfavourable solvent interactions by the hydrophilic side arms resulting in a core-shell structure.

Even in a good solvent for both the backbone and side arms, graft copolymers are reported to segregate into unimolecular core-shell structures.[16, 17] As unimolecular micelles do not possess a critical micelle concentration (cmc), such assemblies are of particular interest in intravenous drug delivery, where conventional micelles would disassemble into unimers upon dilution in the bloodstream. Alternatively, graft copolymers self-assemble into loose micellar aggregates, where the aggregation number is typically low as a consequence of the increased number of hydrophilic blocks per hydrophobic block in comparison to assemblies comprised of linear block copolymers. Whether graft copolymers self-assemble into unimolecular or multi-molecular micelles is dependent on grafting density, the number of side arms and the composition of the side arms and backbone, as these factors determine how well the hydrophilic arms can shield the hydrophobic backbone. The preparation of particles with a diverse range of morphologies including vesicles, compound micelles and lamellae have also been reported *via* the self-assembly of graft copolymers with more complex compositions, for example, block copolymer or mixed arm systems.[18-26]

The properties of cyclic graft copolymers are relatively unexplored, although a few examples of their distinct behaviour in comparison to linear graft copolymers have been reported. Huang and coworkers found that cyclic poly(ethylene glycol)-*g*-poly(styrene) could extract significantly more dye than linear poly(ethylene glycol)-*g*-poly(styrene).[27] On average one molecule of cyclic graft copolymer could encapsulate up to 6 dye molecules, whereas the equivalent linear graft copolymers could only encapsulate ≤ 0.7 dye molecules per polymer. This difference in encapsulation behaviour was attributed to the

ability of the cyclic graft copolymers to act as nanocages to encapsulate multiple dye molecules, whereas several linear graft copolymers were needed to encapsulate a single dye molecule (Figure 5.1). Meanwhile, Szoka and coworkers reported that cyclic graft copolymers display longer *in vivo* circulation times and higher tumor accumulation compared to linear graft copolymer analogues.[28] Similarly, there are very few reports of the self-assembly of cyclic graft copolymers. Li *et al*. reported the preparation of large spherical micelles (D_{av}(TEM) = *ca*. 100 nm) from cyclic poly(ε-caprolactone)$_{208}$-*g*-poly(ethylene oxide)$_{24}$ with a very low grafting density; only 4% of ε-caprolactone units were attached to a PEO chain.[29] Whereas, Schappacher and Deffieux reported the preparation of polymeric nanotubes *via* the self-assembly of densely grafted cyclic poly(chloroethyl vinyl ether) with a mixture of poly(styrene) (PS) and poly(isoprene) (PI) side arms in heptane.[30] Analysis by AFM revealed the nanotubes possessed a PS core and PI corona with an overall

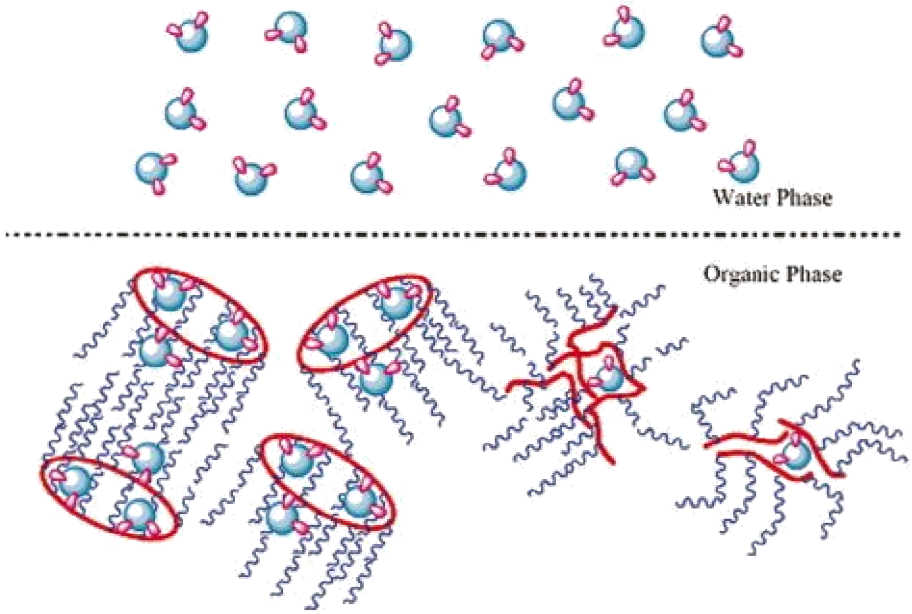

Figure 5.1. Extraction of hydrophilic dye molecules by cyclic and linear poly(ethylene glycol)-*g*-poly(styrene) copolymers.[27]

diameter of *ca*. 100 nm and length of *ca*. 700 nm, where the diameter of the nanotubes corresponded to the diameter of the cyclic graft copolymers, suggesting that self-assembly had occurred in a cofacial manner between cyclic grafts.

In Chapters 3 and 4 procedures for the synthesis of well-defined linear and cyclic graft copolymers were developed using a combination of ROP and RAFT polymerisation techniques. In this chapter, the solution properties of cyclic graft copolymers comprised of a hydrophobic polycarbonate backbone and hydrophilic poly(*N*-acryloylmorpholine) side arms are compared with the properties of equivalent linear graft copolymers. It is shown that the self-assembly and thermoresponsive behaviour of graft copolymers can be dramatically modified through cyclisation of the polymer backbone.

5.2 Results and Discussion

5.2.1 Linear and Cyclic Graft Copolymer Synthesis

A series of linear and cyclic graft copolymers with equivalent compositions and molecular weights were prepared *via* a combination of ring-opening polymerisation (ROP) and reversible addition-fragmentation chain transfer (RAFT) polymerisation as previously reported in Chapters 3 and 4. A RAFT CTA-functional cyclic carbonate monomer (**1**) and an ethyl-functional cyclic carbonate monomer (**2**) were copolymerised using 1,4-butanediol as the ROP initiator to afford hydroxyl-terminated telechelic polycarbonates (Scheme 5.1). For the preparation of cyclic graft copolymers, subsequent end-group modification *via* reaction with 4-pentynoic anhydride yielded alkyne-functional telechelic polycarbonates. Cyclisation was achieved through copper-catalysed cycloaddition with a diazide small molecule linker under *pseudo*-high dilution, where the small molecule linker contained a disulfide unit to enable cleavage of the cyclic polycarbonate backbone. Subsequent RAFT polymerisation using the optimised conditions reported in Chapter 3 yielded well-defined cyclic graft copolymers. To prepare the equivalent linear graft copolymers, RAFT polymerisation proceeded directly after ROP.

The comonomer feed ratio of cyclic carbonate monomers **1** and **2** was 1:1, therefore, a polymer side arm was grown from *ca*. 50% of the repeat units of the polycarbonate backbone during RAFT polymerisation. The graft copolymer arms were composed of the hydrophilic, biocompatible poly(acrylamide), poly(*N*-acryloylmorpholine) (poly(NAM)) and a series of linear and cyclic graft copolymers with different arm lengths (*ca*. 20, 30, 50 and 110) were prepared

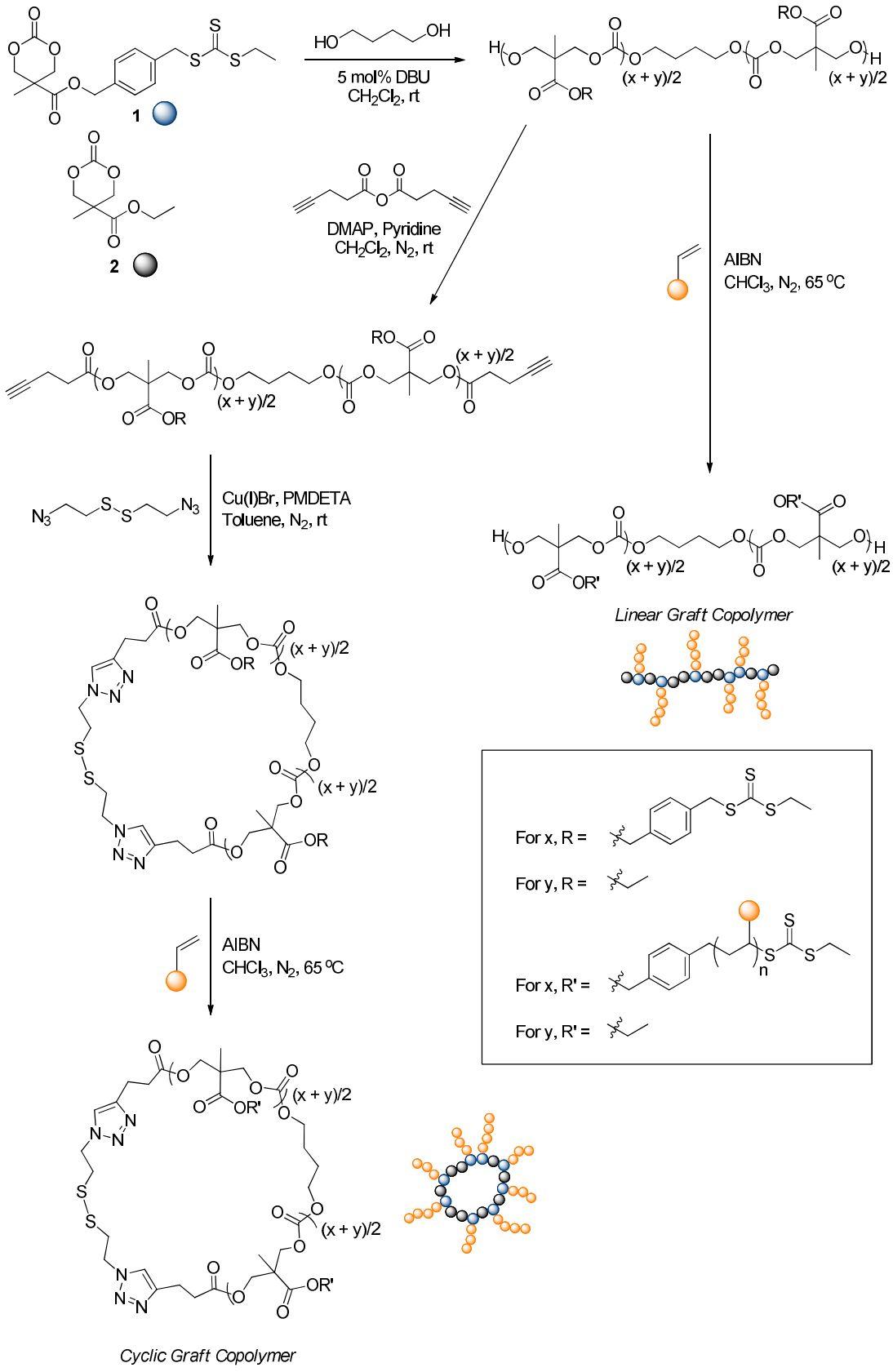

Scheme 5.1. Synthesis of linear and cyclic graft copolymers *via* ROP and RAFT polymerisation.

by variation of the equivalents of *N*-acryloylmorpholine used during polymerisation (Table 5.1 and Figure 5.2). To ensure the equivalent linear and cyclic graft copolymers had very similar compositions and enable a good comparison between their properties, RAFT polymerisations were targeted to give linear and cyclic grafts with the same poly(NAM) arm length. Furthermore, the cyclic and linear graft copolymers were derived from the same starting polycarbonate so in each case possessed the same number of RAFT CTA initiation sites.

Table 5.1. Characterisation of cyclic and linear graft copolymers.

Polymer	Structure	Arm DP[a]	M_n(NMR) (kDa)[a]	M_n(SEC) (kDa)[b]	$Đ_M$[b]
P1	*cyclic*-poly(**2**$_{11}$-*co*-**1**$_{11}$-*g*-NAM$_{19}$)	19	37.3	16.1	1.50
P2	*linear*-poly(**2**$_{11}$-*co*-**1**$_{11}$-*g*-NAM$_{19}$)	19	37.0	15.7	1.38
P3	*cyclic*-poly(**2**$_{11}$-*co*-**1**$_{11}$-*g*-NAM$_{32}$)	32	58.1	23.0	1.46
P4	*linear*-poly(**2**$_{11}$-*co*-**1**$_{11}$-*g*-NAM$_{28}$)	28	51.3	18.0	1.44
P5	*cyclic*-poly(**2**$_{11}$-*co*-**1**$_{11}$-*g*-NAM$_{50}$)	50	86.8	45.3	1.47
P6	*linear*-poly(**2**$_{11}$-*co*-**1**$_{11}$-*g*-NAM$_{47}$)	47	81.6	37.5	1.41
P7	*cyclic*-poly(**2**$_{11}$-*co*-**1**$_{11}$-*g*-NAM$_{112}$)	112	186	60.5	1.66

[a]Determined by ^{1}H NMR spectroscopy. [b]Determined by SEC analysis in $CHCl_3$ using poly(styrene) standards. Conditions: [CTA]:[AIBN] = 1:0.1 in $CHCl_3$ at 65 °C.

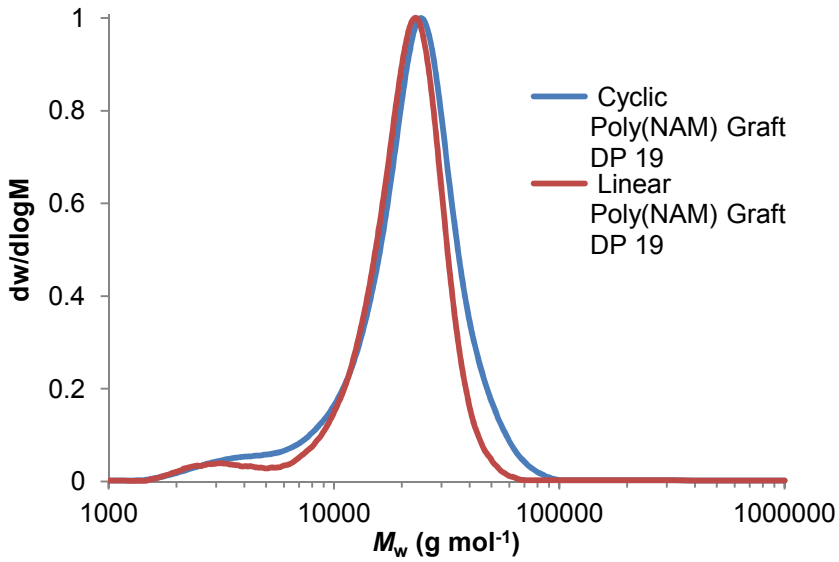

Figure 5.2. SEC chromatograms of *cyclic*-poly(**2**$_{11}$-*co*-**1**$_{11}$-*g*-NAM$_{19}$) (**P1**, M_n = 16.1 kDa, $Đ_M$ = 1.50) and *linear*-poly(**2**$_{11}$-*co*-**1**$_{11}$-*g*-NAM$_{19}$) (**P2**, M_n = 15.7 kDa, $Đ_M$ = 1.38).

5.2.2 Formation of Unimolecular Graft Copolymer Micelles

Solutions of cyclic and linear graft copolymers **P3** – **P7** in water, a selective solvent for the poly(NAM) side arms, and THF, a good solvent for both the polycarbonate backbone and poly(NAM) side arms, were analysed by dynamic light scattering at a concentration of 2 mg/mL. Comparison of the number average hydrodynamic diameters (D_h) of **P3** – **P7** in both solvents revealed that the linear and cyclic graft copolymers did not aggregate upon dissolution in water and instead formed unimolecular micelles, where the hydrophobic polycarbonate backbone formed the core and the hydrophilic poly(NAM) side arms formed the corona (Table 5.2). The values of D_h for the graft copolymers in THF were found to be slightly larger than values of D_h for the graft copolymers in water, as THF can penetrate both the corona and core of the graft copolymer unimolecular micelles, whereas water is excluded from the

Table 5.2. DLS analysis of linear and cyclic graft copolymers, **P3** – **P7**.

Polymer	Topology	Arm DP[a]	$D_h(H_2O)$ (nm)[b]	D_h(THF) (nm)[b]
P3	Cyclic	32	7.6 ± 0.5	7.9 ± 0.4
P4	Linear	28	6.7 ± 0.4	7.2 ± 0.5
P5	Cyclic	50	10 ± 1	12 ± 1
P6	Linear	47	7.7 ± 0.6	8.9 ± 0.2
P7	Cyclic	112	12 ± 0.4	14 ± 0.04

[a]Determined by ^{1}H NMR spectroscopy. [b]Determined by DLS analysis, number average solution diameter.

hydrophobic core. The formation of unimolecular micelles from graft copolymers **P3** – **P7** demonstrates that a poly(NAM) arm length ≥ 30 and a grafting density of *ca.* 50%, is sufficient to protect the hydrophobic polycarbonate backbone from unfavourable solvent interactions.

It was also observed that D_h increased with increasing poly(NAM) arm length for both the cyclic and liner graft copolymers (Table 5.2 and Figure 5.3). Furthermore, although values of D_h were found to be similar for cyclic and linear graft copolymers with the same poly(NAM) arm length, cyclic graft copolymers consistently displayed slightly larger values of D_h than the equivalent linear graft copolymer (Figure 5.4). For example, cyclic and linear graft copolymers with poly(NAM) arm lengths of 32 and 28 respectively exhibited number average solution diameters of 7.6 and 6.7 nm. Cyclic and linear graft copolymers with poly(NAM) arm lengths of 50 and 47 exhibited larger values of D_h (cyclic D_h = 10 nm, linear D_h = 7.8 nm). Cyclic graft copolymer **P7**, with a poly(NAM) arm length of 112, exhibited the largest value of D_h at 12 nm.

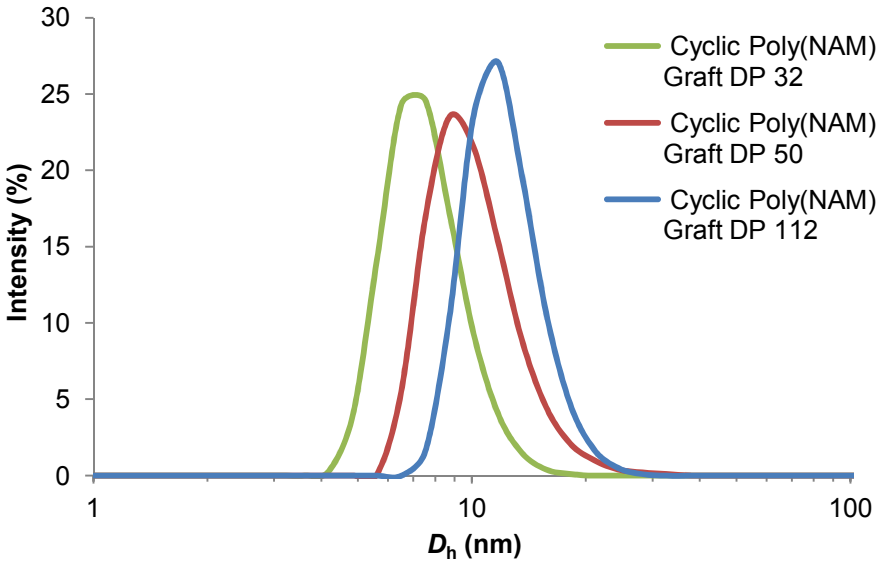

Figure 5.3. DLS analysis of *cyclic*-poly(**2**$_{11}$-*co*-**1**$_{11}$-*g*-NAM) with poly(NAM) arm lengths 32 (**P3**), 50 (**P5**) and 112 (**P7**).

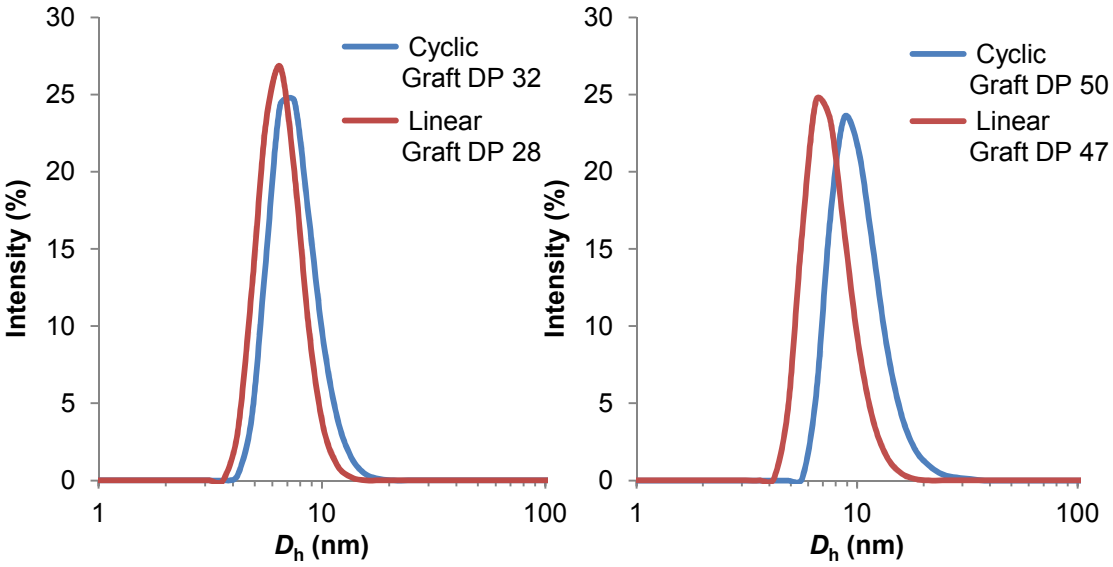

Figure 5.4. DLS analysis of (left) *cyclic*-poly(**2**$_{11}$-*co*-**1**$_{11}$-*g*-NAM$_{32}$) (**P3**, D_h = 7.6 nm) and *linear*-poly(**2**$_{11}$-*co*-**1**$_{11}$-*g*-NAM$_{28}$) (**P4**, D_h = 6.7 nm), (right) *cyclic*-poly(**2**$_{11}$-*co*-**1**$_{11}$-*g*-NAM$_{50}$) (**P5**, D_h = 10 nm) and *linear*-poly(**2**$_{11}$-*co*-**1**$_{11}$-*g*-NAM$_{47}$) (**P6**, D_h = 7.8 nm).

To gain further insight into the solution conformations of these unimolecular micelles, solutions of **P5** and **P6** in water and 1,4-dioxane were analysed by small angle x-ray scattering (SAXS) at a concentration of 0.5 mg/mL. A clear difference was observed in the shape of the curves for the cyclic and linear graft

copolymers in both water and 1,4-dioxane for plots of scattering intensity ($I(q)$) *versus* the scattering vector (q) (Figures 5.5 and 5.6). Fitting the data to a

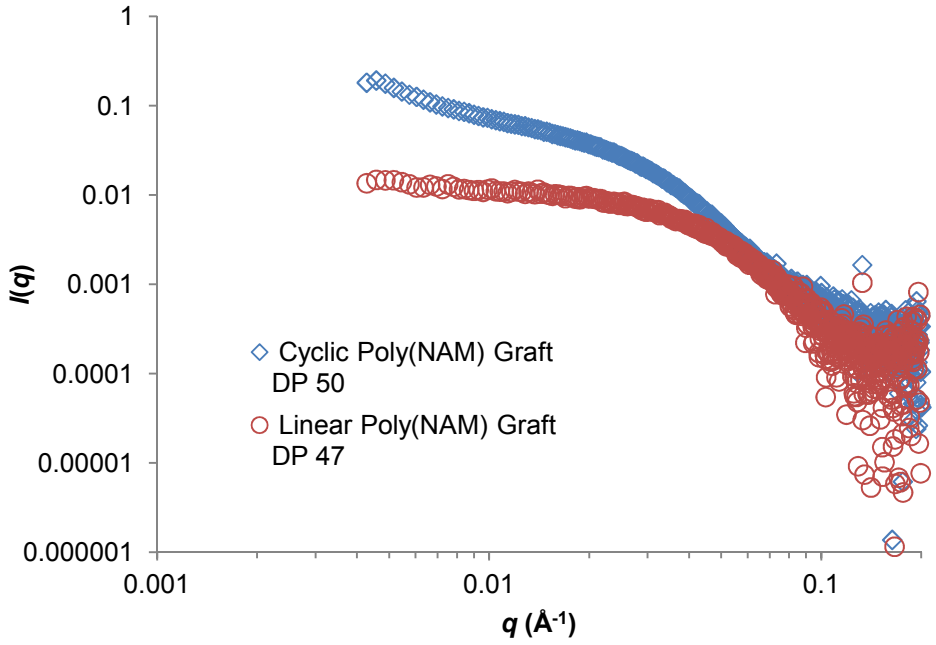

Figure 5.5. SAXS profiles of *cyclic*-poly(**2**$_{11}$-*co*-**1**$_{11}$-*g*-NAM$_{50}$) (**P5**) and *linear*-poly(**2**$_{11}$-*co*-**1**$_{11}$-*g*-NAM$_{47}$) (**P6**) in water at 0.5 mg/mL.

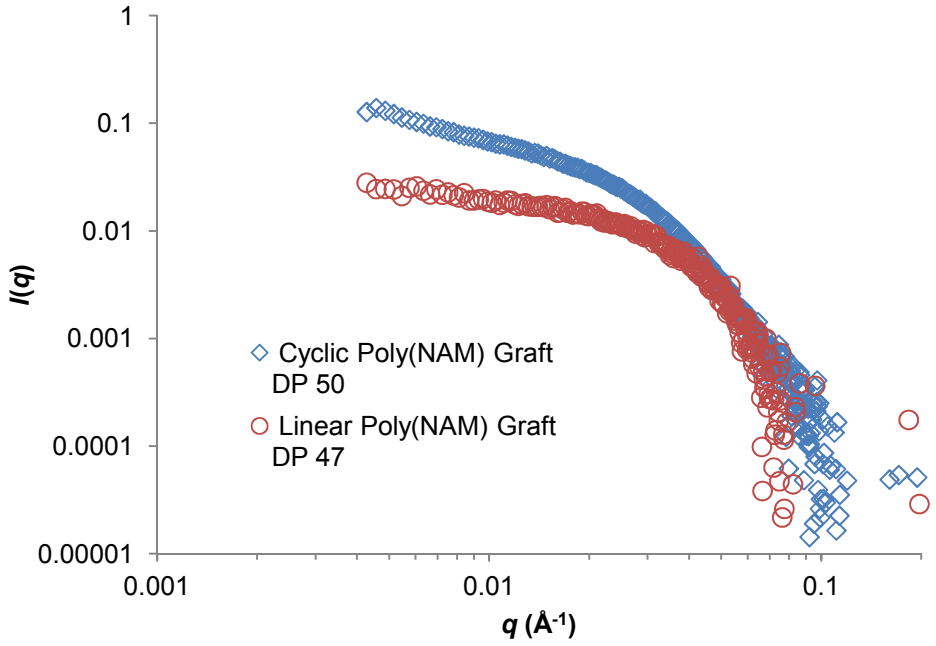

Figure 5.6. SAXS profiles of *cyclic*-poly(**2**$_{11}$-*co*-**1**$_{11}$-*g*-NAM$_{50}$) (**P5**) and *linear*-poly(**2**$_{11}$-*co*-**1**$_{11}$-*g*-NAM$_{47}$) (**P6**) in 1,4-dioaxane at 0.5 mg/mL.

Guinier-Porod model provided some information about the size and shape of the graft copolymers in solution. Dimension parameters of 0.16 and 0.20 were determined for linear graft copolymer **P6**, in water and 1,4-dioxane respectively, indicative of a spherical conformation (Table 5.3). Whereas, dimension parameters of 0.65 and 0.63 were calculated for cyclic graft copolymer **P5**, in water and 1,4-dioxane respectively, suggestive of an elongated rod-like conformation.

A range of other models were used to fit the data and obtain further structural information about **P5** and **P6**. As a consequence of the graft architecture of the polymers and their deviation from a Gaussian coil into a core-shell structure, unimer models (Debye model and Polydisperse Gaussian Coil model) did not provide a good fit for the data of either the linear or cyclic graft copolymers. For the linear graft copolymers, the best fit was found using a polydisperse core-shell spherical model with a polydisperse core and constant shell thickness, in both water and dioxane. For the cyclic graft copolymers, in accordance with data analysis using the Guinier-Porod model, the best fit was obtained using a cylindrical model with dispersity in the radius, in both water and dioxane (Figure 5.7, see appendix for further information). In agreement with DLS analysis, both linear and cyclic graft copolymers displayed smaller solution diameters in water, a selective solvent for the poly(NAM) arms, compared to 1,4-dioxane, a good solvent for both the polycarbonate backbone and poly(NAM) side arms (Table 5.3).

Table 5.3. Guinier-Porod fit for SAXS analysis of cyclic and linear poly(NAM) graft copolymers **P5** and **P6**.

Polymer	Topology	Solvent	R_g (nm)[a]	s[a,b]
P5	Cyclic	H_2O	4.3 ± 0.01	0.65
		1,4-dioxane	4.5 ± 0.01	0.63
P6	Linear	H_2O	3.5 ± 0.02	0.16
		1,4-dioxane	4.5 ± 0.05	0.20

[a]Determined by SAXS analysis. [b]Dimension parameter, s = 0 for spherical objects, s = 1 for rod-like objects.

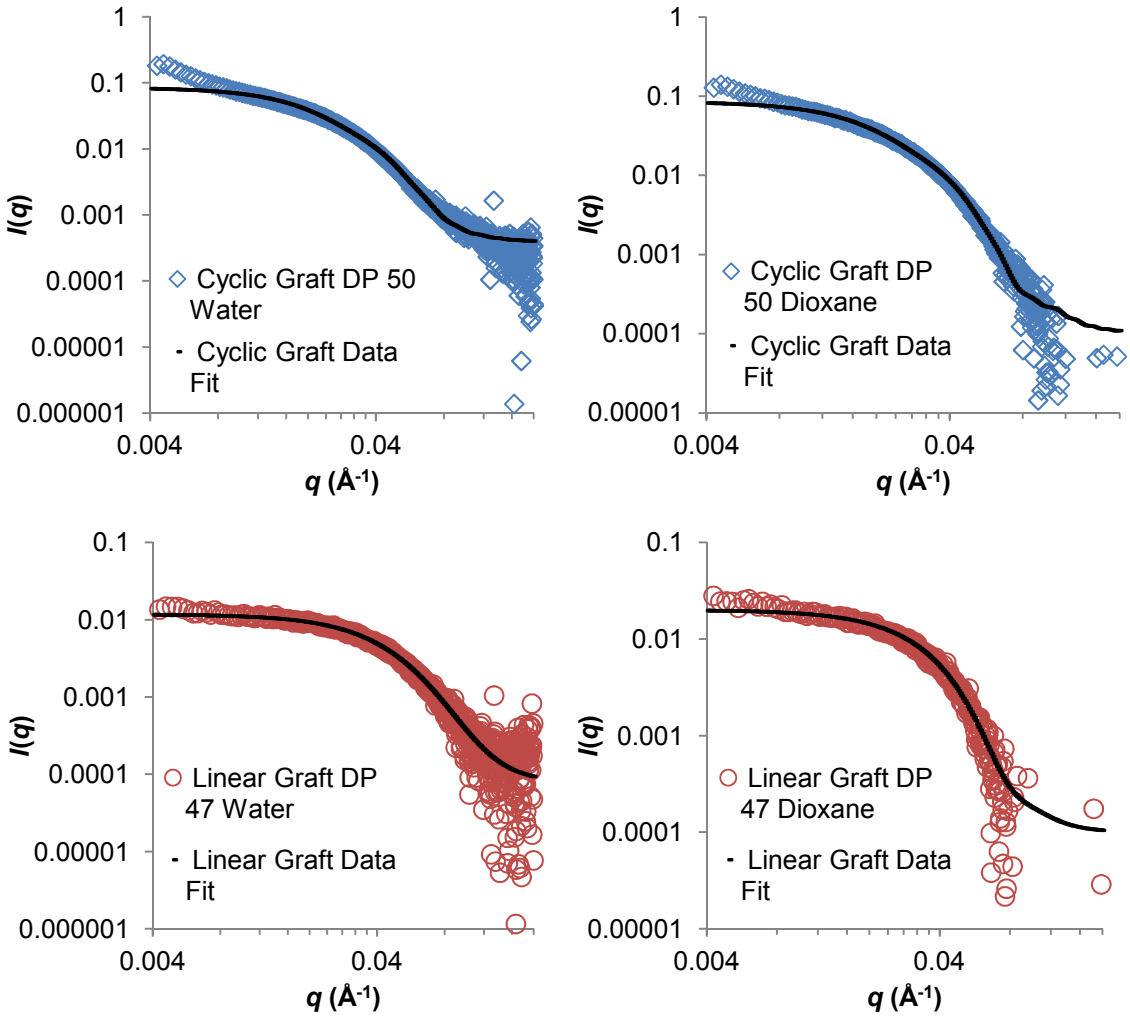

Figure 5.7. SAXS profiles and data fitting for **P5** and **P6** in water and 1,4-dioxane; (top left) **P5** in water, cylindrical model with dispersity on the radius, (top right) **P5** in 1,4-dioxane, cylindrical model with dispersity on the radius, (bottom left) **P6** in water, spherical model for polydisperse micelle, (bottom right) **P6** in 1,4-dioxane, spherical model for polydisperse micelle.

5.2.2.1 Formation of Unimolecular Graft Copolymer Micelles: Thermoresponsive Behaviour

In aqueous solution poly(NAM) homopolymer does not exhibit an observable temperature induced cloud point and is therefore considered to be permanently water soluble. However, the phase transition temperatures of lower critical solution temperature (LCST) thermoresponsive polymers can be lowered through the introduction of hydrophobicity into the polymer chain. Additionally, the LCST is dependent on the architecture of the polymer, for example, polymers with a branched or grafted architecture are known to display lower phase transition temperatures as a consequence of the close proximity of their side arms.[31] The grafted architecture of polymers **P3** – **P6** and the attachment of the poly(NAM) side arms to a hydrophobic polycarbonate backbone may lower the LCST of the poly(NAM) side arms, resulting in an observable cloud point. Furthermore, the cloud point temperatures of **P3** – **P6** may exhibit a difference depending on whether they possess a cyclic or linear topology.

The cloud point temperatures of graft copolymers **P3** – **P6** in nanopure water were determined spectrophotometrically, by measuring the turbidity of the solutions at 1 mg/mL, with a 1 °C/min heating and cooling rate. A large difference was observed in the cloud point temperatures of the cyclic and linear graft copolymers. For graft copolymers with a poly(NAM) arm length of *ca*. DP 30, the linear graft copolymer displayed a cloud point temperature of 47 °C, whereas the cloud point temperature for the equivalent cyclic graft copolymer was significantly higher at 67 °C (Figure 5.8). Furthermore, for graft copolymers with poly(NAM) arm lengths of *ca*. DP 50 the cloud point

temperature of the linear graft was found to be 74 °C, however no cloud point was observed below 100 °C for the equivalent cyclic graft copolymer (Figure 5.9). The dramatic difference in cloud point temperature between linear and

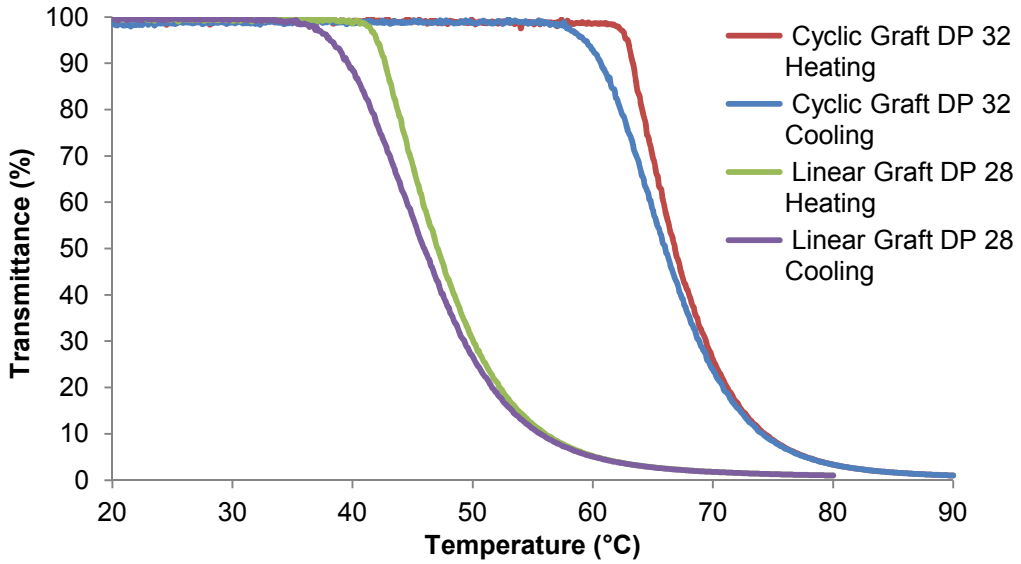

Figure 5.8. Plot of percentage transmittance (%) against temperature (°C) for *cyclic*-poly(**2**$_{11}$-*co*-**1**$_{11}$-*g*-NAM$_{32}$) (**P3**) and *linear*-poly(**2**$_{11}$-*co*-**1**$_{11}$-*g*-NAM$_{28}$) (**P4**) at 1 mg/mL in nanopure water, heating/cooling rate = 1 °C/min.

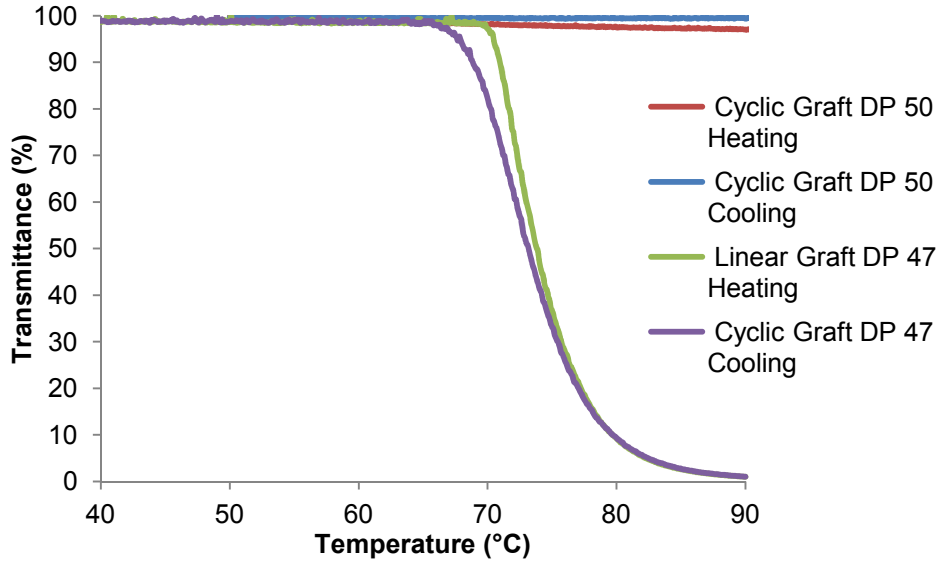

Figure 5.9. Plot of percentage transmittance (%) against temperature (°C) for *cyclic*-poly(**2**$_{11}$-*co*-**1**$_{11}$-*g*-NAM$_{50}$) (**P5**) and *linear*-poly(**2**$_{11}$-*co*-**1**$_{11}$-*g*-NAM$_{47}$) (**P6**) at 1 mg/mL in nanopure water, heating/cooling rate = 1 °C/min.

cyclic graft copolymers provides further evidence of their different solution conformations. Furthermore, the observed difference in cloud point temperature is significantly larger than the difference between cloud point temperatures reported for non-grafted cyclic and linear polymers.[32-34] As expected, the cloud point temperature of both the cyclic and linear graft copolymers increased as arm length and consequently hydrophilic content increased. To the best of our knowledge this is the first time the lower critical solution temperatures of polymers comprised of poly(NAM) have been reported.

5.2.3 Self-Assembly of Cyclic and Linear Graft Copolymers

In an attempt to induce self-assembly of the cyclic and linear graft copolymers to yield multi-molecular micelles, the length of the poly(NAM) side arms was reduced. A reduction of poly(NAM) arm length will reduce the ability of the hydrophilic polymer side arms to shield the hydrophobic polycarbonate backbone from unfavourable solvent interactions and also increase the relative hydrophobic content of the graft copolymer, therefore encouraging self-assembly. Furthermore, the conformational differences observed between cyclic and linear graft copolymers in solution are expected to affect their respective self-assembly behaviour. To this end, analogous cyclic and linear graft copolymers (**P1** and **P2** respectively) were prepared with poly(NAM) arm lengths of DP 19 and a hydrophobic weight fraction of 19%.

5.2.3.1 Self-Assembly of Cyclic and Linear Graft Copolymers: Self-Assembly Technique

Initially three methods were investigated for the self-assembly of cyclic and linear graft copolymers **P1** and **P2**; direct dissolution of the polymers in 18.2 mΩ·cm water (0.5 mg/mL), solvent switch from THF to water and the thin film hydration technique. For the solvent switch procedure, the cyclic and linear graft copolymers were dissolved in THF (1 mg/mL), a good solvent for both the poly(NAM) side arms and polycarbonate backbone, before the dropwise addition of 18.2 mΩ·cm water at a rate of 0.6 mL/h. THF was subsequently removed by exhaustive dialysis against nanopure water for 3 days, resulting in a final polymer concentration of *ca*. 0.5 mg/mL. For the thin film hydration technique, the relevant graft copolymer was dissolved in chloroform in a round bottom flask before solvent evaporation to leave a thin film of polymer coating the flask. After the subsequent addition of 18.2 mΩ·cm water the polymer films were allowed to hydrate overnight.

In the case of the cyclic graft copolymer assemblies of **P1**, analysis of the resulting aqueous solutions by DLS revealed the consistent formation of large nanostructures of *ca.* 150 – 170 nm for each of the self-assembly techniques employed (Table 5.4). Conversely, for the analogous assemblies of the linear graft copolymer **P2**, a large disparity in particle size for the different assembly techniques was observed by DLS analysis. Large structures were observed for solutions prepared *via* direct dissolution and the solvent switch method, whereas only small particles were observed for the solution prepared *via* the thin film hydration technique. Comparison between DLS analysis of the linear graft copolymer in THF and solutions prepared *via* thin film hydration revealed

Table 5.4. DLS analysis of **P1** and **P2** aggregates prepared *via* different techniques.

Assembly technique		Cyclic graft copolymer P1	Linear graft copolymer P2
Direct dissolution	D_h (nm)[a]	170	200
	PD[a]	0.147	0.362
Solvent switch	D_h (nm)[a]	170	115
	PD[a]	0.564	0.659
Thin film hydration	D_h (nm)[a]	150	7.1
	PD[a]	0.283	0.609

[a]Determined by DLS analysis, number average solution diameters.

structures with the same value of D_h, suggesting that either no aggregation had occurred *via* thin film hydration and only unimers were present in solution or that the aggregates formed were unstable and redissolved. Additionally, the dispersities of the linear graft copolymer assemblies were consistently larger than those of the equivalent cyclic graft copolymer assemblies.

5.2.3.2 Self-Assembly of Cyclic and Linear Graft Copolymers: Reproducibility

Following these initial observations, a more detailed study of the self-assembly behaviour of cyclic and linear graft copolymers **P1** and **P2** was undertaken. In all further self-assembly studies, direct dissolution was the chosen method of assembly allowing fast and facile particle preparation. Firstly, the reproducibility of particle size (D_h) for the cyclic and linear graft copolymers at a concentration of 0.5 mg/mL was studied by DLS analysis (Figure 5.10). In the case of the cyclic graft copolymer assemblies, well-defined aggregates of

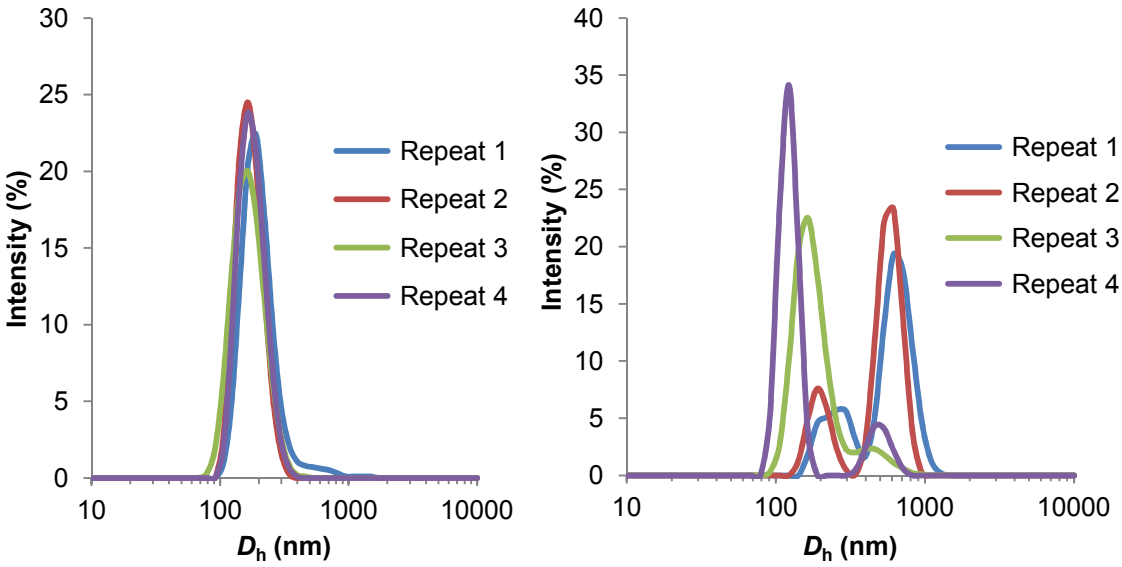

Figure 5.10. DLS analysis of (left) *cyclic*-poly($\mathbf{2}_{11}$-*co*-$\mathbf{1}_{11}$-*g*-NAM_{19}) (**P1**) and (right) *linear*-poly($\mathbf{2}_{11}$-*co*-$\mathbf{1}_{11}$-*g*-NAM_{19}) (**P2**) in 18.2 mΩ·cm water at 0.5 mg/mL.

extremely consistent values of D_h (170 - 210 nm) and low dispersities (< 0.17) were produced each time. In contrast, the aggregates prepared from linear graft copolymer, **P2**, exhibited significantly different particle sizes for each repeat (D_h = 200 – 600 nm), as well as broader dispersity values (*ca*. 0.4). Furthermore, examination of the correlation functions for these linear graft copolymer assemblies revealed that for many runs the data could not be fit by the Cumulant analysis method.

5.2.3.3 Self-Assembly of Cyclic and Linear Graft Copolymers: Effect of Concentration

The effect of concentration on aggregates of cyclic and linear graft copolymers **P1** and **P2** was also investigated. DLS analysis of aqueous solutions of the linear graft copolymer revealed a significant increase in D_h as the concentration of **P2** increased from 0.1 to 2 mg/mL (Figure 5.11). In contrast, analysis of aqueous solutions of cyclic graft copolymer **P1** over the same concentration range

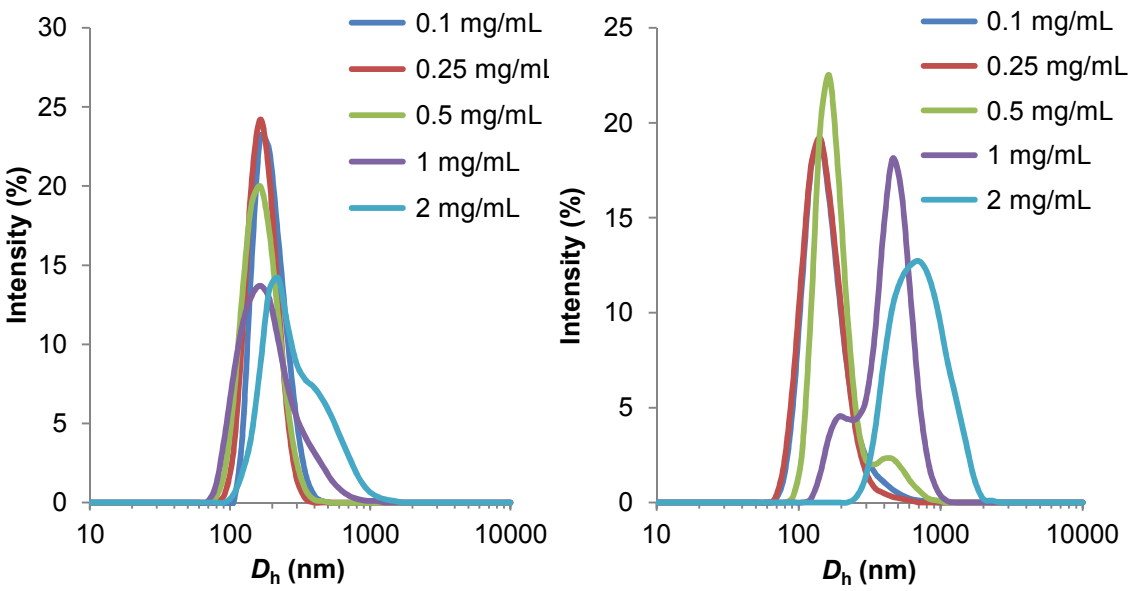

Figure 5.11. DLS analysis of (left) *cyclic*-poly($\mathbf{2}_{11}$-*co*-$\mathbf{1}_{11}$-*g*-NAM_{19}) (**P1**) and (right) *linear*-poly($\mathbf{2}_{11}$-*co*-$\mathbf{1}_{11}$-*g*-NAM_{19}) (**P2**) at varying concentrations.

revealed little difference in particle size as concentration increased. Some aggregation of these nanostructures was however observed at higher concentrations (≥ 2 mg/mL). Again, the assemblies prepared from cyclic graft copolymer **P1** possessed lower dispersity values than the equivalent linear assemblies. These findings further support the formation of well-defined nanostructures prepared from cyclic graft copolymer **P1**, in contrast to the formation of ill-defined aggregates prepared from linear graft copolymer **P2**. The size and morphology of the aggregates of cyclic graft copolymer **P1** were further investigated by cryogenic transmission electron microscopy (cryo-TEM). At a concentration of 2 mg/mL, large spherical structures were observed with an average particle diameter of 207 ± 61 nm; therefore in good agreement with the particle size determined by DLS analysis (Figures 5.12 and 5.13). However, as a consequence of the high hydrophilic content of the assemblies and solvation of the poly(NAM) corona, poor image contrast was observed and

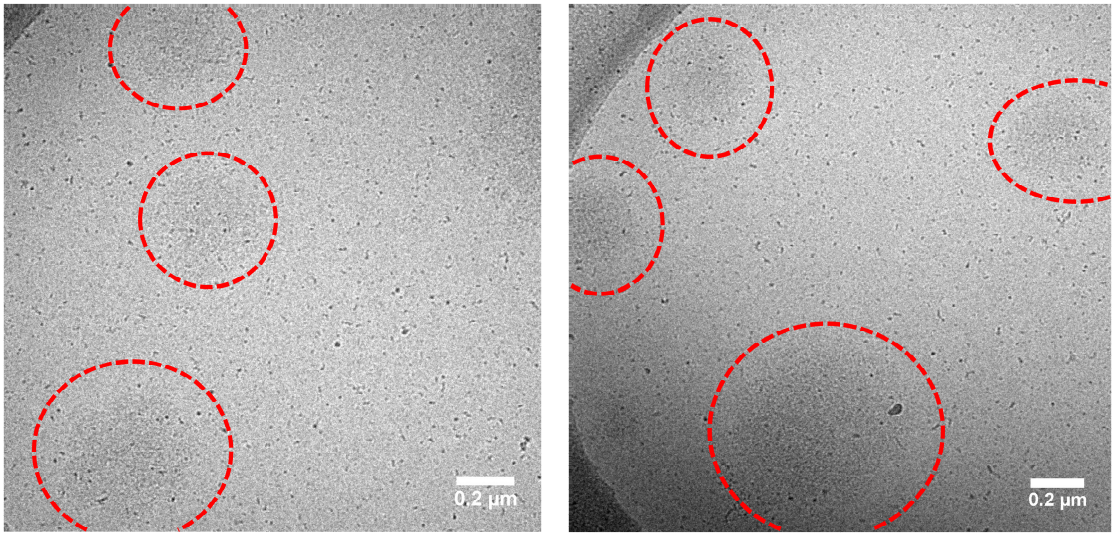

Figure 5.12. Cryo-TEM images of cyclic-poly($\mathbf{2}_{11}$-*co*-$\mathbf{1}_{11}$-*g*-NAM_{19}) (**P1**) at 2 mg/mL, Particles highlighted by dashed red circles.

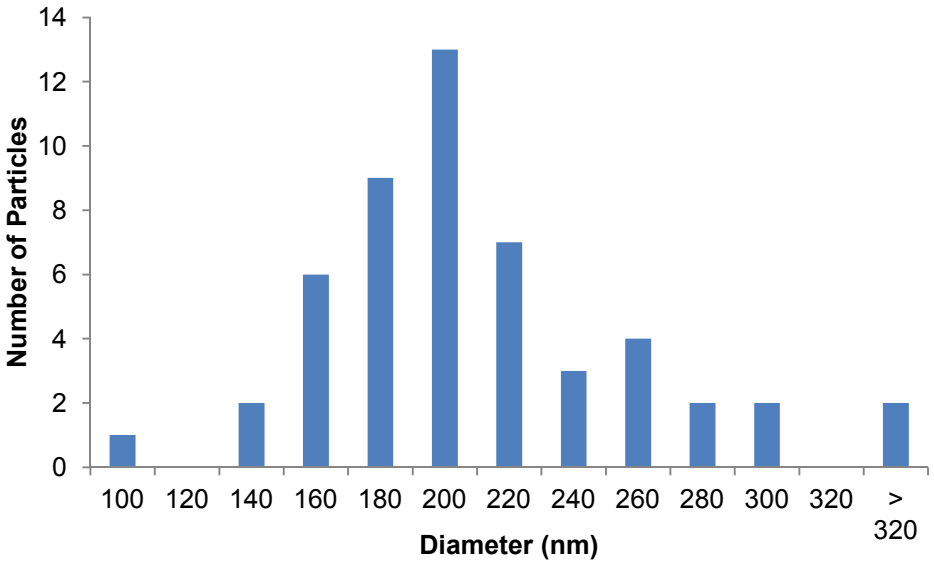

Figure 5.13. Cryo-TEM size histogram of *cyclic*-poly($\mathbf{2}_{11}$-*co*-$\mathbf{1}_{11}$-*g*-NAM_{19}) (**P1**) at 2 mg/mL.

it could not be determined whether the spherical aggregates were solid or possessed a bilayer structure indicative of vesicles. Interestingly, when cryo-TEM of cyclic graft copolymer **P1** was performed at a lower concentration of 0.5 mg/mL, predominantly short worm-like particles with an average length of 18 ± 7 nm were observed, with only a few larger spherical aggregates present

(Figures 5.14 and 5.15). The worm-like structures are significantly smaller than the nanostructures observed by DLS analysis at this concentration and this discrepancy in particle size is attributed to the significant weighting of larger particles by light scattering analyses, giving undue prominence to the small population of large particles.

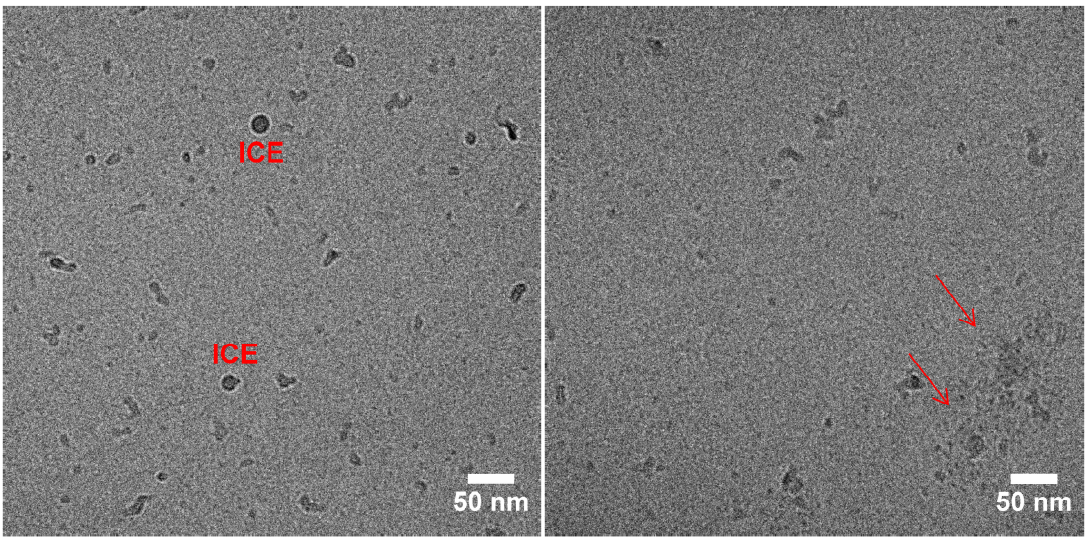

Figure 5.14. Cryo-TEM images of *cyclic*-poly(**2**$_{11}$-*co*-**1**$_{11}$-*g*-NAM$_{19}$) (**P1**) at 0.5 mg/mL, arrows indicate presence of larger spherical assemblies, ice contamination highlighted.

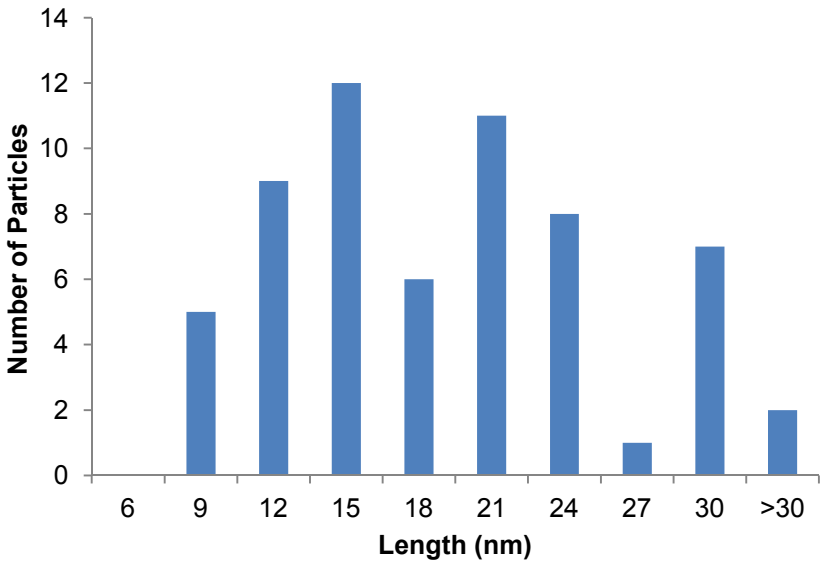

Figure 5.15. Cryo-TEM size histogram of *cyclic*-poly(**2**$_{11}$-*co*-**1**$_{11}$-*g*-NAM$_{19}$) (**P1**) at 0.5 mg/mL.

5.2.3.4 Self-Assembly of Cyclic and Linear Graft Copolymers: Critical Micelle Concentration and Kinetic Stability

To probe the thermodynamic stability of the linear and cyclic graft copolymer assemblies, the critical micelle concentrations of the particles were determined by fluorescence spectroscopy, using pyrene as the fluorescent probe. Pyrene exhibits a change in excitation and emission spectra when its environment is changed from polar to non-polar. A clear shift in the excitation spectra of pyrene of the excitation maxima from *ca*. 339 to 335 nm is observed when pyrene enters the hydrophobic core of a particle. Comparison of the intensity of these two peaks ($I_{339}/I_{334.5}$) over a range of polymer concentrations allows determination of the cmc; where the cmc is taken as the inflection point in the graph of $I_{339}/I_{334.5}$ *versus* polymer concentration. Linear and cyclic graft copolymer solutions ranging in concentration from 0.0003 to 2 mg/mL, were left to stir overnight in the presence of 6×10^{-7} mol/L of pyrene, before analysis by fluorescence spectroscopy, where excitation spectra were recorded in the range λ = 300 – 375 nm and λ_{em} = 390 nm. The cmc for the cyclic graft copolymer was determined as 0.09 g/L (Figure 5.16), whereas the cmc of the linear graft copolymer was found to be higher, at 0.23 g/L (Figure 5.17). Consequently, the assemblies of cyclic graft copolymer **P1** are more thermodynamically stable than the assemblies of linear copolymer graft **P2**.

This difference between values of cmc also suggests that the cyclic graft copolymer topology enables a greater number of favourable hydrophobic interactions in the core of the assembly, compared to a linear graft copolymer topology.

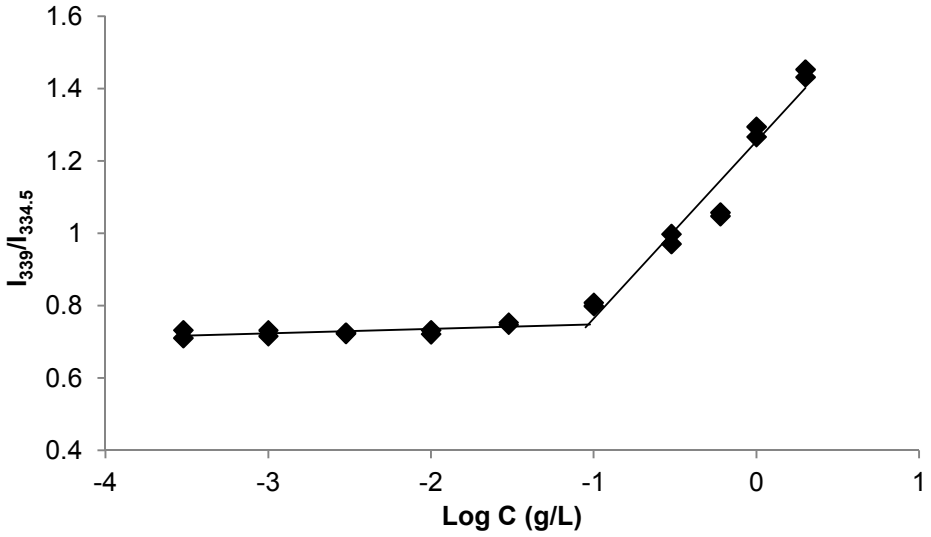

Figure 5.16. Concentration dependence of pyrene $I_{339}/I_{334.5}$ intensity ratio for *cyclic*-poly(**2**$_{11}$-*co*-**1**$_{11}$-*g*-NAM$_{19}$) (**P1**).

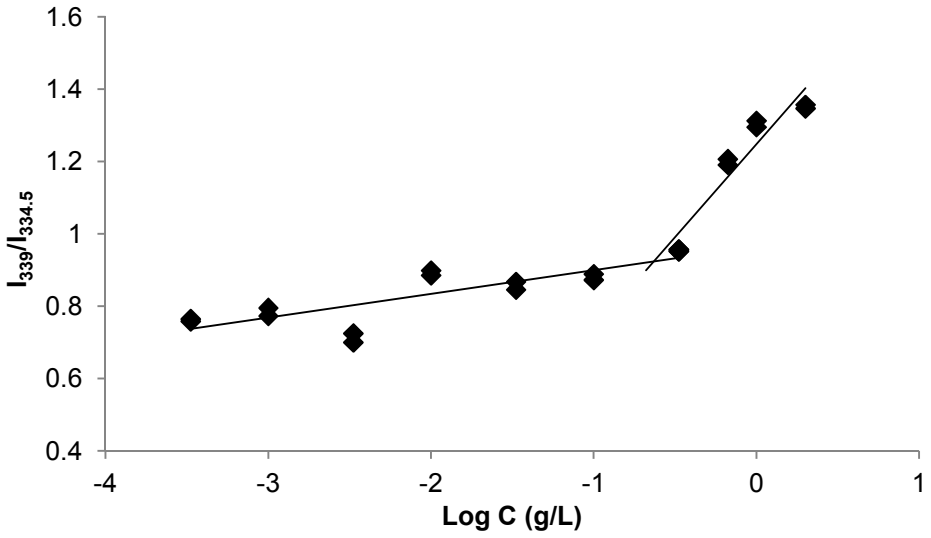

Figure 5.17. Concentration dependence of pyrene $I_{339}/I_{334.5}$ intensity ratio for *linear*-poly(**2**$_{11}$-*co*-**1**$_{11}$-*g*-NAM$_{19}$) (**P2**).

The assemblies of cyclic and linear graft copolymers, **P1** and **P2**, were also monitored over time to gauge their kinetic stability. Following the assemblies over time by DLS analysis it was observed that nanostructures prepared from the linear graft copolymer **P2** had disassembled after 48 h, to afford unimers with an average solution diameter (D_h) of *ca.* 7.5 nm. Furthermore, particle

disassembly was found to occur over the entire range of polymer concentrations investigated ([**P2**] = 0.25 – 2.0 mg/mL) (Figure 5.18). In contrast, DLS analysis revealed that assemblies prepared from the equivalent cyclic graft copolymer, **P1**, remained stable for several weeks; most notably no significant change in particle size or dispersity was observed (Figures 5.19).

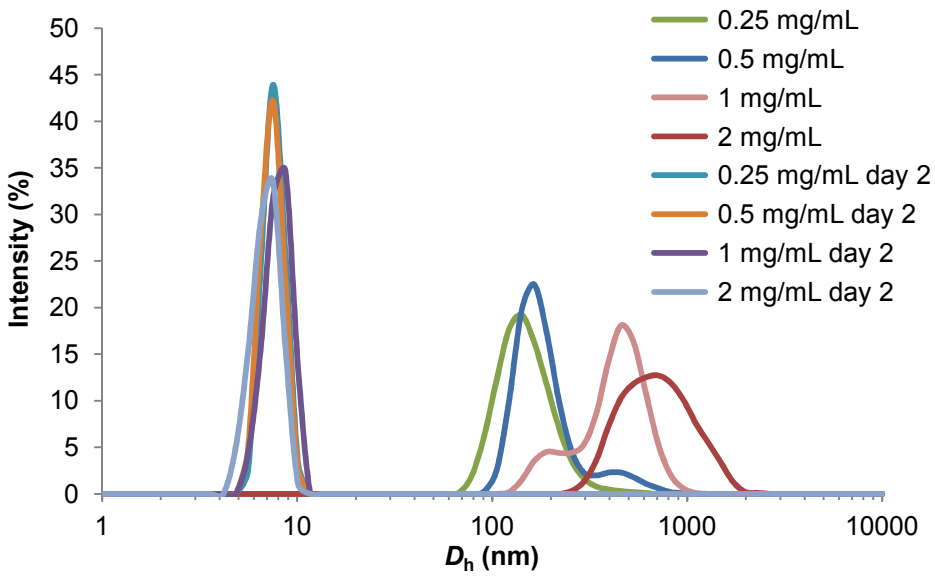

Figure 5.18. DLS analysis of *linear*-poly(**2**$_{11}$-*co*-**1**$_{11}$-*g*-NAM$_{19}$) (**P2**) after 0 h and 2 days.

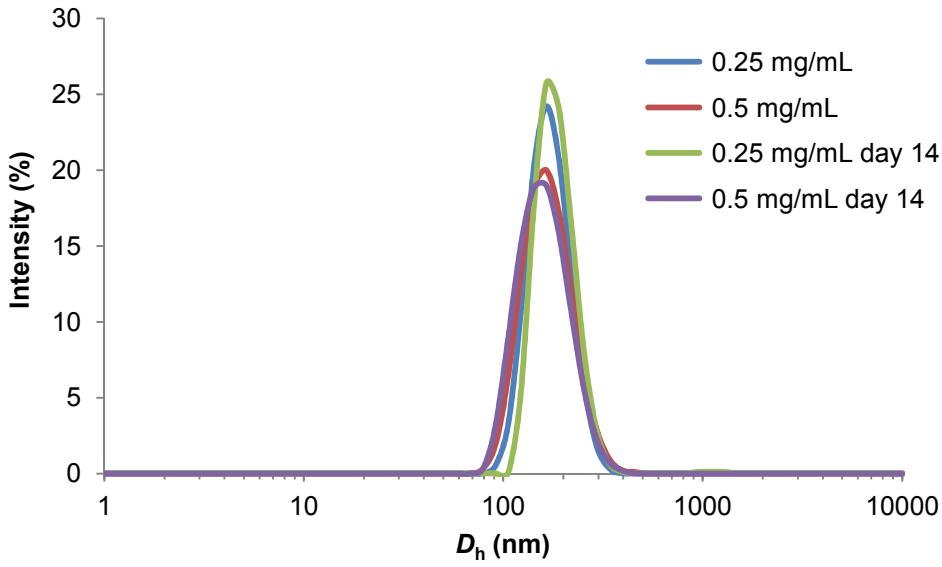

Figure 5.19. DLS analysis of *cyclic*-poly(**2**$_{11}$-*co*-**1**$_{11}$-*g*-NAM$_{19}$) (**P1**) after 0 h and 14 days.

These findings strongly suggest that assemblies comprised of cyclic graft copolymers possess both greater thermodynamic and kinetic stability than assemblies comprised of analogous linear graft copolymers.

5.2.3.5 Self-Assembly of Cyclic and Linear Graft Copolymers: Disulfide Cleavage

The cyclic graft copolymer **P1** contains a disulfide moiety, which upon reduction will cleave the cyclic polycarbonate backbone of **P1** and yield a linear graft copolymer. As a consequence of the different stabilities exhibited by assemblies of cyclic and linear graft copolymers **P1** and **P2**, it was hypothesised that reduction of the disulfide bond of **P1** may trigger particle disassembly. To test this hypothesis, a reducing agent, either dithiothreitol (DTT) or L-glutathione, was added to a solution of cyclic graft copolymer **P1**, assembled at a concentration of 0.5 mg/mL and with D_h = 170 nm. Initially, a large excess of DTT (10 mM) was added to a solution of aggregates of **P1** and left overnight. DLS analysis after 16 h revealed the complete loss of large self-assembled nanostructures and the presence of only very small species with solution diameters that correspond to unimolecular micelles (D_h = 7.4 nm, PD = 0.464) (Figure 5.20) This dramatic change in particle size is consistent with cleavage of the disulfide bond of the cyclic graft copolymer to yield linear graft copolymers, followed by spontaneous disassembly of the relatively unstable aggregates to yield unimolecular micelles.

The use of L-glutathione as a reducing agent was also investigated. L-glutathione is an *in vivo* reducing agent that is present at micromolar concentrations in extracellular environments and at millimolar concentrations

in intracellular environments. This large difference in intra- and extracellular concentrations has been exploited for drug delivery applications, where particles remain stable during circulation, but rapidly disassemble upon cell entry. Assemblies of cyclic graft copolymer **P1** were left for 16 h in the presence of varying concentrations of L-glutathione (10 mM, 1 mM and 10μM) before analysis by DLS (Figure 5.21). DLS analysis of solutions with 10 and 1 mM L-glutathione revealed the complete loss of large particles and the appearance of very small particles, again consistent with the successful cleavage of the disulfide bond of **P1** followed by particle disassembly. The newly formed linear graft copolymers remained as unimolecular micelles and did not reassemble over time. In contrast, aggregates in the presence of 10 μM of L-glutathione solution remained intact, although a small amount of aggregation between particles was observed.

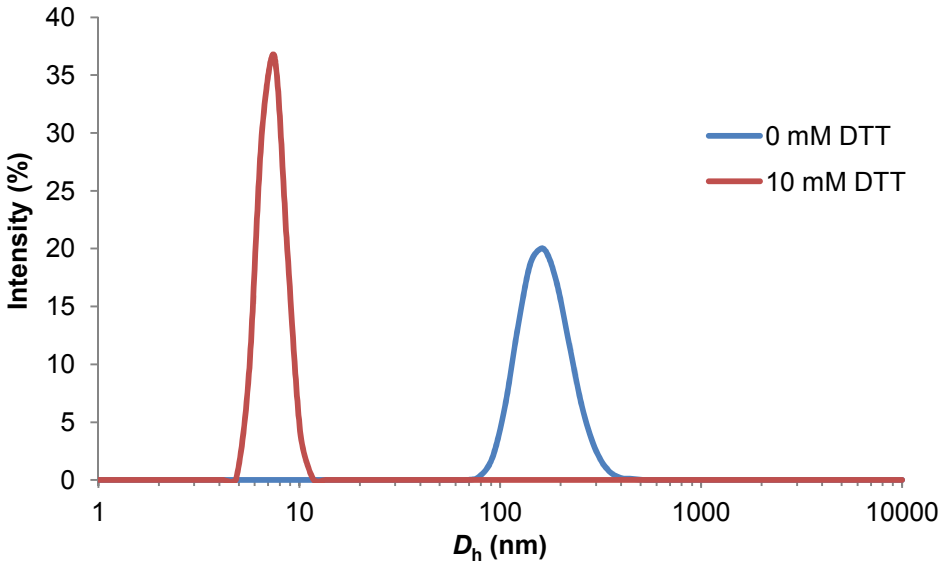

Figure 5.20. DLS analysis of *cyclic*-poly(**2**$_{11}$-*co*-**1**$_{11}$-*g*-NAM$_{19}$) (**P1**) before and after treatment with 10 mM dithiothreitol.

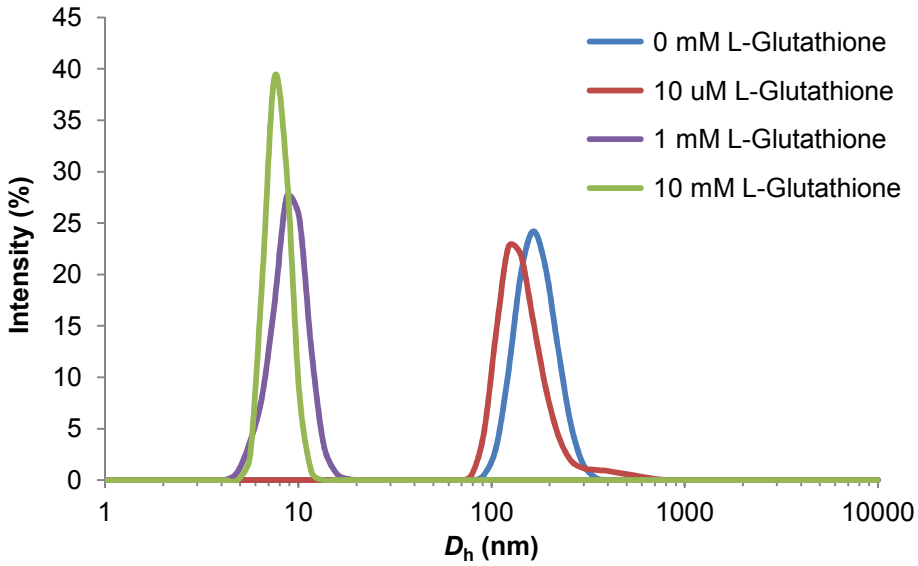

Figure 5.21. DLS analysis of *cyclic*-poly(**2**$_{11}$-*co*-**1**$_{11}$-*g*-NAM$_{19}$) (**P1**) before and after treatment with varying concentrations of L-glutathione.

5.2.3.6 Self-Assembly of Cyclic and Linear Graft Copolymers: Thermoresponsive Behaviour

It was demonstrated above that linear and cyclic graft copolymers comprised of a hydrophobic polycarbonate backbone and poly(NAM) side arms exhibit thermoresponsive behaviour. As such, the thermoresponsive behaviour of nanostructures prepared from cyclic and linear graft copolymers **P1** and **P2** was also investigated. Whilst monitoring the particle size of the assemblies of cyclic graft copolymer **P1** by DLS analysis, as temperature was varied between 5 and 65 °C, several notable trends were observed. Particle size increased from D_h = 175 to 410 nm, as temperature was increased from 25 to 40 °C (Figure 5.22). At temperatures ≥ 40 °C the polymer solution became extremely turbid, indicative of macroscopic aggregation between particles. Furthermore, inspection of the scattering intensity data for assemblies of cyclic graft copolymer **P1** as temperature was increased from 5 and 65 °C, revealed an

abrupt increase in scattering intensity at 30 °C, suggestive of a phase transition (Figure 5.23).

It was also observed through DLS analysis that particle size decreased with decreasing temperature at temperatures ≤ 15 °C, as evidenced by a reduction of both D_h and scattering intensity (count rate). At *ca.* 10 °C a transition from

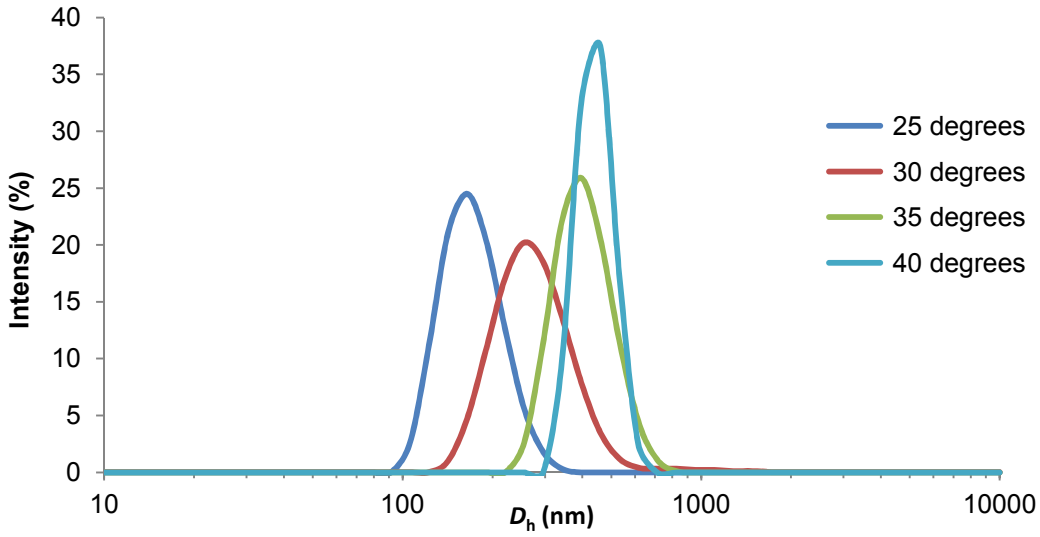

Figure 5.22. DLS analysis of *cyclic*-poly(**2**$_{11}$-*co*-**1**$_{11}$-*g*-NAM$_{19}$) (**P1**) at varying temperatures (25 – 40 °C, 0.5 mg/mL).

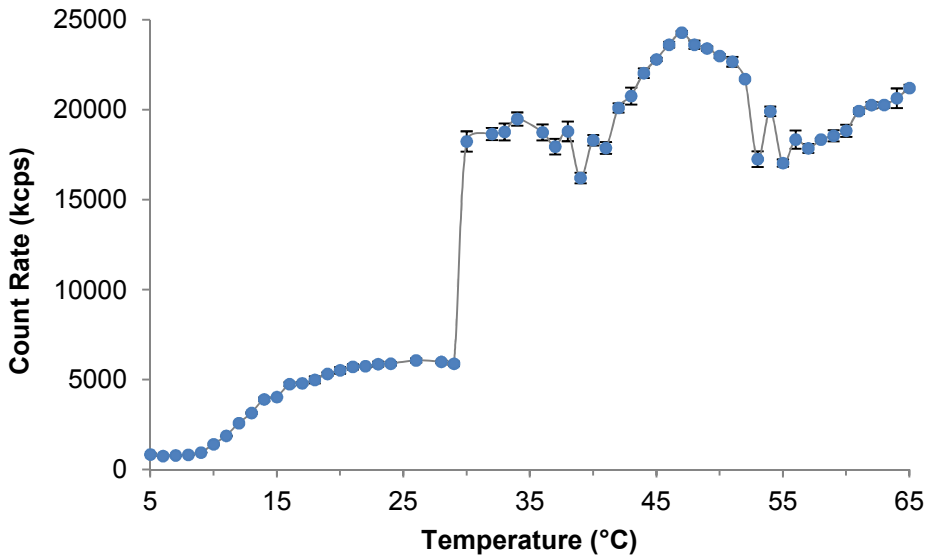

Figure 5.23. Temperature dependence of count rate for *cyclic*-poly(**2**$_{11}$-*co*-**1**$_{11}$-*g*-NAM$_{19}$).

assembled structures to significantly smaller species was observed, where the resulting species possessed solution diameters consistent with those of unimolecular micelles (D_h = 7.6 nm, PD = 0.669) (Figure 5.24). Upon heating the polymer solution back to 25 °C, particles of the original size with narrow dispersities (D_h = 210 nm, PD = 0.125) were reformed, showing that this particle to unimer transition was reversible. The cooling-heating cycle between 25 and 5 °C was repeated twice more, again showing fully reversible transitions (Figure 5.25) and the time scale for both disassembly and reassembly was noted to be fast, requiring as little as 10 minutes. Furthermore, with each temperature cycle the dispersity of the assemblies decreased. Thus, the thermoresponsive behaviour of cyclic graft copolymer **P1** is twofold; at low temperatures (≤ 10 °C), when interactions between water and the poly(NAM) arms are strongest, the poly(NAM) arms are sufficiently hydrophilic to protect the hydrophobic polycarbonate backbone from unfavourable solvent interactions and a unimolecular micelle configuration is adopted. As

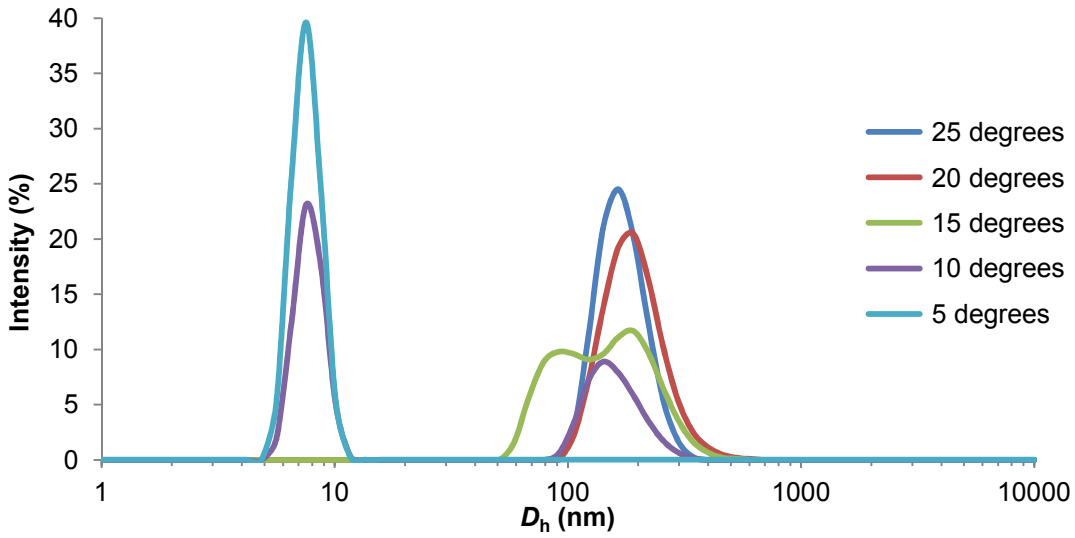

Figure 5.24. DLS analysis of *cyclic*-poly(**2**$_{11}$-*co*-**1**$_{11}$-*g*-NAM$_{19}$) (**P1**) at varying temperatures (25 – 5 °C, 0.5 mg/mL).

temperature is increased, interactions between poly(NAM) arms and water still predominate, however, interactions between poly(NAM) arms of the corona increase and the polymer self-assembles in order to protect the hydrophobic polycarbonate core. As temperature is increased further, interactions between the poly(NAM) arms increase further and the polymer undergoes macroscopic aggregation as water is expelled from the poly(NAM) corona.

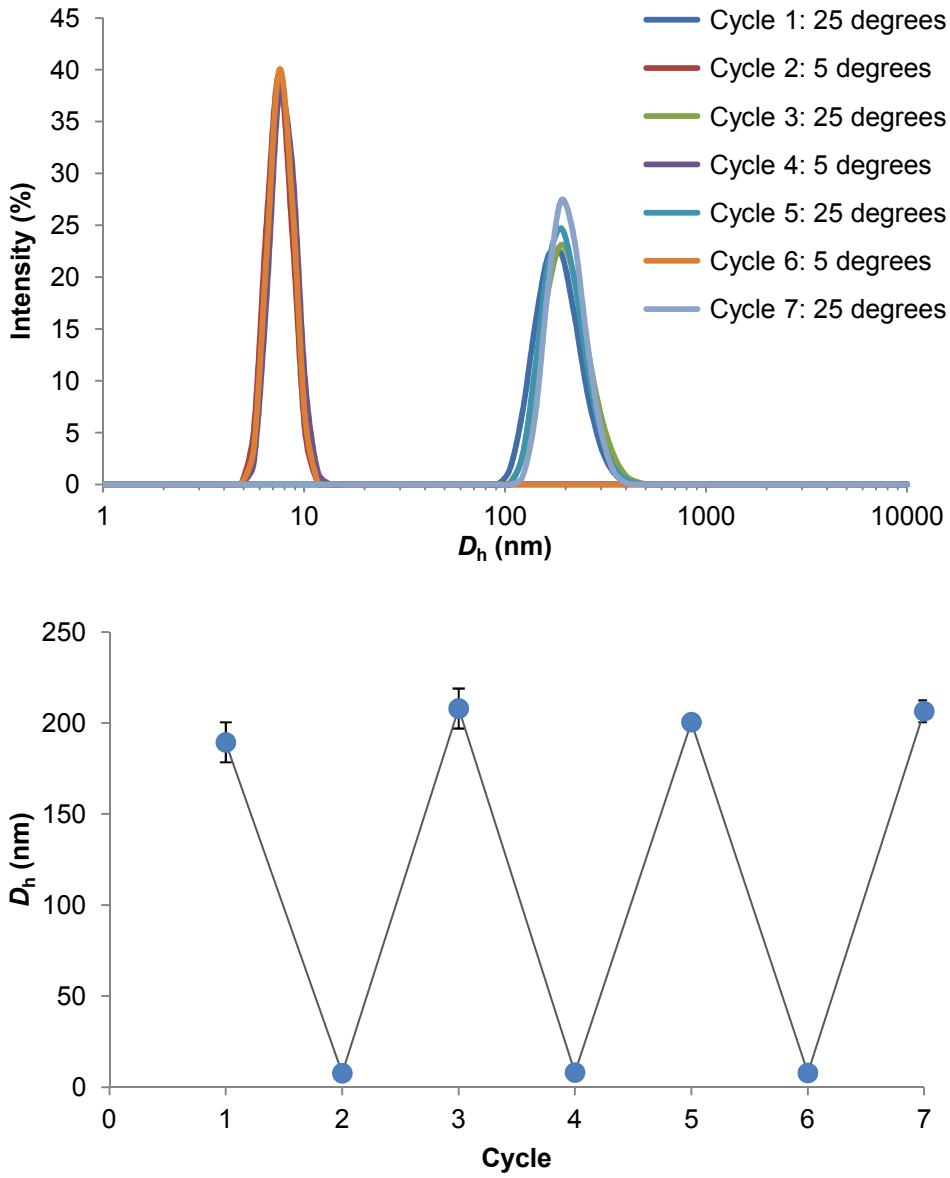

Figure 5.25. DLS analysis of *cyclic*-poly($\mathbf{2}_{11}$-*co*-$\mathbf{1}_{11}$-*g*-NAM_{19}) (**P1**) showing changes in particle size with temperature cycles between 25 and 5 °C.

The thermoresponsive behaviour of nanostructures prepared from linear graft copolymer **P2** was also investigated. As the temperature of a 0.5 mg/mL solution of **P2** was increased, the solution became increasingly turbid. DLS analysis revealed an increase in both D_h and count rate as temperature was increased from 15 to 55 °C, indicative of aggregation between particles (Figure 5.26). However, in contrast to the thermoresponsive behaviour of cyclic graft copolymer **P1**, no well-defined phase transition was observed. When the solution temperature of the linear graft copolymer **P2** was decreased, DLS analysis revealed little change in values of D_h and a transition from particle to unimer was not observed (Figure 5.27). Furthermore, the dispersity of the assemblies increased as the temperature decreased and DLS data quality reduced until at 5 °C all runs were too poor for Cumulant analysis. The ill-defined thermoresponsive behaviour of aggregates of linear graft copolymer **P2** in comparison to aggregates of the cyclic graft copolymer **P1**, may result from

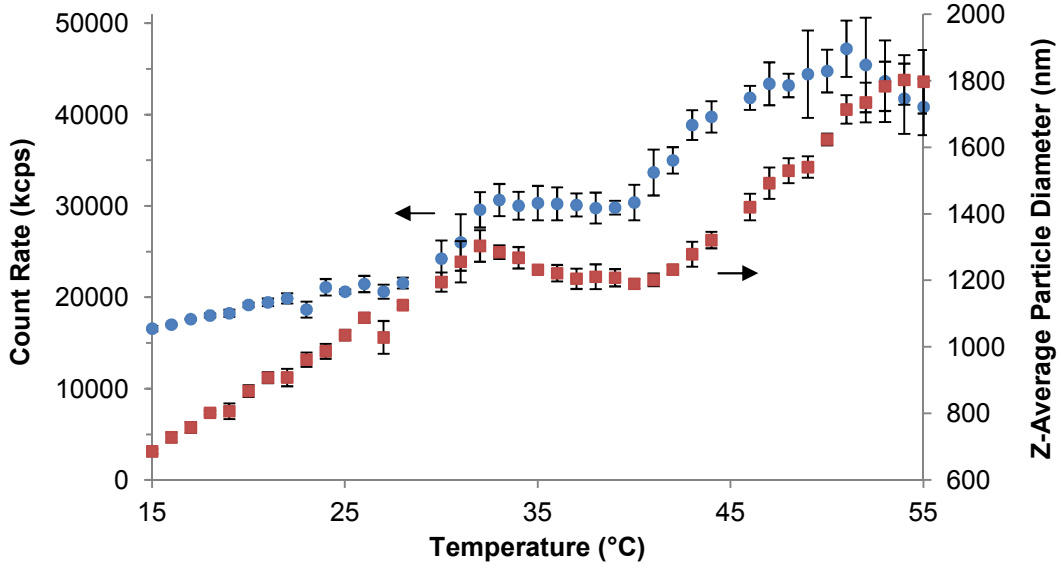

Figure 5.26. Temperature dependence of count rate (blue circle) and Z-average particle size (red square) for *linear*-poly(**2**$_{11}$-*co*-**1**$_{11}$-*g*-NAM$_{19}$) (**P2**).

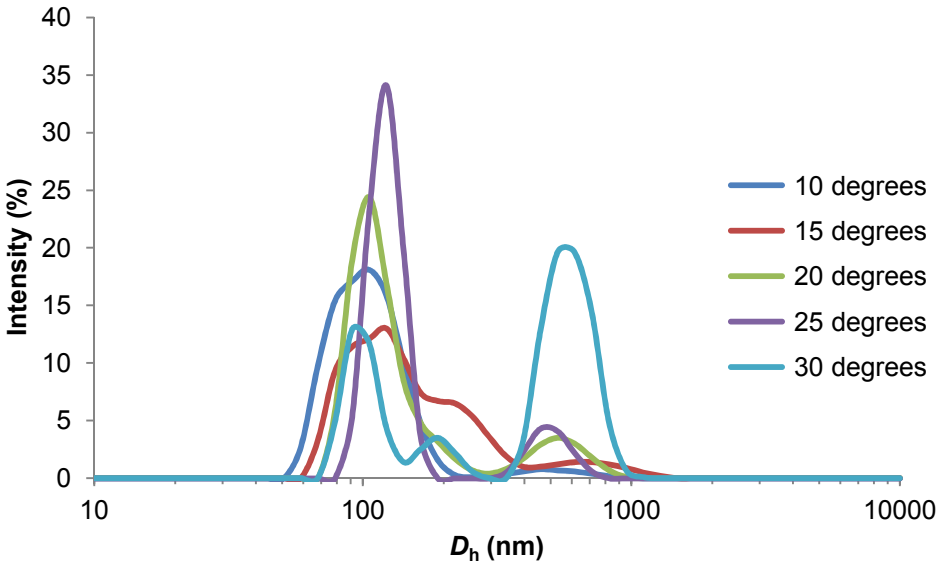

Figure 5.27. DLS analysis of *linear*-poly($\mathbf{2}_{11}$-*co*-$\mathbf{1}_{11}$-*g*-NAM_{19}) (**P2**) at varying temperatures (10 – 30 °C).

the poorly defined nature of the aggregates of **P2**. Therefore, although the linear graft copolymer **P2** forms macroscopic aggregates as temperature is increased, no defined cloud point is exhibited. In contrast, the well-defined nanostructures prepared from **P1** lead to the observation of well-defined phase transitions.

5.3 Conclusions

In conclusion, cyclic polycarbonate-*g*-poly(NAM) copolymers have been shown to display unique solution properties and self-assembly behaviour in comparison to their linear polycarbonate-*g*-poly(NAM) counterparts. Whereas linear graft copolymers adopt a spherical unimolecular micelle conformation, cyclic graft copolymers adopt a rod-like unimolecular micelle conformation. Furthermore, cyclic polycarbonate-*g*-poly(NAM) was found to exhibit cloud point temperatures at least 20 °C higher than the equivalent linear graft copolymers. Cyclic graft copolymers also displayed unique behaviour in comparison to linear graft copolymers during self-assembly. Whereas cyclic polycarbonate-*g*-poly(NAM) formed well-defined and relatively stable nanostructures, linear polycarbonate-*g*-poly(NAM) formed ill-defined aggregates with extremely poor stability. Cyclic and linear graft copolymers were also shown to exhibit distinct thermoresponsive behaviour in their self-assembled states.

5.4 References

1. C. Feng, Y. Li, D. Yang, J. Hu, X. Zhang and X. Huang, *Chem. Soc. Rev.*, 2011, **40**, 1282-1295.
2. Y. Kawakami, *Prog. Polym. Sci.*, 1994, **19**, 203-232.
3. L. Wang, D. Wan, Z. Zhang, F. Liu, H. Xing, Y. Wang and T. Tang, *Macromolecules*, 2011, **44**, 4167-4179.
4. D. Uhrig, R. Schlegel, R. Weidisch and J. Mays, *Eur. Polym. J.*, 2011, **47**, 560-568.
5. S. S. Sheiko, B. S. Sumerlin and K. Matyjaszewski, *Prog. Polym. Sci.*, 2008, **33**, 759-785.
6. M. Zhang and A. H. E. Müller, *J. Polym. Sci., Part A: Polym. Chem.*, 2005, **43**, 3461-3481.
7. J. Bolton, T. S. Bailey and J. Rzayev, *Nano Lett.*, 2011, **11**, 998-1001.
8. R. Fenyves, M. Schmutz, I. J. Horner, F. V. Bright and J. Rzayev, *J. Am. Chem. Soc.*, 2014, **136**, 7762-7770.
9. J. Rzayev, *Macromolecules*, 2009, **42**, 2135-2141.
10. J. Rzayev, *ACS Macro Lett.*, 2012, **1**, 1146-1149.
11. M. Pitsikalis, J. Woodward, J. W. Mays and N. Hadjichristidis, *Macromolecules*, 1997, **30**, 5384-5389.
12. C. Price and D. Woods, *Polymer*, 1974, **15**, 389-392.
13. A. Kreig, A. A. Lefebvre, H. Hahn, N. P. Balsara, S. Qi, A. K. Chakraborty, M. Xenidou and N. Hadjichristidis, *J. Chem. Phys.*, 2001, **115**, 6243-6251.
14. S. Pispas, N. Hadjichristidis and J. W. Mays, *Macromolecules*, 1996, **29**, 7378-7385.

15. Z. Tuzar, P. Kratochvil, K. Procházka, K. Contractor and N. Hadjichristidis, *Makromol. Chem.*, 1989, **190**, 2967-2973.

16. N. Hadjichristidis and J. Roovers, *J. Polym. Sci., Polym. Phys. Ed.*, 1978, **16**, 851-858.

17. D. Rahlwes, J. E. L. Roovers and S. Bywater, *Macromolecules*, 1977, **10**, 604-609.

18. J. X. Zhang, L. Y. Qiu and K. J. Zhu, *Macromol. Rapid Commun.*, 2005, **26**, 1716-1723.

19. H. Yang, L. Jia, C. Zhu, A. Di-Cicco, D. Levy, P.-A. Albouy, M.-H. Li and P. Keller, *Macromolecules*, 2010, **43**, 10442-10451.

20. H. J. Lee, S. R. Yang, E. J. An and J.-D. Kim, *Macromolecules*, 2006, **39**, 4938-4940.

21. J. Xu, Q. Fu, J. M. Ren, G. Bryant and G. G. Qiao, *Chem. Commun.*, 2013, **49**, 33-35.

22. B. Li, G. Chen, F. Meng, T. Li, J. Yue, X. Jing and Y. Huang, *Polym. Chem.*, 2012, **3**, 2421-2429.

23. Y.-L. Luo, W. Yu, F. Xu and L.-L. Zhang, *J. Polym. Sci., Part A: Polym. Chem.*, 2012, **50**, 2053-2067.

24. K. Sui, H. Liang, X. Zhao, Y. Ma, Y. Zhang and Y. Xia, *Macromol. Chem. Phys.*, 2012, **213**, 1717-1724.

25. Y. Li, M. Du, Y. Li, L. Sui, G. Lu and X. Huang, *J. Polym. Sci., Part A: Polym. Chem.*, 2012, **50**, 4783-4789.

26. R. K. Iha, B. A. van Horn and K. L. Wooley, *J. Polym. Sci., Part A: Polym. Chem.*, 2010, **48**, 3553-3563.

27. X. Pang, G. Wang, Z. Jia, C. Liu and J. Huang, *J. Polym. Sci., Part A: Polym. Chem.*, 2007, **45**, 5824-5837.

28. N. Nasongkla, B. Chen, N. Macaraeg, M. E. Fox, J. M. J. Fréchet and F. C. Szoka, *J. Am. Chem. Soc.*, 2009, **131**, 3842-3843.

29. H. Li, R. Jérôme and P. Lecomte, *Macromolecules*, 2008, **41**, 650-654.

30. M. Schappacher and A. Deffieux, *Science*, 2008, **319**, 1512-1515.

31. B. Jiang, L. Zhang, J. Yan, Q. Huang, B. Liao and H. Pang, *J. Polym. Sci., Part A: Polym. Chem.*, 2014, **52**, 2442-2453.

32. Y. Satokawa, T. Shikata, F. Tanaka, X.-p. Qiu and F. M. Winnik, *Macromolecules*, 2009, **42**, 1400-1403.

33. J. Xu, J. Ye and S. Liu, *Macromolecules*, 2007, **40**, 9103-9110.

34. X.-P. Qiu, F. Tanaka and F. M. Winnik, *Macromolecules*, 2007, **40**, 7069-7071.

6 Conclusions and Future Work

6.1 Conclusions

In conclusion, the synthesis and ring-opening polymerisation of novel, functional cyclic carbonate monomers has been reported and applied to the preparation of linear and cyclic graft copolymers containing a degradable polycarbonate backbone. In the first approach, a norbornene-functional cyclic carbonate monomer was prepared and subsequently ring-opened to yield well-defined polycarbonates with norbornene functionality. The pendent norbornene groups were exploited as extremely versatile reactive handles for further post-polymerisation modification of the polycarbonates. Quantitative functionalisation was demonstrated through reaction with azides in thermally promoted 1,3-dipolar cycloaddition reactions, tetrazines in inverse electron demand Diels-Alder reactions and thiols in radical addition reactions. Additionally, multi-functional polycarbonates were prepared by performing all three modification reactions in a one-pot multi-step procedure. Despite the great potential of this approach to prepare libraries of functional polycarbonates, some limitations were encountered when applied to the preparation of graft copolymers. When thiol-functional polymers were grafted-to the norbornene-functional polycarbonates only low grafting yields were achieved and as such this approach was deemed unsuitable for the preparation of graft copolymers.

The successful preparation of graft copolymers with a degradable polycarbonate backbone was however achieved through the synthesis, ring-opening and subsequent reversible addition-fragmentation chain transfer (RAFT) polymerisation of a RAFT CTA-functional cyclic carbonate monomer. The novel cyclic carbonate was designed to allow the preparation of graft

copolymers *via* a R-group RAFT approach and consequently enabled the preparation of polycarbonate based graft copolymers with significantly higher grafting densities than previously reported. Optimisation of the conditions for both ROP and RAFT polymerisation allowed the preparation of well-defined degradable graft copolymers with controlled and predictable grafting densities and arms lengths, and a range of side arm compositions. Furthermore, the preparation and self-assembly of polycarbonate-*g*-poly(NiPAm) copolymers enabled access to thermoresponsive, degradable particles.

The optimised methodology for the preparation of well-defined degradable graft copolymers *via* consecutive ROP and RAFT was further expanded to allow the synthesis of cyclic graft copolymers. RAFT CTA-functional cyclic polycarbonates were prepared *via* ROP of the RAFT-CTA cyclic carbonate monomer and subsequent end-group functionalisation to install alkyne functionality at both polymer chain-ends. Cyclisation was achieved through copper catalysed azide-alkyne cycloaddition with a diazide functional linker. Finally, RAFT polymerisation from the CTA sites located along the polycarbonate backbone yielded well-defined cyclic graft copolymers. This represents the first time RAFT has been used to prepare cyclic graft copolymers in a grafting-from approach and greatly expands the range of possible side arm compositions.

Investigation of the solution properties and self-assembly behaviour of a range of graft copolymers with hydrophilic poly(*N*-acryloylmorpholine) (poly(NAM)) side arms revealed that linear and cyclic graft copolymers display very distinct properties. Whereas, linear graft copolymers were found to adopt a unimolecular spherical core-shell conformation in water, cyclic graft

copolymers assumed a unimolecular rod-like structure. Furthermore, cyclic graft copolymers with poly(NAM) side arms displayed significantly greater cloud point temperatures than the equivalent linear graft copolymer. Reduction of the length of the hydrophilic poly(NAM) side arms was found to induce self-assembly, where cyclic graft copolymers formed well-defined aggregates but linear graft copolymers formed relatively ill-defined and unstable aggregates.

In summary, this thesis has developed methods for the preparation of well-defined linear and cyclic graft copolymers with a degradable polycarbonate backbone and furthermore, has greatly expanded the range of accessible graft compositions and grafting densities of degradable graft copolymers. Initial investigations into the differing solution and self-assembly properties of linear and cyclic graft copolymers have revealed distinct differences in their behaviour, which provides a plethora of opportunities for further research.

6.2 Future Work

Having established procedures for the preparation of cyclic and linear graft copolymers and identified their unique solution and self-assembly behaviour, there are many opportunities for future work. For example, further investigation into the effects of arm length on the self-assembly and solution properties of the linear and cyclic graft copolymers, as well exploring the effect of grafting density, side arm composition and polycarbonate ring size. It would also be desirable to gain a greater understanding of the origins of the different solution properties displayed by the cyclic and linear graft copolymers and to this end, computational modeling and simulations may provide some insight.

The unimolecular micelles prepared from cyclic and linear graft copolymers in Chapter 5 show promise as drug delivery vehicles as a consequence of their lack of critical micelle concentrations. Further exploration could probe their ability to encapsulate small molecule hydrophobic guests and determine whether a difference is displayed between the spherical unimolecular micelles prepared from linear graft copolymers and the rod-like unimolecular micelles prepared from cyclic graft copolymers. Furthermore, non-spherical particles have been reported to exhibit longer *in vivo* circulation times in comparison to spherical particles. The greater thermal stability of cyclic graft copolymers with poly(NAM) arms in comparison to the equivalent linear graft copolymers may also be beneficial in some applications where elevated temperatures are required.

Although the norbornene-functional polycarbonates prepared in Chapter 2 could not be successfully utilised in the preparation of graft copolymers, they may find application *in vivo* through functionalisation with fluorescent or biologically relevant molecules.

7 Experimental

7.1 Materials

1,8-Diazabicyclo[5.4.0]undec-7-ene (DBU) and (-)-sparteine were dried over CaH_2, distilled and stored under inert atmosphere. Benzyl alcohol and 1,4-butanediol were dried and stored over 3 Å molecular sieves. 4-Methoxybenzyl alcohol was dried over 3 Å molecular sieves in dry CH_2Cl_2. 1-(3,5-bis(trifluoromethyl)phenyl)-3-cyclohexylthiourea (**5**, Chapter 2) was synthesised as reported and dried over CaH_2 in dry THF.[1] Monomer **4** (Chapter 2) and monomers **5** and **7** (Chapter 3) were dried over 3 Å molecular sieves in dry CH_2Cl_2. Methyl acrylate (MA) and styrene were distilled over CaH_2 and stored below 4 °C. *N*-isopropylacrylamide (NiPAm) was recrystallised from a 9:1 mixture of hexanes/acetone and stored below 4 °C. Tetrahydropyran acrylate (THPA),[2] triethylene glycol methyl ether acrylate[3] and *S*-dodecyl-*S*'-(α,α'-dimethyl-α''-acetic acid) trithiocarbonate (DDMAT)[4] were prepared as previously reported and stored below 4 °C. AIBN (2,2'-azo-bis(isobutyronitrile)) was recrystallised twice from methanol and stored in the dark below 4 °C. Benzyl azide,[5] triethylene glycol monomethyl ether azide,[6] 4-pentynoic anhydride[7] and ethyl pent-4-ynoate[8] were synthesised according to methods reported in the literature. $CDCl_3$ was dried over 3 Å molecular sieves, distilled and degassed before use. CH_2Cl_2 and THF were purified over Innovative Technology SPS alumina solvent columns and degassed before use. Nanopure water with a resistivity of 18 mΩ·cm was prepared using a Millipore Simplicity UV ultrapure water purification system. All other solvents and chemicals were obtained from Sigma-Aldrich or Fisher Scientific and used as received.

7.2 General Considerations

7.2.1 Techniques

Ring-opening polymerisations were performed under inert atmosphere in a glovebox. RAFT polymerisations were carried out under oxygen-free conditions using standard Schlenk-line techniques. Thiol-ene reactions were performed in a Metalight QX1 lightbox.

7.2.2 Small Molecule Characterisation

^{1}H and ^{13}C NMR spectra were recorded on a Bruker DPX-400, AC-400, or DRX-500 spectrometer at 298 K. Chemical shifts are reported as δ in parts per million (ppm) and referenced to the chemical shift of the residual solvent resonances ($CHCl_3$: ^{1}H δ = 7.26 ppm; ^{13}C δ = 77.16 ppm). Mass spectra were recorded on a Bruker Esquire 2000 ESI spectrometer. Elemental analysis (CHN analysis) was performed in duplicate by Warwick Analytical Services. UV-Vis spectra were recorded using a Perkin-Elmer UV-Vis Spectrometer (Lambda 35). IR spectra were recorded using a Perkin-Elmer Spectrum 100 FT-IR spectrometer. Spectra were an accumulation of 16 scans with the background subtracted.

7.2.3 Polymer Characterisation

Size exclusion chromatography (SEC) analysis in $CHCl_3$ was conducted on a Varian Polymer Laboratories PL-GPC 50 plus integrated SEC system with differential refractive index and ultraviolet detectors equipped with a guard column (Varian Polymer Laboratories PLGel 5 μM, 50 × 7.5 mm) and two mixed D columns (Varian Polymer Laboratories PLGel 5 μM, 300 × 7.5 mm). The

mobile phase was $CHCl_3$ at a flow rate of 1.0 mL min^{-1}. SEC analysis in DMF was conducted on a Varian Polymer Laboratories PL-GPC 50 plus integrated SEC system with differential refractive index and ultraviolet detectors equipped with a guard column (Varian Polymer Laboratories PLGel 5 μM, 50 × 7.5 mm) and two mixed D columns (Varian Polymer Laboratories PLGel 5 μM, 300 × 7.5 mm). The mobile phase was DMF with 5 mM NH_4BF_4 at a flow rate of 1.0 mL min^{-1}. SEC analysis in THF was conducted on a system composed of a Varian 390-LC-Multi detector suite fitted with differential refractive index, light scattering, and ultraviolet detectors equipped with a guard column (Varian Polymer Laboratories PLGel 5 μM, 50 × 7.5 mm) and two mixed D columns (Varian Polymer Laboratories PLGel 5 μM, 300 × 7.5 mm). The mobile phase was THF with 2% triethylamine at a flow rate of 1.0 mL min^{-1}. SEC samples were calibrated against Varian Polymer Laboratories Easi-Vials linear poly(styrene) standards (162 - 2.4 × 10^5 g mol^{-1}) or Varian Polymer Laboratories Easi-Vials linear poly(methyl methacrylate) standards (690 - 1.9 × 10^6 g mol^{-1}) using Cirrus v3.3 software. MALDI-ToF (matrix-assisted laser desorption ionisation time of flight) spectra were recorded using a Bruker Daltronics Ultraflex II MALDI-ToF mass spectrometer, equipped with a nitrogen laser delivering 2 ns laser pulses at 337 nm with a positive ion ToF detection performed using an accelerating voltage of 25 kV. Samples were spotted onto a Bruker ground steel MALDI-ToF analytical plate through application of a small portion of a solution containing trans-2-[3-(4-*tert*-butylphenyl)-2-methyl-2-propylidene]malonitrile (DCTB) as a matrix (20 μL of a 10 mg mL^{-1} solution in THF), sodium trifluoroacetate as a cationisation agent (5 μL of a 10 mg mL^{-1} solution in THF), and analyte (5 μL of a 10 mg mL^{-1} solution in THF) followed by

solvent evaporation. The samples were measured in reflectron ion mode and calibrated by comparison to 2 × 10^3 poly(ethylene oxide) standards. Lower critical solution temperature (LCST) measurements were recorded using a Perkin-Elmer UV/vis Spectrometer (Lambda 35) equipped with a Peltier temperature controller at 500 nm with a heating/cooling rate of 1 °C min^{-1}. An average of three heating/cooling cycles were reported for each sample. Glass transition temperatures (T_g) were determined using a Mettler Toledo DSC1-STAR Differential Scanning Calorimeter (DSC) under a nitrogen stream (50 mL min^{-1}). Changes in heat flow were recorded between -40 and 240 °C over two cycles with a scan rate of 10 °C min^{-1} and a 5 minute isotherm at either end of the temperature range. The instrument was calibrated using indium metal standards supplied by Mettler Toledo and analysis of the data was performed using the STARe software package (version 9.30).

7.2.4 Particle Characterisation

Dynamic light scattering (DLS) measurements were taken on a Malvern Zetasizer NanoS instrument with a 4 mW He- Ne 633 nm laser module and the data analysed using Malvern DTS 5.02 software and both Cumulants and Distribution analysis methods. Measurements were taken at a detection angle of 173°. The hydrodymanic diameter (D_h) was calculated from the Stokes-Einstein equation $D_h = kT/(3\pi\eta D_{app})$, where k is the Boltzmann constant, T is the temperature, η is the viscosity of the solvent and D_{app} the apparent diffusion coefficient, where $D_{app} = \Gamma/q^2$. q is the scattering vector and $q = (4\pi n/\lambda)\sin(\theta/2)$, where θ is the scattering angle, λ is the laser wavelength and n is the refractive index of the solvent. Γ is the relaxation rate of the scatters and

is determined *via* the Cumulants or Distribution method of analysis. The Z-average diameter refers to an intensity-weighted mean diameter of the particles derived from the Cumulants analysis method. The intensity-weighted size distribution is derived from the Distribution analysis method and the volume- and number- weighted size distributions are derived from the intensity-weighted distribution using Mie theory. D_h only coincides with the real hydrodynamic diameter when the measured sample consists of monodisperse spherical particles. Transmission Electron Microscopy (TEM) samples were prepared by drop deposition and freeze drying of the solution onto copper/carbon grids that had been deposited with a thin film of graphene oxide prior to use. Micrographs were collected at magnifications ranging from 8 to 100 K and calibrated digitally. TEM was performed using a JEOL TEM-2011 operating at 200 kV. Cryogenic TEM was performed using a JEOL 2010F TEM operated at 200 kV and imaged using a Gatan Ultrascan 4000 camera. Histograms of number-average particle diameters were generated from the analysis of a minimum of 50 particles from at least three different micrographs using Image J software. SAXS measurements were recorded at the Australian Synchrotron facility at a photon energy of 11 keV and a sample to detector distance of 3.252 m to give a q range of 0.004 to 0.2 $Å^{-1}$. q is the scattering vector and is related to the scattering angle (2θ) and the photon wavelength (λ) by $q = 4\pi\sin(\theta)/\lambda$. The scattering from a blank (H_2O or 1,4-dioxane) was measured and subtracted for each measurement and data were normalised for total transmitted flux using a quantitative beamstop detector and absolute scaled using water as an absolute intensity standard. The two-dimensional SAXS images were converted into one-dimensional SAXS profiles ($I(q)$ *versus* q)

by circular averaging. NCNR Data Analysis IGOR PRO software was used to plot and analyse SAXS data and the models used for form fitting were taken from the NCNR package. See the appendix for further details of these models and the fitting parameters. Scattering length densities (SLD) were calculated using the "Scattering Length Density Calculator" provided by the NIST Center for Neutron Research, using the equation SLD = $\Sigma Z r_e / V_m$, where V_m is molecular volume, Z is atomic number and r_e is electron radius. Critical micelle concentrations were determined using fluorescence spectroscopy on a Cary Eclipse single-beam Perkin-Elmer LS55 fluorometer, using a slit width of 5.0 nm and excitation wavelength of 390 nm.

7.3 Experimental Procedures for Chapter 2

7.3.1 Synthesis of acetonide-protected 2,2-bis(hydroxymethyl)propionic acid (1)

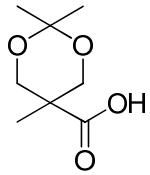

Acetonide-protected 2,2-bis(hydroxymethyl)propionic acid (**1**) was prepared according to a literature procedure.[9] 2,2-Bis(hydroxymethyl)propionic acid (bis-MPA) (10.0 g, 76.1 mmol), 2,2-dimethoxypropane (14.0 mL, 114 mmol) and *p*-toluenesulfonic acid (0.724 g, 3.80 mmol) were dissolved in acetone (70 mL) and the solution was stirred at room temperature. After 2 h ammonium hydroxide was added until the reaction mixture was neutralised and the solvent was removed *in vacuo*. The residue was dissolved in CH_2Cl_2 and washed with water (2 × 50 mL) and the organic layer dried over $MgSO_4$. CH_2Cl_2 was removed

under reduced pressure to yield a white solid (8.24 g, 47.3 mmol, 62%). Characterisation data were in accordance with that previously reported.[9]

^{1}H NMR (400 MHz, $CDCl_3$, ppm): δ = 8.54 (br s, 1H, COO*H*), 4.17 (d, 2H, CH_2O, $^3J_{H\text{-}H}$ = 11.8 Hz), 3.64 (d, 2H, CH_2O, $^3J_{H\text{-}H}$ = 11.8 Hz), 1.43 (s, 3H, C(CH_3)$_2$), 1.39 (s, 3H, C(CH_3)$_2$), 1.16 (s, 3H, CH_3). **^{13}C NMR** (100 MHz, $CDCl_3$, ppm): δ = 179.9 (*C*=O), 98.4 (*C*(CH$_3$)$_2$), 66.3 (*C*H$_2$O), 42.0 (*C*(CH$_3$)), 25.4 (C(*C*H$_3$)$_2$), 22.1 (C(*C*H$_3$)$_2$), 18.6 (*C*H$_3$).

7.3.2 Synthesis of norbornene functionalised acetonide protected bis-MPA (2)

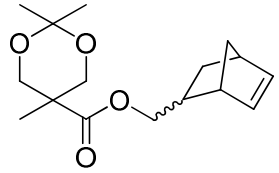

N-Ethyl-*N*′-(3-dimethylaminopropyl)carbodiimide hydrochloride (15.4 g, 80.5 mmol) was added to a solution of **1** (13.4 g, 76.7 mmol) and 4-(dimethylamino)pyridine (0.468 g, 3.83 mmol) in dry CH_2Cl_2 (300 mL) at 0 °C. The solution was allowed to warm to room temperature and stirred for 30 min before the addition of 5-norbornene-2-methanol (a mixture of *endo* and *exo* isomers) (10.0 g, 80.5 mmol). Following stirring of the solution for a further 48 h under nitrogen, the reaction mixture was washed with water (3 × 250 mL) and brine (1 × 250 mL) and the organic layer was dried over $MgSO_4$. CH_2Cl_2 was removed under reduced pressure and the crude product was purified by column chromatography (silica, ethyl acetate: petroleum ether (1:4)) to yield a colourless oil (14.5 g, 51.6 mmol, 67%).

^{1}H NMR (400 MHz, $CDCl_3$, ppm): *endo* isomer δ = 6.15 (m, 1H, C*H*=CHCH$_{bridgehead}$(CH$_{2\text{-}bridge}$)CH(CH$_2$)CH$_2$O), 5.94 (m, 1H, CH=C*H*CH$_{bridgehead}$(CH$_{2\text{-}bridge}$)CH(CH$_2$)CH$_2$O), 4.19 (d, 2H, C(CH$_3$)C*H*$_2$O, $^{3}J_{H\text{-}H}$ = 11.8 Hz), 3.91 (m, 1H, C*H*$_2$OC(O)C(CH$_3$)), 3.73 (m, 1H, C*H*$_2$OC(O)C(CH$_3$)), 3.64 (d, 2H, C(CH$_3$)C*H*$_2$O, $^{3}J_{H\text{-}H}$ = 11.8 Hz), 2.88 (m, 2H, CH$_{bridgehead}$CH$_{2\text{-}bridge}$C*H*$_{bridgehead}$CH(CH$_2$)CH$_2$O), 2.81, (m, 1H, C*H*$_{bridgehead}$CH$_{2\text{-}bridge}$CH$_{bridgehead}$CH(CH$_2$)CH$_2$O), 2.42 (m, 1H, CH$_{bridgehead}$(CH$_{2\text{-}bridge}$)C*H*(CH$_2$)CH$_2$O), 1.83 (m, 1H, CH$_{bridgehead}$(CH$_{2\text{-}bridge}$)CH(C*H*$_2$)CH$_2$O), 1.44 (m, 1H, C*H*$_{2\text{-}bridge}$), 1.42 (s, 3H, C(C*H*$_3$)$_2$), 1.39 (s, 3H, C(C*H*$_3$)$_2$), 1.25 (m, 1H, C*H*$_{2\text{-}bridge}$), 1.19 (s, 3H, C(C*H*$_3$)), 0.56 (m, 1H, CH$_{bridgehead}$(CH$_{2\text{-}bridge}$)CH(C*H*$_2$)CH$_2$O); *exo* isomer δ = 6.08 (m, 2H, C*H*=C*H*), 4.21 (m, 1H, C*H*$_2$OC(O)C(CH$_3$)), 4.19 (d, 2H, C(CH$_3$)C*H*$_2$O, $^{3}J_{H\text{-}H}$ = 11.8 Hz), 4.05 (m, 1H, C*H*$_2$OC(O)C(CH$_3$)), 3.64 (d, 2H, C(CH$_3$)C*H*$_2$O, $^{3}J_{H\text{-}H}$ = 11.8 Hz), 2.83 (m, 1H, C*H*$_{bridgehead}$CH$_{2\text{-}bridge}$CH$_{bridgehead}$CH(CH$_2$)CH$_2$O), 2.69 (m, 1H, CH$_{bridgehead}$CH$_{2\text{-}bridge}$C*H*$_{bridgehead}$CH(CH$_2$)CH$_2$O), 1.75 (m, 1H, CH$_{bridgehead}$(CH$_{2\text{-}bridge}$)C*H*(CH$_2$)CH$_2$O), 1.42 (s, 3H, C(C*H*$_3$)$_2$), 1.39 (s, 3H, C(C*H*$_3$)$_2$), 1.35 (m, 2H, C*H*$_{2\text{-}bridge}$), 1.35 (s, 3H, C(C*H*$_3$)), 1.27 (m, 1H, CH$_{bridgehead}$(CH$_{2\text{-}bridge}$)CH(C*H*$_2$)CH$_2$O), 1.18 (m, 1H, CH$_{bridgehead}$(CH$_{2\text{-}bridge}$)CH(C*H*$_2$)CH$_2$O). **^{13}C NMR** (100 MHz, $CDCl_3$, ppm): both isomers δ = 174.3 (*C*=O), 174.1 (*C*=O), 137.6 (*C*H=CHCH$_{bridgehead}$(CH$_{2\text{-}bridge}$)CH(CH$_2$)CH$_2$O), 137.0 (*C*H=CHCH$_{bridgehead}$(CH$_{2\text{-}bridge}$)CH(CH$_2$)CH$_2$O), 136.2 (CH=*C*HCH$_{bridgehead}$(CH$_{2\text{-}bridge}$)CH(CH$_2$)CH$_2$O), 132.2 (CH=*C*HCH$_{bridgehead}$(CH$_{2\text{-}bridge}$)CH(CH$_2$)CH$_2$O), 98.1 (C(*C*H$_3$)$_2$), 68.9 (*C*H$_2$OC(O)C(CH$_3$)), 68.2 (*C*H$_2$OC(O)C(CH$_3$)), 66.1 (*C*H$_2$O), 49.4 (*C*H$_{2\text{-}bridge}$), 45.0 (*C*H$_{2\text{-}bridge}$), 43.9 (CH$_{bridgehead}$CH$_{2\text{-}bridge}$*C*H$_{bridgehead}$CH(CH$_2$)CH$_2$O), 43.6 (CH$_{bridgehead}$CH$_{2\text{-}bridge}$*C*H$_{bridgehead}$CH(CH$_2$)CH$_2$O), 42.2 (*C*H$_{bridgehead}$CH$_{2\text{-}bridge}$CH$_{bridgehead}$CH(CH$_2$)CH$_2$O), 41.9 (*C*(CH$_3$)), 41.6 (*C*H$_{bridgehead}$CH$_{2\text{-}}$

$_{bridge}CH_{bridgehead}CH(CH_2)CH_2O$), 38.1 ($CH_{bridgehead}C\mathit{H}(CH_2)CH_2O$), 37.8 ($CH_{bridgehead}C\mathit{H}(CH_2)CH_2O$), 29.5 ($CH_{bridgehead}(CH_{2\text{-}bridge})CH(\mathit{C}H_2)CH_2O$), 28.8 ($CH_{bridgehead}(CH_{2\text{-}bridge})CH(\mathit{C}H_2)CH_2O$), 24.6 ($C(\mathit{C}H_3)_2$), 24.5 ($C(\mathit{C}H_3)_2$), 23.0 ($C(\mathit{C}H_3)_2$), 22.9 ($C(\mathit{C}H_3)_2$), 18.8 ($\mathit{C}H_3$). Anal. Calcd for $C_{16}H_{24}O_4$: C, 68.5; H, 8.6%. Found: C, 68.1; H, 8.6%. MS (ESI +ve): m/z 303 $[M+Na]^+$.

7.3.3 Synthesis of norbornene-functional diol (3)

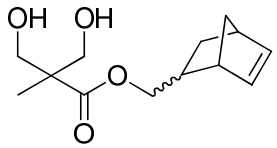

Dowex 50W-X2 acidic resin (5.0 g) was added to a stirred solution of **2** (14.5 g, 46.4 mmol) in MeOH (200 mL). After stirring at room temperature for 16 h, the resin was removed by filtration before concentration of the solution *in vacuo* to yield **3** as a white solid (12.7 g, 52.7 mmol, 98%).

^{1}H NMR (400 MHz, $CDCl_3$, ppm): *endo* isomer δ = 6.17 (m, 1H, $C\mathit{H}$=$CHCH_{bridgehead}(CH_{2\text{-}bridge})CH(CH_2)CH_2O$), 5.94 (m, 1H, CH=$C\mathit{H}CH_{bridgehead}(CH_{2\text{-}bridge})CH(CH_2)CH_2O$), 3.96 (m, 1H, $C\mathit{H}_2OC(O)C(CH_3)$), 3.92 (d, 2H, $C(CH_3)C\mathit{H}_2O$, $^3J_{H\text{-}H}$ = 11.2 Hz), 3.78 (m, 1H, $C\mathit{H}_2OC(O)C(CH_3)$), 3.72 (d, 2H, $C(CH_3)C\mathit{H}_2O$, $^3J_{H\text{-}H}$ = 11.2 Hz), 2.88 (m, 2H, $CH_{bridgehead}CH_{2\text{-}bridge}C\mathit{H}_{bridgehead}CH(CH_2)CH_2O$), 2.83 (m, 1H, $C\mathit{H}_{bridgehead}CH_{2\text{-}bridge}CH_{bridgehead}CH(CH_2)CH_2O$) 2.44 (m, 1H, $CH_{bridgehead}(CH_{2\text{-}bridge})C\mathit{H}(CH_2)CH_2O$), 2.40 (br s, 2H, $O\mathit{H}$), 1.85 (m, 1H, $CH_{bridgehead}(CH_{2\text{-}bridge})CH(C\mathit{H}_2)CH_2O$), 1.46 (m, 1H, $C\mathit{H}_{2\text{-}bridge}$), 1.27 (m, 1H, $C\mathit{H}_{2\text{-}bridge}$), 1.07 (s, 3H, $C(C\mathit{H}_3)$), 0.58 (m, 1H, $CH_{bridgehead}(CH_{2\text{-}bridge})CH(C\mathit{H}_2)CH_2O$); *exo* isomer δ = 6.09 (m, 2H, $C\mathit{H}$=$C\mathit{H}$), 3.93 (d, 2H, $C(CH_3)C\mathit{H}_2O$, $^3J_{H\text{-}H}$ = 11.2 Hz), 4.22 (m, 1H, $C\mathit{H}_2OC(O)C(CH_3)$), 3.73 (d, 2H, $C(CH_3)C\mathit{H}_2O$, $^3J_{H\text{-}H}$ = 11.2 Hz), 4.10 (m, 1H,

C*H*$_2$OC(O)C(CH$_3$)), 2.85 (m, 1H, C*H*$_{bridgehead}$CH$_{2\text{-}bridge}$CH$_{bridgehead}$CH(CH$_2$)CH$_2$O), 2.70 (m, 1H, CH$_{bridgehead}$CH$_{2\text{-}bridge}$C*H*$_{bridgehead}$CH(CH$_2$)CH$_2$O), 2.40 (br s, 2H, O*H*), 1.77 (m, 1H, CH$_{bridgehead}$(CH$_{2\text{-}bridge}$)C*H*(CH$_2$)CH$_2$O), 1.35 (m, 1H, C*H*$_{2\text{-}bridge}$), 1.30 (m, 1H, C*H*$_{2\text{-}bridge}$), 1.28 (m, 1H, CH$_{bridgehead}$(CH$_{2\text{-}bridge}$)CH(C*H*$_2$)CH$_2$O), 1.18 (m, 1H, CH$_{bridgehead}$(CH$_{2\text{-}bridge}$)CH(C*H*$_2$)CH$_2$O), 1.08 (s, 3H, C(C*H*$_3$)). **^{13}C NMR** (100 MHz, CDCl$_3$, ppm): both isomers δ = 176.1 (*C*=O), 176.0 (*C*=O), 137.8 (*C*H=CHCH$_{bridgehead}$(CH$_{2\text{-}bridge}$)CH(CH$_2$)CH$_2$O), 137.1 (*C*H=CHCH$_{bridgehead}$(CH$_{2\text{-}bridge}$)CH(CH$_2$)CH$_2$O), 136.2 (CH=*C*HCH$_{bridgehead}$(CH$_{2\text{-}bridge}$)CH(CH$_2$)CH$_2$O), 132.2 (CH=*C*HCH$_{bridgehead}$(CH$_{2\text{-}bridge}$)CH(CH$_2$)CH$_2$O), 69.2 (*C*H$_2$OC(O)C(CH$_3$)), 68.5 (*C*H$_2$OC(O)C(CH$_3$)), 68.3 (*C*H$_2$O), 49.5 (*C*H$_{2\text{-}bridge}$), 49.3 (*C*H$_{2\text{-}bridge}$), 45.1 (*C*(CH$_3$)), 44.0 (CH$_{bridgehead}$CH$_{2\text{-}bridge}$*C*H$_{bridgehead}$CH(CH$_2$)CH$_2$O), 43.7 (CH$_{bridgehead}$CH$_{2\text{-}bridge}$*C*H$_{bridgehead}$CH(CH$_2$)CH$_2$O), 42.3 (*C*H$_{bridgehead}$CH$_{2\text{-}bridge}$CH$_{bridgehead}$CH(CH$_2$)CH$_2$O), 41.7 (*C*H$_{bridgehead}$CH$_{2\text{-}bridge}$CH$_{bridgehead}$CH(CH$_2$)CH$_2$O), 38.1 (CH$_{bridgehead}$C*H*(CH$_2$)CH$_2$O), 37.8 (CH$_{bridgehead}$C*H*(CH$_2$)CH$_2$O), 29.6 (CH$_{bridgehead}$(CH$_{2\text{-}bridge}$)CH(*C*H$_2$)CH$_2$O), 28.9 (CH$_{bridgehead}$(CH$_{2\text{-}bridge}$)CH(*C*H$_2$)CH$_2$O), 17.3 (*C*H$_3$). Anal. Calcd for C$_{13}$H$_{20}$O$_4$: C, 65.0; H, 8.4%. Found: C, 64.9; H, 8.4%. MS (ESI +ve): m/z 263 [M+Na]$^+$.

7.3.4 Synthesis of norbornene-functional cyclic carbonate monomer (4)

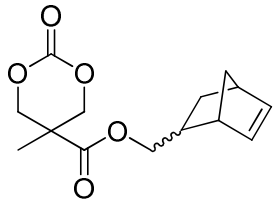

A solution of triphosgene (9.26 g, 31.2 mmol) in dry CH$_2$Cl$_2$ (100 mL) was added in stepwise portions over 30 minutes to a solution of **3** (12.5 g, 52.0 mmol) and pyridine (25.0 mL, 0.312 mol) in dry CH$_2$Cl$_2$ (150 mL) at -78 °C under nitrogen.

The reaction was stirred for 1 h at -78 °C and for a further 2 h at room temperature before being washed with saturated aqueous NH_4Cl solution (200 mL), 1 M HCl (3 × 150 mL) and saturated aqueous $NaHCO_3$ solution (150 mL). The organic layer was dried over $MgSO_4$ and reduced under vacuum to yield a white solid that was recrystallised from hot cyclohexane to yield **4** as a white crystalline solid (10.2 g, 38.5 mmol, 74%.)

^{1}H NMR (400 MHz, $CDCl_3$, ppm): *endo* isomer δ = 6.18 (m, 1H, C*H*=CHCH$_{bridgehead}$(CH$_{2\text{-}bridge}$)CH(CH$_2$)CH$_2$O), 5.93 (m, 1H, CH=C*H*CH$_{bridgehead}$(CH$_{2\text{-}bridge}$)CH(CH$_2$)CH$_2$O), 4.70 (d, 2H, C(CH$_3$)C*H*$_2$O, $^3J_{H\text{-}H}$ = 10.9 Hz), 4.20 (d, 2H, C(CH$_3$)C*H*$_2$O, $^3J_{H\text{-}H}$ = 10.9 Hz), 3.97 (m, 1H, C*H*$_2$OC(O)C(CH$_3$)), 3.82 (m, 1H, C*H*$_2$OC(O)C(CH$_3$)), 2.86 (m, 2H, C*H*$_{bridgehead}$), 2.42 (m, 1H, CH$_{bridgehead}$(CH$_{2\text{-}bridge}$)C*H*(CH$_2$)CH$_2$O), 1.86 (m, 1H, CH$_{bridgehead}$(CH$_{2\text{-}bridge}$)CH(C*H*$_2$)CH$_2$O), 1.48 (m, 1H, C*H*$_{2\text{-}bridge}$), 1.33 (s, 3H, C(C*H*$_3$)), 1.27 (m, 1H, C*H*$_{2\text{-}bridge}$), 0.57 (m, 1H, CH$_{bridgehead}$(CH$_{2\text{-}bridge}$)CH(C*H*$_2$)CH$_2$O); *exo* isomer δ = 6.09 (m, 2H, C*H*=C*H*), 4.71 (d, 2H, C(CH$_3$)C*H*$_2$O, $^3J_{H\text{-}H}$ = 10.9 Hz), 4.26 (m, 1H, C*H*$_2$OC(O)C(CH$_3$)), 4.21 (d, 2H, C(CH$_3$)C*H*$_2$O, $^3J_{H\text{-}H}$ = 10.9 Hz), 4.12 (m, 1H, C*H*$_2$OC(O)C(CH$_3$)), 2.84 (m, 1H, C*H*$_{bridgehead}$CH$_{2\text{-}bridge}$CH$_{bridgehead}$CH(CH$_2$)CH$_2$O), 2.66 (m, 1H, CH$_{bridgehead}$CH$_{2\text{-}bridge}$C*H*$_{bridgehead}$CH(CH$_2$)CH$_2$O), 1.76 (m, 1H, CH$_{bridgehead}$(CH$_{2\text{-}bridge}$)C*H*(CH$_2$)CH$_2$O), 1.39 (m, 1H, C*H*$_{2\text{-}bridge}$), 1.35 (s, 3H, C(C*H*$_3$)), 1.32 (m, 1H, CH$_{bridgehead}$(CH$_{2\text{-}bridge}$)CH(C*H*$_2$)CH$_2$O), 1.30 (m, 1H, C*H*$_{2\text{-}bridge}$), 1.17 (m, 1H, CH$_{bridgehead}$(CH$_{2\text{-}bridge}$)CH(C*H*$_2$)CH$_2$O). **^{13}C NMR** (100 MHz, $CDCl_3$, ppm): both isomers δ = 171.2 (C(CH$_3$)*C*=OOCH$_2$), 171.1 (C(CH$_3$)*C*=OOCH$_2$), 147.6 (CH$_2$O*C*=OOCH$_2$0), 137.8 (*C*H=CHCH$_{bridgehead}$(CH$_{2\text{-}bridge}$)CH(CH$_2$)CH$_2$O), 137.0 (*C*H=CHCH$_{bridgehead}$(CH$_{2\text{-}bridge}$)CH(CH$_2$)CH$_2$O), 136.0 (CH=*C*HCH$_{bridgehead}$(CH$_{2\text{-}bridge}$)CH(CH$_2$)CH$_2$O), 131.9 (CH=*C*HCH$_{bridgehead}$(CH$_{2\text{-}bridge}$)CH(CH$_2$)CH$_2$O), 73.0 (*C*H$_2$OC=OO*C*H$_2$), 70.2

($CH_2OC(O)C(CH_3)$), 69.5 ($CH_2OC(O)C(CH_3)$), 49.4 ($CH_{2\text{-bridge}}$), 45.0 ($CH_{2\text{-bridge}}$), 43.8 ($CH_{bridgehead}CH_{2\text{-bridge}}CH_{bridgehead}CH(CH_2)CH_2O$), 43.5 ($CH_{bridgehead}CH_{2\text{-bridge}}CH_{bridgehead}CH(CH_2)CH_2O$), 42.1 ($CH_{bridgehead}CH_{2\text{-bridge}}CH_{bridgehead}CH(CH_2)CH_2O$), 41.5 ($CH_{bridgehead}CH_{2\text{-bridge}}CH_{bridgehead}CH(CH_2)CH_2O$), 40.2 ($C(CH_3)$), 37.9 ($CH_{bridgehead}CH(CH_2)CH_2O$), 37.6 ($CH_{bridgehead}CH(CH_2)CH_2O$), 29.4($CH_{bridgehead}(CH_{2\text{-bridge}})CH(CH_2)CH_2O$), 28.7 ($CH_{bridgehead}(CH_{2\text{-bridge}})CH(CH_2)CH_2O$), 17.4 ($CH_3$). Anal. Calcd for $C_{14}H_{18}O_5$: C, 63.2; H, 6.8%. Found: C, 62.9.; H, 6.8%. MS (ESI +ve): m/z 289 $[M+Na]^+$.

7.3.5 General procedure for ring-opening polymerisations

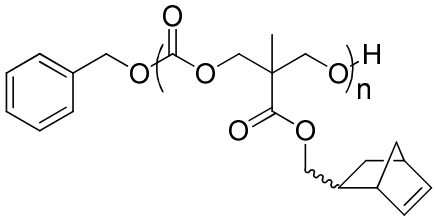

Benzyl alcohol, DBU (1 mol% to monomer), and 1-(3,5-bis(trifluoromethyl)phenyl)-3-cyclohexylthiourea (5 mol% to monomer) were dissolved in dry $CDCl_3$ or dry CH_2Cl_2. **4** was dissolved separately in the same solvent and added to the initiator/catalyst solution. After the desired amount of time the polymerisation was quenched by the addition of Amberlyst 15 H^+ resin. The resin was removed by filtration and the solvent removed under reduced pressure. The residual monomer and catalyst were removed by column chromatography (silica, 100% CH_2Cl_2, then 100% ethyl acetate).

^{1}H NMR (400 MHz, $CDCl_3$, ppm): δ = 7.36 (m, $5H_{end\text{-}group}$, Ar), 6.15 (m, $1H_{backbone\text{-}endo}$, CH=$CHCH_{bridgehead}(CH_{2\text{-bridge}})CH(CH_2)CH_2O$), 6.08 (m, $2H_{backbone\text{-}exo}$, CH=CH), 5.91 (m, $1H_{backbone\text{-}endo}$, CH=$CHCH_{bridgehead}(CH_{2\text{-bridge}})CH(CH_2)CH_2O$), 5.15 (s,

$2H_{end\text{-}group}$, CH_2Ar), 4.29 (m, $4H_{backbone}$, $C{=}OOCH_2C(CH_3)CH_2O$), 4.18 (m, $1H_{backbone\text{-}exo}$, OCH_2Nb), 4.05 (m, $1H_{backbone\text{-}exo}$, OCH_2Nb), 3.89 (m, $1H_{backbone\text{-}endo}$, OCH_2Nb), 3.73 (m, $1H_{backbone\text{-}endo}$, OCH_2Nb), 2.84 (m, $2H_{backbone\text{-}endo}$, $CH_{bridgehead}$), 2.82 (m, $1H_{backbone\text{-}exo}$, $CH_{bridgehead}CH_{2\text{-}bridge}CH_{bridgehead}CH(CH_2)CH_2O$), 2.65 (m, $1H_{backbone\text{-}exo}$, $CH_{bridgehead}CH_{2\text{-}bridge}CH_{bridgehead}CH(CH_2)CH_2O$), 2.40 (m, $1H_{backbone\text{-}endo}$, $CH_{bridgehead}(CH_{2\text{-}bridge})CH(CH_2)CH_2O$), 1.82 (m, $1H_{backobone\text{-}endo}$, $CH_{bridgehead}(CH_{2\text{-}bridge})CH(CH_2)CH_2O$), 1.73 (m, $1H_{backbone\text{-}exo}$, $CH_{bridgehead}(CH_{2\text{-}bridge})CH(CH_2)CH_2O$), 1.44 (m, $1H_{backbone\text{-}endo}$, $CH_{2\text{-}bridge}$), 1.33 (m, $1H_{backbone\text{-}exo}$, $CH_{2\text{-}bridge}$), 1.26 (s, $3H_{backbone}$, $C(CH_3)$), 1.23 (m, $1H_{backbone\text{-}endo}$, $CH_{2\text{-}bridge}$), 1.20 (m, $1H_{backbone\text{-}exo}$, $CH_{bridgehead}(CH_{2\text{-}bridge})CH(CH_2)CH_2O$), 0.54 (m, $1H_{backobone\text{-}endo}$, $CH_{bridgehead}(CH_{2\text{-}bridge})CH(CH_2)CH_2O$).

7.3.6 General procedure for post-polymerisation modifications *via* the 1,3-dipolar cycloaddition of norbornenes and azides

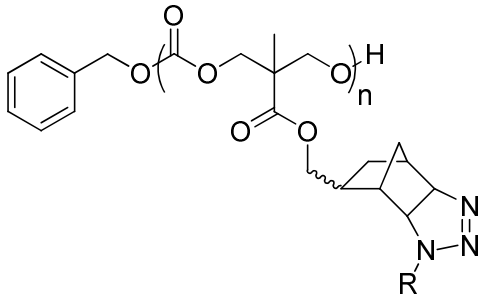

Benzyl azide (10 eq. per Nb moiety) was added to a solution of norbornene-functional polycarbonate in 1,4-dioxane ($[Nb]_0$ = 0.04 M) and stirred at 90 °C for 14 h. The solvent was removed *in vacuo,* the residue dissolved in the minimum amount of $CHCl_3$ and precipitated into cold methanol.

7.3.7 General procedure for post-polymerisation modifications *via* the inverse electron demand Diels-Alder reaction between norbornenes and tetrazines

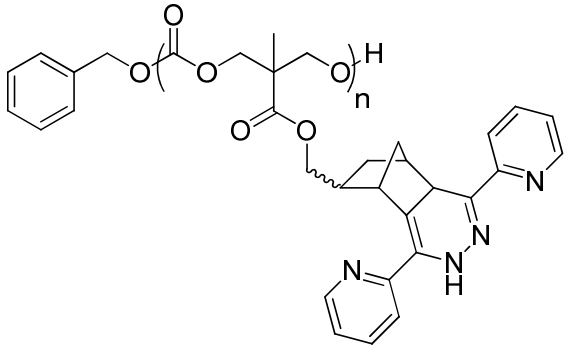

3,6-Di-2-pyridyl-1,2,4,5-tetrazine (1 eq. per Nb moiety) was added to a solution of norbornene-functional polycarbonate in 1,4-dioxane ($[Nb]_0$ = 0.04 M) and stirred at room temperature for 10 h. The solvent was removed *in vacuo,* the residue dissolved in the minimum amount of $CHCl_3$ and precipitated into hexane.

7.3.8 General procedure for post-polymerisation modifications *via* the radical addition of thiols to norbornenes

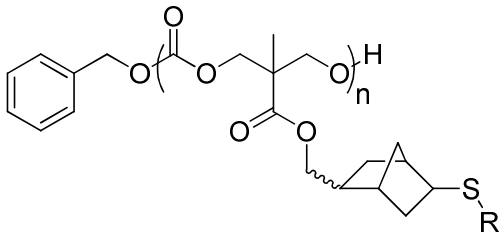

1-Dodecanethiol (1.3 eq. per Nb moiety) and 2-benzyl-2-(dimethylamino)-4'-morpholinobutyrophenone (0.015 eq. per Nb moiety) were added to a solution of norbornene-functional polycarbonate in 1,4-dioxane ([Nb] = 0.04 M) and irradiated with UV light for 1.5 h in a Metalight QX1 lightbox (λ = 320 - 400 nm).

The solvent was removed *in vacuo,* the residue dissolved in the minimum amount of $CHCl_3$ and precipitated into cold methanol.

7.3.9 General procedure for the one-pot three-step modification of norbornene-functional polycarbonates

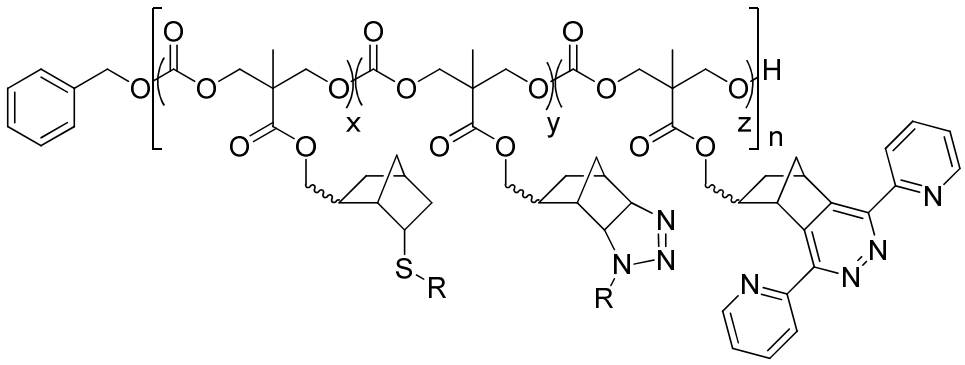

Triethyleneglycol monomethyl ether azide (10 eq. per Nb moiety) was added to a solution of norbornene-functional polycarbonate in 1,4-dioxane ($[Nb]_0$ = 0.04 M) and stirred at 90 °C for 1 h. The reaction was cooled to room temperature before the addition of 3,6-di-2-pyridyl-1,2,4,5-tetrazine (0.5 eq. per remaining Nb moiety) and stirred for 4 h. Finally, 1-dodecanthiol (2 eq. per remaining Nb moiety) and 2-benzyl-2-(dimethylamino)-4'-morpholinobutyrophenone (0.015 eq.) were added and the reaction mixture irradiated for 2 h with UV light. The solvent was removed *in vacuo,* the residue dissolved in the minimum amount of $CHCl_3$ and precipitated into hexane.

7.3.10 General procedure for the preparation of poly(*N*-isopropylacrylamide) *via* RAFT polymerisation

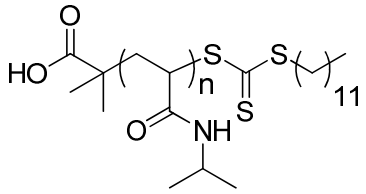

The appropriate equivalents of *S*-dodecyl-*S*'-(α,α'-dimethyl-α''-acetic acid) trithiocarbonate (DDMAT), AIBN (0.1 eq. to DDMAT) and *N*-isopropylacrylamide were loaded into a dry ampoule and dissolved in $CHCl_3$. The reaction mixture was degassed *via* 4 freeze-pump-thaw cycles and refilled with nitrogen. The polymerisation was initiated by immersion of the ampoule into an oil bath at 65 °C. After the desired length of time the polymerisation was quenched by immersion of the ampoule in liquid nitrogen. The polymer was purified by precipitation into diethyl ether.

^{1}H NMR (400 MHz, $CDCl_3$, ppm): δ = 7.11 – 6.01 (br m, $1H_{backbone}$, N*H*), 3.98 (m, $1H_{backbone}$, NHC*H*$(CH_3)_2$), 3.32 (m, $2H_{end\text{-}group}$, SC*H*$_2$), 3.15 (m, $1H_{backbone}$, C*H*CONH), 2.13 (m, $1H_{backbone}$, C*H*CONH), 1.80 -1.36 (m, $2H_{backbone}$, C*H*$_2$CHCO), 1.24 (m, $20H_{end\text{-}group}$, $SCH_2(CH_2)_{10}CH_3$), 1,24 (m, $6H_{end\text{-}group}$, $C(CH_3)_2$), 1.12 (m, $6H_{backbone}$, $NHCH(CH_3)_2$), 0.86 (t, $3H_{end\text{-}group}$, $SCH_2(CH_2)_{10}CH_3$).

7.3.11 General procedure for the end-group reduction of poly(*N*-isopropylacrylamide)

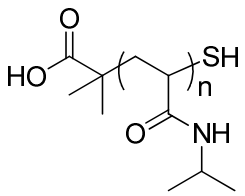

A solution of poly(*N*-isopropylacrylamide) in THF was degassed *via* 3 freeze-pump-thaw cycles in an ampoule. In a separate ampoule, a solution of hydrazine (20 eq.) was also degassed *via* 3 freeze-pump-thaw cycles. The degassed hydrazine solution was transferred *via* cannula to the poly(NiPAm) solution (final concentration = 4 mM), which was stirred under N_2 for 2 h. The polymer was isolated as a white solid *via* precipitation into diethyl ether.

^{1}H NMR (400 MHz, $CDCl_3$, ppm): δ = 7.09 – 5.90 (br m, $1H_{backbone}$, N*H*), 4.00 (m, $1H_{backbone}$, NHC*H*$(CH_3)_2$), 2.23 (m, $1H_{backbone}$, C*H*CONH), 1.80 – 1.10 (m, $2H_{backbone}$, CH_2CHCO), 1.25 (m, $6H_{end\text{-}group}$, C(CH_3)$_2$), 1.14 (m, $6H_{backbone}$, NHCH(CH_3)$_2$).

7.3.12 General procedure for the attempted preparation of polycarbonate-*g*-poly(*N*-isopropylacrylaimde)

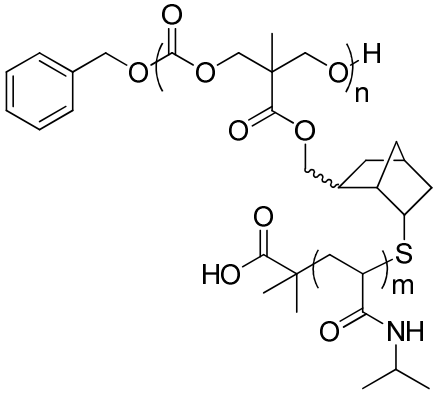

The appropriate equivalents of thiol-terminated poly(NiPAm) and 2-benzyl-2-(dimethylamino)-4'-morpholinobutyrophenone were added to a solution of norbornene-functional polycarbonate in THF ([Nb] = 0.015 M) and irradiated with UV light for 9 h.

7.4 Experimental Procedures for Chapter 3

7.4.1 Synthesis of RAFT CTA (2)

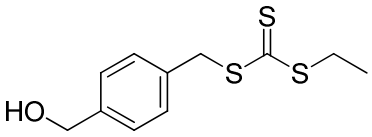

Ethanethiol (2.36 mL, 31.9 mmol) and carbon disulfide (5.76 mL, 95.8 mmol) were added to a suspension of potassium triphosphate (7.45 g, 35.1 mmol) in acetone (300 mL) and stirred for 5 h at room temperature. 4-(chloromethyl)benzyl alcohol (5.00 g, 31.9 mmol) was added and the mixture was stirred for a further 72 h. The solvent was removed *in vacuo* and the residue was dissolved in CH_2Cl_2 (300 mL). The organic phase was washed with 1 M HCl (2 × 200 mL), water (2 × 200 mL) and brine (1 × 200 mL). The organic layer was dried over $MgSO_4$. CH_2Cl_2 was removed under reduced pressure to yield a yellow solid (7.53 g, 29.1 mmol, 91%).

^{1}H NMR (400 MHz, $CDCl_3$, ppm): δ = 7.36 – 7.30 (m, 4H, Ar), 4.68 (d, 2H, ArCH_2OH, $^3J_{H\text{-}H}$ = 6.0 Hz), 4.61 (s, 2H, ArCH_2S), 3.38 (q, 2H, SCH_2CH$_3$, $^3J_{H\text{-}H}$ = 7.4 Hz), 1.64 (t, 1H, OH, $^3J_{H\text{-}H}$ = 6.0 Hz), 1.36 (t, 3H, CH$_2$CH_3, $^3J_{H\text{-}H}$ = 7.4 Hz). **^{13}C NMR** (125 MHz, $CDCl_3$, ppm): δ = 223.5 (*C*=S), 140.5 (OCH$_2$*C*), 134.6 (*C*CH$_2$S), 129.6 (OCH$_2$C*C*H), 127.4 (*C*HCCH$_2$S), 65.1(O*C*H$_2$C$_6$H$_4$), 41.1 (C$_6$H$_4$*C*H$_2$S), 31.5 (S*C*H$_2$CH$_3$), 13.2 (*C*H$_3$). Anal. Calcd for $C_{11}H_{14}OS_3$: C 51.1; H 5.5%. Found: 51.4; H, 5.5%. MS (ESI +ve): m/z 281 $[M+Na]^+$.

7.4.2 Synthesis of RAFT CTA functionalised acetonide protected bis-MPA (3)

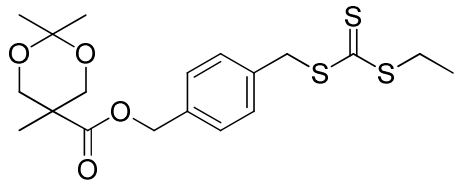

N-Ethyl-*N*′-(3-dimethylaminopropyl)carbodiimide hydrochloride (0.840 g, 4.38 mmol) was added to a solution of **1** (0.730 g, 4.19 mmol) and 4-(dimethylamino)pyridine (0.0256 g, 0.210 mmol) in dry CH_2Cl_2 (50 mL) at 0 °C. The solution was allowed to warm to room temperature and stirred for 30 min before the addition of **2** (1.13 g, 4.38 mmol). Following stirring of the solution for a further 44 h, the reaction mixture was washed with water (3 × 25 mL) and the organic layer was dried over $MgSO_4$. CH_2Cl_2 was removed under reduced pressure and the crude product was purified by column chromatography (silica, ethyl acetate: petroleum ether (1:1)) to yield a yellow solid (1.09 g, 2.63 mmol, 63%).

^{1}H NMR (400 MHz, $CDCl_3$, ppm): δ = 7.35 – 7.28 (m, 4H, Ar), 5.17 (s, 2H, ArCH_2O), 4.60 (s, 2H, ArCH_2S), 4.22 (d, 2H, C(CH_3)CH_2O, $^3J_{H\text{-}H}$ = 11.8 Hz), 3.66 (d, 2H, C(CH_3)CH_2O, $^3J_{H\text{-}H}$ = 11.8 Hz), 3.38 (q, 2H, SC$H_2$$CH_3$, $^3J_{H\text{-}H}$ = 7.4 Hz), 1.43 (s, 3H, C(CH_3)$_2$,), 1.37 (s, 3H, C(CH_3)$_2$,), 1.35 (t, 3H, SCH_2CH_3, $^3J_{H\text{-}H}$ = 7.4 Hz), 1.18 (s, 3H, C(CH_3)CH_2O). **^{13}C NMR** (125 MHz, $CDCl_3$, ppm): δ = 223.3 (*C*=S), 174.0 (*C*=O), 135.5 (OCH_2C), 135.2 (CCH_2S), 129.4 (OCH_2CCH), 128.1 ($CHCCH_2S$), 98.1 (*C*(CH_3)$_2$), 66.2 ($OCH_2C_6H_4$), 66.0 ($CH_2OC{=}OOCH_2$), 41.9 (CCH_3), 40.8 (CCH_2S), 31.4 (CH_2CH_3), 24.9 (C(*C*H_3)$_2$), 22.4 (C(*C*H_3)$_2$), 18.6 (C*C*H_3), 13.1 (CH_2CH_3). Anal. Calcd for $C_{16}H_{26}O_4S_3$: C, 55.0; H, 6.3%. Found: C, 55.0; H, 6.3%. MS (ESI +ve): m/z 437 $[M+Na]^+$.

7.4.3 Synthesis of RAFT CTA-functional diol (4)

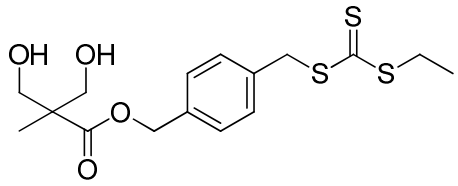

Dowex 50W-X2 acidic resin (0.200 g) was added to a stirred solution of **3** (0.400 g, 0.964 mmol) in MeOH (50 mL). After stirring at room temperature for 16 h, the resin was removed by filtration before concentration of the solution *in vacuo* to yield **4** as a yellow soild (0.361 g, 0.964 mmol, 100%).

^{1}H NMR (400 MHz, $CDCl_3$, ppm): δ = 7.35–7.28 (m, 4H, Ar), 5.17 (s, 2H, ArCH_2O), 4.60 (s, 2H, ArCH_2S), 3.92 (d, 2H, C(CH_3)CH_2O, $^{3}J_{H\text{-}H}$ = 11.2 Hz), 3.72 (d, 2H, C(CH_3)CH_2O, $^{3}J_{H\text{-}H}$ = 11.2 Hz), 3.38 (q, 2H, SC$H_2$$CH_3$, $^{3}J_{H\text{-}H}$ J = 7.4 Hz), 2.41 (br s, 2H, OH), 1.35 (t, 3H, SCH_2CH_3, $^{3}J_{H\text{-}H}$ = 7.4 Hz), 1.07 (s, 3H, C(CH_3)CH_2O). **^{13}C NMR** (125 MHz, $CDCl_3$, ppm): δ = 223.4 (*C*=S), 175.7 (*C*=O), 135.6 (OCH_2C), 135.3 (CCH_2S), 129.6 (OCH_2CCH), 128.3 ($CHCCH_2S$), 68.5 (CH_2OH), 66.4 ($OCH_2C_6H_4$), 49.4 (CCH_3), 40.9 ($C_6H_4CH_2S$), 31.5 (CH_2CH_3), 17.2 (CCH_3), 13.2 (CH_2CH_3). Anal. Calcd for $C_{16}H_{22}O_4S_3$: C, 51.3; H, 5.9%. Found: C, 51.4; H, 5.8%. MS (ESI +ve): m/z 397 $[M+Na]^+$.

7.4.4 Synthesis of RAFT CTA-functional carbonate monomer (5)

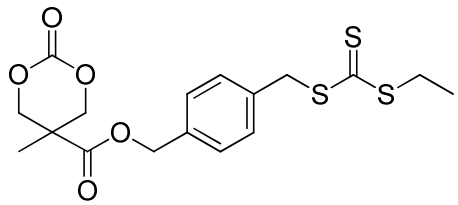

A solution of triphosgene (2.50 g, 8.42 mmol) in dry CH_2Cl_2 (30 mL) was added in stepwise portions over 30 minutes to a solution of **4** (4.67 g, 12.7 mmol) and pyridine (6.00 mL, 74.9 mmol) in dry CH_2Cl_2 (70 mL) at -78 °C. The reaction

was stirred for 1 h at -78 °C and for a further 2 h at room temperature before being washed with saturated aqueous NH_4Cl solution (50 mL), 1M HCl (3 × 50 mL) and saturated aqueous $NaHCO_3$ solution (50 mL). The organic layer was dried over $MgSO_4$ and reduced under vacuum to yield a yellow solid that was recrystallised from THF/diethyl ether to yield **5** as a yellow solid (3.86 g, 9.64 mmol, 76%).

^{1}H NMR (400 MHz, $CDCl_3$, ppm): δ = 7.37–7.26 (m, 4H, Ar), 5.19 (s, 2H, ArCH_2O), 4.70 (d, 2H, C(CH_3)CH_2O, $^3J_{H\text{-}H}$ = 10.8 Hz), 4.61 (s, 2H, ArCH_2S), 4.20 (d, 2H, C(CH_3)CH_2O, $^3J_{H\text{-}H}$ = 10.8 Hz), 3.38 (q, 2H, SC$H_2$$CH_3$, $^3J_{H\text{-}H}$ = 7.4 Hz), 1.36 (t, 3H, SCH_2CH_3, $^3J_{H\text{-}H}$ = 7.4 Hz), 1.33 (s, 3H, C(CH_3)CH_2O). **^{13}C NMR** (125 MHz, $CDCl_3$, ppm): δ = 223.3 (*C*=S), 171.0 (C(CH_3)*C*=OOCH_2), 147.5 (CH_2O*C*=O$OCH_2$0), 136.1 (OCH_2C), 134.4 (*C*CH_2*S*), 129.7 (OCH_2C*C*H), 128.6 (*C*HCCH_2S), 73.0 (*C*H_2OC=OO*C*H_2), 67.5 (O*C*$H_2C_6H_4$), 40.7 (C_6H_4*C*H_2*S*), 40.3 (*C*CH_3), 31.5 (*C*H_2CH_3), 17.6 (C*C*H_3), 13.1 (CH_2*C*H_3). Anal. Calcd for $C_{17}H_{20}O_5S_3$: C, 51.0; H, 5.0%. Found: C, 50.7; H, 4.9%. MS (ESI +ve): m/z 423 $[M+Na]^+$.

7.4.5 Synthesis of ethyl-functional diol (ethyl-2,2-bis(hydroxymethyl)propionate)

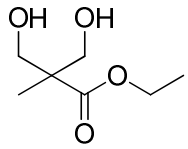

The ethyl-functional diol (ethyl-2,2-bis(hydroxymethyl)propionate) was prepared according to the literature.[10] Amberlyst 15 H^+ ion exchange resin (4.6 g) was added to a solution of bis-MPA (15 g, 0.112 mol) in ethanol (100 mL) and heated at reflux for 16 h. After this time, the solution was allowed to cool to

room temperature and the resin was subsequently removed *via* filtration. Solvent was removed *in vacuo* to yield a white residue. CH_2Cl_2 (120 mL) was added and the mixture filtered to remove unreacted bis-MPA, the filtrate was dried over $MgSO_4$. CH_2Cl_2 was removed *in vacuo* to yield a colourless liquid (15.1 g, 93.0 mmol, 83%). Characterisation data were in accordance with that previously reported.[10]

^{1}H NMR (400 MHz, $CDCl_3$, ppm): δ = 4.17 (q, 2H, C=OC*H*$_2$CH$_3$, $^3J_{H\text{-}H}$ = 7.2 Hz), 3.84 (d, 2H, C(CH$_3$)C*H*$_2$O, $^3J_{H\text{-}H}$ = 11.2 Hz), 3.66 (d, 2H, C(CH$_3$)C*H*$_2$O, $^3J_{H\text{-}H}$ = 11.2 Hz), 3.38 (br s, 2H, O*H*), 1.25 (t, 3H, C=OCH$_2$C*H*$_3$, $^3J_{H\text{-}H}$ = 7.2 Hz), 1.04 (s, 3H, C*C*H$_3$). **^{13}C NMR** (100 MHz, $CDCl_3$, ppm): δ = 176.0 (*C*=O), 67.5 (C(CH$_3$)*C*H$_2$O), 61.1 (C=O*C*H$_2$CH$_3$), 49.2 (*C*CH$_3$), 17.2 (C*C*H$_3$), 14.2 (C=OCH$_2$*C*H$_3$).

7.4.6 Synthesis of ethyl-functional cyclic carbonate monomer (5-methyl-5-ethoxycarbonyl-1,3-dioxan-2-one) (7)

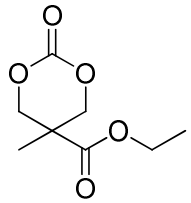

Triethylamine (19.3 mL, 193 mmol) was added *via* dropwise addition to a solution of ethyl-2,2-bis(hydroxymethyl)propionate (7.5 g, 46.2 mmol) and ethyl chloroformate (8.81 mL, 92.5 mmol) in THF (80 mL) at 0 °C. The reaction was subsequently stirred at room temperature for 16 h. NEt_3.HCl salts were removed *via* filtration and the solvent removed *in vacuo* to yield a white residue. The crude product was dissolved in CH_2Cl_2 (50 mL), washed with water (3 × 30 mL) and the organic layer dried over $MgSO_4$. Solvent was removed *in vacuo* and the product was isolated as a white solid after

recrystallisation from hot toluene (5.30g, 28.2 mmol, 61%). Characterisation data were in accordance with that previously reported.[10]

^{1}H NMR (400 MHz, $CDCl_3$, ppm): δ = 4.69 (d, 2H, C(CH_3)CH_2O, $^3J_{H\text{-}H}$ = 10.8 Hz), 4.26 (q, 2H, C=OC$H_2$$CH_3$, $^3J_{H\text{-}H}$ = 7.1 Hz), 4.20 (d, 2H, C(CH_3)CH_2O, $^3J_{H\text{-}H}$ = 10.8 Hz), 1.33 (s, 3H, CCH_3), 1.30 (t, 3H, C=OCH$_2$CH_3, $^3J_{H\text{-}H}$ = 7.1 Hz). **^{13}C NMR** (100 MHz, $CDCl_3$, ppm): δ = 171.2 (C(CH_3)C=OOCH$_2$), 147.7 (CH$_2$OC=OOCH$_2$0), 73.2 (C(CH_3)CH$_2$O), 62.4 (C=OCH$_2$CH$_3$), 40.2 (CCH$_3$), 17.7 (CCH$_3$), 14.1 (C=OCH$_2$$CH_3$).

7.4.7 General procedure for ring-opening polymerisations

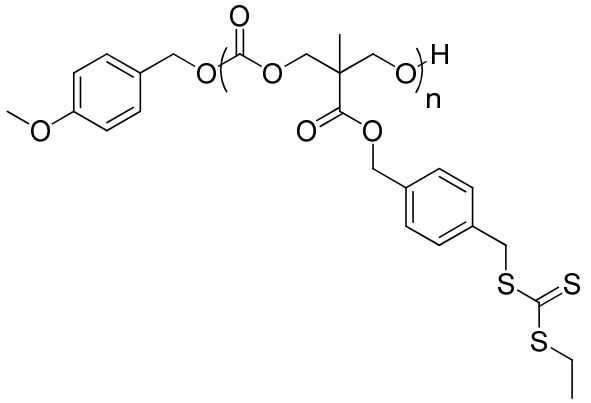

1,8-Diazabicyclo[5.4.0]undec-7-ene (DBU) (5 mol% to monomer) was added to a solution of **5** and 4-methoxybenzyl alcohol in dry CH_2Cl_2 or $CDCl_3$ (taken from a stock solution of 4-methoxybenzyl alcohol in dry CH_2Cl_2 or $CDCl_3$). After the desired amount of time the polymerisation was quenched by the addition of Amberlyst 15 H^+ ion exchange resin. The resin was removed by filtration and CH_2Cl_2 removed under reduced pressure. The unreacted monomer and residual catalyst were removed by column chromatography (silica, 100% CH_2Cl_2, then 100% ethyl acetate).

^{1}H NMR (400 MHz, $CDCl_3$, ppm): δ = 7.27 (m, 4H$_{backbone}$, Ar), 6.87 (m, 2H$_{end\text{-}group}$, Ar), 5.10 (m, 2H$_{backbone}$, OCH_2Ar), 5.04 (s, 2H$_{end\text{-}group}$, CH_2Ar), 4.73 (m, 2H$_{backbone}$,

SCH_2Ar), 4.57 (m, 4H$_{backbone}$, C=OOCH_2C(CH$_3$)CH_2O), 3.79 (s, 3H$_{end\text{-}group}$, OCH_3), 3.36 (m, 2H$_{backbone}$, SCH_2CH$_3$), 2.42 (m, 1H$_{end\text{-}group}$, OH), 1.35 (m, 3H$_{backbone}$, SCH$_2$CH_3), 1.23 (m, 3H$_{backbone}$, CCH_3).

7.4.8 General procedure for ring-opening copolymerisations

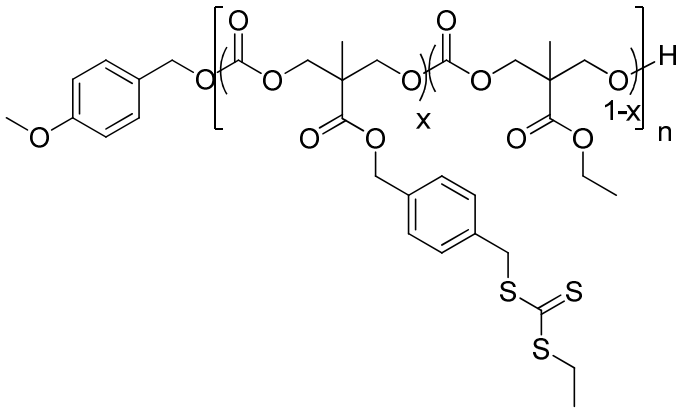

1,8-Diazabicyclo[5.4.0]undec-7-ene (DBU) (5 mol% to total monomer) was added to a solution of cyclic carbonate **5**, cyclic carbonate **7** and 4-methoxybenzyl alcohol in dry CH_2Cl_2 (taken from a stock solution of 4-methoxybenzyl alcohol in dry CH_2Cl_2). After the desired amount of time the polymerisation was quenched by the addition of Amberlyst 15 H^+ ion exchange resin. The resin was removed by filtration and CH_2Cl_2 removed under reduced pressure. The unreacted monomers and residual DBU were removed by column chromatography (silica, 100% CH_2Cl_2, then 100% ethyl acetate).

^{1}H NMR (400 MHz, $CDCl_3$, ppm): δ = 7.28 (m, 4H$_{backbone\text{-}\mathbf{5}}$, Ar), 6.88 (m, 2H$_{end\text{-}group}$, Ar), 5.12 (m, 2H$_{backbone\text{-}5}$, OC$H_2$Ar), 5.07 (m, 2H$_{end\text{-}group}$, C$H_2$Ar), 4.61 (m, 2H$_{backbone\text{-}\mathbf{5}}$, SC$H_2$Ar), 4.28 (m, 8H$_{backbone\text{-}\mathbf{5+7}}$, C=OOC$H_2$C(CH$_3$)C$H_2$O), 4.18 (m, 2H$_{backbone\text{-}\mathbf{7}}$, OC$H_2CH_3$), 3.10 (m, 3H$_{end\text{-}group}$, OC$H_3$), 3.37 (m, 2H$_{backbone\text{-}\mathbf{5}}$, SC$H_2CH_3$), 1.35 (m, 3H$_{backbone\text{-}\mathbf{5}}$, SCH$_2CH_3$), 1.24 (m, 6H$_{backbone\text{-}\mathbf{5+7}}$, CC$H_3$), 1.20 (m, 3H$_{backbone\text{-}\mathbf{7}}$, OCH$_2CH_3$).

7.4.9 General procedure for RAFT polymerisations

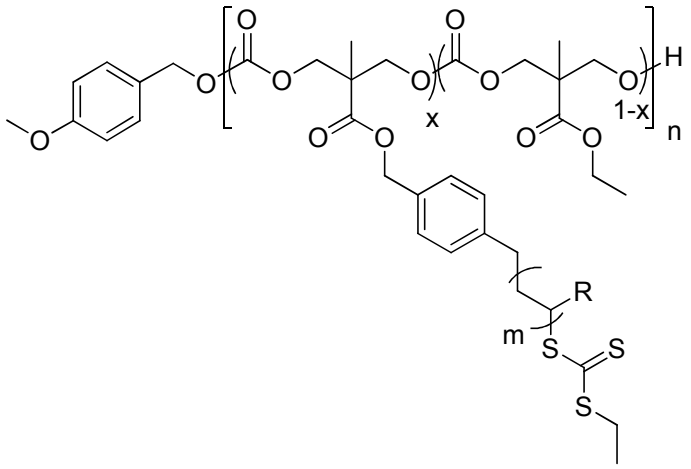

The appropriate equivalents of RAFT CTA-functional polycarbonate, AIBN (0.1 eq. to total RAFT CTA groups) and methyl acrylate were loaded into a dry ampoule and dissolved in $CHCl_3$. The reaction mixture was degassed *via* 4 freeze-pump-thaw cycles and refilled with nitrogen. The polymerisation was initiated by immersion of the ampoule into an oil bath at 65 °C. After the desired length of time the polymerisation was quenched by immersion of the ampoule in liquid nitrogen.

^{1}H NMR (400 MHz, $CDCl_3$, ppm): δ = 7.22 – 7.12 (m, 4H$_{PC}$, Ar), 5.10 (m, 2H$_{PC}$, OCH_2Ar), 4.87(m, 2H$_{PC}$, SCH_2Ar), 4.27 (m, 8H$_{PC}$, C=OOCH_2C(CH_3)CH_2O), 4.17 (m, 2H$_{PC}$, OC$H_2$$CH_3$), 3.66 (s, 3H$_{PMA}$, OC$H_3$), 3.37 (m, 2H$_{PC}$, SC$H_2$$CH_3$), 2.30 (m, 1H$_{PMA}$, CH_2C*H*C=OOCH_3), 2.00 - 1.40 (m, 2H$_{PMA}$, CH_2CHC=OOCH_3), 1.35 (m, 3H$_{PC}$, SCH_2CH_3), 1.23 (m, 6H$_{PC}$, CCH_3), 1.20(m, 3H$_{PC}$, OCH_2CH_3).

7.4.10 Preparation of polycarbonate-*g*-poly(*N*-isopropylacrylaimde) micelles

Polymer **P10** was dissolved in 18.2 MΩ·cm water at a concentration of 1.0 mg/mL at 4 °C. The solution was allowed to stir for 1 h prior to analysis and then stored at 4 °C.

DLS: $D_{h(\text{number average})}$ = 12 ± 0.4 nm, PD = 0.33. TEM: D_{av} = 12 ± 2 nm.

7.5 Experimental Procedures for Chapter 4

7.5.1 General procedure for ring-opening polymerisations

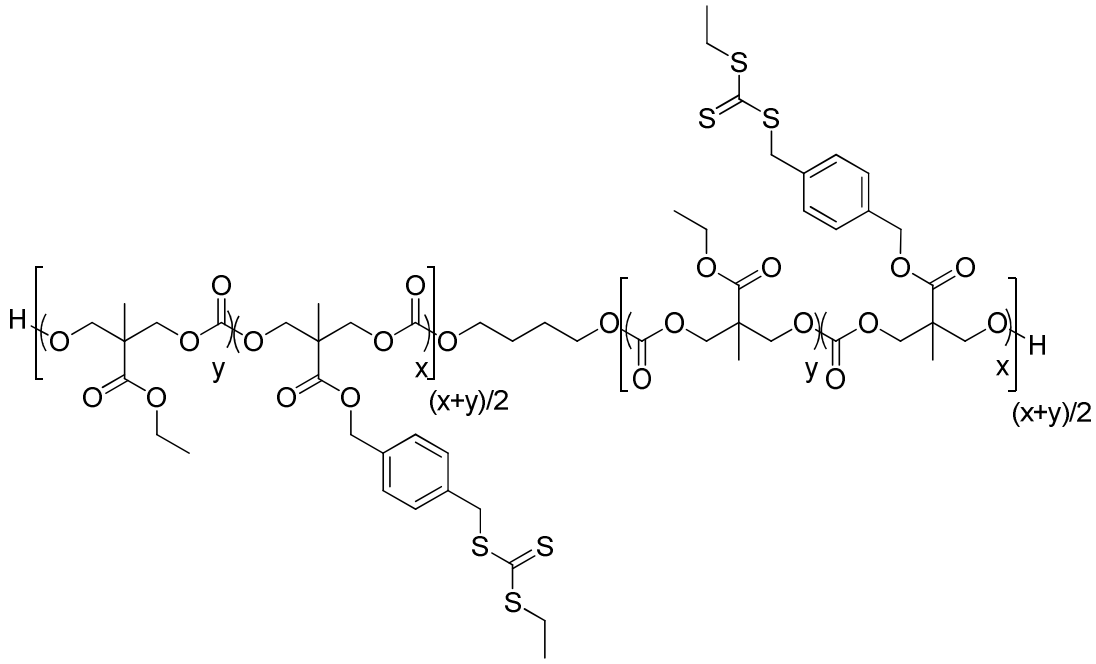

1,8-Diazabicyclo[5.4.0]undec-7-ene (DBU) was added to a solution of the appropriate equivalents of **1**, **2** and 1,4-butanediol (taken from a stock solution of 1,4-butanediol in dry CH_2Cl_2) in dry CH_2Cl_2 and stirred at room temperature. After the desired amount of time the polymerisation was quenched by the addition of Amberlyst 15 H^+ ion exchange resin. The resin was removed by filtration and CH_2Cl_2 removed under reduced pressure. The unreacted

monomers and residual DBU were removed by column chromatography (silica, 100% CH_2Cl_2, then 100% ethyl acetate).

^{1}H NMR (400 MHz, $CDCl_3$, ppm): δ = 7.31 – 7.26 (m, $4H_{backbone\text{-}\mathbf{1}}$, Ar), 5.11 (m, $2H_{backbone\text{-}\mathbf{1}}$, OCH_2Ar), 4.59 (m, $2H_{backbone\text{-}\mathbf{1}}$, SCH_2Ar), 4.28 (m, $8H_{backbone\text{-}\mathbf{1+2}}$, $C{=}OOCH_2C(CH_3)CH_2O$), 4.17 (m, $2H_{backbone\text{-}\mathbf{2}}$, OCH_2CH_3), 4.11 (m, $4H_{end\text{-}group}$, OCH_2CH_2), 3.37 (m, $2H_{backbone\text{-}\mathbf{1}}$, SCH_2CH_3), 1.73 (m, $4H_{end\text{-}group}$, OCH_2CH_2), 1.35 (m, $3H_{backbone\text{-}\mathbf{1}}$, SCH_2CH_3), 1.24 (m, $6H_{backbone\text{-}\mathbf{1+2}}$, CCH_3), 1.21 (m, $3H_{backbone\text{-}\mathbf{2}}$, OCH_2CH_3).

7.5.2 General procedure for alkyne end-group functionalisation

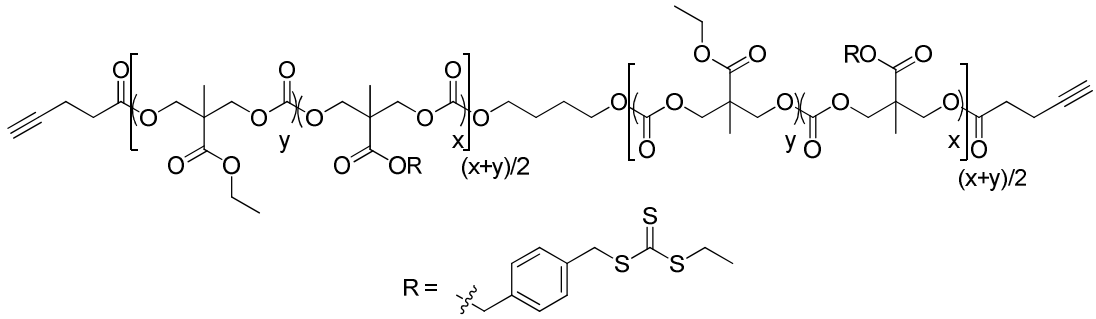

Pyridine (10 eq.) was added to a solution of RAFT CTA-functional polycarbonate, 4-pentynoic anhydride (30 eq.) and DMAP (3 eq.) in dry CH_2Cl_2 and stirred under nitrogen for 36 h. The solution was washed with saturated $NaHSO_4$ (2 ×) and saturated $NaHCO_3$ and the organic layer dried over $MgSO_4$. Solvent was removed *in vacuo*, the polymer residue dissolved in the minimum amount of $CHCl_3$ and precipitated into petroleum ether 40 – 60 °C three times.

^{1}H NMR (400 MHz, $CDCl_3$, ppm): δ = 7.31 – 7.26 (m, $4H_{backbone\text{-}\mathbf{1}}$, Ar), 5.11 (m, $2H_{backbone\text{-}\mathbf{1}}$, OCH_2Ar), 4.59 (m, $2H_{backbone\text{-}\mathbf{1}}$, SCH_2Ar), 4.28 (m, $8H_{backbone\text{-}\mathbf{1+2}}$, $C{=}OOCH_2C(CH_3)CH_2O$), 4.17 (m, $2H_{backbone\text{-}\mathbf{2}}$, OCH_2CH_3), 4.11 (m, $4H_{end\text{-}group}$, OCH_2CH_2), 3.87 (m, $2H_{backbone\text{-}\mathbf{1}}$, SCH_2CH_3), 2.55 (m, $4H_{end\text{-}group}$, CH_2CH_2CCH),

2.50 – 2.42 (m, $4H_{end\text{-}group}$, CH_2CH_2CCH), 1.97 (m, $2H_{end\text{-}group}$, C*H*), 1.73 (m, $4H_{end\text{-}group}$, OCH_2CH_2), 1.34 (m, $3H_{backbone\text{-}\mathbf{1}}$, SCH_2CH_3), 1.24 (m, $6H_{backbone\text{-}\mathbf{1+2}}$, CCH_3), 1.22 (m, $3H_{backbone\text{-}\mathbf{2}}$, OCH_2CH_3).

7.5.3 Synthesis of bis-(mesylate ethyl)disulfide (3)

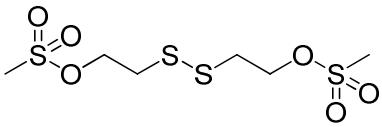

Bis-(mesylate ethyl)disulfide (**3**) was prepared according to literature procedures.[11, 12] Methanesulfonyl chloride (4.01 mL, 51.9 mmol) was added dropwise to a solution of 2-hydroxyethyldisulfide (2 g, 13.0 mmol) and triethylamine (7.23 mL, 51.9 mmol) in CH_2Cl_2 (40 mL) at 0 °C and subsequently left to stir at room temperature for 16 h. The solution was washed with 1M HCl (2 × 20 mL), saturated $NaHCO_3$ (2 × 20 mL) and brine (20 mL) and the organic layer dried over $MgSO_4$. Solvent was removed *in vacuo* to yield **3** as a pale yellow oil, that was used for the next step without further purification.

7.5.4 Synthesis of bis-(azidoethyl)disulfide (4)

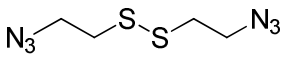

Bis-(azidoethyl)disulfide (**4**) was prepared according to literature procedures.[11, 12] Sodium azide (4.2 g, 64.6 mmol) was added to a solution of **3** (4 g, 12.9 mmol) in DMF (80 mL) and heated at 80 °C for 16 h, during which time a white precipitate formed. The precipitate was removed *via* filtration and solvent removed *in vacuo*. The residue was dissolved in CH_2Cl_2, filtered, washed

with saturated $NaHCO_3$ and the organic layer dried over $MgSO_4$. Solvent was removed *in vacuo* to yield (**4**) as a colourless oil (2.35 g, 11.5 mmol, 89.2%). Characterisation data were in accordance with that previously reported.[11, 12]

^{1}H NMR (400 MHz, $CDCl_3$, ppm): δ = 3.59 (t, 4H, N_3CH_2, $^3J_{H\text{-}H}$ = 6.7 Hz), 2.86 (t, 4H, SCH_2, $^3J_{H\text{-}H}$ = 6.7 Hz). **^{13}C NMR** (100 MHz, $CDCl_3$, ppm): δ = 50.0 (N_3CH_2), 37.7 (SCH_2).

7.5.5 General procedure for cyclisation *via* copper-catalysed azide-alkyne cycloaddition

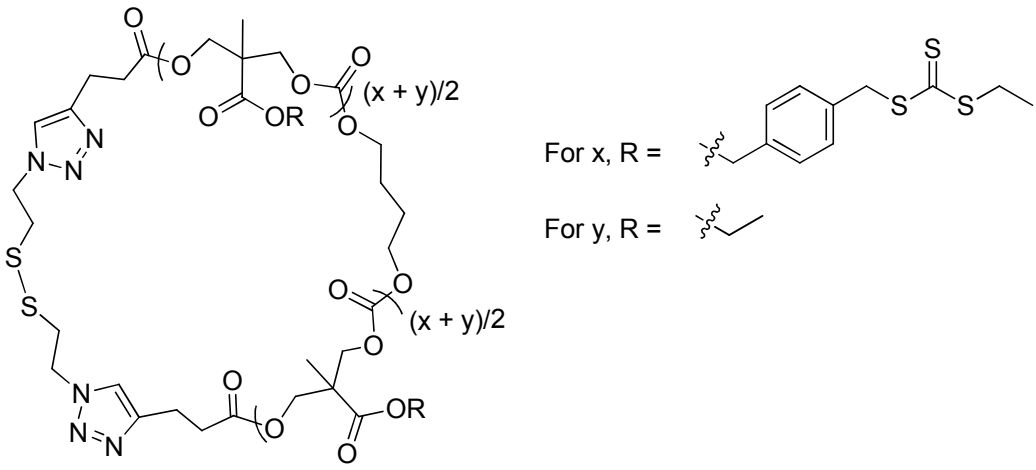

A solution of *N,N,N',N''*-pentamethyldiethylenetriamine (PMDETA) (100 eq.) in toluene (0.05 mM) was bubbled with nitrogen for 1 h. Cu(I)Br (100 eq.) was added and the solution bubbled for a further 30 min. In a separate ampoule a solution of alkyne-terminated RAFT CTA-functional polycarbonate (1 eq.) and **4** (1 eq.) in toluene (1 mM) was degassed *via* 3 freeze-pump-thaw cycles. The degassed solution of polymer and **4** was transferred into a gas-tight glass syringe and added at a rate of 0.3 mL/h to the solution of PMDETA and Cu(I)Br whilst stirred. After complete addition the solution was stirred for a further 3 h, then washed with saturated $NaHCO_3$ (3 ×) and brine (3 ×) and the organic layer

dried over $MgSO_4$. Toluene was removed *in vacuo* and the polymer residue was dissolved in CH_2Cl_2 and stirred in the presence of Cuprisorb beads overnight. The beads were removed *via* filtration and the polymer was precipitated into petroleum ether 40 – 60 °C.

^{1}H NMR (400 MHz, $CDCl_3$, ppm): δ = 7.31 – 7.25 (m, $4H_{backbone\text{-}\mathbf{1}}$, Ar), 5.12 (m, $2H_{backbone\text{-}\mathbf{1}}$, OCH_2Ar), 4.59 (m, $2H_{backbone\text{-}\mathbf{1}}$, SCH_2Ar), 4.28 (m, $8H_{backbone\text{-}\mathbf{1+2}}$, $C{=}OOCH_2C(CH_3)CH_2O$), 4.17 (m, $2H_{backbone\text{-}\mathbf{2}}$, OCH_2CH_3), 4.12 (m, $4H_{end\text{-}group}$, OCH_2CH_2), 3.37 (m, $2H_{backbone\text{-}\mathbf{1}}$, SCH_2CH_3), 3.14 – 2.59 (m, $12H_{end\text{-}group}$, CH_2SSCH_2 + CH_2CH_2CCH + CH_2CH_2CCH), 1.73 (m, $4H_{end\text{-}group}$, OCH_2CH_2), 1.35 (m, $3H_{backbone\text{-}\mathbf{1}}$, SCH_2CH_3), 1.24 (m, $6H_{backbone\text{-}\mathbf{1+2}}$, CCH_3), 1.22 (m, $3H_{backbone\text{-}\mathbf{2}}$, OCH_2CH_3).

7.5.6 Model small molecule copper-catalysed azide-alkyne cycloaddition (5)

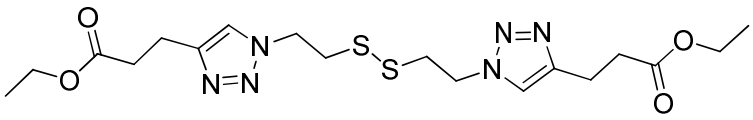

Solutions of ethyl pent-4-ynoate (0.300 g, 2.38 mmol) and **4** (0.194 g, 0.950 mmol) in toluene (13 mL) and PMDETA (119 µL, 0.570 mmol) and Cu(I)Br (0.081 g, 0.565 mmol) in toluene, in separate ampoules, were degassed *via* 3 freeze-pump-thaw cycles. The PMDETA and Cu(I)Br solution was transferred *via* cannula to the solution of ethyl pent-4-ynoate and **4** and stirred for 6 h. The crude product was isolated *via* filtration, dissolved in CH_2Cl_2, washed with saturated $NaHCO_3$ (3 × 10 mL) and brine (3 × 10 mL) and the organic layer dried over $MgSO_4$. Solvent was removed *in vacuo* to yield **5** as a white solid (0.404 g, 0.884 mmol, 93.1%).

^{1}H NMR (400 MHz, $CDCl_3$, ppm): δ = 7.43 (s, 2H, C=C*H*), 4.59 (t, 4H, N_3CH_2, $^3J_{H\text{-}H}$ = 6.7 Hz), 4.11 (q, 4H, CH_2CH_3, $^3J_{H\text{-}H}$ = 7.1 Hz), 3.14 (t, 4H, SCH_2, $^3J_{H\text{-}H}$ = 6.7 Hz), 3.03 (t, 4H, C=OC*H*$_2$, $^3J_{H\text{-}H}$ = 7.3 Hz), 2.71 (t, 4H, CH_2CH_2C=CH, $^3J_{H\text{-}H}$ = 7.3 Hz), 1.22 (t, 6H, CH_3, $^3J_{H\text{-}H}$ = 7.1 Hz). **^{13}C NMR** (100 MHz, $CDCl_3$, ppm): δ = 172.9 (*C*=O), 1.46.8 (*C*=CH), 122.1 (C=*C*H), 60.7 (OCH_2CH_3), 48.7 (N_3CH_2), 37.9 (SCH_2), 33.8 (C=OCH_2), 21.1 (CH_2C=CH), 14.4 (CH_3).

7.5.7 General procedure for RAFT polymerisations

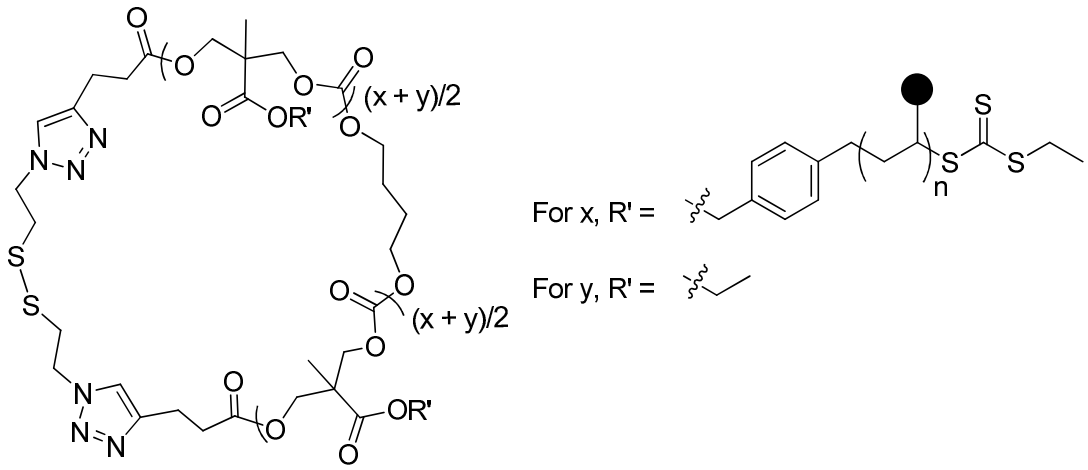

The appropriate equivalents of RAFT CTA-functional cyclic polycarbonate, AIBN (0.1 eq. to toal RAFT CTA groups) and monomer were loaded into a dry ampoule and dissolved in $CHCl_3$. The reaction mixture was degassed *via* 4 freeze-pump-thaw cycles and refilled with nitrogen. The polymerisation was initiated by immersion of the ampoule into an oil bath at 65 °C. After the desired length of time the polymerisation was quenched by immersion of the ampoule in liquid nitrogen.

^{1}H NMR (400 MHz, $CDCl_3$, ppm): δ = 7.22 – 7.15 (m, 4H$_{PC}$, Ar), 5.18 (m, 2H$_{PC}$, SCH_2Ar), 5.10 (m, 2H$_{PC}$, OCH_2Ar), 4.27 (m, 8H$_{PC}$, C=O$OCH_2C(CH_3)CH_2O$), 4.17 (m, 2H$_{PC}$, OCH_2CH_3), 3.63 – 3.31 (m, 4H$_{PNAM}$, NCH_2CH_2O), 3.37 (m, 2H$_{PC}$, SCH_2CH_3),

2.76 – 2.30 (m, $1H_{PNAM}$, $CH_2CHC{=}ON(CH_2)_2$), 1.90 – 1.50 (m, $2H_{PNAM}$, $CH_2CHC{=}ON(CH_2)_2$), 1.36 (m, $6H_{PC}$, CCH_3), 1.24 (m, $3H_{PC}$, OCH_2CH_3).

7.6 Experimental Procedures for Chapter 5

7.6.1 General procedure for particle preparation *via* direct dissolution

The relevant polymer was dissolved in 18.2 MΩ·cm water and thoroughly mixed using a vortex mixer.

7.6.2 General procedure for particle preparation *via* solvent switch

The relevant polymer was dissolved in THF at 1 mg/mL. 18.2 MΩ·cm water was added to the stirred solution *via* a peristaltic pump at a rate of 0.6 mL/h. After complete water addition, THF was removed *via* exhaustive dialysis against 18.2 MΩ·cm water for 3 days to yield a final concentration of *ca*. 0.5 mg/mL.

7.6.3 General procedure for particle preparation *via* thin film hydration

The relevant polymer was dissolved in $CHCl_3$ in a round bottom flask. $CHCl_3$ was removed *in vacuo* to leave a thin polymer film coating the inside of the flask. 18.2 MΩ·cm water was carefully added down the side of the flask, to prevent disruption of the film, which was left to hydrate for 16 h.

7.6.4 Determination of cmc *via* fluorescence spectroscopy

73 μL of a stock solution of pyrene in acetone (2.47×10^{-6} M) was added to several vials and the acetone subsequently evaporated. Solutions of **P1** and **P2** were prepared *via* direct dissolution in 18.2 MΩ·cm water, with concentrations from 0.0003 to 2 mg/mL. 300 μL of each polymer solution was added to a

pyrene containing vial and stirred overnight to give a final pyrene concentration of 6×10^{-7} M.

7.7 References

1. R. C. Pratt, B. G. G. Lohmeijer, D. A. Long, P. N. P. Lundberg, A. P. Dove, H. Li, C. G. Wade, R. M. Waymouth and J. L. Hedrick, *Macromolecules*, 2006, **39**, 7863-7871.
2. J. E. Kearns, C. D. McLean and D. H. Solomon, *J. Macromol. Sci., Part A: Chem.*, 1974, **8**, 673-685.
3. J.-H. Ryu, R. Roy, J. Ventura and S. Thayumanavan, *Langmuir*, 2010, **26**, 7086-7092.
4. J. Skey and R. K. O'Reilly, *Chem. Commun.*, 2008, 4183-4185.
5. L. S. Campbell-Verduyn, L. Mirfeizi, R. A. Dierckx, P. H. Elsinga and B. L. Feringa, *Chem. Commun.*, 2009, 2139-2141.
6. M. Malkoch, R. Vestberg, N. Gupta, L. Mespouille, P. Dubois, A. F. Mason, J. L. Hedrick, Q. Liao, C. W. Frank, K. Kingsbury and C. J. Hawker, *Chem. Commun.*, 2006, 2774-2776.
7. M. Malkoch, K. Schleicher, E. Drockenmuller, C. J. Hawker, T. P. Russell, P. Wu and V. V. Fokin, *Macromolecules*, 2005, **38**, 3663-3678.
8. I. Tellitu, S. Serna, M. T. Herrero, I. Moreno, E. Domínguez and R. SanMartin, *J. Org. Chem.*, 2007, **72**, 1526-1529.
9. H. Ihre, A. Hult, J. M. J. Fréchet and I. Gitsov, *Macromolecules*, 1998, **31**, 4061-4068.
10. K. Fukushima, R. C. Pratt, F. Nederberg, J. P. K. Tan, Y. Y. Yang, R. M. Waymouth and J. L. Hedrick, *Biomacromolecules*, 2008, **9**, 3051-3056.
11. Y. Wang, R. Zhang, N. Xu, F.-S. Du, Y.-L. Wang, Y.-X. Tan, S.-P. Ji, D.-H. Liang and Z.-C. Li, *Biomacromolecules*, 2010, **12**, 66-74.

12. A. B. J. Withey, G. Chen, T. L. U. Nguyen and M. H. Stenzel, *Biomacromolecules*, 2009, **10**, 3215-3226.

Appendix

Guinier Porod model provided by the NCNR package. Parameters Kn refer to the following:

K0 scale
K1 dimension variable s
K2 Rg (A)
K3 Porod exponent (A)
K4 background (cm^{-1})

PolyCoreForm model provided by the NCNR package. Parameters Kn refer to the following:

K0 scale
K1 average core radius (A)
K2 core polydispersity
K3 shell thickness (A)
K4 SLD core (A^{-2})
K5 SLD shell (A^{-2})
K6 SLD solvent (A^{-2})
K7 background (cm^{-1})

P6 h2o_dat_i[0,791]

GuinierPorod(coef_GP,WMCF_TempDestWave,WMCF_TempXWave)
V_chisq= 1576.36;V_npnts= 790;V_numNaNs= 0;V_numINFs= 0;
Coefficient values ± one standard deviation
K0 =0.0056955 ± 0.000188
K1 =0.1628 ± 0.00786
K2 =35.003 ± 0.225
K3 =3.3643 ± 0.0691
K4 =2.6332e-005 ± 8.54e-006
fit time = 0.980137 seconds

P6 h2o_dat_i[3,464]

Debye(coef_deb,WMCF_TempDestWave,WMCF_TempXWave)
V_chisq= 8653.97;V_npnts= 462;V_numNaNs= 0;V_numINFs= 0;
Coefficient values ± one standard deviation
K0 =0.014205 ± 6.54e-005
K1 =60.647 ± 0.217
K2 =1e-005 ± 0
fit time = 0.570081 seconds

P6 h2o_dat_i[13,439]

PolyCoreForm(coef_pcf,WMCF_TempDestWave,WMCF_TempXWave)
V_chisq= 740.781;V_npnts= 427;V_numNaNs= 0;V_numINFs= 0;
Coefficient values ± one standard deviation
K0 =0.0042714 ± 0.00284
K1 =22.082 ± 0.627
K2 =0.48761 ± 0.0135
K3 =0 ± 0
K4 =9.7483e-006 ± 9.6e-008
K5 =6.0873e-007 ± 0
K6 =9.46e-006 ± 0
K7 =8e-005 ± 0
fit time = 0.443818 seconds

P6 dioxane_dat_i[2,168]

GuinierPorod(coef_GP,WMCF_TempDestWave,WMCF_TempXWave)
V_chisq= 288.534;V_npnts= 167;V_numNaNs= 0;V_numINFs= 0;
Coefficient values ± one standard deviation
K0 =0.0085501 ± 0.000558
K1 =0.19524 ± 0.0147
K2 =44.65 ± 0.537
K3 =3.5674 ± 0.532
K4 =3e-005 ± 0
fit time = 0.906032 seconds

P6 dioxane_dat_i[9,253]
PolyCoreForm(coef_pcf,WMCF_TempDestWave,WMCF_TempXWave)
V_chisq= 573.672;V_npnts= 245;V_numNaNs= 0;V_numINFs= 0;
Coefficient values ± one standard deviation
K0 =0.0069901 ± 0.0111
K1 =48.542 ± 0.892
K2 =0.23593 ± 0.0111
K3 =0 ± 0
K4 =9.7679e-006 ± 1.43e-007
K5 =6.0873e-007 ± 0
K6 =9.587e-006 ± 0
K7 =0.0001 ± 0
fit time = 0.356397 seconds

P5 h2o_dat_i[13,515]
GuinierPorod(coef_GP,WMCF_TempDestWave,WMCF_TempXWave)
V_chisq= 1081.47;V_npnts= 503;V_numNaNs= 0;V_numINFs= 0;
Coefficient values ± one standard deviation
K0 =0.0040258 ± 7.23e-005
K1 =0.64507 ± 0.00403
K2 =42.778 ± 0.142
K3 =3.5955 ± 0.0223
K4 =0.0002441 ± 7.28e-006
fit time = 0.718703 seconds

P5 h2o_dat_i[15,464]
PolyCoreForm(coef_pcf,WMCF_TempDestWave,WMCF_TempXWave)
V_chisq= 10137;V_npnts= 450;V_numNaNs= 0;V_numINFs= 0;
Coefficient values ± one standard deviation
K0 =0.004396 ± 0.289
K1 =35.632 ± 0.35
K2 =0.5 ± 0.00512
K3 =0 ± 0
K4 =9.7989e-006 ± 1.11e-005
K5 =6.0873e-007 ± 0
K6 =9.46e-006 ± 0
K7 =0.00025 ± 0
fit time = 0.469801 seconds

P5 h2o_dat_i[19,477]
Cyl_PolyRadius(coef_cypr,WMCF_TempDestWave,WMCF_TempXWave)
V_chisq= 2824.1;V_npnts= 459;V_numNaNs= 0;V_numINFs= 0;
Coefficient values ± one standard deviation
K0 =0.00090742 ± 1.15
K1 =37.851 ± 0.0547
K2 =255.54 ± 1.01
K3 =0.3 ± 0
K4 =1.0211e-005 ± 0.000477
K5 =9.46e-006 ± 0
K6 =0.00039556 ± 4.95e-006
fit time = 2.14163 seconds

P5 dioxane_dat_i[6,758]
GuinierPorod(coef_GP,WMCF_TempDestWave,WMCF_TempXWave)
V_chisq= 6106.68;V_npnts= 753;V_numNaNs= 0;V_numINFs= 0;
Coefficient values ± one standard deviation
K0 =0.0040658 ± 6.49e-005
K1 =0.63374 ± 0.00349
K2 =45.49 ± 0.135
K3 =5.2205 ± 0.0743
K4 =3e-005 ± 0
fit time = 1.55001 seconds

P5 dioxane_dat_i[13,280]
PolyCoreForm(coef_pcf,WMCF_TempDestWave,WMCF_TempXWave)
V_chisq= 4187.72;V_npnts= 268;V_numNaNs= 0;V_numINFs= 0;

Coefficient values ± one standard deviation
K0 =0.0038558 ± 0.0105
K1 =38.689 ± 0.485
K2 =0.5 ± 0.00623
K3 =0 ± 0
K4 =9.9119e-006 ± 4.42e-007
K5 =6.0873e-007 ± 0
K6 =9.587e-006 ± 0
K7 =0.0001 ± 0
fit time = 0.564801 seconds

P5 dioxane_dat_i[17,214]
Cyl_PolyRadius(coef_cypr,WMCF_TempDestWave,WMCF_TempXWave)
V_chisq= 1094.49;V_npnts= 198;V_numNaNs= 0;V_numINFs= 0;
Coefficient values ± one standard deviation
K0 =0.00095663 ± 1.38
K1 =46.12 ± 1.6
K2 =272.45 ± 1.54
K3 =0.19191 ± 0.0268
K4 =1.0231e-005 ± 0.000463
K5 =9.587e-006 ± 0
K6 =0.0001 ± 0.000116
fit time = 0.535684 seconds